

**THE BIOLOGICAL EFFECTS OF TITANIUM CORROSION PRODUCTS ON
GINGIVAL EPITHELIUM**

By

Joanna Mary Batt

BDS, MJDF, FHEA

A thesis submitted to the University of Birmingham for the degree of

DOCTOR OF PHILOSOPHY

School of Dentistry

College of Medical and Dental Sciences

University of Birmingham

August 2017

UNIVERSITY OF
BIRMINGHAM

University of Birmingham Research Archive

e-theses repository

This unpublished thesis/dissertation is copyright of the author and/or third parties. The intellectual property rights of the author or third parties in respect of this work are as defined by The Copyright Designs and Patents Act 1988 or as modified by any successor legislation.

Any use made of information contained in this thesis/dissertation must be in accordance with that legislation and must be properly acknowledged. Further distribution or reproduction in any format is prohibited without the permission of the copyright holder.

Abstract

Implanted titanium (Ti) devices such as dental implants have been shown to produce metallic species within adjacent tissues. The effect of the presence of these species within oral epithelial tissues is currently not well characterised or known. This thesis investigates the effects of TiO₂ nanoparticles (TiO₂ NPs) at a range of concentrations on oral epithelial cells in the context of cell viability, cellular functions and interactions via a variety of methods. A co-culture model was established, and the difficulties of using a nano-scale insoluble stimulus were explored, and high content screening techniques were shown to be potentially more appropriate methods than conventional assays in this context. Interactions between TiO₂ NPs and oral epithelial cells were imaged and investigated using a variety of imaging techniques. Oral epithelial cells were shown to take up TiO₂ NPs within vacuole type structures. Cell viability appeared to not be affected at lower concentrations. Gene expression changes of oral epithelial cells in response to TiO₂ NPs in the presence and absence of pathogenic bacteria were investigated. Cytokines important in cell-cell signalling were shown to bind TiO₂ NPs, therefore creating potential for TiO₂ NPs within tissues to modify immune responses within tissues adjacent to implanted Ti devices.

Dedication

I would like to dedicate this thesis to my family. Thank you for all your support and reminding me what are the true priorities in life. Special thanks to my husband for believing that I could do this and his refreshing dislike of Dentistry, my daughter (who was born somewhere between chapters 7 and 8), and bump who has helped me in finishing my write up.

Acknowledgements

I would like to thank Professor Owen Addison, Professor Iain Chapple, and Dr Mike Milward for their support, help and guidance throughout these last few years and introducing me to the world of 'proper' science! I hope in years to come I can extend the same guidance to others that you have shown me.

I would also like to thank colleagues who have helped me immeasurably; Dr Helen Wright, Dr Naomi Hubber, and all the other PhD students with whom I shared some years, particularly Martin, Helen, Pip and Sonam.

Table of contents

List of Figures

List of Tables

Abbreviations

Chapters

Page
number

Chapter 1 - Introduction	1
1.1 Use of Titanium as a biomaterial	2
1.1.1 <i>Physical properties and presentation</i>	2
1.1.2 <i>Suitability as a biomedical alloy</i>	2
1.1.3 <i>Ti surface stability conferred by Titanium Oxide layer (TiO₂)</i>	3
1.1.4 <i>Classification of Ti</i>	4
1.2 Use of Ti in dental implants	5
1.2.1 <i>History of dental implants</i>	5
1.2.2 <i>Osseointegration</i>	5
1.2.3 <i>The development of modern “root form” Ti implants</i>	7
1.2.4 <i>“Success, survival and failure” criteria for dental implants</i>	10
1.3 Peri-implant disease	11
1.3.1 <i>Definitions of peri-implant diseases</i>	11
1.3.2 <i>Prevalence of peri-implant diseases</i>	11
1.3.3 <i>The pathogenesis of peri-implant disease</i>	12
1.3.4 <i>The role of and composition of microflora in the peri-implant milieu</i>	13
1.3.5 <i>The role of host responses in the progression of peri-implant disease</i>	15
1.3.6 <i>Treatment of peri-implant diseases</i>	17
1.4 Stability of Ti surfaces in vivo	18
1.4.1 <i>Corrosion of Ti</i>	18
1.4.2 <i>Evidence of release in non-wear situations</i>	20
1.4.3 <i>The potential bio-consequences of free Ti in tissues</i>	22
1.5 The role of epithelium in implant soft tissue outcomes	24
1.5.1 <i>Structure of the peri-implant tissues</i>	24
1.5.2 <i>Structure and function of the oral epithelial tissues</i>	26
1.5.3 <i>Link between soft tissues and long term implant health</i>	28
1.5.4 <i>Epithelium, the bacterial challenge and inflammation</i>	30
1.5.5 <i>Cell-cell signalling and immune cell recruitment</i>	31
1.6 Aims and objectives	31
1.6.1 <i>Justification for project</i>	31
1.6.2 <i>Aims of the project</i>	32
 Chapter 2 – Materials and methods	 33
2.1 Titanium stimuli	34
2.1.1 <i>Titanium oxide stimulus preparation</i>	34
2.1.2 <i>Addition to cell culture medium</i>	35
2.2 H400 cell culture	35
2.2.1 <i>Cell culture media and reagents</i>	35
2.2.2 <i>H400 cell culture and passage</i>	36
2.3 Use of cell viability assays	40
2.3.1 <i>CellTiter-Glo® assay</i>	41

2.3.2 CytoTox-ONETM	43
2.3.3 Caspase-Glo® 3/7 assay	44
2.3.4 Sytox® Green Nucleic Acid Stain	45
2.3.5 MTT assay	46
2.4 Primary oral epithelial cell culture	47
2.4.1 Primary epithelial cell culture using a 3T3 feeder layer	47
2.4.2 Primary epithelial cell culture using the explant method	49
2.5 RNA isolation and Polymerase Chain Reaction (PCR)	50
2.5.1 RNA isolation from cultured cells	50
2.5.2 RNA purification and DNase digestion	52
2.5.3 RNA quantification	53
2.5.4 Reverse transcription (RT)	53
2.5.5 Purification and concentration of cDNA	54
2.5.6 Semi quantitative PCR	54
2.5.7 Quantitative Real Time Polymerase Chain Reaction (qPCR)	57
2.6 Immunocytochemistry	61
2.6.1 Staining for NF-κB activation using the SuperSensitive® Link-Detection Kit overview	61
2.6.2 Stimulation of H400 cells prior to ICC	65
2.6.3 Quantification of NF-κB translocation	65
2.7 Immunofluorescence staining of cultured cells	68
2.8 Microscopy techniques	70
2.8.1 Transmission electron microscopy (TEM)	70
2.8.2 Reflectance confocal microscopy	72
2.9 Reactive Oxygen Species (ROS) production of neutrophils	73
2.9.1 Neutrophil isolation reagent preparation	75
2.9.2 ROS generation assay reagent preparation	77
2.9.3 ROS assay protocol	76
2.9.4 Preparation of bacterial stimuli	78
2.9.5 Chemotaxis assay	80
2.10 Enzyme linked immunosorbent assays (ELISAs)	83
2.10.1 ELISA protocol	84
2.11 High Content Screening (HCS) sample preparation	85
2.11.1 HCS methods (general)	86
Chapter 3 - Development and validation of in vitro models of oral epithelium	89
3.1 H400 cell growth and morphology	91
3.1.1 H400 morphology assessment	92
3.1.2 H400 morphology assessment – results	95
3.1.3 Conclusions from H400 growth characterisation and cell counts	98
3.2 Primary oral epithelial cell isolation and culture	99
3.2.1 Primary epithelial cell culture methods	100
3.2.2 Results of primary epithelial cell culture	100
3.2.3 Conclusions from primary oral epithelial cell culture	104
3.2.4 Characterisation of explant cellular outgrowth	105
3.2.5 Conclusions of characterisation following culture of epithelial cells from gingival tissues	108
3.3 Use of relevant stimuli and potential interactions of Ti products with known assays	109

3.3.1 Cell Titer-Glo® verification with TiO ₂ NPs	110
3.3.2 MTT ([3-(4,5-Dimethylthiazol-2-yl)-2,5-Diphenyltetrazolium Bromide]) Assay	110
3.3.3 LDH (Lactate dehydrogenase) assay	112
3.3.4 CaspaseGlo® 3/7 assay	113
3.3.5 Conclusions from assay verifications	113
3.4 Chapter conclusions	114
Chapter 4 - Imaging of interactions between TiO₂ NPs and oral epithelial cells	116
4.1 Light microscopy and findings	117
4.2 Transmission Electron Microscopy (TEM)	118
4.2.1 Limitations of TEM imaging	122
4.2.2 Treatment with an endocytosis inhibitor	123
4.3 Reflectance confocal microscopy	125
4.4 Imaging of TiO ₂ NP accumulation in primary oral epithelial cells	127
4.5 Conclusions from cell images and justification for further investigation	130
4.6 Synchrotron micro-focussed X-ray Fluorescence (SR-XRF)	130
4.6.1 SR-XRF methods	131
4.6.2 SR-XRF results	132
4.7 Chapter conclusions	134
Chapter 5 - Effects of interactions between TiO₂ NPs and oral epithelial cells on cell viability, growth and immune responses	136
5.1 Conventional cell viability assays	137
5.1.1 ATP activity measured by CellTiter-Glo®	138
5.1.2 LDH concentration measured by CytoTox-ONE™	139
5.1.3 CaspaseGlo® 3/7	141
5.1.4 Cell viability results from conventional assays	142
5.1.5 Sytox® green staining	145
5.2 High Content Screening (HCS)	147
5.2.1 Cell viability using HCS	148
5.2.2 Cell count and cell death	151
5.2.3 Cell morphology	152
5.2.4 Further work informed by HCS results	152
5.2.5 Cell cycle as examined using HCS	153
5.2.6 Conclusions from HCS viability and initial assays	155
5.3 Effects of TiO ₂ NPs on Nuclear Factor kappa-light-chain-enhancer of activated B cells (NFκB) activation	156
5.3.1 Activation of NFκB in H400 cells	157
5.4 TiO ₂ NPs as a potential modifier of epithelial responses to bacteria	160
5.4.1 NFκB responses of oral epithelial cells to bacterial LPS with and without pre-treatment with TiO ₂ NPs – method	160
5.4.2 NFκB responses of oral epithelial cells to bacterial LPS with and without pre-treatment with TiO ₂ NPs – results and discussion	161
5.4.3 Co-stimulation of H400 cells with heat killed <i>Fusobacterium nucleatum</i> and TiO ₂ NPs	162
5.4.4 Co-stimulation of H400 cells with heat killed <i>Fusobacterium nucleatum</i> and TiO ₂ NPs – discussion	163
5.4.5 HCS investigation of NFκB responses to bacteria with and without TiO ₂ NPs- method	163

5.4.6 HCS investigation of NFκB responses to bacteria with and without TiO ₂ NPs- results	164
5.4.7 HCS investigation of NFκB responses to bacteria with and without TiO ₂ NPs- discussion	167
5.5 Chapter conclusions	167
Chapter 6 - Effects of interactions between TiO₂ NPs and oral epithelial cells on gene expression	169
6.1 DNA microarray	170
6.1.1 Affymetrix GeneChip method	172
6.1.2 GeneChip data analysis	173
6.1.3 GeneChip results – DNA microarray data	174
6.1.4 GeneChip results - DNA microarray data interpretation and discussion - Ontological grouping	177
6.1.5 GeneChip results - DNA microarray data interpretation and discussion – Common genes between 6 hr and 24 hr samples	180
6.1.6 GeneChip results - DNA microarray data interpretation and discussion – robustness of microarray data	184
6.2 Confirmatory Polymerase Chain Reaction (PCR)	185
6.2.1 Confirmatory PCR – methods	185
6.2.2 Confirmatory PCR – results and conclusion	186
6.2.3 Confirmatory PCR– Primary oral epithelial cells –aim and method	186
6.2.4 Confirmatory PCR – Primary oral epithelial cells –results and conclusion	187
6.3 Co-stimulation qPCR (Quantitative Real Time PCR)	188
6.3.1 Co-stimulation qPCR - aims	188
6.3.2 Co-stimulation qPCR - method	188
6.3.3 Co-stimulation qPCR - results	190
6.3.4 Co-stimulation qPCR - discussion	190
6.4 Chapter conclusions	191
Chapter 7 - Effects of the presence of TiO₂ NPs on cell to cell signalling processes	193
7.1 Cytokine release from H400 cells as detected using ELISAs (Enzyme Linked Immunosorbant Assays)	194
7.1.1 ELISA standard curves in the presence and absence of TiO ₂ NPs - methods	196
7.1.2 ELISA standard curves in the presence and absence of TiO ₂ NPs – results	197
7.1.3 ELISA standard curves in the presence and absence of TiO ₂ NPs - conclusions	197
7.1.4 ELISAs performed on supernatants from H400 cells - aims	198
7.1.5 ELISAs performed on supernatants from H400 cells - methods	198
7.1.6 ELISAs performed on supernatants from H400 cells - results	199
7.1.7 ELISAs performed on supernatants from H400 cells - conclusions	200
7.2 Interactions between TiO ₂ NPs and IL8 / IFNγ	200
7.2.1 Interaction between TiO ₂ NPs and IL8 –ELISA investigation method	201

7.2.2 Demonstration of IL8 / TiO ₂ NP binding	203
7.2.3 Chemotaxis assay as a functional measure of IL8 activity in the presence and absence of TiO ₂ – aims and method	205
7.2.4 Chemotaxis assay as a functional measure of IL8 activity in the presence and absence of TiO ₂ – results	207
7.2.5 Chemotaxis assay as a functional measure of IL8 activity in the presence and absence of TiO ₂ – conclusion	210
7.3 Reactive Oxygen Species (ROS) production	211
7.3.1 ROS generation by neutrophils in response to stimulation by H400 supernatants - method	212
7.3.2 ROS generation by neutrophils in response to stimulation by H400 supernatants – results and conclusions	214
7.3.3 H400 growth in RPMI (Roswell Park Memorial Institute) medium	215
7.3.4 ROS assay using supernatants from H400 cell culture as priming agents to freshly isolated neutrophils	217
7.3.5 ROS assay using supernatants from H400 cell culture as priming agents to freshly isolated neutrophils – results	218
7.3.6 ROS assay using supernatants from H400 cell culture as priming agents to freshly isolated neutrophils – conclusions	218
7.3.7 Effect of TiO ₂ NPs on the priming action of IFN γ	219
7.4 Chapter conclusions	220
Chapter 8 - Discussion, conclusions and further work	221
8.1 Discussion	222
8.1.1 Epithelial structure and function	222
8.1.2 Implant derivatives within oral epithelial cells and associated tissues	223
8.1.3 Effects of TiO ₂ NPs on the viability of oral epithelial cells	226
8.1.4 Intracellularisation of TiO ₂ NPs by epithelial cells	227
8.1.5 Dose responses of epithelial cells to TiO ₂ NPs	228
8.1.6 Interference of TiO ₂ NPs in suspension with known assays and difficulties of using conventional assays only	229
8.1.7 Effects of TiO ₂ on inflammation involving oral epithelial cells	230
8.2 Relevance of findings in the clinical context of peri-implant disease	231
8.3 Overall conclusions	234
8.4 Future work	236
References	237

List of Figures

Figure number	Figure title	Page
1.1	Crystalline structures of Anatase, Brookite and Rutile (Jolivet et al., 2010)	4
1.2	Illustration highlighting the anatomical differences between a natural tooth and a single unit root form implant supported restoration	7
1.3	X-ray fluorescence map of peri-implant epithelium showing significant accumulation of Ti in the peri-implant soft tissues	21
1.4	High resolution X-ray fluorescence map of peri-implant epithelium showing significant accumulation of Ti in the both epithelial and connective tissue layers	21
1.5	Nano-focussed Ti (red) X-ray fluorescence map of peri-implant epithelium	22
1.6	Peri-implant tissues (A) compared with periodontal tissues	25
1.7	Diagram (bucco-lingual Section) through the periodontal tissues	26
1.8	Gingival epithelial tissue viewed under Transmission Electron Microscopy	28
2.1	Diagram representing a cell count of cells stained with trypan blue exclusion	40
2.2	The luciferase reaction which takes place using the CellTiter-Glo® assay	41
2.3	Standard curve for LDH content in wells using CytoTox-ONE™ assay	43
2.4	Bands of GAPDH expression selected and the intensity of each 'blot' is generated by AIDA image analysis software	56
2.5	PCR gel image at 30, 35 and 40 cycles	57
2.6	Amplification of YWHAZ gene	59
2.7	Amplification curve, efficiency standard curve and melt curve for YWHAZ housekeeper gene	60
2.8	Diagrammatic representation of an indirect ICC system	62
2.9	Layout of multiwell slides for ICC	62
2.10	Expected result showing positive control for immunocytochemistry	66
2.11	Expected result showing negative diluent control for immunocytochemistry	66
2.12	H400 control well from stained NF-κB slide	67
2.13	H400 cells with E. coli LPS stimulated well from a stained NF-κB slide	67
2.14	Hunting curve for cell counts	68
2.15	Diagram of indirect immunofluorescence	69
2.16	Diagram of the ROS luminol/isoluminol based assay	75
2.17	Diagram of Percoll blood separation tube following centrifugation	76
2.18	Diagram and photograph of an Insall chamber	81
2.19	Diagram illustrating sandwich ELISA process to detect target proteins within a sample.	83
2.20	Diagram representing the different parameters which can be measured using HCS imaging techniques	87
3.1	Diagram representing a section of a modified Neubauer haemocytometer	94
3.2	Diagram showing eyepiece graticule superimposed over cells in situ	94
3.3	Light microscopy images illustrating H400 cell growth from 1-4 days post seeding showing increasing growth to confluence	95
3.4	H400 cells showing morphological features of epithelial cells	96
3.5	Hunting curves for single cell suspension count using a haemocytometer (a) and in-situ count using an eyepiece graticule (b)	96
3.6	Cell counts of single cell suspension using haemocytometer (a) and cell counts of in-situ cells within a monolayer using an eyepiece graticule (b)	97
3.7	Appearance of epithelial cells growing out from biopsy tissue on a 3T3 fibroblast feeder layer before passaging and reseeded	100

3.8	Mixed epithelial and fibroblastic appearance of primary epithelial cells grown on a 3T3 feeder layer following cell passage	101
3.9	Light microscopy images showing explanted oral epithelial tissue exhibiting epithelial appearance of primary cells growing outwards in a 'cobblestone' formation from a tissue biopsy at 5 and 7 days post placement into a culture flask	102
3.10	Typical light microscopy image showing cells cultured from explanted epithelial tissue	103
3.11	Primary oral cells 14 days post passage showing a mixed morphology of epithelial and fibroblastic appearance	104
3.12	Representative image of tissue outgrowth stained for cytokeratin expression	106
3.13	Images of agarose gel showing expression of cytokeratins and vimentin	107
3.14	Expression of vimentin in different cell types	118
3.15	Absorbance of samples containing known concentrations of TiO ₂ NPs and LDH	114
3.16	Absorbance for cell culture media containing 0-1000 ppm TiO ₂ NPs and H400 cells	111
3.17	Absorbance of samples containing known concentrations of TiO ₂ NPs and LDH	112
4.1	A representative image of H400 cells cultured in a 25cm ² cell culture flask without addition of TiO ₂ NPs (a) and after the addition of 100 ppm TiO ₂ NPs to cell culture medium for 24 h (b)	117
4.2	A representative image of H400 cells cultured in a 25cm ² cell culture flask without addition of TiO ₂ NPs (a) and after the addition of 100 ppm TiO ₂ NPs to cell culture medium for 48 h (b)	118
4.3	A section through a detached (trypsinised) and fixed H400 cell viewed using TEM	119
4.4	Control (not exposed to TiO ₂ NPs) H400 cells imaged using TEM	120
4.5	H400 cells washed (<1 min) with cell culture media supplemented with 100ppm TiO ₂ NPs imaged using TEM	120
4.6	H400 cells cultured with 10 ppm TiO ₂ NPs in medium for 24 h imaged using TEM	120
4.7	H400 cells cultured for 24h in growth media containing 100ppm TiO ₂ NPs imaged using TEM	121
4.8	H400 cells cultured with 1000ppm TiO ₂ NP containing medium for 24h imaged using TEM	121
4.9	H400 cells cultured with (a) 100ppm TiO ₂ NP containing medium for 24h and 0.1% DMSO and (b) H400 cells cultured with 100ppm TiO ₂ NP containing medium for 24h with 80 µM Dynasore Hydrate	124
4.10	H400 cells cultured with 1 ppm TiO ₂ NPs for 0, 3, 6 and 9h then and viewed under reflectance microscopy	125
4.11	H400 cells cultured with 10 ppm TiO ₂ NPs for 0, 3, 6 and 9h then and viewed under reflectance microscopy	126
4.12	H400 cells cultured with 100 ppm TiO ₂ NPs for 0, 3, 6 and 9h then and viewed under reflectance microscopy	126
4.13	Graph showing % cells with visible TiO ₂ NP agglomerations following exposure to 0-100 ppm TiO ₂ NPs for 0-9 h	127
4.14	TEM images showing primary human gingival epithelial cells exposed to TiO ₂ 100 ppm for 6 h	128
4.15	Reflectance microscopy images of primary human gingival epithelial cells exposed to 10ppm TiO ₂ NPs for 6h	128

4.16	Reflectance microscopy images of primary human gingival epithelial cells exposed to 10 ppm TiO ₂ NPs for 9h	129
4.17	XFR images showing relative fluorescence of Potassium, Calcium and Titanium in control H400 cells	132
4.18	A representative XRF image of representative fluorescence of S, Ca and Ti in H400 cells exposed to TiO ₂ 10 ppm for 24h	132
4.19	X-ray fluorescence of Ca and Ti two groups (a and b) of H400 cells exposed to TiO ₂ 10 ppm for 24 h	134
5.1	CellTiter-Glo® luminescence (RFU) for H400 cells treated with 0, 1, 10, 100 and 1000 ppm TiO ₂ NPs for 0 h, 3 h, 6 h and 24 h	138
5.2	Fluorescence (RFU) generated using CytoTox-ONE™ assay of known LDH concentrations	140
5.3	LDH levels, Caspase 3 and 7 levels and percentage of cells positive for trypan blue stain within a 96-well plate	141
5.4	Conventional viability assays performed at time-points up to 24 h on H400 cells exposed to up to 5000 ppm TiO ₂ NPs	143
5.5	Exemplar images showing Sytox® green stained cells in a population of H400 cells co cultured with TiO ₂ NPs at concentrations of 0-1000 ppm and the proportion of positively stained cells within a number of images counted	146
5.6	Selected HCS images showing cell viability 6 days following addition of TiO ₂ NPs at a variety of concentrations	150
5.7	H400 cell count (A) and percentage cell death of the whole population (B) as measured by HCS over 7 days	151
5.8	H400 cells stained with CellMask plasma membrane stain, DAPI nuclear stain and combined images at 6 days post exposure to 1000 ppm TiO ₂ NPs (a) and control cells (b)	152
5.9	Cell cycle diagram	154
5.10	HCS analysis of cell populations exposed to differing concentrations of TiO ₂ NPs	155
5.11	H400 cells stained for the identification of NFκB translocation	157
5.12	Graph showing activation of H400 cells exposed to the stimuli listed in the below table for 1 h	158
5.13	Nuclear:cytoplasmic intensity of NFκB stained with a flurophore of H400 cells exposed to 0-100 ppm TiO ₂ NPs	159
5.14	A one-way ANOVA and post-hoc Tukey tests demonstrated a significant difference between NFκB activation in response to 20 mg/mL LPS when pre-treated with TiO ₂	161
5.15	The % activated H400 cells exposed to heat killed FN for 1 h +/- TiO ₂ 10 ppm for 24 h previously or exposed to FN and TiO ₂ concurrently for 1 h	162
5.16	Nuclear:cytoplasmic intensity ratio of fluorophore conjugated to NFκB in oral epithelial cells when stimulated with FN (<i>Fusobacterium nucleatum</i>), LPS (<i>E.Coli</i> LPS) and PG (<i>Porphyromonas gingivalis</i>) over time	164
5.17	Example images showing fluorescent signal from H400 cells stained for NFκB translocation	165
5.18	Example images showing fluorescent signal from H400 cells stained for NFκB translocation following 10 ppm TiO ₂ treatment for 24 h	165
5.19	Example images showing fluorescent signal from H400 cells stained for NFκB translocation following FN exposure for 1 h	166
5.20	Example images showing fluorescent signal from H400 cells stained for NFκB translocation following 10 ppm TiO ₂ treatment for 24h and FN exposure for 1 h	166

6.1	Illustration of a DNA microarray chip	171
6.2	Diagrams showing ontological grouping by function of genes with altered expression as labelled in H400 cells exposed to TiO ₂ NPs 100 ppm for 6 h compared with a control cell sample	178
6.3	Diagrams showing ontological grouping by function of genes with altered expression as labelled in H400 cells exposed to TiO ₂ NPs 100 ppm for 24 h compared with a control cell sample	179
6.4	Venn diagrams showing down-regulated, up-regulated and altered expression of genes in H400 cells at 6 h (blue) and 24 h (yellow) TiO ₂ exposure at 100 ppm compared with respective control cells as detected by the AffyChip	181
6.5	Example graph of the levels of expression of ID1 in each sample replicate	185
6.6	Images of agarose gels showing agreement of up- or down- regulation between PCR and microarray data on a selection of genes	186
6.7	Primary epithelial cell semi-quantitative PCR data showing a down-regulation of ID1 and 3 in cells exposed to TiO ₂ for 6h and an up-regulation of ID2	187
6.8	Histograms showing ID1 (a), ID2 (b) and ID3 (c) expression using qPCR of H400 samples	190
7.1 (a-e)	A plot of cytokine concentration (replicate points shown) against absorbance (arbitrary units, AU) derived from ELISA (n=2) for the serially diluted specific standard and for the serially diluted specific standard following exposure to 100ppm TiO ₂ NPs for 24 h and centrifugation to remove insoluble contents	197
7.2	ELISA data showing absorbances representing cytokine concentration in supernatants	199
7.3	A plot of IL8 concentration (mean and SEM) against absorbance (arbitrary units) derived from ELISA (n=3) for the IL8 standard (0 ppm) serially diluted in standard reagent diluent (a) and human serum (1 in 10) (b) and for the IL8 standard following exposure to 1, 10, 100 and 1000 ppm of TiO ₂ NPs for 1 h then serially diluted in reagent diluent or human serum (1 in 10), respectively before centrifugation to remove insoluble contents	202
7.4	Sections taken from an imperial Blue stained protein gel	204
7.5	Examples of first (left) and last (right) frames of 40 frames of a chemotaxis video showing the coloured lines where a selection of randomly chosen cells were tracked	206
7.6	Box-whisker plots showing data points plus mean and SD for Speed, Velocity and Chemotactic Index of neutrophils exposed to the positive and negative (control chemoattractant and to the experimental chemoattractants.	207
7.7	Chemotaxis vector plots showing the proportion and directionality of movement of cells in each segment during the observation period related to Figure 7.6	208
7.8	Box-whisker plots showing data points, mean and SD of data for Speed, Velocity and Chemotactic Index of neutrophils exposed to the positive and negative control chemoattractant and to the experimental chemoattractants (IL8 at initially 200 ng/mL) exposed to 1, 10, 100, 1000 ppm of TiO ₂ NPs for 1 h before centrifugation to remove the insoluble NPs	209
7.9	Chemotaxis vector plots showing the proportion and directionality of movement of cells in each segment during the observation period related to Figure 7.8	210
7.10	Plot showing verification of use of Luminol and assay described in Section 2.9 to detect oxidative burst	213

7.11	ROS curve showing RLU generated by addition of supernatants as listed below to wells containing neutrophils and luminol over time	214
7.12	Cell free simulated ROS burst generated by H ₂ O ₂ addition to wells containing luminol and media as listed, TiO ₂ was suspended in water	215
7.13	A typical optical micrograph illustrating the growth of H400 cells at 24 h and 48 h post seeding at 2 x 10 ⁵ cells in standard H400 cell culture medium	216
7.14	A typical optical micrograph illustrating the growth of H400 cells at 24 h and 48 h post seeding at 2 x 10 ⁵ cells in RPMI medium	216
7.15	A typical optical micrograph illustrating the growth of H400 cells at 24 h and 48 h post seeding at 2 x 10 ⁵ cells initially in standard H400 cell culture medium, then exchanging medium post 24 h to RPMI	217
7.16	Box and whisker plot to show relative oxidative burst responses of neutrophils stimulated with ops <i>Sa</i> when primed with RPMI based supernatant from H400 cells	218
7.17	ROS generation of neutrophils primed with 110 units of IFN γ +/- TiO ₂ NPs (50ppm) then stimulated with PMA compared with control cells (no primer or stimulation) and cells primed with PBS then stimulated with PMA	219
8.1	Diagrammatic representation of cell-cell signalling involving oral epithelial cells and related cell types during periodontal inflammation and associated bone resorption (Sahingur and Yeudall, 2015)	231

List of Tables

Table number	Table title	Page
1.1	Elastic moduli of selected materials (Ratner, 2013)	2
1.2	Physical properties of Ti grades. Reproduced from Elias et al., 2008	5
1.3	Implant success scale recreated from Misch et al., 2008	10
1.4	Bacterial colonisation of implant surfaces separated into Socransky's groupings	14
1.5	Documented reported toxicological effects of Ti particles on different human cell types, including the Ti species identified, the cell type and the author / date.	23
1.6	Maturation features in non-keratinised epithelium (Nanci and Ten Cate, 2008)	27
2.1	Ti stimulus preparation	34
2.2	Seeding densities of epithelial cells	39
2.3	DMEM supplementation	47
2.4	Primary cell culture medium	48
2.5	Wash-PBS	49
2.6	Serum free culture medium	50
2.7	PCR cycling	55
2.8	qPCR primers	58
2.9	qPCR reagent mix	58
2.10	qPCR cycling protocol used	58
2.11	Cp data of housekeeping genes	59
2.12	Concentrations of stimuli for H400 cells prior to immunocytochemistry staining	65
2.13	Percoll densities	75
2.14	Lysis buffer	76
2.15	ROS assay protocol	78
2.16	H400 conditions prior to ELISA testing	85
2.17	Gel electrophoresis sample preparation	87
3.1	Similarities and differences between H400 cells and primary oral epithelial cells (keratinocytes)	92
4.1	Quantification of H400 cells associated with no Ti, small and large agglomerations	133
5.1	H400 cell preparation prior to NFkB staining	161
5.2	H400 co-culture conditions prior to NFkB staining	162
6.1	H400 RNA sample preparation	172
6.2	Genes showing altered expression at 6 h in H400 cells exposed to TiO ₂ NPs compared with control cells (fold change >1.5 and p < 0.001)	174-5
6.3	Genes showing altered expression at 24 h in H400 cells exposed to TiO ₂ NPs compared with control cells (fold change >1.5 and p < 0.001)	175-6
6.4	H400 plating conditions prior to qPCR	189
7.1	ELISA sample preparation	198
7.2	ELISA data shown in Figure 7.14 summarised	200
7.3	Protein gel sample preparation	203

List of Abbreviations

ACTB Beta-Actin

Al	Aluminium
AP-1	Activation Protein 1
ASTM	American Society for Testing and Materials
ATCC	American Type Culture Collection
ATP	Adenine Triphosphate
ATPase	adenosine triphosphatase
AU	Arbitrary Units
BAHA	Bone Anchored Hearing Aid
BSA	Bovine Serum Albumin
Ca	Calcium
Ca ²⁺	Calcium ion
CBCT	Cone Beam Computerised Tomography
cdk	Cyclin-dependent kinase
CI	Chemotactic Index
CO ₂	Carbon Dioxide
CP	Commercially Pure
Cp	Crossing point
DAB	Diaminobenzidine
DAPI	4',6-diamidino-2-phenylindole
DMEM	Dulbecco's Modified Eagle's Medium
DMSO	Dimethyl Sulphoxide
DNA	Deoxyribonucleic Acid
D-PBS	Dulbecco's Phosphate Buffered Saline
EDTA	Ethylenediaminetetracetic acid
EGF	Epithelial Growth Factor
ELISA	Enzyme Linked Immunosorbent Assay
F	Fluoride
FCS	Foetal Calf Serum
FITC	Fluorescein Isothiocyanate
FMLP	N-Formylmethionyl-leucyl-phenylalanine
FN	Fusobacterium Nucleatum
FTIR	Fourier Transform Infrared (spectroscopy)
GAPDH	Glyceraldehyde-3-Phosphate-Dehydrogenase
GM-CSF	Granulocyte Macrophage Colony-stimulating Factor
GTPase	Guanosinetriphosphatase
H ₂ O ₂	Hydrogen Peroxide
hBD-2	Human Beta Defensin 2
HCl	Hydrochloric Acid
HCS	High Content Screening
HEGF	Human Epithelial Growth Factor
HEPES	4-(2-hydroxyethyl)-1-piperazineethanesulfonic acid)
HLH	Helix-loop-helix trabscription factors
HOCl	Hydrochlorous Acid
HRP	Horseradish Peroxidase
HRP	Horseradish Peroxidase
ICC	Immunocytochemistry
IF	Immunofluorescence
IFN-γ	Interferon gamma
IgG	Immunoglobulin G
IL-1β	Interleukin-1 beta
IL6	Interleukin 6

IL8 / CXCL8	Interleukin 8
ITS-X	Insulin-Transferrin-Selenium-ethanolamine
I- κ B	Inhibitor of Nuclear Factor Kappa B
KHCO ₃	Potassium bicarbonate
LDH	Lactate Dehydrogenase
LPS	Lipopolysaccharide
MACC	Mechanically Assisted Crevice Corrosion
Mg ²⁺	Magnesium ion
MOI	Multiplication of Infection
mRNA	Messenger RNA
MTT	3-(4,5-Dimethylthiazol-2-yl)-2,5-diphenyl tetrazolium bromide
NaCl	Sodium chloride
NADH	Nicotinamide Adenine Dinucleotide - Hydrogen (reduced)
NaOH	Sodium Hydroxide
Nb	Niobium
NF κ B	Nuclear Factor Kappa B
NH ₄ Cl	Ammonium Chloride
NPs	Nanoparticles
OECs	Oral epithelial cells
opsSA	Opsonised Staphylococcus Aureus
PBS	Phosphate Buffered Saline
PCR	Polymerase Chain Reaction
PD	Probing Depth
PDL	Periodontal ligament
<i>Pg</i>	Porphyromonas gingivalis
PMNs	Polymorphonuclear neutrophils
pRb	Retinomablastoma protein
qPCR	Quantitative Real Time Polymerase Chain Reaction
RANKL	Receptor Activator of Nuclear Factor Kappa-B
RAU	Relative Absorbance Units
REDOX	Reduction-oxidation reaction
RFU	Relative Fluorescence Units
RLU	Relative Light Units
RNA	Ribonucleic Acid
RO	Reverse Osmosis
ROS	Reactive Oxygen Species
RPMI	Roswell Park Memorial Institute
RT	Reverse Transcriptase
RT	Room temperature
<i>Sa</i>	Staphylococcus aureus
SCC	Squamous Cell Carcinoma
SD	Standard Deviation
SEM	Standard Error of Mean
SFM	Serum Free Medium
SN	Supernatant
SR-XRF	Synchrotron micro-focussed X-ray Fluorescence
SSL-D	SuperSensitive® Link Detection Kit
Ta	Tantalum
TEM	Transmission Electron Microscopy
Ti	Titanium
TiO ₂	Titanium Oxide

TJA	Total Joint Arthroplasty
TLR	Toll-like Receptor
TMB	Tetramethylebenzidine
TNF α	Tumour Necrosis Factor Alpha
V	Vanadium
WBC	White Blood Cell
XANES	X-Ray Absorption Near Edge Structure
XRF	X-ray Fluorescence
YWHAZ	Tyrosine-3/tryptophan,5-monooxygenase activation protein, zeta polypeptide
Zr	Zirconium

Chapter 1

Introduction

1.1 The use of Titanium as a biomaterial

1.1.1 *Physical properties and presentation*

Titanium (Ti) is a silver coloured transition metal, with notable characteristics of having both a relatively low density (4.507 g/cm^3) (Boyer et al., 2004) and a high strength. Its atomic number is 22 and its atomic weight is 47.88 (Boyer et al., 2004). Ti exists in an elemental (unalloyed) form, structured as hexagonal close packed crystals, known as its α phase. This phase is stable up to 882.5°C whereupon it transforms into a body centred cubic structure, known as the β phase, up to its melting point at 1668°C (Ratner, 2013).

Ti and alloys of Ti are popular as biomedical materials due to their favourable physical properties, corrosion resistance, and most importantly their perceived biocompatibility. Ti in its unalloyed form is described as Commercially Pure (CP), which is presented in various “Grades” for biomedical applications, which are discriminated by their purity. For many biomedical applications improved mechanical properties than those conferred by CPTi are required. To achieve this Ti is alloyed and common alloying elements include Aluminium (Al), Vanadium (V), Niobium (Nb), Tantalum (Ta) and Zirconium (Zr). CPTi is most commonly used to manufacture dental implants, whilst Ti alloys are widely used in dental applications and for the fabrication of orthopaedic prostheses.

1.1.2 *Suitability as a biomedical alloy*

Among metals, Ti is often favoured as a biomedical material as it has both a high yield strength and possesses an elastic modulus that is closer to that of bone than alternatives (Ratner, 2013) (Table 1). Under standard testing conditions Ti exhibits high corrosion resistance and possesses suitable strength for it to be used in load bearing applications (Bertrand et al., 2010).

Material	CPTi	Ti-6Al-4V	Ti-35Nb-5Ta-7Zr	Stainless steel	Bone
Elastic Modulus (GPa)	105	110	55	205-210	10-40

Table 1.1 - Elastic moduli of selected materials (Ratner, 2013)

In the orthopaedic context, there is a long and successful history of the use of Ti (Cook et al., 1988), mainly in the form of an alloy with Al and V (Ti-6%Al-4%V, wt%) which is used in fixation screws, plates, and components of Total Joint Arthroplasties (TJA). Other Ti based materials commonly used in orthopaedic surgery include the alloy with Al and Nb, Ti6Al7Nb which is incorporated in hip replacement units. (Cadosch et al., 2009a). One of the desirable features of Ti and its alloys, is the ability to manufacture components in a variety of different ways, including casting, drawing, pressing, subtractive machining and laser sintering. This flexibility in manufacturing route is particularly useful to achieve the complex shapes and surface finishes demanded by orthopaedic and dental implantable devices (Liu et al., 2004).

Ti has been described as the most well tolerated metal by the human body (Ratner, 2013). It is widely accepted that Ti and its alloys are “relatively ‘bioinert’” (Li et al., 2010, Tschernitschek et al., 2006) and hence Ti is commonly reported as being a “biocompatible material”. The term “biocompatibility” is frequently used by both medical professionals and laypeople. It has been defined as:

“the ability of a material to perform with an appropriate host response in a specific application” (Donaruma, 1988).

Importantly this definition can be interpreted according to both the material and the context in which it is being used. Therefore, to broadly classify any material as biocompatible or not is unwise. However, in many applications, Ti has indeed been shown to induce minimal responses from the body *in vivo*.

1.1.3 *Ti surface stability conferred by a Titanium Oxide surface layer (TiO₂)*

Ti itself is a highly reactive metal, and Ti surfaces in physiological environments are covered by a thin but resilient oxide layer (TiO₂) (Kasemo, 1983). This layer forms spontaneously under atmospheric conditions (Branemark et al., 2001) and so any interactions described in a biomedical setting between Ti and tissues are actually referring to the interaction between the surface oxide layer and the tissue contents. The naturally formed surface oxide layer is typically 3-7 nm thick (Wang et al., 2016) and has been characterised as consisting mainly of rutile and anatase crystalline forms

of TiO_2 (Effah et al., 1995) (Figure 1.1). The structure of these two forms is described as Ti atoms surrounded octahedrally by six oxygen atoms (Jolivet et al., 2010).

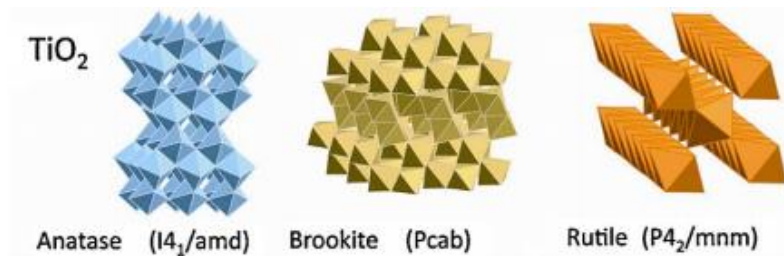


Figure 1.1 - Crystalline structures of Anatase, Brookite and Rutile (Jolivet et al., 2010).

The physio-chemical behaviour of the TiO_2 oxide layer depends on its chemical composition and thickness, which are sensitive to the manufacturing conditions and post-processing surface treatments (Li et al., 2004). Considerable research into the surface treatment of Ti materials has been undertaken, with the aim of optimising interactions between biological tissues and the material (Sul et al., 2002, Klokkevold et al., 1997, Germanier et al., 2006). It is therefore important to note that this wide range of different surface treatments for Ti based biomedical devices will inevitably result in differences in surface oxide layer formation and structure.

1.1.4 *Classification of Ti*

Ti can be classified according to different systems. The American Society for Testing and Materials (ASTM) has classified 23 Ti 'Grades' as biomedical materials (Elias, 2008). Of these, CPTi is preferred for the manufacture of dental implants, and is graded 1-4 by the ASTM. Grade 1 Ti is the purest and also has the most ductility (ability to deform under tensile stress) but has the lowest yield strength (Elias, 2008). However, this is typically of less importance in a dental rather than an orthopaedic setting. Contrastingly, Grade 4 is the least pure (containing ~1 wt% Fe), has the least ductility and highest yield strength (Table 1.2). Grades 2 and 4 are the most common grades of CPTi for dental implant manufacture. A summary of the properties of the CPTi grades and of the alloy Ti-6Al-4V (also known as ASTM grade 5) is shown in Table 1.2.

	ASTM Grade				Ti6AlV
Property	1	2	3	4	5
Yield Strength (MPa)	170	275	380	483	795
Ultimate Tensile Strength (MPa)	240	345	450	550	860
Elongation (%)	24	20	18	15	10
Elastic Modulus (GPa)	103-107	103-107	103-107	103-107	114-120

Table 1.2 - Physical properties of Ti grades. Reproduced from Elias et al., 2008

1.2 The use of Ti in dental implants

1.2.1 *History of dental implants*

Early attempts to produce a replacement for missing teeth have been identified as long ago as the end of the first or beginning of the second century AD, as reported in a Gallo-Roman necropolis in France (Crubzy et al., 1998). Cruzby reported the discovery of a wrought iron dental implant in the upper right second premolar of a male, over the age of 30. Modern implantology has been developed hugely since its infancy in the 1940s and 1950s, when a variety of implants were being placed, both to replace whole arches as well as individual teeth (Misch, 1999). Implants were being placed transosteally (through the bone) and also on top of the bone, beneath the periosteum (subperiosteally) as well as the approach which has continued to be developed into contemporary implant dentistry, within the bone (endosteally) (Caswell, 1991). At this stage of implant development, a variety of materials were being used which included cobalt-chromium-molybdenum (Goldberg and Gershkoff, 1949). Throughout the 1960s and 1970s, different designs and materials were placed, including endo-osseous “blade” designs made of surgical stainless steel (Linkow and Dorfman, 1991), and intramucosal implanted devices to aid the stability of maxillary removable dentures (Weiss and Judy, 1974). Problems with these early implant designs were unpredictability of soft tissue outcomes, leading to loss or instability of the implanted device, as well as infection (Caswell, 1991).

1.2.2 *Osseointegration*

Osseointegration is defined as

“a direct structural and functional connection between ordered, living bone and the surface of a load carrying implant” (Branemark, 1983).

Osseointegration was discovered serendipitously by Brånemark, a Swedish orthopaedic surgeon in 1952, in a study which was investigating imaging of blood flow in the tibias of rabbits. Brånemark observed that Ti chambers which had been placed within the bones of rabbits could not be removed at the end of the experiment, therefore were assumed to be integrated within the bone itself (Brånemark, 1959). The applications for orthopaedic and indeed dental implant surgery of this finding were noted by a number of groups, and research then focussed on the use of Ti as a material to produce dental implants.

Osseointegration continues to be the subject of a large amount of scientific research, and the evidence suggests that Ti has an excellent capacity to become osseointegrated (Brånemark et al., 2001, Albrektsson et al., 1994). The absence of soft tissue between an implant surface and living bone has also been used to define osseointegration (Carlsson et al., 1986); however the ability to determine the presence of soft tissue between the implant and bone is limited in a clinical setting, so the definition provided here is likely to be more clinically useful. Histological examination of implanted devices is not possible without removing the device, so determination of osseointegration *in vivo* is performed by clinical and radiographic examinations alone.

Osseointegration occurs via a series of complex events following implant insertion into a prepared bone site:

- Proteins and biomolecules will adsorb to the implant surface from the blood (Junker et al., 2009);
- An inflammatory process occurs, after which the peri-implant blood clot begins to be replaced by fibrin, which allows anchorage of bone forming cells to the implant surface (Junker et al., 2009);
- This weak initial bony attachment is strengthened and remodelled over time by osteogenic cells, to form an organised bone structure (Junker et al., 2009).

Early animal studies demonstrated the potential of Ti as a material with the ability to osseointegrate (Carlsson et al., 1986), a process shown to rely on a number of factors such as stability, sterility and surface finish of Ti implanted devices (Albrektsson et al., 1994). Implants which failed to osseointegrate have been shown to lack a consistent

surface, including variability in the surface oxide layer (Arys et al., 1998). A drive to enhance and speed up osseointegration has contributed to the development of modern implant systems.

1.2.3 The development of modern “root form” Ti implants

A series of *in vivo* studies following Brånemark’s initial discovery of the osseointegration potential of Ti (Weiss and Rostoker, 1981), led to the development of root form Ti implant geometries. Adell et al., trialled Ti implants in humans over 15 years (Adell et al., 1981), with over 2700 fixtures being placed in 410 jaws of 310 edentulous patients. Within this study, 81 % of maxillary fixtures and 91 % of mandibular fixtures were described as being stable during the follow-up period (Adell et al., 1981), therefore osseointegrated Ti root form dental implants were established as a viable treatment option for restoration of edentulous areas.

In contemporary dentistry, CPTi is most often used for the manufacture of dental implants which are osseointegrated (Albrektsson et al., 1994) and support supragingival restorations. Implant retained restorations can be in the form of removable or fixed prostheses. Figure 1.2 shows a diagrammatic representation of a modern root form dental implant retained single unit restoration.

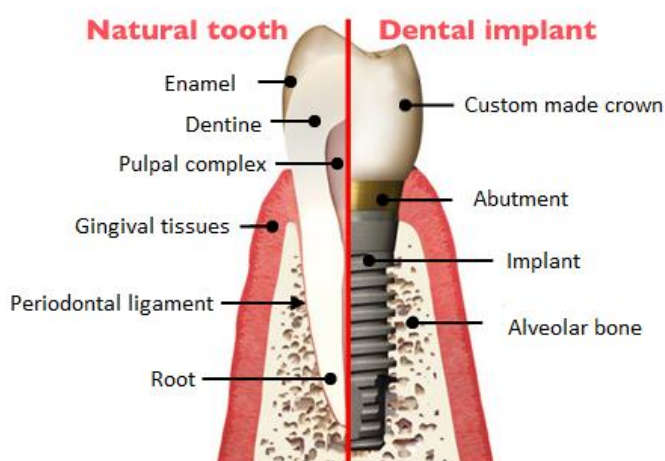


Figure 1.2 – Illustration highlighting the anatomical differences between a natural tooth and a single unit root form implant supported restoration. Diagram from abostonsmile.com (2012).

The move towards the root form design shown in Figure 1.2 was driven by the need to:

- Shorten the osseointegration time (Esposito et al., 2013);
- Optimise the bone and soft tissue contour surrounding an implant to enhance function and aesthetics;
- Aid oral hygiene maintenance and therefore soft tissue health;
- Optimise the long term retention of implants.

Ti root form implants were established as a robust treatment option in the 1980s. However, many more variables exist with regard to the design, placement and restoration of these implants, so a large body of research has taken place in order to continually optimise various aspects of the implant restoration processes.

Size and number of implants

The size and number of implants required to adequately restore an edentulous area is still unclear, and clinicians tend to select configurations, sizes and locations based on traditional prosthodontic practice and their own clinical experience and judgement (Lindhe et al., 2008). The size of a “standard” implant is approximately 4-5 mm in diameter, and is used for anterior or premolar tooth replacement, while a wider >5 mm diameter implant may be used for molar tooth replacement. The size of the implant is often key to the aesthetic success, as a wide crown narrowing down to a small diameter implant may appear aesthetically unacceptable (Lazzara, 1993) and impede adequate plaque removal. However, the available bone in both quantity and quality in all dimensions may limit implant diameter selection. The amount of bone present can be examined radiographically using plain film radiography, through Cone Beam Computerised Tomography (CBCT) scans, and clinically using palpation and bone mapping. The length of an implant is also a feature that must be determined by the clinician, as bone should cover the entire threaded section of the implant, and a longer implant will have a higher surface area available for osseointegration (Olate et al., 2010). Implants should be placed so the transition from the intraoral restoration to the implant itself is at a biologically and aesthetically acceptable level when compared with any surrounding natural teeth, to avoid an artificial aesthetic result. If insufficient bone is present in either a horizontal (buccal-palatal) or vertical dimension, there are a number of surgical options to increase the potential implant bearing bone volume:

- Bone augmentation using either autogenous bone in either a block or chips harvested from a distant site, or the use of bone substitutes (such as BioOss®, a granular bovine origin bone substitute). These techniques can be used alongside surgery such as sinus lift procedures to further enhance the available space for implant placement (Balaji, 2013).
- Procedures such as distraction osteogenesis, where force is applied across an ossifying interface to accelerate the formation of new bone in the site to be restored (Vega and Bilbao, 2010).

Soft tissue quantity and quality

Treatment planning when restoring a patient's dentition using dental implants can be complex, as many factors need to be taken into account other than the quantity and quality of bone available for implant placement. Soft tissue profiles surrounding implants will affect not only the aesthetics of a restored dental implant, but also the ease of oral hygiene maintenance, as interference from overhanging restoration margins will impede patient plaque control. Poor oral hygiene surrounding a dental implant is a key risk factor in reducing the long term prognosis of the implant and is discussed in Section 1.3.3 (Jepsen et al., 2015, Renvert et al., 2014). The quantity and quality of both keratinised and non-keratinised soft tissues in an edentulous area should be clinically examined and taken into account during the treatment planning process in order to maximise aesthetic and functional outcomes.

Surface finish of implants

Over 1300 different implant systems exist with a variety of shapes, dimensions, surface materials, thread design, surface topography and surface modification (Junker et al., 2009). The surface finish, coating and topography of dental implants has been shown to affect osseointegration and the eventual "success" of the restoration (Dohan Ehrenfest et al., 2010). A positive correlation exists between surface roughness and osseointegration (Shalabi et al., 2006) when comparing etched surfaces to polished Ti implants. Furthermore, surface wettability and hydrophilicity has been shown to promote osseointegration (An et al., 2012). Many contemporary implant manufacturers treat the surfaces of implants with different bioactive molecules or

bone morphogenetic proteins (Avila et al., 2009) with the aim of increasing the likelihood and speed of osseointegration.

1.2.4 *“Success, survival and failure” criteria for dental implants*

Dental implants are a popular, successful and largely predictable way of restoring spaces (Klokkevold and Newman, 2000) where teeth have been lost or are congenitally absent. According to the American Academy of Implant Dentistry, three million Americans have dental implants and that number is increasing every year. “Success” rates are difficult to ascertain, as statistics can be used to “prove” a number of frequently opposing views. Moreover, much of the published literature focuses on small cohorts or describes systems and approaches that may be outdated.

Implant “success” and “survival” are now more frequently used terms to describe implant outcomes (Misch et al., 2008), and were outlined in 2008 at the Pisa Consensus Conference of the International Congress of Oral Implantologists:

Implant quality scale group	Clinical conditions
Success (optimum health):	No pain or tenderness upon function, no mobility, <2 mm radiographic bone loss from initial surgery, no exudate history.
Satisfactory survival:	No pain on function, no mobility, 2-4 mm radiographic bone loss, no exudates history.
Compromised survival:	May have pain on function, no mobility, radiographic bone loss >4 mm (less than half the length of implant body), probing depth >7 mm, may have exudates history
Failure (clinical or absolute):	Any of the following: pain on function, mobility, radiographic bone loss > half length of the implant body, uncontrolled exudate, loss of implant.

Table 1.3 – Implant success scale recreated from Misch et al., 2008.

Therefore, to define “failure” as simply the loss of an implant is no longer acceptable, as a successful implant by this measure could have a variety of problems which indicate it is failing, such as bone loss, suppuration and mobility, but if it has not been lost completely then it would have been classed as “survival”. For example Roos-Jansaker et al., demonstrated in a longitudinal observational study of 218 patients (999 implants) over 9-14 years that implant based survival (defined as implant retention only) rates were 95.6 %, however analysis of the same data demonstrated a success

rate of 88.5 % (Roos-Jansaker et al., 2006). It is also important to recognise that many implants are not examined radiographically on a regular basis with X-rays frequently taken only if there is a suspicion of a clinical problem. Therefore, many implants which are still symptom free may exhibit bone loss which is otherwise undetected. Another important factor when interpreting implant success rates is that many practitioners would classify an implant as being “successful” after initial osseointegration has taken place, and will not consider problems occurring later in the life of the restoration as a “failure”. There is an important biological distinction to be made between immediate failure (within 6 months) and failure after osseointegration has occurred. The former reflects failed osseointegration and the latter has a distinctly altered pathogenic process, referred to as “peri-implantitis”.

1.3 Peri-implant disease

1.3.1 *Definitions of peri-implant diseases*

The presence of peri-implant inflammation potentially causing bone loss is a known complication of dental implant rehabilitation (Lindhe and Meyle, 2008). Inflammatory conditions involving the peri-implant tissues (referred to collectively as peri-implant diseases) can be categorised as:

- Peri-implant mucositis (reversible inflammation localised to the soft tissues)
- Peri-implantitis (a more advanced lesion where supporting bone is lost), defined as $\geq 1\text{mm}$ bone loss after the first year of installation together with bleeding and/or suppuration (Sanz et al., 2012).

1.3.2 *Prevalence of peri-implant diseases*

A recent systematic review and meta-analysis of 9 studies (from 504 screened studies), based upon 6283 implants in 1497 patients, with a mean follow up of 5-13 years demonstrated a prevalence of peri-implant mucositis of 64% and peri-implantitis of almost 20% (Atieh et al., 2013). In this study, the patient was used as the basis of the analysis, i.e. how many patients with implants had peri-implantitis present in their

mouths, where peri-implantitis was defined as a Probing Depth (PD) ≥ 5 mm and bone loss of ≥ 2 mm.

Mucositis is characterised by bleeding on probing and a clinical appearance of reddened, inflamed gingivae adjacent to an implant supported prosthesis in the absence of suppuration. Radiographic examination reveals no associated bone loss. Peri-implant mucositis is reversible, and can be treated successfully with non-surgical debridement and oral hygiene improvement (Renvert et al., 2008). Bone loss associated with peri-implantitis usually presents in a circumferential pattern and is diagnosed by radiographic or surgical examination, and cannot be reversed by simple mechanical debridement (Renvert et al., 2008).

Many similarities have been drawn between peri-implantitis and periodontitis (defined as a chronic inflammatory disease that affects the supporting tissues of the dentition (Aisenberg, 1952)). Both are chronic inflammatory diseases caused by an aberrant host response to a bacterial challenge. Soft tissue explants from sites exhibiting peri-implantitis show an inflammatory infiltrate rich in innate immune cells and B cells and plasma cells (Berglundh et al., 2004), and are very similar to lesions found in periodontal disease (Esposito et al., 1997). However, peri-implant lesions do not respond predictably to non-surgical or surgical therapies, and it is claimed that the progression of peri-implantitis is similar to the progression of bone loss seen in furcation lesions with limited access to maintain oral hygiene (Renvert et al., 2014).

As both periodontal disease and peri-implantitis appear to have similar aetiologies and clinical presentation, it is often assumed that patients who are more at risk from periodontal disease will be more at risk from peri-implantitis (Heitz-Mayfield and Lang, 2010). Genetic factors, tobacco use, poor oral hygiene, poorly controlled glycaemia and various other co-morbidities have been shown to be significant risk factors for periodontal disease (Heitz-Mayfield, 2005), and are therefore thought to also pose similar risks for development of peri-implantitis.

1.3.3 *The pathogenesis of peri-implant disease*

Peri-implant diseases are inflammatory diseases which involve a number of complex interactions. The current understanding is that there is not one discrete causative

agent, but a pathogenic challenge from polymicrobial agents coupled with an abnormal host response produces the inflammation and tissue destruction seen in peri-implantitis (Renvert et al., 2014). The key risk factors for peri-implant disease are common with those for periodontitis:

- Poor oral hygiene, leading to an increased bacterial load adhered to the implant surface;
- A history of periodontal disease;
- Poorly controlled diabetes mellitus;
- Smoking or other tobacco use (Heitz-Mayfield and Lang, 2010).

Whenever a new surface is introduced to the oral environment, an opportunity for colonisation with a microbial biofilm is presented (Nociti et al., 2001). An implant surface is no exception, and these surfaces will become rapidly colonised by bacteria (Lindhe et al., 2008). The composition of this biofilm and the host response are considered to determine the probability of a peri-implant lesion developing, although current understanding is that further modifying factors may play a role in disease progression (Levin, 2013).

1.3.4 *The role of, and composition of microflora in the peri-implant milieu*

To date, the majority of research in the field of peri-implantitis has focused on the bacterial challenge and the host's response to the biofilm, as the likely causative agents of peri-implant disease. Implant surfaces are colonised by bacteria and at 28 days post-placement, a complex biofilm has been shown to form on Ti implants in the oral environment (Lindhe et al., 2008). Peri-implant soft tissues take several weeks to fully mature, and so the early biofilm will be initially in contact with immature epithelial tissue. Biofilms are complex ecosystems containing bacteria in an extracellular matrix, which can be highly resistant to antimicrobial agents (Donlan, 2002). The bacterial biofilm is in direct contact with the host tissues, and will illicit an immune response. The likely microbial succession on the surface of a dental implant (Lindhe et al., 2008) is illustrated in Table 1.4 and is organised into coloured complexes according to Socransky's classification (Socransky et al., 1998).

Early colonisers			Late colonisers	
<i>Actinomyces</i> :	Green complex	Yellow / Purple complex	Orange complex	Red complex
<i>A. genenscrae</i> <i>A. israelii</i> <i>A. naeslundii</i>	<i>A. actinomycetemcomitans</i> <i>C. gingivalis</i> <i>C. ochracea</i> <i>C. sputigena</i> <i>E. corrodens</i>	<i>S. gordonii</i> <i>S. intermedius</i> <i>S. mitis</i> <i>S. oralis</i> <i>S. sanguinis</i> <i>A. odontolyticus</i> <i>V. parvula</i>	<i>C. gracillis</i> <i>C. rectus</i> <i>C. showae</i> <i>E. nodatum</i> <i>F. nucleatum **</i> <i>F. periodonticum</i> <i>P. micros</i> <i>P. intermedia</i>	<i>T. forsythia</i> <i>P. gingivalis **</i> <i>T. denticola</i>

Table 1.4 – Bacterial colonisation of implant surfaces separated into Socransky's groupings. Starred bacterial species were selected as stimuli for oral epithelial cell responses in this thesis (Socransky et al., 1998).

Where disease is present and implants are failing, the composition of the microflora within the implant surface biofilm changes from that in health (Mombelli and Décaillet, 2011). In (clinically) healthy implants, the biofilm consists of almost exclusively aerobic cocci and non-motile rods. In failing implants, a much larger proportion of motile rods, spirochaetes and fusiform bacteria are present (Lindhe et al., 2008), indicating that these types of anaerobic bacteria are potentially associated with peri-implant disease. However, it is also possible that these bacteria are simply more able to colonise an area that is chronically inflamed which will have an altered pH, available nutrient profile (including iron from haemoglobin) and altered biofilm composition to a healthy site.

A recent study demonstrated that periodontally significant bacteria such as *Treponema*, *Prevotella*, *Campylobacter* and *Eubacteria* are the dominant species in the peri-implantitis biofilm. In addition the levels of *Treponema*, *Campylobacter* and *Eubacterium* were significantly higher in both peri-implant health and disease than in periodontitis (Kumar et al., 2012). Generally, peri-implant samples were also found to contain a higher proportion of Gram-negative bacteria than sub-gingival samples in periodontitis patients (Kumar et al., 2012). These findings suggest that Gram-negative bacteria probably play an important role in peri-implant disease pathogenesis, but whether they colonise following the development of inflammation, or drive the initial inflammatory response remains to be determined.

Peri-implant biofilms have been and continue to be the subject of extensive research. While it is highly probable that there is no clear causative organism for peri-implantitis, it is likely that:

- Implant surfaces are covered in an acquired pellicle of proteins, peptides and other proteins very similar to those found on natural teeth in the oral cavity;
- This creates an environment suited to colonisation by various bacterial species, and biofilm formation;
- As a biofilm matures it becomes more complex with a predominance of Gram-negative anaerobic motile bacteria;
- The peri-implant *milieu* surrounding implants in partially dentate patients with periodontitis contains more periodontal pathogens than those in patients who are either edentulous or do not have periodontitis (Lindhe et al., 2008). This appears to increase the long term risk of peri-implantitis, therefore indicating that known periodontal pathogens may also play a role in peri-implantitis;
- The introduction of species such as *P. gingivalis* in animal models (such as dogs) has been shown to initiate and progress ligature associated lesions (Nociti et al., 2001), implying certain periodontal pathogens may be of particular importance in the initiation of or progression of peri-implant disease.

1.3.5 *The role of host responses in the progression of peri-implant disease*

It is interesting to note that in large studies of implant failure, peri-implantitis appears to cluster in certain patients. The aforementioned study by Roos-Jansaker et al., (Roos-Jansaker et al., 2006) found that implant loss appeared to cluster in a few patients (a group of 22 out of a total of 218 patients lost 46 implants; of these, 8 patients lost more than one fixture), indicating a strong association between implant complications and patient phenotype. Current thoughts on the progression of peri-implant mucositis to peri-implant disease is that the process is similar to the progression of gingivitis to periodontitis in susceptible patients (Heitz-Mayfield and Lang, 2010). The disease process is initiated by key bacteria present within the biofilm which cause a complex host immune inflammatory response. A key cell is the neutrophil which has been shown to be hyperactive and hyper-reactive in periodontally susceptible patients, and

as a result neutrophils are implicated in the tissue damage characteristic of the disease process (Ling et al., 2015, Matthews et al., 2007).

Polymorphonuclear leukocytes (PMNLs)

The host response to a bacterial challenge in the context of periodontal disease has been the subject of a large body of research (Chapple, 2006, Wright et al., 2008, Matthews et al., 2007). PMNLs are known to form a key role in the host response to bacterial pathogens. The crevicular epithelium is intimately related to the plaque biofilm and key periodontal pathogens have been shown to elicit a pro-inflammatory response via activation of NFκB (Milward et al., 2007). This inflammatory response induces a wide range of pro-inflammatory sequelae including (PMNL) neutrophil recruitment.

Neutrophils are the first line of defence in immune cell recruitment. They are numerous in the circulating blood, and are produced in the bone marrow of a healthy adult at the rate of approximately 10^{11} cells per day (Mollinedo et al., 1999). Neutrophils are recruited to the site of bacterial challenge in response to the release of cytokines from the host tissues (Baggiolini et al., 1989, Mollinedo et al., 1999), where their function is to phagocytose and kill invading organisms. During maturation, neutrophils develop granules that enable microbial killing by the cell to take place by one or more of three killing mechanisms: phagocytosis, degranulation and NETosis (cellular killing via release of decondensed chromatin and granular contents (Remijnen et al., 2011)).

One of the mechanisms by which neutrophils can kill bacteria is by releasing Reactive Oxygen Species (ROS). However, these species not only kill bacteria, but if released in excess are also capable of causing host tissue damage. Patients with periodontal disease have been shown to exhibit a hyperactive and hyper-reactive phenotype (Matthews et al., 2007). In such situations the susceptible patient shows a disproportionate response to bacterial challenge which contributes to the tissue damage observed in periodontal lesions (Matthews et al., 2007). In health, a fine balance exists between ROS production from neutrophils and local levels of antioxidants which are able to modulate ROS activity. However, if excess ROS are

produced and /or local antioxidant defences are compromised this can result in local tissue damage characteristic of the periodontal lesion (Chapple, 2006, Dias et al., 2013). The mechanisms by which ROS can cause tissue damage are:

- Oxidation of low molecular weight molecules, proteins and lipids
- DNA strand breaks and base hydroxylation (Matthews et al., 2007).

It is highly likely therefore that the nature of the host responses taking place within the tissues in response to a pathogenic challenge will impact upon the amount and type of tissue damage which occurs during any inflammatory disease process, including peri-implant diseases.

1.3.6 *Treatment of peri-implant diseases*

Peri-implantitis can lead to pain, loss of function, infection and implant loss. These have a negative impact on the patient in both physical and psychological terms, and also financial implications for both the patient and the health service provider. Due to the increased life expectancy of the population and the increasing number of implants being placed it is reasonable to assume that the incidence of this condition will increase further over time (Levin, 2013).

A wide range of treatment modalities have been proposed to manage peri-implantitis (Lindhe and Meyle, 2008) including debridement, the use of local or systemic antimicrobials, photodynamic therapy, and surgical interventions including surgical debridement, implantoplasty, regenerative material placement or implant removal. However, there is a lack of consensus on a “gold standard treatment” (Levin, 2013). This was confirmed by a recent review which concluded there is no reliable evidence supporting a single effective intervention in the treatment of peri-implantitis (Bidra, 2012). However, it is agreed that the prevention of peri-implantitis by maintaining optimal oral hygiene is an essential aspect of good patient care (Jepsen et al., 2015).

1.4 Stability of Ti surfaces *in vivo*

1.4.1 Corrosion of Ti

Ti is frequently described as an “inert” biomaterial that is resistant to corrosion in a physiological setting. As previously discussed, all favourable biological interactions with Ti implant surfaces are mediated by a surface oxide layer of a few nanometres thickness. Any disruption of the TiO₂ surface leads to rapid re-passivation due to an immediate reaction between the exposed ‘bare’ metal and oxygen in the environment. However a number of scenarios where sustained disruption of the surface oxide layer can occur *in vivo* are now recognised, and consequently the extent to which metals really are inert in a biomedical setting is now being more carefully considered (Cadosch et al., 2009a).

Theories of Ti release into tissues

Clinical evidence demonstrating the deterioration of metal implant surfaces *in vivo* has been widely reported and it is accepted that released metal ions, wear and/or corrosion products may have biological consequences (Addison et al., 2012, Cadosch et al., 2009a, Olmedo et al., 2008, Olmedo et al., 2012, Thomas et al., 2004). Metal release from bearing surfaces of articulating orthopaedic devices is ubiquitous with their design and is principally due to tribological and tribocorrosion mechanisms (Cadosch et al., 2009a). In contrast, metal release from ‘passive surfaces’ that are not subjected to obvious wear has been more difficult to explain, but key mechanisms that may be operative include:

- Mechanically assisted crevice corrosion;
- Physiochemical corrosion;
- Cellular-gated corrosion (biocorrosion) mechanisms (Cadosch et al., 2009a).

Although Ti has superior corrosion resistance when compared with other metals (Ratner, 2013), it has been shown that Ti will corrode in certain physiological environments, and is capable of producing a variety of potentially bioactive corrosion products (Cadosch et al., 2009a, Addison et al., 2012, Olmedo et al., 2008, Jonas et al., 2001, Torgersen et al., 1995). *In vitro* experiments have shown that although in many simulated physiological conditions Ti has high corrosion resistance (Kedici et al., 1998),

factors such as pH, inorganic ions such as Fluoride (F^-) (Stajer et al., 2008, Schiff et al., 2002, Nakagawa et al., 1999) and relevant biomolecules such as lipopolysaccharide (Yu et al., 2015a) may reduce this resistance leading to significantly enhanced metal release. These modifying factors are of particular interest in the field of dental implants, as the oral environment into which abutments or threaded sections of Ti implants are exposed varies widely in pH, and for example, F^- is a ubiquitous additive in oral hygiene products. The oral pH varies as a result of dietary intake, saliva buffering capacity, oral hygiene practices and is also strongly influenced by certain medical conditions, for example gastric oesophageal reflux disorder (Filipi et al., 2011, Piangprach et al., 2009). Many oral pathogens are also known to be acidogenic and are found in dental implant biofilms.

Recently it has been shown that the inflammatory biomolecule H_2O_2 , and albumin, the most common protein in tissue fluid, act synergistically to significantly increase metal ion release from Ti6Al4V alloys when tested in physiological saline (Yu et al., 2015b). These findings would not have been predicted by standard *in vitro* tests performed with either species as a stimulus alone. The findings highlight our lack of understanding of how the contents of biological environments can influence the stability of metal surface oxide layers *in vivo*. Such findings may help explain why Ti levels detected in peri-implant tissues and fluids associated with inflammation are elevated (Olmedo et al., 2012).

Biocorrosion

Biocorrosion is corrosion which occurs as a consequence of, or is enhanced by, the presence of prokaryotic or eukaryotic cells. From a structural perspective, the loss of material is minimal, and therefore is unlikely to produce any functional change in the implanted device. However, generation of potentially bioactive particles and their subsequent release into tissues surrounding an implanted device may stimulate biological responses which may influence peri-implant tissue outcomes. It is now accepted that corrosion of metallic materials implanted *in vivo* is inevitable and leads to the production of insoluble and soluble corrosion products which have been associated with inflammation, and in the case of certain orthopaedic implants, device failure (Cadosch et al., 2009a). It has also been suggested that certain cell types such as

osteoclasts and innate immune cells are able to corrode metal surfaces such as stainless steel (Cadosch et al., 2009b, Cadosch et al., 2009a). Whilst the exact mechanisms involved in such corrosive processes have not yet been characterised, it is highly likely from the current body of evidence that there is an interaction between bacterial or host cells and the implanted metal surfaces.

1.4.2 *Evidence of metal release in the absence of wear*

Whilst physical wear processes such as those observed between two bearing surfaces of artificial joints can potentially generate large amounts of wear debris, there is a growing body of evidence to support the hypothesis that potentially bioactive debris is generated even in the absence of obvious tribology (Sections 1.4.1 and 1.4.2).

Evidence of corrosion *in vivo* of cemented Ti femoral stems has been established, showing clear corrosion visible on non-articulated areas following implant retrieval. The corrosion has been attributed to mechanically assisted crevice corrosion (MACC) processes that lead to sustained disruption of passive oxide surfaces (Thomas et al., 2004). Ti species have been identified in tissue samples adjacent to failing Bone Anchored Hearing aids (BAHs), which, like dental implants, are transmucosal CPTi implanted devices which have no articulating parts. Corrosion products have been identified at up to 800 µm from the implant site, and include both metallic and oxide based species, including both rutile and anatase (Addison et al., 2012). It was hypothesised that these Ti species within the tissues had formed from MACC (between the abutment and osseointegrated fixture) and through cellular gated corrosion mechanisms. Figures 1.3-1.5 show unpublished images generated using synchrotron X-ray Fluorescence mapping (method detailed in Section 4.6.1) of peri-implant epithelium, showing the presence of Ti in surrounding tissues. These images were taken of tissue adjacent to failing BAHs which are percutaneous, non-articulated devices, fabricated from Grade 4 CPTi.

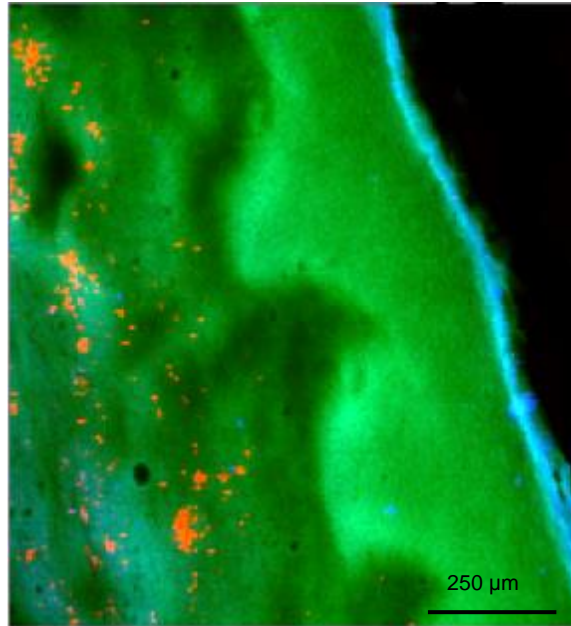


Figure 1.3 - X-ray fluorescence map of peri-implant epithelium showing significant accumulation of Ti (red) in the peri-implant soft tissues. Measurements taken of a 5 μm thickness tissue section, using a 5 μm focussed X-ray beam footprint at 5.7 KeV at I-18 beamline, Diamond Light Source, UK. Three colour elemental image – (Green = Phosphorous, Blue = Potassium, Red = Titanium).

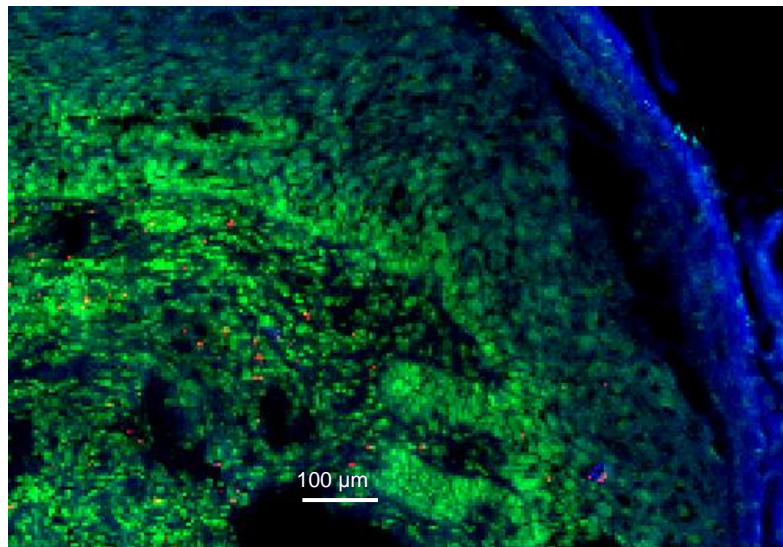


Figure 1.4 - High resolution, X-ray fluorescence map of peri-implant epithelium showing significant accumulation of Ti in the both epithelial and connective tissue layers. Measurements taken on a 5 μm thickness tissue Section mounted on Si_3N_4 , using a 600 nm focussed X-ray beam footprint at 5.7 KeV at beamline, ID-21, ESRF, Grenoble, France. Three colour elemental image – (Green = Phosphorous, Blue = Potassium, Red = Titanium).

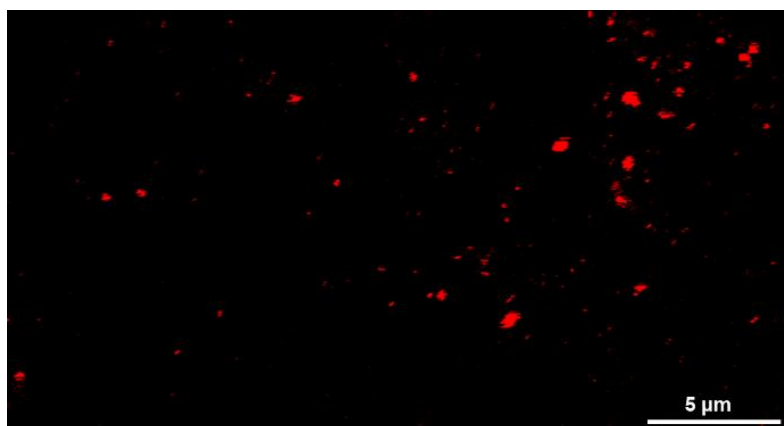


Figure 1.5 - Nano-focussed Ti (red) X-ray fluorescence map of peri-implant epithelium –focused region taken from Figure 1.4. Measurements taken on a 5 μm thickness tissue Section mounted on Si_3N_4 , using a 50 nm focussed X-ray beam with a 17.5 KeV pink beam, using beamline ID-16-B, ESRF, Grenoble, France. Demonstrates a disperse distribution of Ti particles (red) ranging in size from 1-2 μm down to single pixel (50 nm) scale.

Figures 1.3-1.5 show the presence of a variety of sizes of Ti particles within epithelium, or in sub-epithelial tissues adjacent to an implanted device. The presence of Ti distant to the surface and speciation (not metallic) suggests that these species are generated by means other than mechanical wear.

1.4.3 *The potential biological consequences of free Ti in tissues*

Ti ions and particles have been reported to be pro-inflammatory, increasing the production of cytokines such as IL8, (Haleem-Smith et al., 2012, Wilson et al., 2000) from mesenchymal and epithelial cells, and Tumour Necrosis Factor alpha ($\text{TNF}\alpha$) and Receptor Activator of Nuclear Factor Kappa-B ligand (RANKL) in fibroblasts (Irshad et al., 2013, Qian et al., 2013). Particles in the ultrafine size bracket (<100 nm in diameter) have shown stronger pro-inflammatory effects at an equal mass dose to fine TiO_2 particle sizes (Singh et al., 2007). TiO_2 has also been shown to induce apoptosis in bronchial epithelial cells (Park et al., 2008). Therefore, it is widely reported in the literature that while Ti in bulk has many favourable properties with regard to biocompatibility, Ti species when in contact with the tissues in an ionic or particulate form can be highly bioactive.

Ti Species	Cell type	Author, year
Anatase, rutile	HaCaT (human immortalised keratinocyte)	Jin et al., 2011
Mixture of anatase and rutile	H1299 (Human non-small lung cancer cells)	Lee et al., 2009
Anatase/rutile	Rat lung tissue	Silva et al., 2013
Ultrafine anatase/rutile and fine anatase	A549 (human lung epithelial cells)	Singh et al., 2007
Anatase and rutile	Human monoblastoid cell line	Vamanu et al., 2008
Anatase and rutile	Human lymphocytes	Tavares et al., 2014
Pure Ti	Human osteoblasts	Choi et al., 2005
Anatase	BEAS-2B (human bronchial epithelial cell line)	Gurr et al., 2005
Rutile	Human fibroblasts	Irshad et al., 2013
TiO ₂ (unspecified)	BEAS-2B	Park et al., 2008
Ti	Human fibroblasts	Qian et al., 2013
Anatase	HaCaT cells	Tucci et al., 2013
Anatase	A549	Srivastava et al., 2013
Anatase	Human dermal fibroblasts	Prasad et al., 2013
Anatase	HEK-293 (human embryonic kidney cell line)	Meena et al., 2012
Anatase	HeLa (human cervical adenocarcinoma cells)	Ramkumar et al., 2012
Anatase/rutile	Human foetal lung fibroblasts	Zhang et al., 2011
TiO ₂ (unspecified)	HUVEC (human umbilical vein endothelial cells)	Montiel-Dávalos et al.
Rutile/anatase	CaCo-2 (human epithelial colorectal adenocarcinoma cells)	Gerloff et al., 2012
Anatase	HepG2 (human hepatocellular liver carcinoma cell line)	Shukla et al., 2013
Anatase/rutile	Primary human foreskin keratinocytes	Simon et al., 2011
Anatase	A431 (human epidermal cell line)	Shukla et al., 2011
Anatase	NCTC2544 (human keratinocyte cell line)	Kocbeck et al., 2010
Rutile	<i>In vivo</i> rat pulmonary tissues	Warheit et al., 1997

Table 1.5 - Documented reported toxicological effects of Ti particles on different cell types, including the Ti species identified, the cell type and the author / date.

To date, very little research has been carried out into the effects of Ti species on oral epithelium. Due to the reported bioactive potential of Ti species over a range of cell types it is proposed that Ti released by dental implants may have deleterious effects on cells, which are in intimate contact or are adjacent to the device. Any interactions

between Ti species and host epithelial cells may be a potential modifying factor in a soft tissue reaction to a prosthesis.

1.5 The role of epithelium in implant soft tissue outcomes

The function of oral epithelial cells and tissue has long been established as a protective one, whereby surface cells are shed, eliminating adherent bacteria, and form a constantly renewed tissue of cells adhered tightly together (Squier and Kremer, 2001a). However, far from being a simple physical barrier tissue, the oral epithelium has a more complex role in protecting the body from invasion by pathogens than was originally described. It is now established that stimulation of the oral epithelium by (periodontal) pathogens leads to specific transcriptional events aimed at mounting a pro-inflammatory protective response (Milward et al., 2007).

1.5.1 The *structure of the peri-implant tissues*

While the clinical and histopathological features of periodontitis and peri-implantitis have many similarities, there are also important structural differences between the periodontal and peri-implant tissues (Figure 1.6).

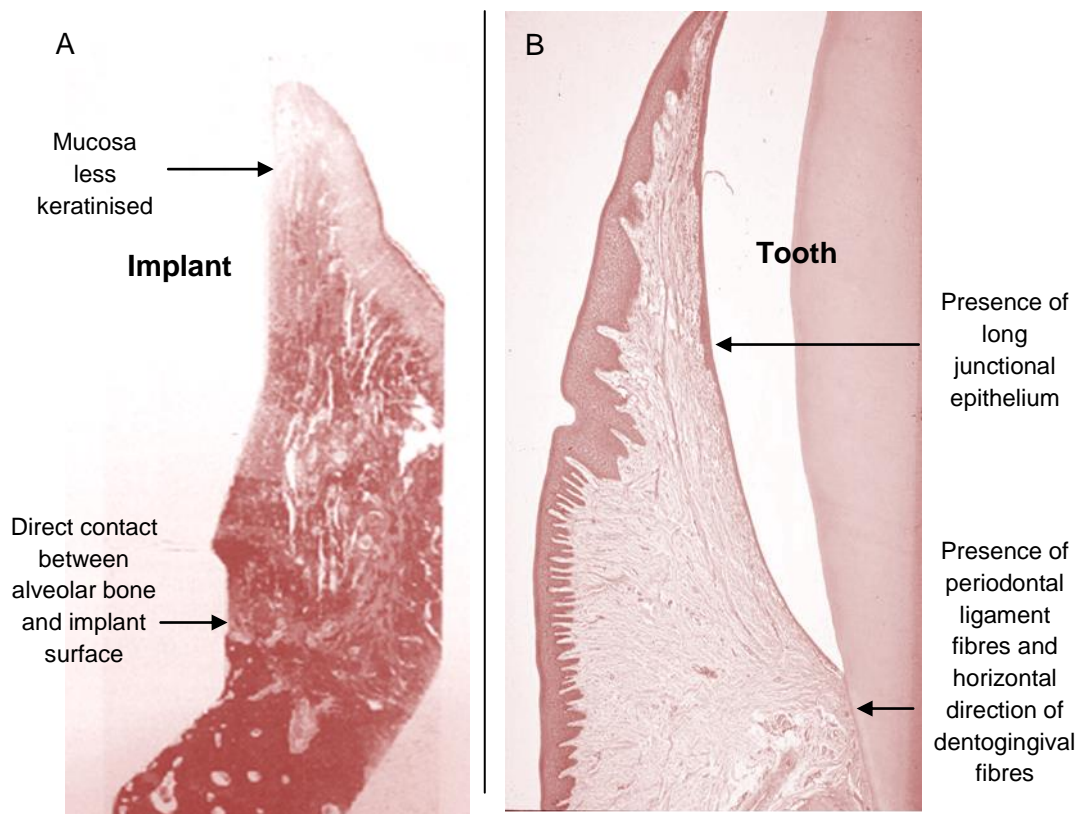


Figure 1.6 – Comparison of peri-implant tissues (A) with periodontal tissues (B). (A) adapted from Lindhe et al., 2008 and (B) courtesy of Professor ILC Chapple.

As shown in Figure 1.6, important differences between the periodontal and peri-implant tissues exist. Peri-implant tissues (compared with periodontal tissues) are:

- Less keratinised
- Have attachment fibres which run parallel to the implant surface as opposed to investing into the cementum of a tooth (dentogingival fibres)
- Less vascularised
- Apically to have connective tissue cells in contact with an implant – in the periodontal situation the tissue in contact with a tooth is epithelial (Lindhe et al., 2008)
- No periodontal ligament containing undifferentiated mesenchymal stem cells.

Despite these differences, the overwhelming similarity of peri-implant and periodontal tissues means the disease process within these structures are often expected to be similar. Therefore, the role of epithelial cells in periodontitis has potentially important ramifications for their role in peri-implant disease initiation and progression.

1.5.2 *The structure and function of the oral epithelial tissues*

Oral epithelial cells are defined as those cells found in oral tissues, which cover surfaces and form linings. Epithelium can be stratified or non-stratified, keratinised or non-keratinised. Epithelial cells join tightly together to form epithelia through a variety of mechanisms, including tight junctions, desmosomes, adherens and gap junctions. The oral epithelium is a stratified squamous epithelium which maintains its integrity by a continuous renewal process, where cells are produced in the deepest layer by mitosis, and undergo differentiation as they migrate passively towards the epithelial surface (Nanci and Ten Cate, 2008). The specific structure and function of the mucosa varies in accordance to its location within the oral cavity.

The gingival epithelium can be divided into the oral epithelium, the sulcular epithelium, and the junctional epithelium (Figure 1.7).

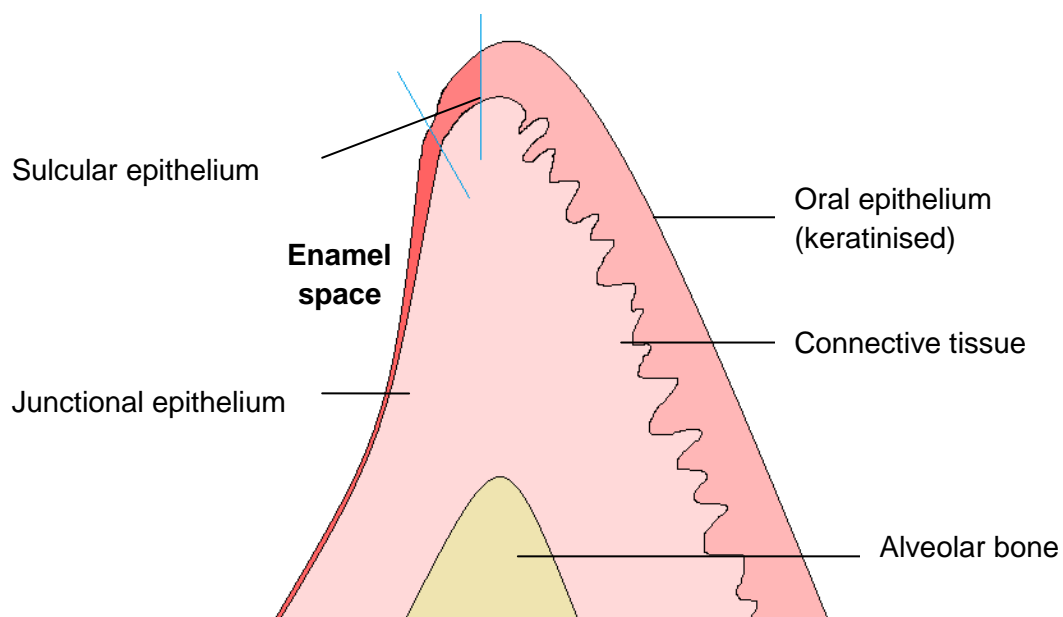


Figure 1.7 - Diagram (bucco-lingual Section) through the periodontal tissues.

These epithelia together form the dentogingival junction. In the absence of inflammation (via periodontal disease or trauma) the junctional epithelium forms a tight junction with fibres of the periodontal ligament that insert into the cementum of the tooth (Nanci and Ten Cate, 2008). It is important to appreciate the wide variety of

bacteria and bacterial products that will colonise the tooth surface, meaning the protective role of the junctional epithelium is essential in maintaining periodontal health. In the presence of inflammation however, the junctional epithelium migrates apically (Bosshardt and Lang, 2005). During this process, a periodontal pocket is formed, and the resulting pocket lining epithelium differs in structure and function to the junctional epithelium. Pocket lining epithelium is a barrier epithelium with Rete ridges as opposed to a semi-permeable membrane. A summary of the different features of the cell layers of non-keratinised epithelium is shown in Table 1.6. In humans, the outer surface of the gingival epithelium is usually para-keratinised, while the inner (crevicular) surface is non-keratinised.

Cell layer	Features
Basal	Cuboidal or columnar cells; site of most cell divisions
Prickle / spinosum	Larger ovoid cells; filaments become more numerous
Intermediate	Slightly flattened cells containing many filaments
Superficial	Slightly flattened cells; fewer organelles present but nuclei persist

Table 1.6 – Maturation features in non-keratinised epithelium (Nanci and Ten Cate, 2008)

Although there is some distinction between the epithelial cell layers in non-keratinised epithelium, this is far less pronounced than in keratinised epithelium. All epithelium is separated from the underlying connective tissue by a structure known as the basal lamina, which acts as a filter and barrier, as well as having important cell signalling properties (Nanci and Ten Cate, 2008).

Figure 1.8 shows an electron micrograph of a gingival epithelial cell biopsy. Clearly visible are the cell-cell junctions, and gross structure of the epithelial cells.

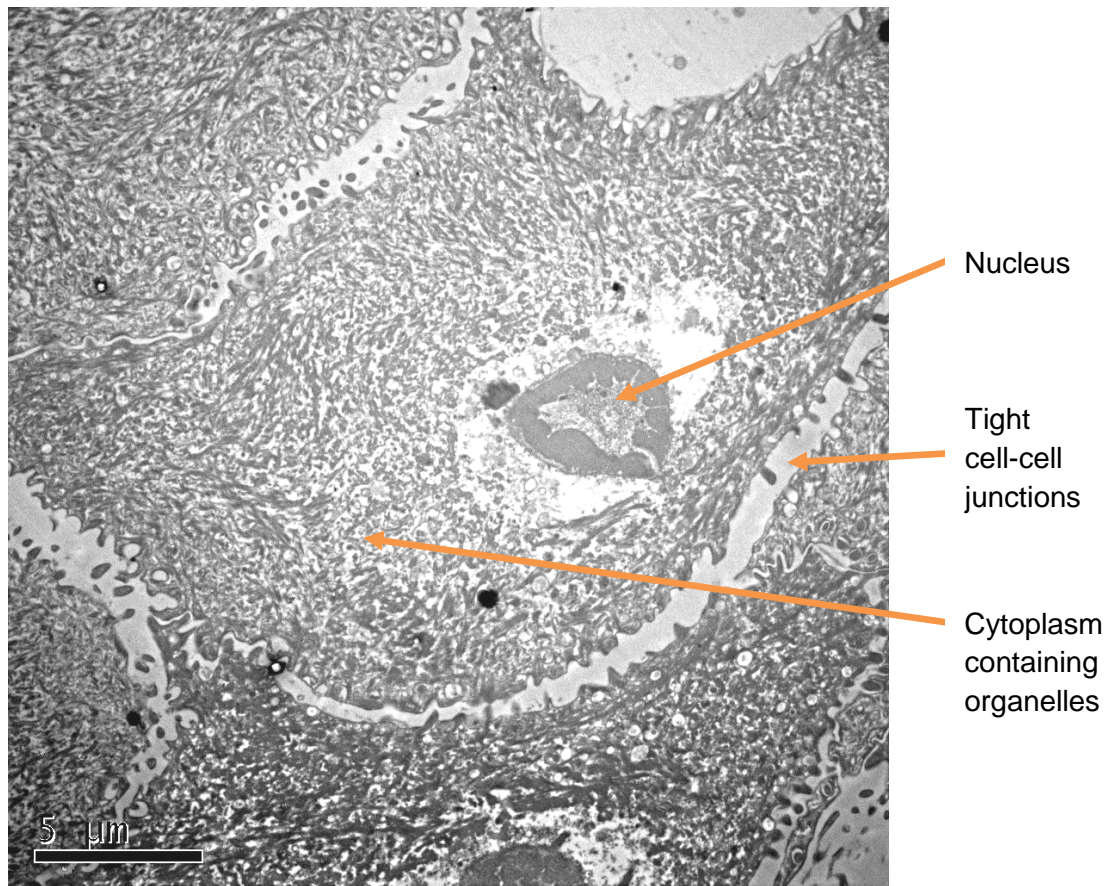


Figure 1.8 – Gingival epithelial tissue viewed under Transmission Electron Microscopy (TEM) (see Section 2.8.1 for sample preparation technique).

The functions of the oral epithelial tissues

Far from being a simple physical barrier, the oral epithelium has a number of other functions which differ according to the region of the mouth in which the mucosa is located. Areas such as the palate and gingivae are keratinised, and although significantly less permeable than other non-keratinised areas such as the buccal mucosa, still have some permeability (Wertz and Squier, 1991). Aside from this protective function as a semi-permeable barrier, the oral mucosa has been shown to have an important role in responding to pathogens and is discussed in Section 1.5.4.

1.5.3 *The link between soft tissues and long term implant health*

It has long been established that healthy soft tissues surrounding teeth or implants will act as a barrier to subgingival plaque formation. The peri-implant soft tissues can establish a cuff-like barrier tightly adherent to the Ti implant abutment (Berglundh et al., 1991). The width of keratinised mucosa surrounding an implant has also been

shown to be important in influencing soft tissue outcomes, and a smaller band of keratinised mucosa adjacent to an implant may create an increased risk of soft tissue mucositis at that site (Schrott et al., 2009). It is logical to presume that the more cleansable an implant is the more effective oral hygiene measures will be. Given that oral hygiene maintenance and regular disruption of the peri-implant biofilm will decrease the bacterial challenge, it follows that those implants where oral hygiene maintenance is possible will be more likely to have favourable long term soft tissue outcomes than those where oral hygiene measures are compromised. Maintenance of oral hygiene measures, and therefore long term implant health, are potentially compromised in the following situations:

- The patient is not compliant with oral hygiene regime (either not willing or unable to comply)
- Soft tissues surrounding the implant are hypertrophic, causing plaque accumulation
- Soft tissues have receded surrounding an implant, exposing the complex anatomy of the threaded part of the implant and allowing plaque accumulation
- Poorly designed implant based restoration which will compromise oral hygiene maintenance
- Implant has been placed inappropriately, leading to a lack of adequate soft tissue coverage on one or more aspects of the implant surface
- Presence of subgingival cement from implant superstructure which retains plaque.

It has also been established that a “thinner” mucosal biotype (meaning a pocket measuring probe inserted to the gingival crevice can be seen through the tissues) as opposed to a “thick” biotype (where the probe cannot be seen) predisposes to recession of peri-implant soft tissues (Nisapakultorn et al., 2010), therefore potentially adversely affecting long term soft tissue health.

1.5.4 *Epithelium, the bacterial challenge and inflammation*

Epithelial cells are the first cells (apart from crevicular neutrophils) that pathogens will encounter. Contact between epithelial cells and pathogenic bacteria plays an important role in forming a localised immune response in the periodontal and peri-implant setting. Epithelium can be penetrated by bacterial, viral and fungal pathogens, which may either directly invade the epithelial cells or may travel between epithelial cell junctions (Eick et al., 2006). The ability of pathogens to adhere to epithelial cells or invade epithelial cells stimulates an inflammatory response. Various pathogens that were identified in Section 1.3.4, such as *P. gingivalis*, have been shown to adhere to epithelial cells in large numbers (Yilmaz et al., 2002). This adhesion is aided by a variety of virulence factors including bacterial lipopolysaccharide (LPS) (Lamont and Jenkinson, 1998). Therefore, it is important to appreciate that an immune response can be initiated by contact with, passage between, or invasion of epithelial cells by pathogens. It is likely that in the periodontal or peri-implant context, all three processes will arise due to the structure of the epithelium surrounding an implant, and the biofilm covering the implant surface.

Epithelial cells are now known to be far more than simply a structural barrier, and their role in immune responses in periodontitis is well documented (Milward et al., 2007, Milward et al., 2013). Receptors called Toll-like Receptors (TLRs) are central to this immune response (Philpott et al., 2001), and have the ability to recognise key bacterial components such as lipopolysaccharides (LPS) of Gram-negative bacteria. Activation of TLRs initiates a number of molecular signalling pathways which culminate in the activation of Nuclear Factor Kappa B (NFκB). NFκB is the key pro-inflammatory gene transcription factor, which upon activation splits from its inhibitor (I-κB) and translocates from the cytoplasm of epithelial cells to the nucleus. Here it binds to DNA resulting in gene transcription changes and downstream protein production (e.g. IL8), (Milward et al., 2007). Activation of the pathway will lead to the recruitment of immune cells from the underlying connective tissues, such as neutrophils and macrophages, leading to inflammation, and potentially apoptosis of infected cells.

Although NFκB represents an important pro-inflammatory pathway, it is not the only mechanism by which transcription of inflammatory genes can be upregulated. Other

molecules such as activation protein 1 (AP-1) can also create an immune response (Philpott et al., 2001). There are a variety of complex pathways by which different bacteria may stimulate an immune response from contact with epithelial cells, many of which are as yet uncharacterised. AP-1 and NF κ B are examples of REDOX sensitive transcription factors, meaning that changes in cellular oxidative stress can lead to their activation (Chapple and Matthews, 2007).

1.5.5 *Cell-cell signalling and immune cell recruitment*

Epithelial cells play an important role in cell-to-cell signalling pathways including in the presence of a pathogenic challenge. Signalling molecules are produced to recruit other cell types and initiate an immune response (Yilmaz et al., 2003, Krisanaprakornkit et al., 2000, Milward et al., 2007). Therefore, if this signalling process is in some way compromised (for example by the presence of Ti species) and results in perturbation of the production or function of these cell signalling molecules, immune responses such as neutrophil function or chemotaxis, could be compromised. Neutrophils are the predominant acute inflammatory cells in peri-implant sites, therefore cell signalling between epithelial cells and neutrophils is a potentially important regulator of peri-implant inflammatory outcomes.

1.6 **Aims and objectives**

The introduction and literature review has demonstrated that there is a need to elucidate the effects that implant derived Ti products may have on epithelial cells in the context of peri-implant disease. Currently, little is known about the potential interactions between Ti products and epithelial cells, and how any interactions which may arise could affect cell signalling, immune responses and potentially peri-implant inflammation. These questions will be investigated using a number of techniques with the aim of determining the impact of insoluble Ti products on the epithelium and once elucidated, may offer potential therapeutic targets for treating peri-implant diseases.

1.6.1 *Justification for the research enquiry*

The fact that peri-implant tissues from failed implanted Ti devices have been shown to contain Ti particles that suggests that Ti does not, as initially thought, remain passive

and stable *in vivo*. Insoluble Ti products in the form of TiO₂ NPs have been demonstrated to be co-located with epithelium and with innate immune cell infiltrates in the adjacent tissues. The established evidence from the orthopaedic literature and extensive *in vitro* modelling has shown that Ti in these forms has clear biological reactivity and hence it is possible that when Ti accumulates in peri-implant tissues it will generate epithelial cell responses.

1.6.2 *Aims of the project*

The aims of this project are:

1. To develop a clinically relevant *in vitro* model system to investigate the effects of relevant Ti products on epithelial cell viability.
2. To determine any interactions that may occur between clinically relevant Ti species and epithelial cells and characterise these.
3. To investigate the direct cellular effects of any interactions on epithelial cells.
4. To investigate the molecular effects of any interactions using microarray screening and confirmatory Polymerase Chain Reactions (PCR).
5. To determine any effects these interactions may have on known epithelial cell responses and their role in the inflammatory immune response to known pathogens.

Based on the lack of reported evidence in this area the work reported in this thesis will test the null hypothesis (H₀) that:

“Ti species similar to those released from implanted Ti devices do not elicit significant biological responses from oral epithelial cells”.

Chapter 2

Materials and methods

Synopsis

The aim of this chapter is to provide a general overview of the main cell culture and assay techniques used in this body of work. Cell culture technique, stimulus preparation and overarching experimental methods are described. Due to the breadth of methods used, the specific details of experimental protocols are included within the individual experimental chapters.

2.1 Titanium stimuli

2.1.1 *Titanium oxide stimulus preparation*

To limit the number of experimental variables this study focused predominantly on the use of one Ti stimulus. Many different Ti species could potentially come into contact with oral epithelial cells, however deposits of TiO₂ in anatase form in both nanoscale and larger particle sizes have been detected within the epithelial tissues surrounding transmucosal CPTi implanted devices (Addison et al., 2012, Haleem-Smith et al., 2012, Olmedo et al., 2012). For all work unless otherwise specified, TiO₂ suspensions were prepared using TiO₂ (powder, anatase form, purity 99.7 %, catalogue number 637254, Sigma-Aldrich, UK) in the form of nanoparticles with a particle size of <25 nm.

TiO₂ was weighed using a balance (Ohaus Precision Standard, Ohaus UK) accurate to 3 decimal places in plastic weigh boats. The TiO₂ powder was added to a quantity of reverse osmosis (RO) water (see below) that had been sterilised in an autoclave (Little Sister 2, Eschmann UK) at 134°C for 3 min. The suspension was made up in a sterile 100 mL glass beaker using the following masses of TiO₂:

Ti mass	Amount RO water	Stock concentration	Final working concentration
0.05 g	50 mL	100 µg/mL	10 µg/mL (10 ppm)
0.50 g	50 mL	1000 µg/mL	100 µg/mL (100 ppm)
5.00 g	50 mL	10 000 µg/mL	1000 µg/mL (1000 ppm)
25.00g	50 mL	50 000 µg/mL	5000 µg/mL (5000ppm)

Table 2.1 – Ti stimulus preparation

The beaker containing the TiO₂ / water suspension was then placed within a plastic container with ice and sonified using a Branson Sonifier 250 (Branson Ultrasonics, Danbury, Connecticut USA), according to a published protocol (Taurozzi et al., 2013). A

standard ½" clean titanium horn was inserted centrally within the 100 mL beaker to a depth 1 cm from the base of the vessel. Sonification was performed using a 50 W power output and 80 % duty cycle for 15 min. Sonification was conducted in a positive flow biological hood (MSC12, ThermoScientific, USA) to help maintain sterility. The resultant sonified suspension was stored in sterile conditions within a sterile plastic tube prior to use and re-sonified prior to use if stored for longer than 48 h in order to minimise the chances of settling of the TiO₂ NPs, which would result in a reduction in accuracy of the suspension concentration.

2.1.2 *Addition to cell culture medium*

150 µL of the TiO₂ NP suspension was transferred to a sterile 25 mL universal container which contained 18.75 µL of 80 mg/mL sterile Bovine Serum Albumin (BSA) solution (Sigma-Aldrich, UK) made by adding 0.80 g of BSA granules to 10 mL of sterile RO water. BSA was added to the TiO₂ NPs in order to minimise agglomeration (Taurozzi et al., 2013). The TiO₂ / BSA mixture was then augmented with 14.83 mL of cell culture medium as appropriate to the experiment (see Section 2.1.1) to make 15 mL medium with a known concentration of TiO₂ nanoparticles (NPs) in suspension.

2.2 **H400 (oral epithelial cell line) cell culture**

2.2.1 *Cell culture media and reagents*

Dulbecco's modified Eagle's medium (DMEM)

DMEM was supplemented to form the growth culture media for H400 cells. Ham's F12 DMEM (Life Technologies, UK) was supplemented with L-Glutamine (Sigma-Aldrich, UK), foetal calf serum (FCS) (Labtech, UK) and hydrocortisone (Sigma-Aldrich, UK) to the following concentrations (see below) under aseptic conditions in a biological positive flow hood. For experiments using dynasore hydrate, the FCS was omitted for the final medium replenishment as described in more detail within Section 4.2.2.

L-Glutamine	2 mM final concentration
FCS	10 % v/v final concentration
Hydrocortisone	0.5 ng/mL final concentration

Trypsin ethylenediaminetetraacetic acid (Trypsin-EDTA)

Trypsin-EDTA (Gibco, UK) was used to detach the adherent H400 cell monolayer from the cell culture flask. This allows a single cell suspension to be created to facilitate re-seeding of cells into other flasks or growth receptacles. Trypsin-EDTA used in this work contained 0.5 g/L trypsin and 0.2 g/L EDTA in Hank's balanced salt solution and was purchased ready for use (Sigma-Aldrich, UK). Once received the solution was aseptically split into 5 mL aliquots and stored at -20°C prior to use in order to prevent repeated freeze-thaw cycles and any potential loss of activity. Before use, aliquots were defrosted and warmed to $37 \pm 1^\circ\text{C}$ in a water bath.

Phosphate buffered saline (PBS)

Commercially available Dulbecco's phosphate buffered saline without Ca^{2+} or Mg^{2+} (D-PBS) (Gibco, UK) was used to wash cells prior to detachment from the cell culture plasticware. D-PBS was stored aseptically at $4 \pm 1^\circ\text{C}$ prior to use, then warmed to $37 \pm 1^\circ\text{C}$ before washing cells.

2.2.2 *H400 cell culture and passage*

The H400 cell line is an immortal cell line derived from an oral squamous cell carcinoma (SCC). It is used as a robust model for oral epithelial cells (OECs) (Prime et al., 1990) and is a cell line kept at the University of Birmingham following donation from Professor S Prime. This cell line was derived from a Stage 2 moderately differentiated SCC in the alveolar process of a 55-year-old female, and has been shown to exhibit qualities strongly representative of OECs (Prime et al., 1990). This cell line has been extensively used in studies relating to periodontal disease and inflammatory responses (Milward et al., 2007, Milward et al., 2013, Grant et al., 2010a, Wylie et al., 2010). All experiments were performed between passages 4-30. Cells were archived by freezing in supplemented cell culture medium containing 20 % FCS and 10 % Dimethyl sulphoxide (DMSO), which was added to prevent cell membrane rupture during the freezing process. Once frozen, cells were stored at -80°C.

General cell culture methods

H400 cells were cultured in an incubator (Galaxy S, SLS, UK) at $37 \pm 1^\circ\text{C}$ in a humidified atmosphere and 20 % CO_2 . H400 cells will form a confluent, adherent monolayer when cultured on many different surfaces. Tissue culture treated plasticware was used for the majority of work in this thesis, but H400 cells will also successfully adhere to and divide on untreated (sterilised) glass cover-slips and microscope slides. The majority of H400 cell culture was performed using 75 cm^2 or 25 cm^2 sterile cell culture treated flasks (TC coated plasticware, Corning, New York, U.S.).

All work with H400 cells was performed without the addition of antibiotics or antifungal agents to the cell culture media so as to negate additional confounding factors. As antimicrobials were not included, all experiments were reliant on careful and thorough aseptic technique. All aliquots of reagents were split using sterile single use pipettes in a biological positive flow hood in sterile receptacles, with all cell culture techniques utilising careful aseptic technique. If any flasks became turbid or light yellow in colour, these were presumed infected and disposed of immediately. Antimicrobial-free culture was not possible when initially culturing primary cells due to the non-sterile nature of the tissues from which the cells were cultured when compared to cell lines.

Supplemented DMEM contains phenol red (a pH indicator) which will indicate an acidic pH when the medium is becoming exhausted and requires refreshing, becoming orange, then yellow in colour. H400 cells were cultured to approximately 80 % confluency before use as determined by light microscopy, to allow representative cell responses whilst not risking total confluence which can induce contact inhibition and media exhaustion and result in cell death. The degree of monolayer confluence was assessed using light microscopy at 10x and 20x magnification.

Cell passage / splitting

H400s were split and reseeded (passaged) when an 80% confluent monolayer had been reached, to allow further growth and division of cells following re-seeding into different plasticware or glassware. The process for a 75 cm^2 flask is outlined below.

1. Cells were examined visually using a 10x objective on an inverted light microscope (Primo Vert, Zeiss, Germany) to establish level of confluence.

2. Cell culture medium was removed from the flask using a sterile Pasteur pipette.
3. Cells were washed gently with 5 mL warmed D-PBS ($37 \pm 2^{\circ}\text{C}$) to remove remaining cell culture medium, as the FCS contained in the media will inhibit the action of trypsin-EDTA.
4. 5 mL of warmed ($37 \pm 2^{\circ}\text{C}$) trypsin-EDTA was added to the flask and gently agitated, re-sealed, and incubated at 37°C in a 20 % CO_2 atmosphere for 10 min.
5. After 10 min the level of dissociation was examined using light microscopy as before. If cells were still attached, the flask was incubated for a further 3-4 min and re-examined until full dissociation was achieved.
6. The resulting cell suspension was aseptically removed from the flask and added to an equal volume of pre-warmed H400 culture medium in a sterile 25 mL universal tube. As the medium contains FCS it will stop the action of trypsin thereby preventing undue cellular damage.
7. The suspension was then centrifuged at 1000 rpm for 10 min (IEC Centra CL2, Thermo Scientific, UK) following which the supernatant was removed and discarded with a sterile Pasteur pipette taking care not to disturb the cell pellet.
8. The cell pellet was gently re-suspended in approximately 1 mL cell culture medium ($37 \pm 2^{\circ}\text{C}$), and the cell concentration quantified by counting using a haemocytometer before re-seeding the correct number of cells into fresh medium in an appropriate cell culture vessel.
9. H400s were visually inspected at 24 and 48 h to assess cellular adherence, growth and morphology. When H400s were seeded at an appropriate density, the medium was changed after approximately 4 days and confluency was reached in approximately 5-7 days post passage.

Cell freezing / recovery from storage

To retrieve archived frozen cells, a vial containing cells was warmed quickly to 37°C in a water bath and added to 9 mL of pre-warmed cell culture medium. The suspension was spun at 800 rpm for 10 min, then the supernatant discarded and the pellet re-

suspended in 1 mL warmed cell culture medium. The suspension was then added to a flask containing a total of 10 mL of warm supplemented DMEM, and incubated and monitored as previously indicated above.

To freeze aliquots of H400s, 1×10^6 cells in 1 mL supplemented DMEM containing 20 % FCS and 10 % dimethyl sulphoxide (DMSO, Sigma-Aldrich, UK) were placed into 2 mL sterile cryo-vials (Corning, USA). The vials were wrapped in cotton wool to ensure slow freezing and stored at -80°C until needed, upon which they were defrosted and seeded as previously described. Long term storage of H400s has traditionally been undertaken in liquid nitrogen, however all H400s used in this work were successfully stored at -80°C for a number of months with no loss of viability on retrieval from storage (data not shown).

Cell growth in well plates

Experiments were undertaken to establish the ideal seeding densities when using different cell culture plasticware. Table 2.2 shows a list of seeding densities in number of cells and expected time to confluency:

Vessel	Cell count	Volume of medium	Time to “just” confluence
96-well plate	8×10^3 cells per well	100 μL or 200 μL	48-72 h
6 well plate	1×10^5 cells per well	2 mL	48-72 h
25 cm^2 flask	2×10^5 cells per flask	5 mL	5-7 days
75 cm^2 flask	5×10^5 cells per flask	10 mL	5-7 days
Transwells in 24 well plate	3×10^4 cells per top chamber	300 μL	3-5 days

Table 2.2 – Seeding densities of epithelial cells

The seeding densities in Table 2.2 were used for the majority of experiments however these were adapted if the time to confluence needed to be reduced or extended. The stage in the cell cycle and potential cell behaviour may be altered if a significantly different length of time between seeding and confluency occurs. Therefore, if cells had not achieved the appropriate degree of growth expected, they were discarded and new cultures set up in order to maximise experimental consistency.

Cell growth on coverslips and glass slides

For certain staining and histological techniques, H400s were grown on sterile microscope slides (Hendley-Essex, UK) and coverslips (Scientific Laboratory Supplies, UK). The H400 cell line did not require collagen coating of microscope slides or other glassware in order to adhere sufficiently. All glassware was sterilised by immersion in 70 % alcohol for 30 s then rinsed in sterile D-PBS before use. Cells were cultured on coverslips (1.5 mm thickness, 13 mm diameter, Scientific Laboratory Supplies, Nottingham, UK) in standard 24, 12 or 6 well sterile tissue culture plates (Corning, New York, U.S.) containing 1, 1.5 or 2 mL cell culture medium respectively.

Trypan blue staining

Cell viability was determined using a trypan blue exclusion staining protocol. Trypan blue 0.4 % (Gibco, UK) was added to the cell suspension at a ratio of 1:1, mixed gently by hand for 60 s at room temperature and a cell count then performed using a haemocytometer (Figure 2.1). Positively stained cells appear blue and are assigned as non-viable as trypan blue cannot pass the cell membrane of viable cells. Viability is expressed as a percentage of total cell number and is expected to be in excess of 90%.

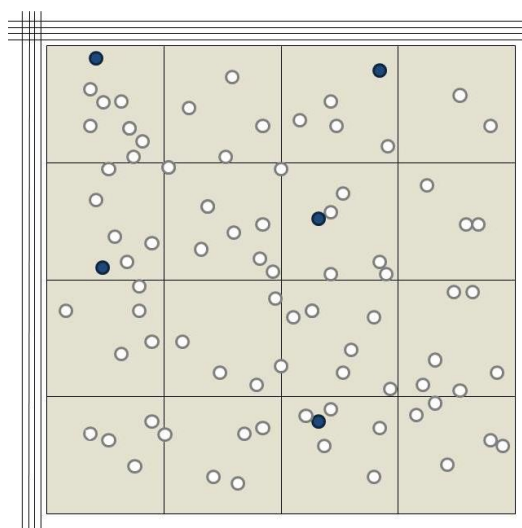


Figure 2.1 – Diagram representing a cell count of cells stained with trypan blue exclusion (5/80 cells = 94 % viability). Blue cells would be counted as non-viable.

2.3 Use of cell viability assays

There are many different methods of assessing cell viability within a population. As will be discussed further in Chapter 3, there are potential interactions between the

insoluble nanoparticles (NPs) and assays, therefore it is imperative that all assays used were validated for use in the presence of TiO₂ NPs. This body of work employed a number of assays to determine cell “viability”, and utilized indirect pathways in conjunction with direct pathways to build a clear picture of the likely status of cells in response to NP exposure.

2.3.1 *CellTiter-Glo® assay*

CellTiter-Glo® (Promega, UK) is a commercially available luminescence-based assay. The assay provides a substrate (luciferin) which is converted to oxyluciferin, through a reaction that releases light. This reaction is dependent upon the presence of ATP and oxygen present in viable cells.

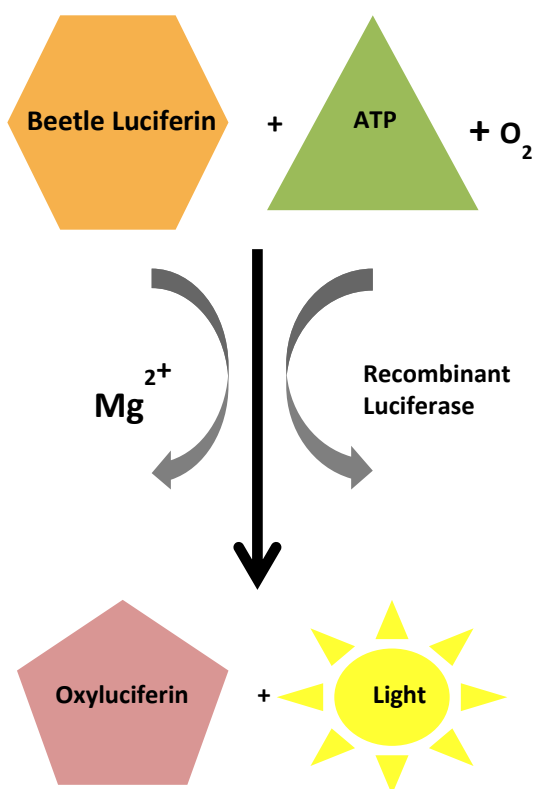


Figure 2.2 – The luciferase reaction which takes place using the CellTiter-Glo® assay. Mono-oxygenation of luciferin occurs and is catalysed by luciferase in the presence of oxygen, Mg²⁺ and ATP. The output measured is light produced during this process in arbitrary units.

Non-viable cells produce no ATP, therefore will not catalyse the reaction contained in the assay resulting in no light output (Riss and Moravec, 2004). Light output is measured after a short incubation period using a luminometer (Berthold, Bad Wildbad, Germany). The assay lyses the cells, so can only be carried out once per sample.

For all the work in this thesis using CellTiter-Glo®, the following protocol was adopted with the light output measured in Relative Light Units (RLU) per well.

1. H400 cells were seeded into a cell culture treated 96-well white walled plate (Appleton Woods, Birmingham, UK) and exposed to a relevant stimulus according to the specific experimental design, along with the relevant controls (both cell free and stimulus free). Whenever possible the outer wells of the plate were not used to avoid excess evaporation of medium during incubation. The total medium volume in each well was either 100 or 200 μ L depending upon whether 100 μ L of supernatant was needed for another assay (for example an LDH assay, see Section 2.3.2).
2. Following incubation with stimuli determined by the specific experimental design, the 96-well plate was removed from the incubator.
3. The supernatant was removed from the cell monolayer. Wells were then washed 3 times with 100 μ L warmed D-PBS to remove any remaining stimulus as far as possible. 100 μ L of fresh warmed cell culture medium was then pipetted into the well.
4. CellTiter-Glo® reagent (at room temperature, $23 \pm 2^\circ\text{C}$, made up as per manufacturer's protocol) was added in an equal volume to the cell culture medium in each well.
5. The plate was covered with the lid, and incubated for a minimum of 10 min at room temperature. The manufacturer reports this signal to be stable for up to 60 min, but all plates in this thesis were read within 30 min to ensure accuracy and consistency between experimental repeats.
6. Plates were read using a TriStar² 942 multifunction plate reader (Berthold, Bad Wildbad, Germany) at a temperature of $37 \pm 1^\circ\text{C}$ and a counting time of 0.10 s, as per a protocol on ICE Software (Version 1.0.6.0) or a LB96V luminometer (Berthold, Germany) if the TriStar² was unavailable. Data were captured using WinGlow software (Berthold, Germany).
7. Data were exported to a Microsoft Excel file and analysed according to the objectives of the specific experiment. The data captured was the mean of the

two RLU readings closest to 30 min after the assay reagent was added to the plate.

- Control wells were run for every experiment consisting of cell free wells containing each stimulus used, and wells containing cells but no stimuli.

2.3.2 *CytoTox-ONETM*

CytoTox-ONETM (Promega, UK) is a commercially available fluorometric assay kit used to determine the concentration of the enzyme lactate dehydrogenase (LDH) in a sample. LDH is an intracellular enzyme, released extracellularly into the cell culture medium if a cell membrane becomes damaged (e.g. during necrosis). Therefore, the concentration of LDH in the supernatant of a cell population will increase as the numbers of necrosing or necrotic cells increases. The cell culture medium will contain some LDH due to the inclusion of FCS. Positive samples will fluoresce at an excitation wavelength of 560 nm 590 nm, and appropriate filters were used.

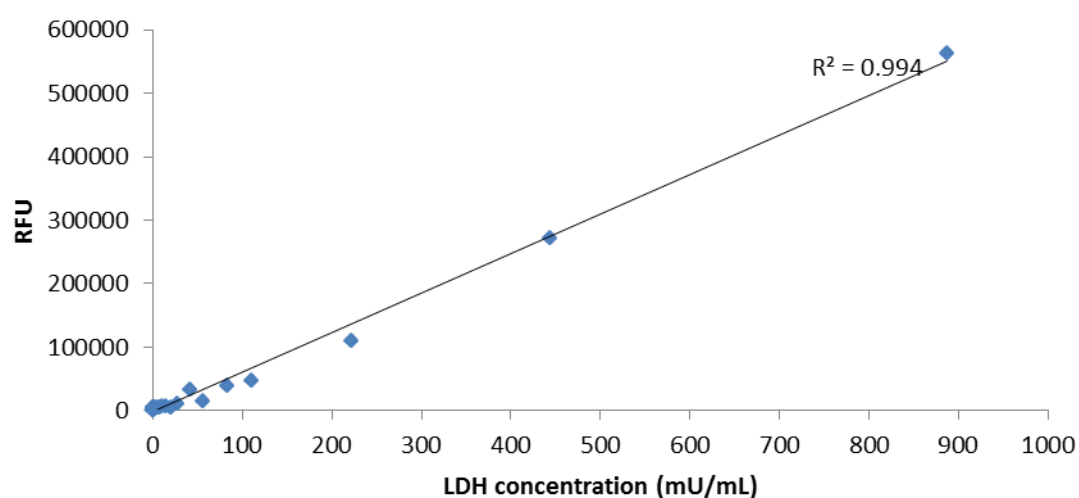


Figure 2.3 - Standard curve for LDH content in wells using CytoTox-ONETM assay demonstrating a linear relationship between the LDH concentration in cell culture medium and the relative fluorescence (in RFU) of the well containing the cell culture medium.

For all the work in this thesis detecting LDH concentrations, the following protocol was used. Data were recorded as Relative Fluorescence Units (RFU) per well.

- Cells were cultured in a tissue culture treated, white walled, clear bottomed 96-well plate (Appleton Woods, Birmingham, UK) with a total volume of 200

µL medium (including any stimulus) for a pre-determined length of time according to the specific objectives of the experiment.

2. At the time of performing the LDH assay, 100 µL of supernatant was removed from the white walled clear bottomed plate the cells were incubated in, and transferred to a plate with black wells in order to read the fluorescence of the sample. White or clear bottomed plates are not compatible with reading fluorescence.
3. An equal volume of CytoTox-ONE™ assay reagent (prepared as per manufacturer's protocol) was added at room temperature to each well.
4. The plate was incubated at room temperature for 10 min. Fluorescence was read using a multimode plate reader (TriStar², Berthold, Bad Wildbad, Germany) with excitation and emission filters of 560 nm and 590 nm respectively at 37 ±1°C, with a count time of 0.1s and lamp energy of 70 %. Data were exported as described in Section 2.3.1. Cell free wells were run as controls in each experiment to ensure no interference from cell culture medium or stimuli. A standard curve was also performed to ensure the assay's accuracy (Figure 2.3).

2.3.3 *Caspase-Glo® 3/7 assay*

Caspase-Glo® 3/7 is a commercially available luminescence assay used to determine the quantity of caspase 3/7 activity in a population of cells. Caspases are enzymes which are activated during apoptosis. Caspases 3 and 7 are detected via:

- cell lysis, which will liberate any caspase present within the cell
- the assay substrate (containing the tetrapeptide sequence DEVD) is in turn cleaved by caspase 3/7 to produce a luminous product (Riss and Moravec, 2004)
- luminescence will be proportional to the amount of luminous product, therefore representative of the amount of caspase 3 and 7 present.

For all the work in this thesis using Caspase-Glo® 3/7, the following protocol was used and data were expressed as Relative Light Units (RLU) per well.

1. Cells were cultured according to Section 2.3.1 in white-walled clear bottomed 96-well plates and stimulated as the specific objectives of the experiment demanded. The total well volume was consistent between wells.
2. After the incubation time necessary for each specific experiment the 96-well plate was removed from the incubator.
3. The supernatant was removed and the cell monolayer was washed 3 times with warmed D-PBS to remove any remaining stimulus as far as possible. Fresh warmed cell culture medium was pipetted into each well.
4. Caspase-Glo® 3/7 reagent (at room temperature, made up as per manufacturer's protocol) was added in an equal volume to the cell culture medium in each well. This was either 50 or 100 µL depending on the specific protocol of the experiment.
5. The plate was covered with the lid and incubated in the dark for a minimum of 30 min at room temperature ($23 \pm 2^{\circ}\text{C}$) as per the manufacturer's protocol. All plates in this thesis were read within 40 min from the addition of the reagent to minimise any change in light output over time.
6. The plate was read and data were collected as for the CellTiter-Glo® assay (see 2.3.1).

2.3.4 *Sytox® Green Nucleic Acid Stain*

Sytox® green is a high affinity nucleic acid stain, which will rapidly stain the nuclei of cells with a non-intact cell membrane. Stained nuclei will fluoresce bright green when excited with a 450 – 490 nm light source. This light output can be measured either with a fluorescence plate reader or visualised using a microscope.

1. H400 cells were cultured in tissue culture compatible, white walled, clear bottomed 96-well plates (Appleton Woods, Birmingham, UK) containing 100 µL cell culture media. The media was changed once approximately 80 % confluence was reached, and new media was added containing TiO₂ NPs in concentrations of 0, 1, 10, 100 and 1000 ppm and incubated for 24 h.
2. The media was aspirated and the cell monolayer washed 3 times with warmed PBS, then 40 µL of warmed PBS was added to each well to avoid the monolayer dessication.

3. 10 μ L of Sytox[®] Green stock solution (S7020, Life Technologies, UK) was added to each well to give a final concentration of 0.2 μ M. The plate was incubated at room temperature for 5 min, then images were captured using an epi-fluorescent microscope (Nikon Eclipse TE300) with a fluorescence filter (excitation 472 nm and emission 520 nm, BrightLine[®] GFP-3035B, Semrock) at x40 magnification. 3 randomly positioned images were taken from each well using a digital camera (Nikon Coolpix 990) using standard settings. This process was completed quickly to avoid the cells becoming non-viable due to lack of cell culture medium and/or being out of the incubator.
4. Images were captured at exposure times of 1500 ms for the laser excitation and 50 ms brightfield, and adjusted using FIJI (ImageJ) software 1.49k (National Institutes of Health, USA) to enhance clarity. The total number of stained cells was counted manually by viewing the captured images and expressed as a percentage of the total cell number.

2.3.5 *MTT assay*

The MTT (3-[4,5-dimethylthiazol-2-yl]-2,5 diphenyl tetrazolium bromide) assay functions via the actions of NAD(P)H dependent enzymes in viable cells, which will reduce the assay substrate tetrazolium dye MTT to its insoluble form which is purple in colour. If more viable cells are present in a sample, the solution will become increasingly purple during the controlled conditions of the assay.

The following protocol was used:

1. H400 cells were cultured in a tissue culture, white walled, clear bottomed 96-well plate (Appleton Woods, Birmingham, UK) with 100 μ L cell culture media. Cells were treated with stimuli as demanded by the specific experimental protocol.
2. MTT substrate (Sigma-Aldrich, UK) was diluted in PBS to form a stock at a concentration of 5 mg/mL. The stock was filtered through a 0.2 μ L syringe filter (Sterilitech, UK) and stored at 4 ± 1 °C in the dark until use.

3. When the assay was due to be performed, 10 μ L of MTT stock solution was added to each well and the plate was incubated for 4h at 37 \pm 1°C with 5 % CO₂.
4. 100 μ L of dimethyl sulfoxide (DMSO, Sigma-Aldrich, UK) was added to each well and thoroughly pipetted to mix and dissolve any crystals of insoluble dye which had formed.
5. The absorbance of each well was measured immediately at 570 nM (ELx800 Universal Microplate Reader, Biotek UK). Data were exported to Microsoft Excel for analysis in the form of a single absorbance value generated for each well.

2.4 Primary oral epithelial cell culture

2.4.1 Primary epithelial cell culture using a 3T3 feeder layer

3T3 cells are a murine cell line now accepted as a well characterised fibroblastic cell line. Cells used were a gift from Dr RM Shelton at the University of Birmingham. The following previously described protocol was used in to establish a ‘feeder layer’ for primary epithelial cells (Gray et al., 1983, Taylor-Papadimitriou et al., 1977). This feeder layer is then treated to prevent cell division within the feeder layer but to maintain cell viability in order to continue to produce the growth factors necessary for primary epithelial cell survival.

3T3 Cell culture media and reagents

Supplemented DMEM

DMEM supplemented with FCS and penicillin-streptomycin (Sigma-Aldrich, UK) was used as the standard cell culture medium for 3T3 cells in accordance with existing in-house protocols. All cell culture reagents and passage were performed in a positive flow biological hood to ensure an aseptic technique. DMEM with high glucose and with L-Glutamine and HEPES buffer (Gibco, UK) was used and supplemented as below:

FCS	Final concentration 10 % v/v
Penicillin/streptomycin	Final concentration 100 U/mL penicillin, 0.1 mg/mL streptomycin

Table 2.3 – DMEM supplementation

Additional cell culture reagents

Additional cell culture reagents were as for H400 cell culture. Trypsin-EDTA and D-PBS reagents used were as previously described for H400 passage. Primary cells were seeded at the same density as H400 cells. All cells were incubated at 37°C in 20 % CO₂.

3T3 feeder layer culture

1. 3T3 cells were cultured in a 75 cm² tissue culture medium treated sterile flask (as for H400 cells, see Section 2.2) until 30 – 40 % confluent (approximately 24 hours post seeding).
2. 3T3 cells were then treated with mitomycin C (4 µg/mL) (Sigma-Aldrich, UK) for 2 h at 37°C in 5 % CO₂ to arrest cell division. Following incubation for 2 h the medium was changed for fresh growth media (without mitomycin C).

Following treatment with mitomycin C, the feeder layer was kept in the incubator until the primary epithelial tissue had been prepared (maximum 2 h).

Culture media for primary epithelial cells – feeder layer method

Primary epithelial cells were cultured in the same media as H400 cells (see 2.2.1) but with additions outlined in Table 2.4.

Penicillin – streptomycin (Sigma-Aldrich, UK)	100 U/mL penicillin, 0.1 mg/mL streptomycin
Amphotericin-B (Sigma-Aldrich, UK)	2.5 µg/mL
Cholera toxin (Sigma-Aldrich, UK)	10 ⁻¹⁰ M
Epithelial Growth Factor (Sigma-Aldrich, UK)	10 ng/mL
Insulin (Sigma-Aldrich, UK)	0.01 mg/mL

Table 2.4 – Primary cell culture medium

Primary tissue treatment

2 mm diameter gingival punch biopsies were collected from healthy volunteers as part of an ongoing clinical trial (NHS R&D Reference: R&D1398, REC Reference Number: 10/H1208/48). Waste tissue was also collected with consent from patients undergoing routine surgery including gingivectomy or third molar extraction. The tissue was stored in transport medium (Ham's F12 DMEM supplemented with 10 % Fetal Calf Serum and 100 U/mL penicillin, 0.1 mg/mL streptomycin [Sigma-Aldrich, UK]) immediately

following collection. As soon as possible (and always within 24 h) the tissue was trypsinised with trypsin-EDTA (see Section 2.2.1) at $4 \pm 1^\circ\text{C}$ overnight to separate the epithelial cell layer from the underlying connective tissue. This was conducted at low temperatures to minimise the uptake of the trypsin-EDTA by the epithelial cells. Separation of the epithelial layer from connective tissue was carried out aseptically under magnification using a sterile scalpel. The epithelial layer was then placed into the flask with the mitomycin C treated 3T3 cells immediately following removal of the 3T3 culture medium.

10 mL pre-warmed epithelial cell culture media (as described in Section 2.4.1) was added and the flask was incubated at $37 \pm 2^\circ\text{C}$, in 5 % CO_2 and monitored using light microscopy for signs of growth.

2.4.2 *Primary epithelial cell culture using the explant method*

An alternative method for culturing primary epithelial cells was explored following problems experienced when using the method described in Section 2.4.1. These issues are described in detail in Section 3.2.3.

Primary epithelial cell culture media and reagents – explant method

The explant method uses different growth media in which to culture cells than previously described. Wash-PBS and cell culture media were made up as indicated in Tables 2.5 and 2.6, and stored aseptically at 4°C until use.

Wash-PBS:

PBS without Mg^{2+} or Ca^{2+} (Gibco, UK) with the addition of the following antimicrobials:

Penicillin /Streptomycin (Sigma-Aldrich, UK)	100U, 0.1mg/mL
Amphotericin B (Sigma-Aldrich, UK)	0.25 $\mu\text{g}/\text{mL}$

Table 2.5 – Wash-PBS

Serum free culture media (SFM):

DMEM with or without Ca^{2+} (Gibco, UK) 75% plus DMEM F-12 (Gibco, UK) 25% with the following supplements:

L-Glutamine (Sigma-Aldrich, UK)	2 mM
Hydrocortisone	0.4 ng/mL
Penicillin / streptomycin (Sigma-Aldrich, UK)	100U, 0.1 mg/mL
Gentamycin (Sigma-Aldrich, UK)	0.1 mg/mL
HEPES buffer (Gibco, UK)	1 in 100 (1M)
ITS-X (Insulin-Transferrin-Selenium-Ethanolamine, Gibco, UK)	1 in 100 (100x)
HEGF (Human Epidermal Growth Factor, Gibco, UK)	10 ng/mL
Choleratoxin (Sigma-Aldrich, UK)	1 µg/mL

Table 2.6 – Serum free culture medium

DMEM without Ca^{2+} was used when cells were growing and multiplying as anticipated. Initially, DMEM with Ca^{2+} was used to aid cellular attachment and proliferation.

Explant method protocol

Biopsy samples or waste tissue were stored in transport medium as previously described (Section 2.4.1). Samples were washed repeatedly in warmed wash-PBS to remove any blood contamination or bacterial contaminants on the tissue surface. A sterile disposable scalpel (Schwann-Morton, UK) was then used to dissect the epithelial layer from any attached connective tissue under 3x magnification. The epithelium was subsequently divided into small pieces of approximately 1-2 mm in diameter. These were then re-washed in wash-PBS and placed onto tissue culture treated polystyrene as required (flasks or well plates were employed, Corning, UK). The tissue was left for 15-20 min to dry slightly and to adhere. Subsequently an appropriate volume (depending on flask or well size) of warmed SFM was gently dropped onto the explanted tissue. The explants were then incubated at $37 \pm 1^\circ\text{C}$ in 5% CO_2 and examined using light microscopy daily. Medium was changed every 4 days.

2.5 RNA isolation and Polymerase Chain Reaction (PCR)

2.5.1 RNA isolation from cultured cells

Cells were cultured in 25 cm^2 flasks and treated with trypsin-EDTA, washed and re-suspended (see Section 2.2.2). The resulting single cell suspension was centrifuged at 1000 rpm for 10 min and the resulting cell pellet was treated with 1 mL TRIreagent® (Sigma-Aldrich, UK) and pipetted thoroughly to mix. The resulting emulsification was

then either frozen and stored at -80°C until RNA isolation or used immediately according to the following protocol. Due to the presence of TiO_2 NPs within the experimental system it was decided to use an alternative method of RNA extraction to the standard filter columns as a precaution, as it was possible that the TiO_2 NPs may interfere with the filtration process.

1. 200 μL of chloroform (Sigma-Aldrich, UK) was added to the homogenised TRI reagent containing the cell lysate in an autoclaved 1.5 mL centrifuge tube (Eppendorf, Germany).
2. The tube was vortexed for 30 s and checked visually to ensure a homogenous colour.
3. The tube was left at room temperature for 5 min.
4. The tube was then centrifuged at 12,000 g for 15 min.
5. The top clear aqueous layer from the tube was carefully removed using a pipette and placed into a clean centrifuge tube. Any remaining TiO_2 NP stimulus was observed at the bottom of the centrifuge tube.
6. 500 μL of isopropanol alcohol (Sigma-Aldrich, UK) was added to the tube and pipetted thoroughly to mix.
7. The tube was left at room temperature ($23 \pm 2^{\circ}\text{C}$) for 10 min.
8. The tube was centrifuged at 12,000 g for 10 min, and the tube was oriented so the resulting pellet could be located after centrifugation.
9. The supernatant was carefully removed, leaving the white pellet containing the RNA in the tube.
10. The RNA pellet was washed with 1 mL of 70 % ethanol made up by adding pure ethanol (Sigma-Aldrich, UK) to RNase free water (Qiagen, UK) in a ratio of 7 parts in 10.
11. The tube was centrifuged at 7,500 g for 10 min.
12. The supernatant was removed and the resulting pellet was left to air dry until clear (after approximately 5-10 min) then dissolved in 50 μL of RNase free water. The resulting sample was then either purified as below or frozen at -80°C until purification.

2.5.2 *RNA purification and DNase digestion*

Before gene expression analysis, the resulting RNA was purified to ensure the quality of the samples was as high as possible. A commercial kit was used (RNeasy® mini kit, Qiagen, UK) with the following protocol.

1. 600 µL of 70 % ethanol was added to the 50 µL RNA in water as prepared above.
2. 650 µL of the resulting mixture was then transferred to the RNeasy spin column in a 2 mL collection tube and centrifuged at 10,000 rpm for 30 s.
3. The flow through was discarded and 350 µL of buffer RW1 was added, then the column was centrifuged at 10,000 rpm for 30 s.
4. The flow through was discarded. 70 µL of DNase I (Qiagen UK, made up according to the manufacturer's instructions) was added directly to the column membrane, taking care not to touch the edge of the column. This was left for 10-15 min at room temperature ($23 \pm 2^{\circ}\text{C}$).
5. 350 µL of RW1 buffer was added and then the column was centrifuged at 10,000 rpm for 30 s.
6. The flow through was discarded. 500 µL of RPE buffer was added and the column was centrifuged at 10,000 rpm for 30 s.
7. The flow through was discarded. 500 µL of RPE buffer was added and the column was centrifuged at 10,000 rpm for 2 min. The flow through was discarded.
8. The column was placed in a new 1.5 mL collection tube and centrifuged at 15,000 rpm for 1 min.
9. The column was placed into a new 1.5 mL collection tube and 30 µL of RNase free water was added. The column was centrifuged at 10,000 rpm for 1 min to elute the purified RNA.

Care was taken to avoid samples becoming degraded so samples were stored on ice whenever possible. Following purification, quantified samples were stored at -80°C until use.

2.5.3 *RNA quantification*

RNA was quantified spectrophotometrically using a Biophotometer (Eppendorf, UK) to establish the concentration of RNA in the samples. A dilution of each RNA sample (2 µL of sample with 68 µL of RNase free water) was produced and placed into a cuvette (Eppendorf, UK). The absorbance at 260 nm was read, with a value of 1 unit at 260 nm at the dilution of 2 µL in 70µL indicating a concentration of 40 µg/mL of RNA or single stranded DNA. Sample purity was also determined by assessing the ratio between absorbances at 260 and 280 nm (A_{260}/A_{280}), with a higher ratio indicating a higher purity (ideal range 1.7+).

2.5.4 *Reverse transcription (RT)*

RT is the process by which cDNA (a DNA strand complementary to the mRNA) is synthesised. RT was performed on samples using the Tetro cDNA Synthesis Kit (Bioline, US) according to the following protocol. Oligo (dT) primer was used to incorporate a sequence of 15-20 thymine bases complementary to the sequence of Adenine bases located at the 3' end of eukaryotic mRNA molecules. Therefore, only mRNA species within the total RNA sample were reverse transcribed due to the fact that other RNA species will not possess poly-A tails.

1. A mastermix was made per sample of the below constituents for each RNA sample processed:
 - 1 µL oligo (dT)₁₈
 - 1 µL 10 nM dNTP
 - 4 µL 5x RT buffer
 - 1 µL reverse transcriptase (200 U/µL)
2. 2 µg of RNA were made up (depending on the quantification result, see Section 2.5.3) per sample to give a final volume of 12 µL in RNase free water in a 0.5 mL Eppendorf plastic tube.
3. 8 µL of mastermix was added per tube.
4. A thermal cycling block (Eppendorf Mastercycler gradient, Eppendorf, UK) was used to incubate samples at 45°C for 30 min followed by 85°C for 5 min. Samples were then held at 4°C.

2.5.5 *Purification and concentration of cDNA*

The resulting cDNA was concentrated and purified to remove unincorporated RT components. RNase free water was added to each sample up to a volume of 500 μ L. This mix was then added to a microcon filter (Amicon 0.5 mL centrifugal filter unit, Millipore, UK) and centrifuged according to the protocol below:

1. Centrifuged at 10,000 rpm for 2 min
2. The level was checked to ensure there was still sample within the filter
3. Centrifuged at 8,000 rpm for 1 min
4. The level was checked again to ensure there was still adequate sample in the filter
5. Centrifuged at 8,000 rpm for 1 min
6. There now should remain approximately 50-60 μ L sample within the filter. The column was then inverted into a new collection tube and centrifuged at 8,000 rpm for 1 min to remove the sample from the filter.

This sequence of filtering ensures cDNA is collected while contaminants are removed in the water which is spun through the filter. The samples were then stored at -20°C until use.

2.5.6 *Semi-quantitative PCR*

Semi-quantitative PCR was performed on agarose gels for all experiments in this work. All samples were prepared using the RedTaq system (Sigma-Aldrich, UK) in 25 μ L reaction volumes in PCR tubes (Eppendorf, UK) as per the following protocol:

- 12.5 μ L RedTaq
- 2 μ L forward and reverse primer mix (primers were purchased from Life Technologies, UK. The primer mix was made by adding 60 μ L RNase free water to 10 μ L of the forward and reverse primer once reconstituted according to the manufacturer's protocol).
- 9.5 μ L RNase free water
- 1 μ L cDNA

The resulting mix was then cycled using the thermal cycling block as before according to the Table 2.8 (altered according to primers used as per information from manufacturer and also according to the amount of target sequence present in the sample):

Reaction stage	Temperature	Time	Repeated cycles dependent upon amount of target sequence
Denaturation	94°C	5 min	
Denaturation	94°C	30 s	
Annealing	Individual to primer	20 s	
Polymerisation	68°C	20 s	
Hold	4°C	indefinite	

Table 2.8 – PCR cycling

Agarose gel preparation and electrophoresis

A 1.5 % agarose gel was prepared in 1 x TAE buffer (40 mM Tris base, 20 mM acetic acid and 1 mM EDTA in distilled water) by adding 0.9 g agarose powder (Bioline, UK) with 60 mL of 1 x TAE buffer. The mixture was heated to boiling point to dissolve the agarose, then cooled slightly before adding 5 µL Web Green Advance DNA Stain (Web Scientific, UK) and mixing. The gel was then poured into a gel tray and sample wells were created using a plastic comb before being left to set at room temperature for approximately 30 min to 1 h.

To run the electrophoresis, the gel was placed in an electrophoresis tank (Fisher Scientific, UK) and immersed in TAE buffer. The sample combs were removed and any resultant air bubbles in the sample wells were gently dislodged. 5 µL of each PCR sample was loaded into each experimental well alongside a DNA ladder (PCRRanger 100bp DNA Ladder, Geneflow, UK) to enable size determination of the DNA products. Electrophoresis was then performed for approximately 20 min at 120 V, or long enough to show adequate band separation before the red tracking dye ran off the gel. After electrophoresis, gel images were captured using the Electrophoresis Documentation and Analysis System (Kodak, UK) under exposure to UV light and analysed using AIDA image analysis software (Fuji, UK).

Sample normalisation

Glyceraldehyde-3-phosphate dehydrogenase (GAPDH) is an enzyme involved in glucose breakdown, and the genetic expression of GAPDH is used as a 'housekeeping' marker to normalise samples of cDNA. This protein should be evenly expressed between samples, therefore if the expression of GAPDH is normalised between samples then any up or down-regulation of other proteins can be attributed to changes within the cells being studied as opposed to the quality or abundance of cDNA within individual samples. An example of normalisation of samples is shown below:

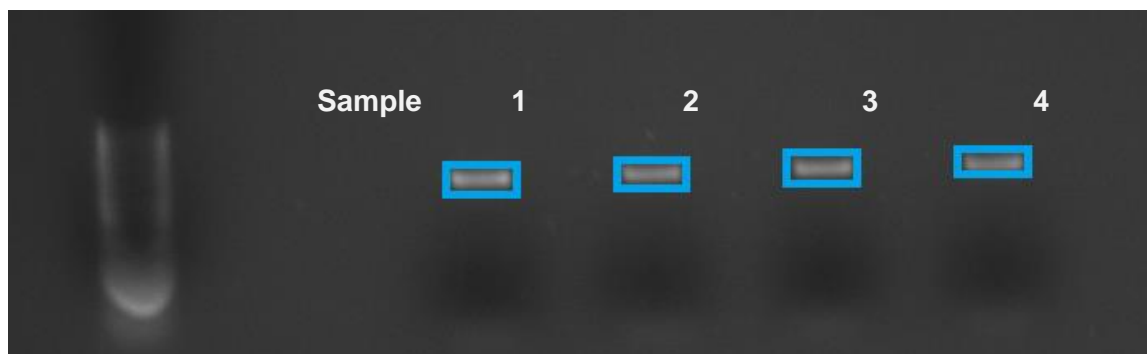


Figure 2.4 – Bands of GAPDH expression selected and the intensity of each 'blot' is generated by AIDA image analysis software. This is then calculated as per the equation below to give the volume of cDNA required from each sample. The brightest blot was used as the band to normalise to. This process is repeated until values within 10-15 % are obtained.

$$\frac{\text{intensity of test band}}{\text{intensity of the brightest band}} \times \text{volume of sample} = \text{volume of cDNA required}$$

Cycle number was also optimised for each different primer and an example is shown in Figure 2.5.

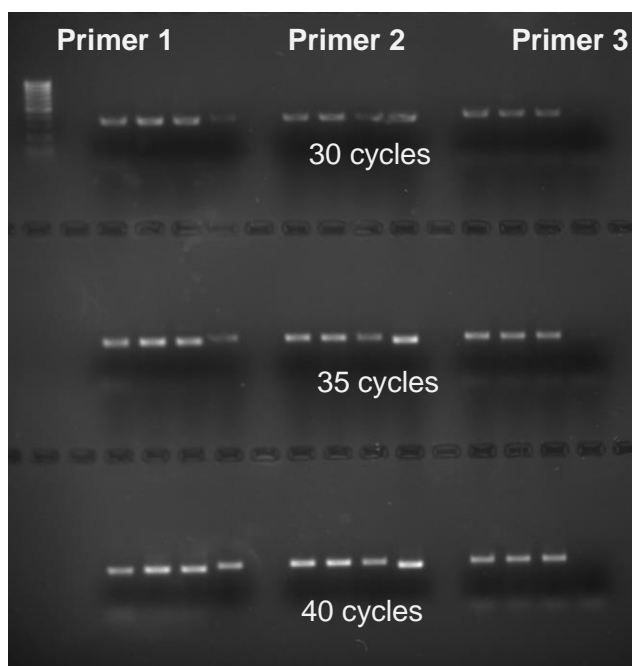


Figure 2.5 – PCR gel image at 30, 35 and 40 cycles for 4 samples and 3 primers tested, showing more definite bars at 35 and 40 cycles compared with 30 cycles for all 3 primers.

Following normalisation of samples according to intensity of initial results and optimisation of cycles for each primer, gels were run accordingly and the intensity of the bands generated gives an approximate quantity of gene product expression, hence “semi-quantitative” PCR.

2.5.7 *Quantitative Real Time Polymerase Chain Reaction (qPCR)*

The PCR method detailed in Section 2.5.6 has limitations due to the fact that it is only semi-quantitative. The alternative method, qPCR, detects changes in protein expression during cycling, instead of identifying an amplification or reduction in gene expression after a set time of cycling. qPCR is carried out in a thermal cycler which can detect the fluorescence emitted by a fluorophore specific to the target protein.

qPCR method and housekeeping gene selection

Reference genes were selected from a panel of targets suggested by the literature. Target genes were chosen to firstly confirm the microarray data findings (see Chapter 6) and secondly to further investigate cytokine expression (see Chapter 7). Specific cDNA primers were purchased (Sigma-Aldrich, UK) as per Table 2.9.

Housekeeping genes	Targets selected
GAPDH	ID1, ID2, ID3 for microarray confirmation
YWHAZ (tyrosine 3/tryptophan, 5-monooxygenase activation protein, zeta polypeptide)	<div>IL8</div> <div>TNFα</div> <div>IL-1β</div> <div>IFN-γ</div> <div>For ELISA comparison</div>
B2M (beta-2-microglobulin)	
ACTB (Beta Actin)	

Table 2.8 – qPCR primers

The thermal cycler used was a Roche LightCycler 480 system. A 96-well microtiter plate (LightCycler® 480) containing a total of 20 μ L per well:

Constituent	Volume in well
cDNA	1 μ L
LightCycler® SYBR green PCR mix (Sigma-Aldrich, UK)	10 μ L
Primers at 0.5 μ M concentration	variable
RNase and DNase free water	variable

Table 2.9 – qPCR reagent mix

The plate was covered, centrifuged for 3 min at 1500 rcf and then placed into the thermal cycler. Samples were amplified in duplicate and two controls for each primer containing no template were included for every run. The cycling protocol is described in Table 2.10, and an example of the output of amplification data in graphical format is in Figure 2.4.

	Temperature (°C)	Time	Cycles
Pre-incubation	98	5 min	1
Denaturation	98	20 s	60
Annealing	60	20 s	60
Extension	72	30 s	60
Melting	98	-	1
Cooling	4	Hold	1

Table 2.10 – The qPCR cycling protocol used.

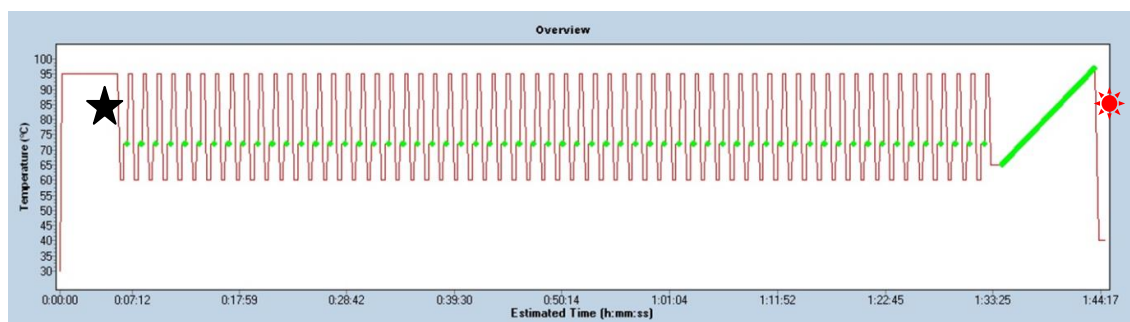


Figure 2.6 - Amplification of YWHAZ gene according to the protocol previously described. Features are: Denaturation (★), Quantification during each denaturing/annealing/extending cycle shown by the green dots, and the melting of the product (☀).

Following cycling, data were gathered and analysed following the manufacturer's instructions from crossing point (Cp) values by methods within the thermal cycler's software (Roche diagnostics version 1.5). The housekeeper gene data were inputted into the BestKeeper algorithm (Pfaffl et al., 2004), and using information on the expression of each housekeeper gene, a panel of results for each is analysed (Cp values, standard deviation and coefficient of variance), and the most appropriate housekeeper for the target cells is recommended. The data generated by BestKeeper are shown in Figure 2.7. The lowest standard deviation implies the most consistent gene, therefore YWHAZ was chosen as an appropriate housekeeper gene from this panel, and used as a reference gene for quantification of the target genes.

	GapdH	YWHAZ	B2M	ACTB
n	9	9	9	9
geo Mean [Cp]	17.31	17.65	19.36	19.50
ar Mean [Cp]	17.32	17.65	19.37	19.50
min [Cp]	16.79	16.73	18.88	19.03
max [Cp]	18.75	18.47	20.70	20.90
std dev [± Cp]	0.40	0.33	0.43	0.39
CV [% Cp]	2.34	1.89	2.20	1.99
min [x-fold]	-1.39	-1.80	-1.38	-1.40
max [x-fold]	2.50	1.69	2.44	2.72
std dev [± x-fold]	1.29	1.24	1.31	1.28

Table 2.11 - Cp data of housekeeping genes

qPCR results and analysis

A set of curves is generated for each gene. Figure 2.7 shows the amplification curve, standard curve and melt curves for the YWHAZ housekeeping gene.

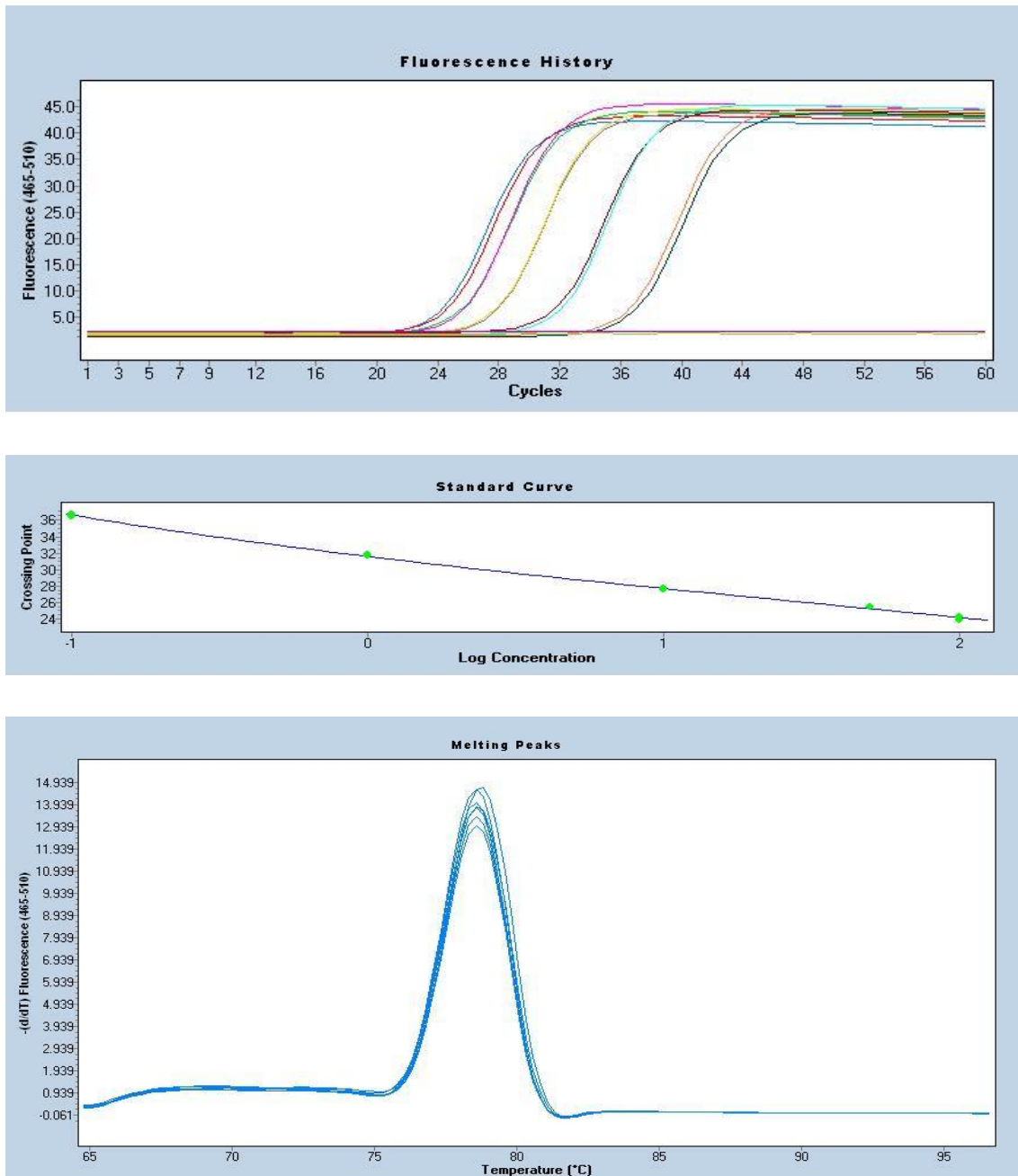


Figure 2.7 – Amplification curve, efficiency standard curve and melt curve for YWHAZ housekeeper gene. The amplification curve is of a series of dilutions of YWHAZ and two no-template controls (flat lines), and this information was used to generate the standard curve by the LightCycler® 480 software. An efficiency of 2.0 is considered to be 100% efficient in this context, and the efficiency of the above curve is 1.93. The melt curve shows a single peak, ensuring that only the target is being amplified by the primers. These curves are produced for each reference gene and target gene.

2.6 Immunocytochemistry

Immunocytochemistry (ICC) is a method where antibodies to specific cellular antigens are counterstained with a label to permit visualisation of either the presence or absence of the target antigen, or localisation of the antigen within a cell. Different labels can be used, for instance fluorescent conjugates or stains visible under light microscopy. These labels can be directly conjugated to the antibody in the case of direct ICC or immunofluorescence (IF), or indirectly linked via a third molecule in the case of indirect ICC or IF.

The method used in this thesis was based on indirect staining of the target antigen with a brown stain visible under light microscopy called the biotin-streptavidin amplified technique (SuperSensitive® Link-Detection Kit, BioGenex). The staining mechanism has been previously used to investigate NFκB activation (Milward et al., 2007, Milward et al., 2013) as the translocation of NFκB from the cytoplasm to the nucleus of activated cells can be visualised using this method. The effects of TiO₂ NPs both alone and alongside known NFκB activating factors was investigated by the following method.

2.6.1 *Staining for NFκB activation using the SuperSensitive® Link-Detection Kit overview*

The protocol for staining described below has four main stages to allow visualisation of the location of NFκB within cells.

- The first stage requires a primary antibody to link to the target antigen (NFκB in this case).
- The second stage involves a link immunoglobulin which specifically binds to the primary antibody.
- The third stage is where a streptavidin label binds to the link molecule and expresses horseradish peroxidase (HRP).
- The final stage is the addition of diaminobenzidine (DAB), a clear stain which oxidises on exposure to peroxide in the label molecule to produce a brown precipitate visible by light microscopy.

Figure 2.8 is a diagrammatic representation of the indirect ICC staining method. After staining with DAB, the nuclei of the cells were counterstained using Mayer’s haematoxylin to allow better visualisation of any translocation of NFκB into the nuclei of the cells during activation. The reagents for this staining system are supplied in kit form from BioGenex. A test was carried out to optimise the use of this system and ascertain the optimum incubation times for the DAB and haematoxylin.

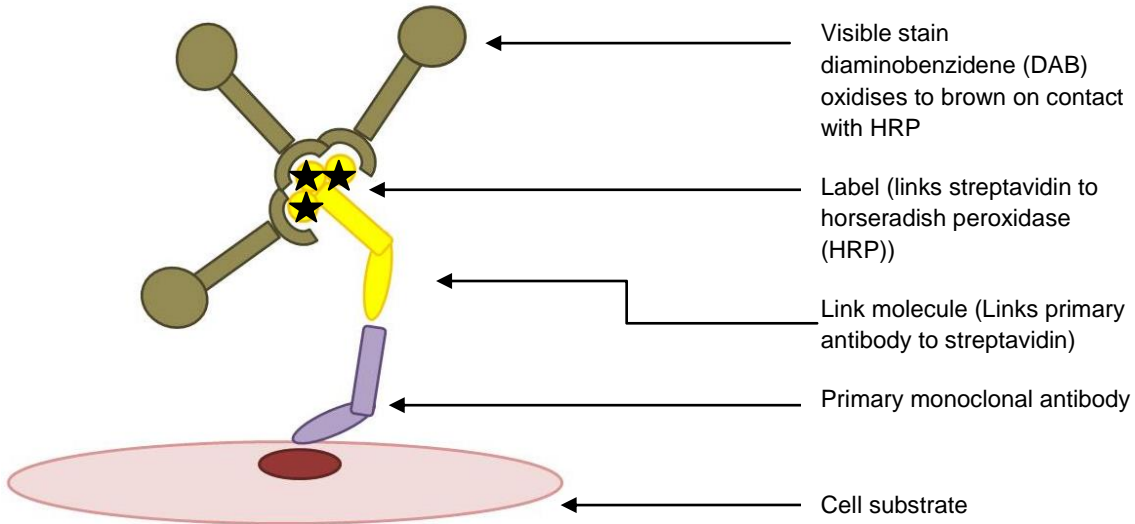


Figure 2.8 – Diagrammatic representation of an indirect ICC system.

Each slide contained a positive and negative control well to ensure that the staining protocol had worked successfully and that any staining seen is likely to be a true result. Figure 2.9 illustrates the layout of each slide.

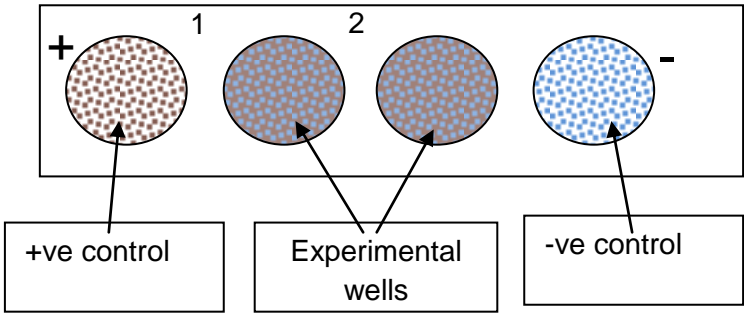


Figure 2.9 – layout of multiwell slides for ICC. Positive control incubated with Ki-67 antibody, negative control incubated with PBS/BSA only.

Positive control: The left well was treated with a monoclonal antibody to the Ki-67 nuclear protein. The expected result would be brown staining confined to only the nucleus of the cells in this well, as Ki-67 is not expressed in the cytoplasm of human cells. Any brown staining in the cytoplasm would therefore imply cross contamination between wells of primary antibodies or a lack of specificity in the staining system.

Negative control: The right well was treated with PBS BSA (1 %) in the place of a primary antibody, therefore the expected result would be no brown staining in the cells. Any brown staining in this well would imply cross contamination of antibody or a lack of specificity in the staining system. Both positive and negative control wells were counterstained with Meyer's haematoxylin so should have blue staining visible in the nuclei.

ICC NFκB staining protocol using the SuperSensitive® Link-Detection Kit (SS L-D)

1. H400 cells were grown on 4 well slides (Hedley-Essex, UK) until approximately 70 – 80 % confluent. Cells were seeded directly into the wells on cleaned 4 well slides at a concentration of 4×10^5 cells in 15 mL supplemented DMEM. The slide was placed into an autoclaved glass petri dish and incubated as described in Section 2.2.2. The glass petri dish and slides were autoclaved prior to use to prevent contamination. The DMEM was changed at day 4 under aseptic conditions as previously described. Cells were cultured for 5 days prior to use to minimise the potential stimulatory effects of passage and re-seeding cells on any inflammatory pathways.
2. Cells were stimulated as described in Section 2.6.2, then removed from the dish and washed quickly in chilled PBS ($4 \pm 1^\circ\text{C}$).
3. Slides were fixed in dry acetone (Sigma-Aldrich, UK) at room temperature for 15 min and then allowed to air dry for 10 min at room temperature.
4. Following fixation, the wells in each slide were circled with a water repellent pen (Sigma-Aldrich, UK) to decrease the likelihood of cross contamination between wells. Primary antibodies were then added to each well as follows:
 - a. Positive control: 100 μL Clone MM1 antibody to Ki-67 (Novacastra™, UK) at a dilution of 1:100 in PBS BSA 1 %.
 - b. Negative control: 100 μL diluent only.

- c. Experimental wells: 100 μ L monoclonal antibody to NF κ B p65 subunit (Clone F-6, Santa Cruz Biotechnology, US) at a dilution of 1:100 in PBS BSA 1 %.
5. Slides were placed in a humidity box at room temperature for 1 h. After this stage, the slides were not allowed at any point to dry.
 6. After 1 h, the antibody was tipped quickly away to prevent cross contamination, and the slides were washed in fresh PBS 3 times for 2 min and gently agitated on an orbital mixing platform.
 7. Every well was then treated with 2-3 drops of 'Link' reagent from the SS L-D. Care was taken to ensure the whole of the well was covered. The slides were incubated for 20 min at room temperature as per the manufacturer's instructions.
 8. Slides were washed as before (step 6) then 2-3 drops of 'Label' from the SS L-D was added to each well. Care was taken to ensure the whole of the well was covered. The slides were incubated for 20 min at room temperature as per the manufacturer's instructions.
 9. Slides were washed as before (step 6) then 2-3 drops of freshly prepared DAB reagent (2 drops of 'Chromagen' added to a 2.5 mL vial of 'Substrate Buffer' from the SS L-D) was added to each well. Care was taken to ensure the whole of the well was covered. The slides were incubated for 5 min at room temperature (optimum time ascertained by initial testing).
 10. Slides were then washed under running water for 2 min and counterstained with 'Haematoxylin' from the SS L-D for 5 min (optimum time ascertained by initial testing).
 11. Slides were then washed in running deionised water for 2 min, then dehydrated through graded alcohol baths and cleared in xylene (Sigma-Aldrich, UK) before being mounted in XAM mounting medium. Slides were kept in the dark and horizontally for a day after mounting to prevent any movement of the mounting medium or coverslip before it was fully dry.

2.6.2 Stimulation of H400 cells prior to ICC

Prior to staining, the cell culture medium was changed on day 4 post-seeding. Old medium was aspirated from the petri dish and discarded, and 15 mL of warmed fresh medium was pipetted into the dish with minimum disruption to the slide. In the case of cells being exposed to TiO₂ NPs, cell culture medium containing 10 ppm anatase NPs (prepared as before) was substituted for plain medium. Cells were stained as per the above protocol on day 5 post seeding. 1 h prior to staining, cells were stimulated as indicated in the table below to activate NFκB nuclear translocation.

E. coli LPS was purchased from Sigma-Aldrich, diluted to a stock concentration of 1mg/mL, and stored in aliquots at -20°C prior to use.

Condition	Stimulant and concentration
Control	Warmed DMEM 300 µL into 15 mL in dish to mirror LPS or FN fluid addition
LPS	<i>E. coli</i> LPS (Sigma-Aldrich, UK) final concentration of 20 or 40 µg/mL in cell culture medium
FN	<i>Fusobacterium nucleatum</i> (heat killed) at a multiplication of infection (MOI) of approximately 100 bacteria per epithelial cell (see Section 2.9.5)

Table 2.12 - Concentrations of stimuli for H400 cells prior to immunocytochemistry staining

2.6.3 Quantification of NFκB translocation

Cell counts were performed using colour images captured by a Zeiss Primovert microscope and a Retiga camera (standard settings) and then analysed using FIJI (ImageJ) software 1.49k (National Institutes of Health, Bethesda MD, USA).

Before cell counts were performed, the positive and negative control wells were studied to ensure they showed the expected results (Figures 2.10 and 2.11):

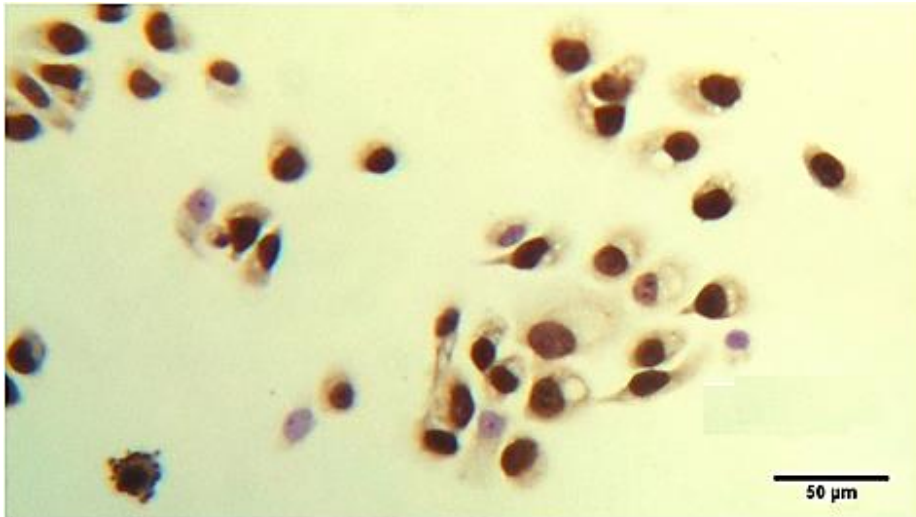


Figure 2.10 - Expected result showing **positive control** for immunocytochemistry (Ki67) well demonstrating DAB staining localised to the nucleus and minimal staining in surrounding cytoplasm.

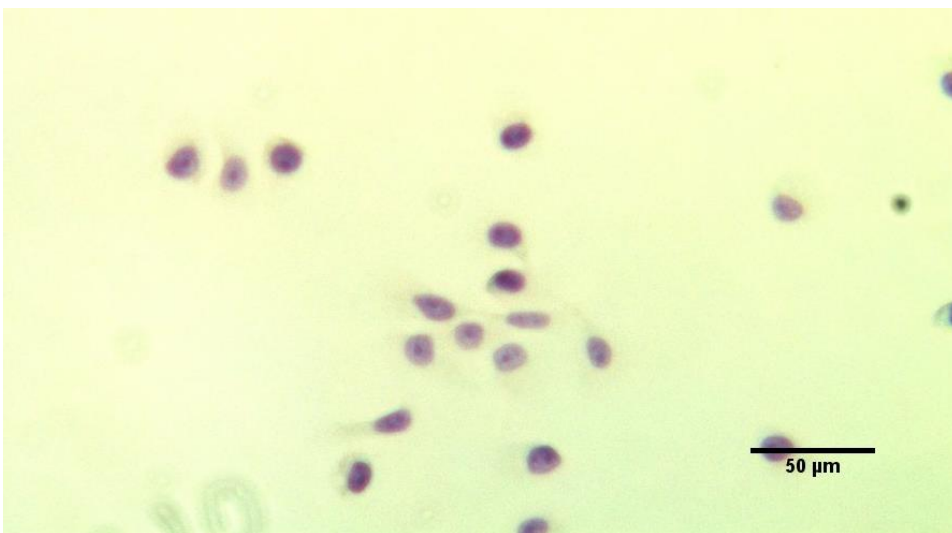


Figure 2.11 - Expected result showing **negative diluent control** demonstrating an absence of DAB staining when the primary antibody is omitted.

Experimental slides were analysed by blinded cell counts as per the images below. Labelled folders of images were given pseudonyms by a third person before counts were performed. Sets of 50 cells taken from the top right of 10 randomly selected areas of the slides were counted and classified as positive or negative. These numbers were then plotted to form Hunting curves to determine how many sets of 50 cells needed to be counted to produce an accurate estimate of the percentage of cells activated.

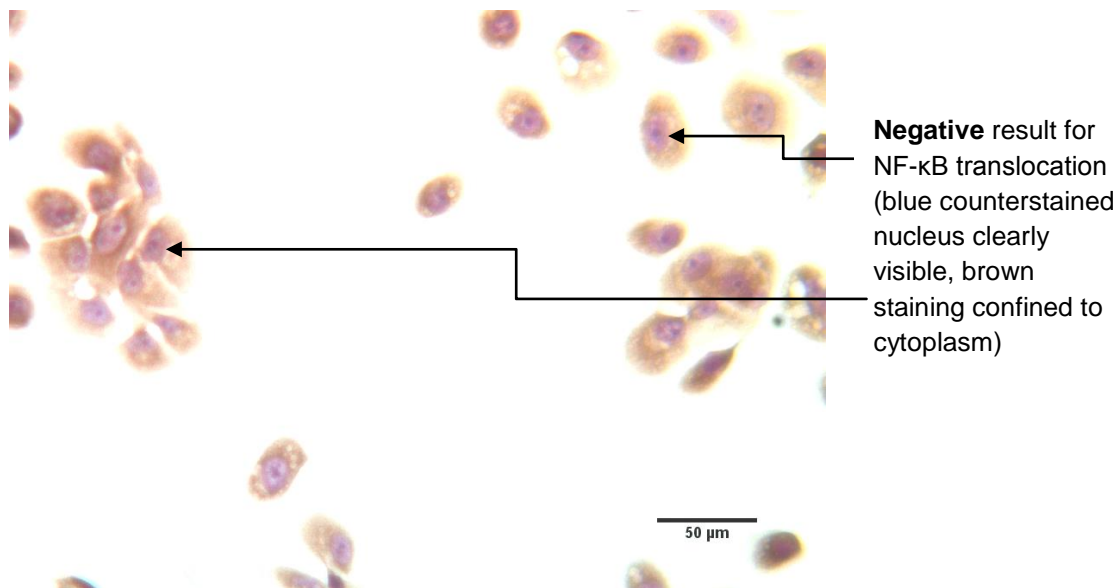


Figure 2.12 - Control well from stained NFκB slide. DAB stained NFκB can be seen in the cytoplasm with minimal translocation to the nucleus.

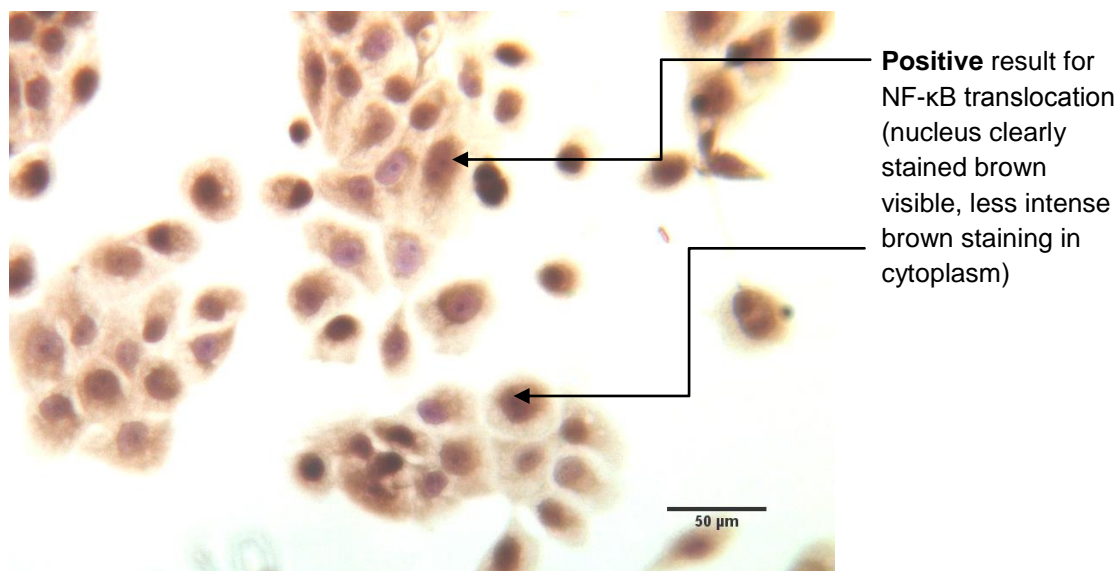


Figure 2.13 – *E. coli* LPS stimulated well from a slide. DAB stained NFκB can be seen translocated to the nucleus, meaning the blue haematoxylin counterstain is no longer clearly visible and nuclei are stained brown. The DAB stain intensity in the cytoplasm is reduced.

In situations where translocation was not clear, cells were counted as negative to minimise the incidence of false positives. Manual cells counts were performed to identify numbers of “positive” and “negative” cells. The number of fields that required cell counts to produce a representative indication of NFκB translocation was determined using Hunting curves.

Hunting curves:

An example of the Hunting curve produced is below. Each graph showed that a reliable mean of positively stained cells was reached after 10 counts of 50 cells. 50 cells were chosen as the number to count on each image. Where there were many more cells present, the 50 cells to the left of the image were counted. If there were fewer the image was discarded.

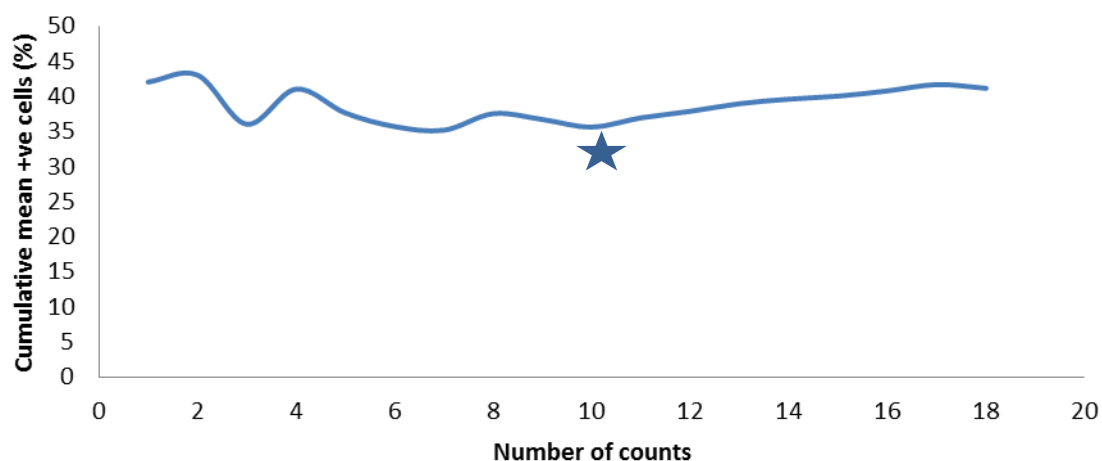


Figure 2.14 – Hunting curve showing cell counts against cumulative mean of percentage of positively stained cells showing 10 counts of 50 cells is adequate for quantification of NFκB activation. This result was consistent between each condition (control and experimental wells).

2.7 Immunofluorescence staining of cultured cells

Indirect immunofluorescence (IF) works on the same principle as immunocytochemistry, however, the stain used is a fluorescent conjugate and visualised using fluorescence microscopy. This method was used to identify the presence of epithelial specific markers (cytokeratins) in tissue grown out from epithelial cell biopsies to ensure the outgrowth was epithelial and not mesenchymal in origin.

The primary antibody chosen must be cross reactive with the species that the cells or tissue were derived from (e.g. anti-cytokeratin IgG produced in mouse). The secondary antibody must be specific to the primary antibody (e.g. goat anti-mouse IgG) and conjugated to a fluorescent label (e.g. FITC).

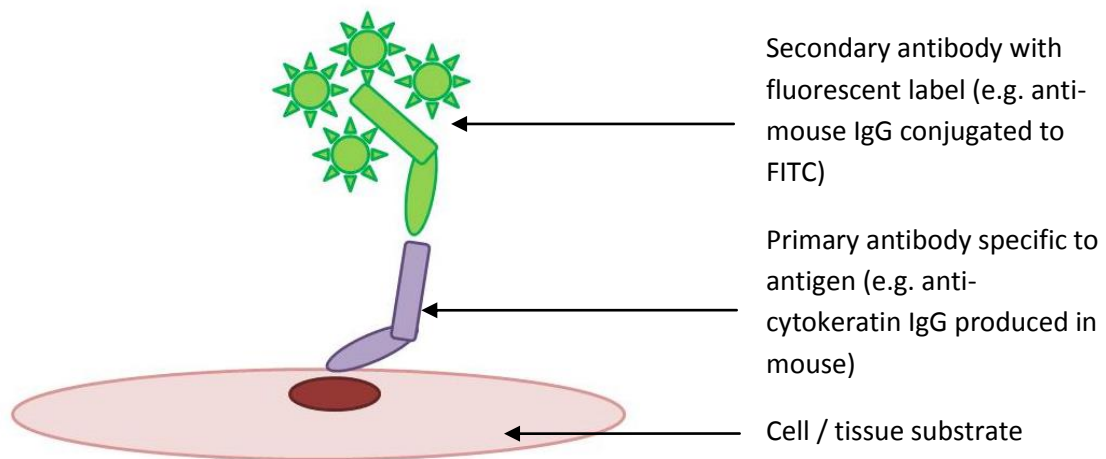


Figure 2.15 - Diagram of indirect immunofluorescence.

1. Coverslips (#1.5 thickness, 13 mm diameter, Scientific Laboratory Supplies, Nottingham, UK) with attached cells were washed 3 times with PBS.
2. Coverslips were fixed in neutral buffered formalin 10 % (Sigma-Aldrich, UK) for 10 min at room temperature, then washed 3x with PBS as before.
3. Coverslips were then washed 3 times with PBS BSA (1 %).
4. A staining tray (large Petri dish, Corning, UK) was lined with a piece of Parafilm®M (Sigma-Aldrich, UK). 50 µL diluted primary antibody was placed on the film, and the coverslip inverted onto the droplet, cell side down.
5. The coverslips were incubated at room temperature away from light for 1 h, then washed in PBS 3 times as before.
6. 50 µL diluted secondary antibody was placed on fresh film, and a coverslip was placed cell side down onto the antibody drop.
7. After incubating for 45 min at room temperature away from light, a glass slide was prepared by placing a drop of Fluoroshield® with DAPI mounting medium (Sigma-Aldrich, UK) onto the surface. The coverslip was washed 3 times in PBS, dried by gently blotting the edge of the coverslip onto tissue, and mounted onto the slide using Fluoroshield® mounting medium with DAPI

(Sigma-Aldrich, UK). The slide was then stored in the dark until dry, and then at -20°C for longer term storage.

2.8 Microscopy techniques

The overall strategy for imaging epithelial cells was to use a variety of methods to image different potential interactions between TiO₂ NPs and either H400 or primary oral epithelial cells. Simple light microscopy enabled visualisation of agglomerations of TiO₂ NPs even following repeated washing of the cell monolayer, however any further visualisation of potential interactions by this method was limited. The capability of visualising interactions in the form of intracellularisation, membrane interactions, internal cell structure and the impact on cellular morphology cannot be provided through one technique alone. Transmission electron microscopy (TEM) was therefore used as a method of cellular imaging as it enables imaging of sectioned cells, thereby allowing visualisation of intracellular structures. Confocal reflectance microscopy was also employed to locate agglomerations of nanoparticles associated either with the cell membrane or intracellularly.

2.8.1 TEM

TEM was used to investigate the appearance of epithelial cells both before and after exposure to Ti stimuli. TEM is a microscopy technique which uses an electron beam to pass through thin sample sections, and is capable of imaging at far higher magnification and resolution than light microscopy. The method however relies upon a complex sample fixation (which may introduce artefacts) and sectioning protocol, and is relatively time consuming to capture images of a good quality and quantity in the context of biological samples. It is necessary to find cleanly sectioned cells which have not been creased or damaged during processing. However, this technique can successfully be used to visualise intracellular structures in detail.

Cell fixation and processing prior to TEM

1. Cells were cultured in appropriate cell culture treated plasticware as previously described. After stimulation with the selected Ti species for a

predetermined time, cell monolayers were washed with warmed PBS (Gibco, UK) 3x to remove as much loose Ti product as possible.

2. Cells were then treated with trypsin-EDTA as previously described for 10 min at 37 °C and 5 % CO₂ and gently agitated to detach from the plasticware.
3. The resulting cell suspension was then transferred to a sterile universal container with an equal volume of warmed supplemented DMEM and centrifuged for 10 min at 1000 rpm.
4. The supernatant was removed and discarded and the resulting cell pellet was re-suspended in an appropriate volume of freshly prepared chilled 2.5 % gluteraldehyde fixative (CEM, University of Birmingham). This was worked out at a ratio of 1 mL fixative per 1×10^6 cells.
5. Cells were kept in fixative at 4°C until transported to the Centre for Electron Microscopy (CEM) at the University of Birmingham. The time in fixative can be between 1 h and several days. Where possible, the samples in this thesis were kept in fixative for less than 3 days.
6. Samples were further processed by staff of the CEM according to the following protocol:
 - a. Secondary fixation in 1 % osmium tetroxide for 1 h.
 - b. Dehydration through graded alcohols – 50, 70, 90 and 100 % alcohols for 2x 15 min each, followed by propylene oxide for 2x 15 min.
 - c. Following dehydration, samples were embedded in propylene oxide: resin at a ratio of 1:1 on a rotator followed by pure resin for 1 h on a rotator.
 - d. Samples were then positioned just under the surface of the resin in embedding moulds and placed in a vacuum for 30 min before allowing back to atmospheric pressure.
 - e. The resin was then polymerised at 60°C for at least 16 h.
 - f. Sectioning of samples at a thickness of 50 – 15 nm was performed using a diamond blade and placed onto electron microscope grids (Formvar film with carbon coating).
7. Following processing, TEM samples were stored in the dark at room temperature prior to examination using a Jeol 1200EX transmission electron

microscope (Jeol, USA) at a power of 80 keV and between x2,000–x10,000 magnifications.

2.8.2 *Reflectance confocal microscopy*

This method of imaging uses a combination of light microscopy to capture a confocal stack of images through a sample and a reflectance mode which can image the reflectance of a specific target particle. In this case, TiO₂ NP agglomerations were imaged using the reflectance mode. The light microscopy and reflectance images are then merged to provide a composite image allowing localisation of the target particle within a tissue.

To obtain the reflectance image, TiO₂ NPs were imaged in the absence of any cells in the reflectance mode, and the microscope was calibrated to the settings which would best visualise these agglomerations. A control cell monolayer was then imaged using the reflectance mode, and this background reflectance was subtracted from the subsequent images captured, therefore allowing visualisation of TiO₂ NP agglomerations within a confocal stack of images. The same stack of images is then captured using light microscopy for orientation of where within the cell the TiO₂ signal is captured.

This technique requires cells to be adherent to a coverslip then fixed before visualisation. The method for culturing and fixing epithelial cells for this technique is listed below.

1. H400s were cultured on sterile coverslips (#1.5 thickness, 13mm diameter, SLS UK) placed into the base of a 6 well cell culture plate. Cells were grown until near confluence, determined by using light microscopy.
2. Cell culture medium was then removed and replaced with media containing 0, 1, 10 or 100 ppm TiO₂ NPs (<25nm diameter) prepared as described in Section 2.1 and incubated for 0, 3, 6, or 9 h.
3. Coverslips were then removed from media, washed 3 times in PBS to remove as much excess anatase as possible, and fixed as per the following protocol:
 - a. Coverslips were immersed in formalin (Sigma-Aldrich, UK) at room temperature for 15 min.

- b. The formalin was then neutralised with NH_4Cl 50 mM (Sigma-Aldrich, UK) in PBS for 7 min.
- c. Coverslips were then washed with fresh NH_4Cl 50 mM once and with room temperature PBS twice.
- d. The coverslips were inverted and mounted on plain glass microscope slides (Hedley Essex, UK) using one drop of Fluoroshield™ with DAPI (Sigma-Aldrich, UK) and air dried in a dark drawer. The edges of the coverslips were then sealed with nail polish.

Each sample was then examined using a confocal microscope (Carl Zeiss Microscopy, Oberkochen, Germany) using 488 nm and 543 nm lasers and an oil objective lens. Reflectance images were captured using an A1R inverted confocal microscope (Nikon Corporation, Tokyo, Japan). Cells were randomly selected and a point in the middle of the z-stack was chosen following identification of the nucleus to ensure images were truly intracellular. The resulting images were captured as TIFF files and analysed using FIJI (ImageJ) software 1.49k (National Institutes of Health, USA).

2.9 *ROS (Reactive Oxygen Species) production by neutrophils*

Neutrophils release ROS as part of their role in the innate immune system to protect the host from pathogenic bacterial challenge. Neutrophil responses can be measured *in vitro* by stimulating harvested neutrophils and measuring ROS release.

Recruitment of neutrophils to the periodontal / peri-implant tissues occurs in response to molecular signals (chemokines) released at the site of injury. Historically it was thought that epithelial cells were simply a barrier cell, and that the sole function of epithelium was to provide a mechanical barrier to injury, be it physical or bacterial. However, there is a mounting body of evidence highlighting a role for epithelial cells to generate a pro-inflammatory response when stimulated, by releasing a variety of both pro and anti-inflammatory cytokines to signal to other cell types including neutrophils. Epithelial cells, specifically H400 cells, have been shown to produce specific cytokines (TNF α , IL-1 β , IL8, MCP-1/CCL2 and GM-CSF) (Milward et al., 2007) in response to a pathogenic challenge. IL8 in particular is important in the recruitment of neutrophils (Milward et al., 2007), therefore the hypothesis for this part of the work

was that cytokines may be produced by H400 cells in response to exposure to Ti products which could potentially promote an innate immune response via neutrophil recruitment.

Primary neutrophils have an *ex vivo* life expectancy of up to 24 h (Ling et al., 2015) and are described as relatively fragile (Payne et al., 1994), therefore may not seem the ideal cell to use *in vitro*. However, some cell lines (such as HL60) have proven to inadequately respond in the same way as freshly isolated primary neutrophils so fail to offer a suitable model to study neutrophil responses. Therefore, this study used primary neutrophils harvested from donors to investigate cellular responses. However, it must be remembered that one of the issues with using cells harvested from human donors is the intra- and inter- donor variability in biological responses.

The ROS production by neutrophils from healthy donors in response to various stimuli was investigated using luminescence assays. Luminol as a substrate produces a light output proportional to the total amount of ROS production by activated neutrophils and is a well-documented technique (Kopprasch et al., 2003) and is detailed in Figure 2.16. Cell membranes are permeable to luminol, therefore both intracellular and extracellular ROS are detected. Isoluminol, a similar substrate to luminol, is also oxidised by ROS to form aminophthalate, but is less able to transverse cell membranes due to the position of the amino group within its structure when compared with luminol (Lundqvist and Dahlgren, 1996). Therefore, isoluminol detects extracellular ROS only.

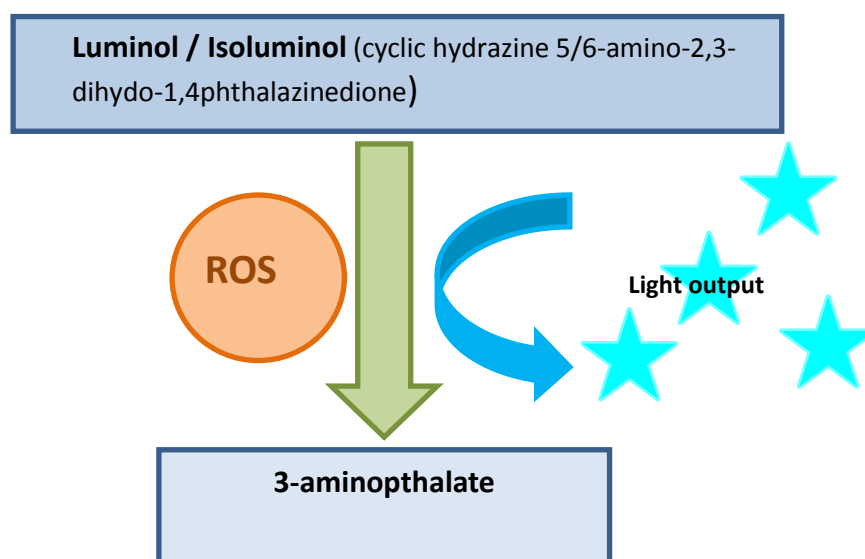


Figure 2.16 – diagram of the ROS luminol/isoluminol based assay.

For assays using isoluminol, supplementary horseradish peroxidase was added to amplify the chemiluminescence, and effectively replaces the intracellular myeloperoxidase which catalyses luminol during intracellular ROS detection. The principal ROS measured by luminol and isoluminol is HOCl, a downstream ROS from superoxide and hydrogen peroxide (Chapple and Matthews, 2007).

2.9.1 Neutrophil isolation reagent preparation

Percoll gradient preparation

Percoll (GE Healthcare UK) densities were prepared as per Table 2.13

	Density 1.079	Density 1.098
Percoll (mL)	19.708	24.823
H₂O (mL)	11.792	6.677
NaCl 1.5M (mL)	3.5	3.5

Table 2.13 – Percoll densities

6 mL of 1.079 density Percoll was carefully layered over 6 mL of 1.098 density Percoll in a 25 mL sterile universal tube (Fisher Scientific UK). These tubes were stored at room temperature for up to 2 h before neutrophil isolation commenced or refrigerated overnight at 4 °C then equilibrated to room temperature before use.

Lysis buffer preparation

Lysis buffer was prepared as below and stored at 4 °C prior to use.

NH₄Cl (Sigma-Aldrich UK)	8.3 g
KHCO₃ (Sigma-Aldrich UK)	1.0 g
EDTA 2H₂O (Sigma-Aldrich UK)	0.04 g
Bovine serum albumin (Sigma-Aldrich UK)	2.5 g
Endotoxin free sterilised water (Versol, Aguetant UK)	1000 mL

Table 2.14 – lysis buffer

Neutrophil isolation protocol

1. Blood was collected from volunteer donors who were not currently taking any anti-inflammatory or anti-microbial medication in 6 mL heparin anticoagulant vacutainers (Greiner UK). Ethical approval (number 10/H1208/48) was in place and all volunteers gave informed consent.
2. 6 mL blood was layered gently over the prepared Percoll gradients using a Pasteur pipette. This was centrifuged for 8 min at 150 rcf followed immediately by 10 min at 1200 rcf (Hettich Universal 320R).
3. Following centrifugation, the layers of separation are as below:

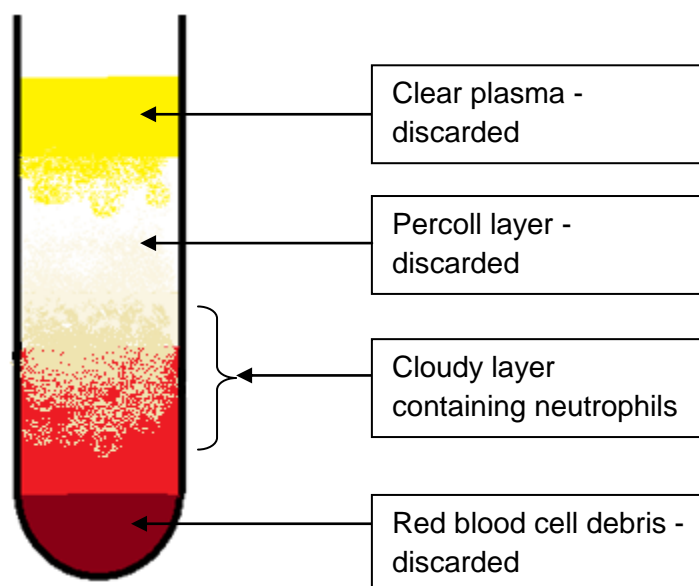


Figure 2.17 – Diagram of Percoll blood separation tube following centrifugation indicating layers generated; notably the cloudy layer containing neutrophils.

The neutrophil containing layer was then transferred into a 50 mL centrifuge tube (Fisher Scientific UK) containing 30 mL lysis buffer.

4. The tube was mixed gently and incubated at room temperature for 6 min or until the cloudy appearance had transformed into a non-turbid solution.
5. The tube was then centrifuged at 500 rcf for 6 min.
6. Following aspiration of supernatant, the resulting neutrophil pellet was re-suspended in approximately 3 mL lysis buffer, mixed gently and incubated for 5 min at room temperature before repeating centrifugation at 500 rcf for 6 min.
7. Following aspiration of the supernatant, the resulting cell pellet was re-suspended in 2 mL PBS (as previously described) and centrifuged at 500 rcf for 6 min in order to remove residual lysis buffer from the neutrophil suspension.
8. Following aspiration of the supernatant, the resulting cell pellet was re-suspended in 2 mL PBS and neutrophils were counted using a haemocytometer and viability determined using trypan blue dye exclusion as previously described (Section 2.2.2).

2.9.2 *ROS generation assay reagent preparation*

Luminol and isoluminol preparation

A 30 mM stock solution of each reagent was prepared by dissolving 0.5 g luminol (Sigma-Aldrich UK) or isoluminol (Sigma-Aldrich UK) in 94.05 mL 0.1 M NaOH. These were stored at 4 °C in the dark prior to use.

When required, a working solution was prepared by diluting 1 mL stock solution in 9 mL PBS (as before) and adjusting the pH to 7.3 as necessary.

Horseradish peroxidase (HRP) preparation

A master stock solution was prepared by dissolving 1000 units HRP (Sigma-Aldrich UK) in 1.0 mL PBS (as before). This was stored at -20°C in aliquots of 105 µL. When required, an aliquot was defrosted and 945 µL PBS was added.

2.9.3 *ROS assay protocol*

1. White, solid bottomed 96-well plates (Appleton Woods UK) were used to perform this assay. Both luminol and isoluminol were used in the same plate if required. Plates were pre-blocked with a 1 % BSA (Sigma-Aldrich UK) solution in PBS overnight at 4 °C to minimise neutrophils adhesion.
2. The plates were washed with fresh PBS before use using a microplate washer (BioTek ELx50).
3. Reagents were added to wells as required.

Reagent	Luminol assay	Isoluminol assay
Luminol	30 µL	-
Isoluminol	-	60 µL
Glucose PBS	45 µL	-
Horseradish Peroxidase (HRP)	-	15 µL
Cell suspension (1×10^5 per well)	100 µL	100 µL
Total volume:	175 µL	175 µL

Table 2.15 – ROS assay protocol

4. The cell suspension was added and the plate was placed into a luminometer (Berthold LB96v) at 37°C for 30 min. Readings were taken every 3 min to generate a background luminescence reading using Winglow software (Berthold Technologies, Bad Wildbad, Germany). This stage ensures any initial stimulation of neutrophils arising from handling and seeding into the plate does not adversely affect any stimulus response.
5. 25 µL stimulus or PBS for negative controls was then added to each well to give a total volume of 200 µL. The luminescence was then read every 3 min for 2 h 30 min and the data collected as before or every 90 s if half a plate was used. If neutrophils were to be primed prior to stimulation 10 µL of primer was added after 30 min, and then neutrophils were stimulated after a further 30 min.

2.9.4 *Preparation of bacterial stimuli*

A number of bacteria were cultured and prepared as neutrophil stimulants for the ROS assay and to investigate cellular responses in the presence of bacterial products.

Fusobacterium nucleatum ssp Polymorphum (FN)

FN is a Gram-negative periodontal pathogen (Settem et al., 2012, Roques et al., 2000), reported to activate neutrophils and epithelial cells via Toll Like Receptors (TLRs) (Kikkert et al., 2007), therefore was highly relevant in this work. Aliquots of heat killed *FN* (American Type Culture Collection [ATCC] 10953) were supplied as a gift from Dr Mike Milward at the University of Birmingham and stored until use at $-20 \pm 1^{\circ}\text{C}$.

Porphyromonas gingivalis (Pg)

Pg is an important Gram-negative anaerobic periodontal pathogen associated with periodontal destruction (Hajishengallis et al., 2011) falling in to the red category of Socransky's classification (Socransky et al., 1998). *Pg* (strain W83) aliquots were supplied as a gift from Dr Mike Milward at the University of Birmingham and stored until use at $-20 \pm 1^{\circ}\text{C}$.

Opsonised Staphylococcus aureus (Ops Sa)

Sa is a Gram-positive bacterium commonly found on the skin and in the oral cavity of healthy individuals. *Sa* has however been isolated at higher levels from pockets of patients with aggressive periodontitis as opposed to chronic periodontitis (Fritschi et al., 2008), and *Sa* also elicits a strong neutrophil response (Brinkmann et al., 2004). *Sa* was opsonised to increase the neutrophil recognition of test bacteria (Voyich et al., 2005). *Sa* (National Collection of Type Cultures 6571, Fisher Scientific) was cultured by inoculation of a mannitol salt agar plate (OXOID) and cultured overnight aerobically at $37 \pm 1^{\circ}\text{C}$, 5% CO_2 . Bacterial colonies were then transferred to a sterile Pyrex bottle containing 500 mL sterile tryptone soya broth (OXOID) using a sterile plastic loop. The broth was cultured overnight (as before) and the resulting culture was divided into 10 50 mL sterile centrifuge tubes (Fisher Scientific) before being subject to the following centrifuge and wash protocol:

- 10 min at 700 rcf then removal of the supernatant
- Pellet was re-suspended in 20 mL sterile PBS (see 2.2.1) and vortexed to redistribute the bacteria
- Resulting suspensions were pooled and centrifuged twice to produce two bacterial pellets

- The pellets were then re-suspended in 20 mL 10 % neutral buffered formalin (Sigma-Aldrich, UK) for 1 h at $22 \pm 1^\circ\text{C}$
- Centrifugation and re-suspension in PBS was repeated twice to remove the fixative
- Bacterial concentration of the resulting suspension was measured by optical density using a spectrophotometer and a look-up table generated in house (Roberts et al., 2002) and diluted in PBS to achieve a concentration of 2.8×10^7 bacteria per 50 mL tube.
- To opsonise the bacteria, tubes were heat treated at 80°C for 20 min followed by the addition of Vigam at a concentration of $33 \mu\text{L}$ per 10^9 cells (a reagent containing active human IgG (Bio Products Laboratory) and incubated overnight on a shaker (Stuart Scientific S120H).
- Following opsonisation bacteria were washed twice more and stored in 1 mL aliquots at $-80 \pm 1^\circ\text{C}$ until use.

2.9.5 Chemotaxis assay

Chemotaxis is defined as the movement of a cell or organism in response to a chemical stimulus gradient established in their local environment. Chemotaxis differs from chemokinesis, which is non-directional movement, while chemotaxis is a directional kinesis of a cell or an organism towards a chemoattractant along a chemical gradient. Neutrophils have been shown to be able to move in response to chemical stimuli in an *in vitro* situation, simulating the *in vivo* response whereby neutrophils are recruited from the peripheral blood supply to an area that is infected or colonised by bacteria. Neutrophils can then fulfil their role in phagocytosis and ROS production to eradicate invading micro-organisms.

In order for neutrophils to produce this co-ordinated, directional cell movement, a number of criteria must be met:

- The chemical stimulus (chemoattractant) can be a variety of substances (chemokines released from cells in the body e.g. IL8, bacterial products), but it has to be detected by the neutrophil.

- Internal signalling must take place within the neutrophil to signal formation of new pseudopods at the leading edge of the cell and retraction at the posterior edge of the cell. This also relies on the neutrophil having accurately identified the direction of the chemoattractant gradient to ensure movement occurs in the correct direction (Andrew and Insall, 2007).
- Neutrophils have a number of transmembrane G-protein coupled receptors which are capable of detecting and activating a complex cascade of signalling leading to directional controlled movement towards a chemoattractant (Hirsch et al., 2000).

Chemotaxis protocol

The Insall chamber was used to visualise chemotaxis (Muinonen-Martin et al., 2010), see Figure 2.18.

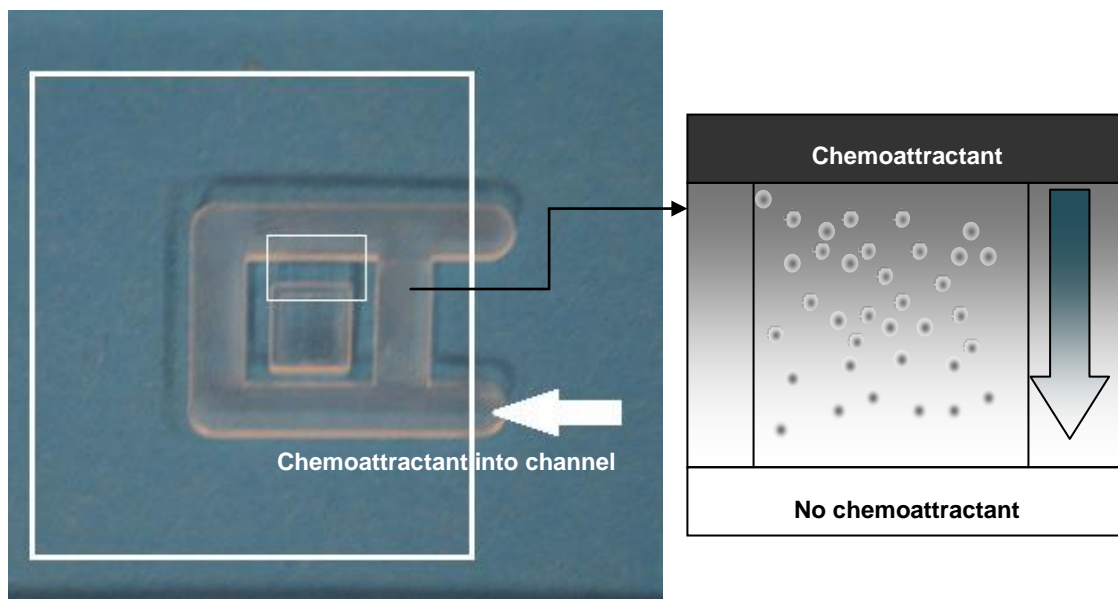


Figure 2.18 – Diagram and photograph of an Insall chamber. The photograph on the left shows the channels scribed into the chamber and the position of the coverslip is shown by the large white rectangle. The small white rectangle shows the detail of the chamber where a gradient of chemoattractant is formed, and the area of the chamber which is visualised in order to track neutrophil chemotaxis. Neutrophils are represented by the small grey circles and the chemoattractant gradient is represented by the grey gradient and highlighted by the blue arrow.

N-formylmethionine leucyl-phenylalanine (fMLP) was used as a positive control as it is a well-established chemoattractant (Nagata et al., 2001, Heit et al., 2008) and would

indicate the ability of isolated neutrophils to undergo chemotaxis. The order of conditions was varied between experimental repeats, but data were only used when cells responded appropriately to the positive control.

1. Neutrophils were isolated from healthy volunteers as described in Section 2.9.2 and reconstituted to a concentration of 1×10^6 cells per mL in RPMI.
2. A coverslip (22 mm, 1.5 thickness, VWR international) was washed in 0.2 M HCl and rinsed in two changes of RO water, dried and blocked with 400 μ L 7.5 % BSA (Sigma-Aldrich, UK). The BSA was then drained from the coverslip and 400 μ L cell suspension was added to the coverslip and incubated at room temperature for 20 min to allow the neutrophils to adhere slightly to the coverslip.
3. The coverslip was then inverted, the excess neutrophil suspension was discarded, and the coverslip was placed onto the Insall chamber which had the inscribed channels pre-loaded with RPMI. Excess moisture was removed from the coverslip using filter paper to ensure the coverslip was adhered to the chamber slide by capillary force.
4. The chemoattractant channel was then loaded from the loading bays (as shown by the large white arrow), ensuring the coverslip was not dislodged by overloading the channel with liquid. This produces a chemoattractant gradient in the area represented in Figure 2.19.
5. Cell movement was recorded by capturing a frame every 30 s for 20 min using a Zeiss Primovert microscope at 20 x magnification (Carl Zeiss Imaging, USA) and a Q Imaging Retiga 2000R camera and QCapture Pro Software (QImaging, Canada).
6. The frames captured were analysed using ImageJ by tracking 15 cells manually to give numerical co-ordinates which were used to calculate cell speed, cell velocity and Chemotactic Index (CI) per video as described by Roberts et al (Roberts et al., 2015).
7. Statistical analysis was carried out using the CircStat tool in MATLAB (Mathworks, USA) to elucidate how significant the movement of the neutrophils was over time.

2.10 *Enzyme linked immunosorbent assays (ELISAs)*

Commercially available ELISAs were used to determine concentrations of inflammatory markers in cell supernatants. Levels were quantified by measuring colour generation in a reaction which is directly related to target levels detected by target specific antibodies. Figure 2.17 summarises the experimental process underpinning ELISA assay.

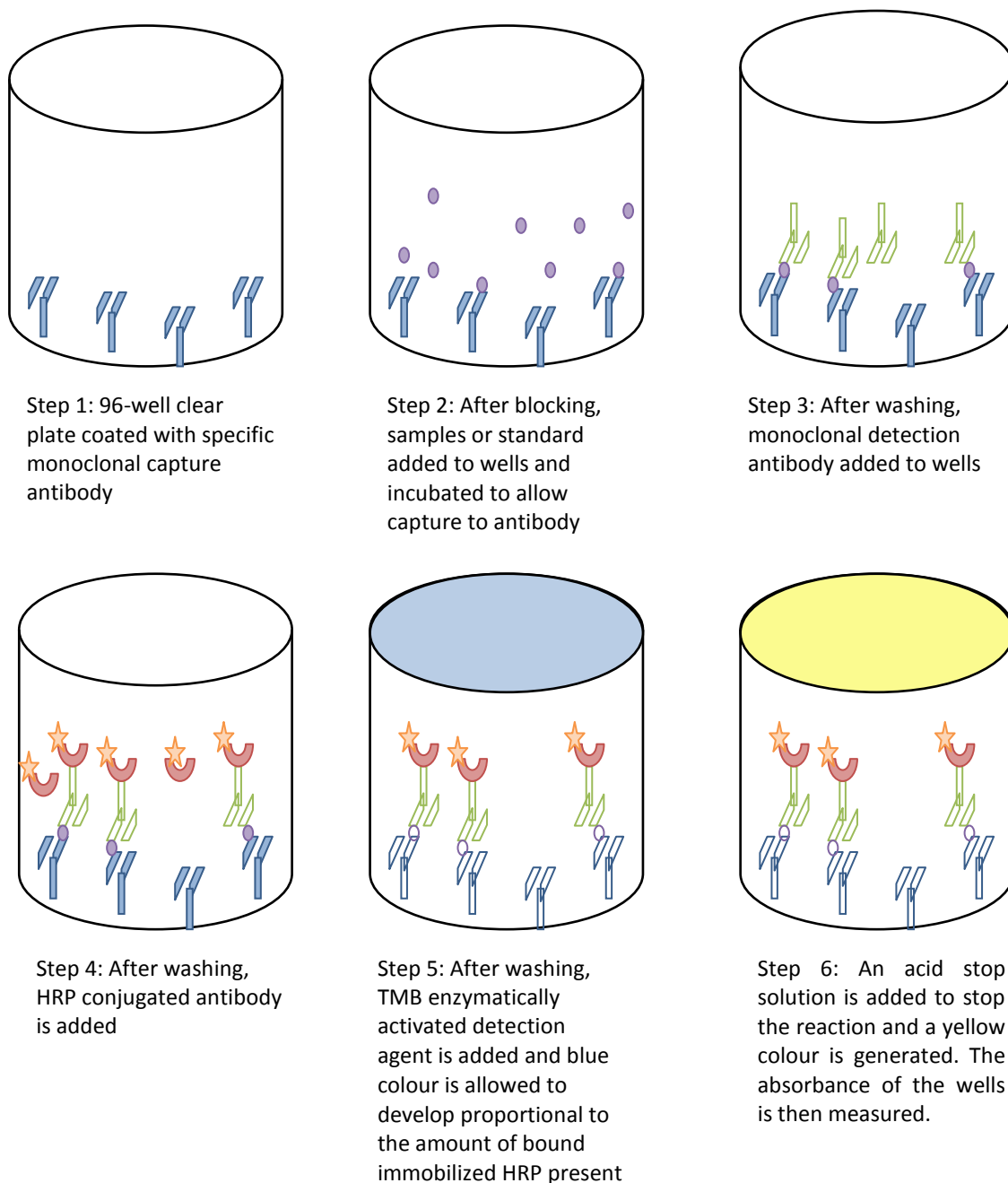


Figure 2.19 – diagram illustrating sandwich ELISA process to detect target proteins within a sample.

2.10.1 *ELISA protocol*

1. ELISAs were all performed using DuoSet ELISA kits (R&D systems, Bio-technique, USA) according to the manufacturer's instructions.
2. Plate preparation: Capture antibodies were diluted in protein free PBS and 100 µL per well was incubated overnight at room temperature or at 4°C (target specific) in covered plates to prevent evaporation or contamination. Plates were then washed 3 times using PBS containing 0.05 % TWEEN-20 (Sigma-Aldrich, UK) the excess blotted on clean paper towels.
3. After washing, wells were blocked with 300 µL of either Reagent Diluent (RD) comprising Tris-buffered saline containing 0.05 % TWEEN-20 and 0.1 % BSA (Sigma-Aldrich, UK) or blocking buffer (PBS containing 1 % BSA) depending on the target. After 1 h, plates were washed following the same wash protocol as above. Plates were then used immediately or stored for up to 48 h at 4°C.
4. Assay performance: Standards were diluted according to specific manufacturer protocol for each target. Cell supernatant samples were prepared as below using 6 well plates with H400 cells cultured to 70-80 % confluence before stimulating as below (Table 2.16). Supernatants were aspirated and centrifuged at 15000 rpm for 5 min (Geneflow SciSPin Micro). All standards and samples were brought to room temperature before use and stored long term at -20°C (standards at stock concentration) or -80°C (supernatants). 100 µL was added to each well and incubated in a covered plate for 2 h at room temperature.

Sample	Cells	TiO ₂ treatment	Bacteria added
1	Cell free	-	-
2	H400	-	-
3	H400	24 h pre-treated 100ppm	-
4	Cell free	-	FN 100:1 for 1 h
5	H400	-	FN 100:1 for 1 h
6	H400	24 h pre-treated at 100ppm	FN 100:1 for 1 h
7	H400	100 ppm with bacteria for 1h	FN 100:1 for 1 h
8	Cell free	-	PG 25:1 for 1 h
9	H400	-	PG 25:1 for 1 h
10	H400	24 h pre-treated at 100ppm	PG 25:1 for 1 h
11	H400	100 ppm with bacteria for 1h	PG 25:1 for 1 h

Table 2.16 – H400 conditions prior to ELISA testing

1. After washing according to the previous protocol, Streptavidin conjugated to HRP was diluted according to the manufacturer's instructions and 100 µL added to each well and incubated at room temperature in the dark for 20 min.
2. After 20 min, the plate was washed again according to the previous protocol. 100 µL of a 50:50 mix of H₂O₂ and TMB (Tetramethylbenzidine) is recommended by the manufacturer, however in this work a TMB Liquid Substrate System for ELISA (Sigma-Aldrich, UK) was used due to its improved safety profile. The plate was incubated for up to 20 min in the dark, checking every 5 min to ensure wells were not becoming too blue.
3. After an appropriate incubation time, 50 µL stop solution (1 M Sulphuric acid) was added to each well to stabilise the reaction, and the blue colour from the TMB changed to yellow. Absorbance was then read at 450 nm (absorbance at 570 nm was subtracted to improve accuracy) using a plate reader (BIO-TEK Elx800, Bio-tek, USA).

2.11 High Content Screening (HCS) sample preparation

High content analysis (HCS) was carried out on H400 cells using a variety of assays and techniques by Imagen Therapeutics (formerly Imagen Biotech, Alderley Edge, UK). All experiments were carried out in sterile black walled, clear bottomed tissue culture

treated 96-well plates (Appleton Woods, UK). Live cells were used for some assays, and for others cells were fixed using paraformaldehyde prior to staining by Imagen Biotech.

For the HCS work, all cells and reagents were supplied by the author and seeded into the appropriate well plates at Imagen Biotech's laboratory in Alderley Edge. Due to the distance from Birmingham, H400 cells were transported at room temperature in a vial containing 1×10^6 cells in 1 mL culture medium in a cryovial, sealed with parafilm, as per established methods (Rainov et al., 2000). The following information describes the methods for HCS as a general technique, and the specific culture techniques, stimuli and protocols for each experiment will be described in the appropriate results in Chapter 5.

2.11.1 *HCS methods (general)*

H400 cells were fixed in 1 % formaldehyde and washed twice with PBS. Primary antibodies were diluted as appropriate according to the specific antibody used, and incubated with the cells in Digitonin (500 μ L/mL, Sigma-Aldrich, UK) to induce increased membrane permeability. Primary antibodies were incubated for 1 h at room temperature ($21 \pm 2^\circ\text{C}$), following which the antibody was decanted and the plate was washed twice with PBS using a plate washer (Tecan UK Ltd, Reading, UK). Secondary antibodies were diluted as appropriate and again incubated for 1 h at room temperature in conjunction with Hoechst 3332 (Invitrogen, UK) to counterstain the nuclei. Following the second incubation the wells were again washed after removal of the secondary antibody mix. 100 μ L of PBS was then added to each well for storage and visualisation. Immunoreactivity staining for biomarkers was performed in triplicate for each experiment and triplicate readings were pooled.

HCS data capture and analysis

Biomarkers of interest were visualised and the intensity quantified using Cellomics ArrayScan® HCS and INCELL Analyser® readers and Compartmental Analysis Bio-Application (V2 Version, Thermo Scientific). Thermo Scientific Software was used for certain specific applications as appropriate (BioApplications). Images were captured of at least 5000 cells per well in ≥ 8 images taken in a spiral pattern outwards from the centre of each well. Images were captured in three channels (386 nm_{EM}, 488 nm_{EM} and

549 nm_{EM}). Each cell was analysed individually to identify the intensity of targets throughout different regions of the cell.

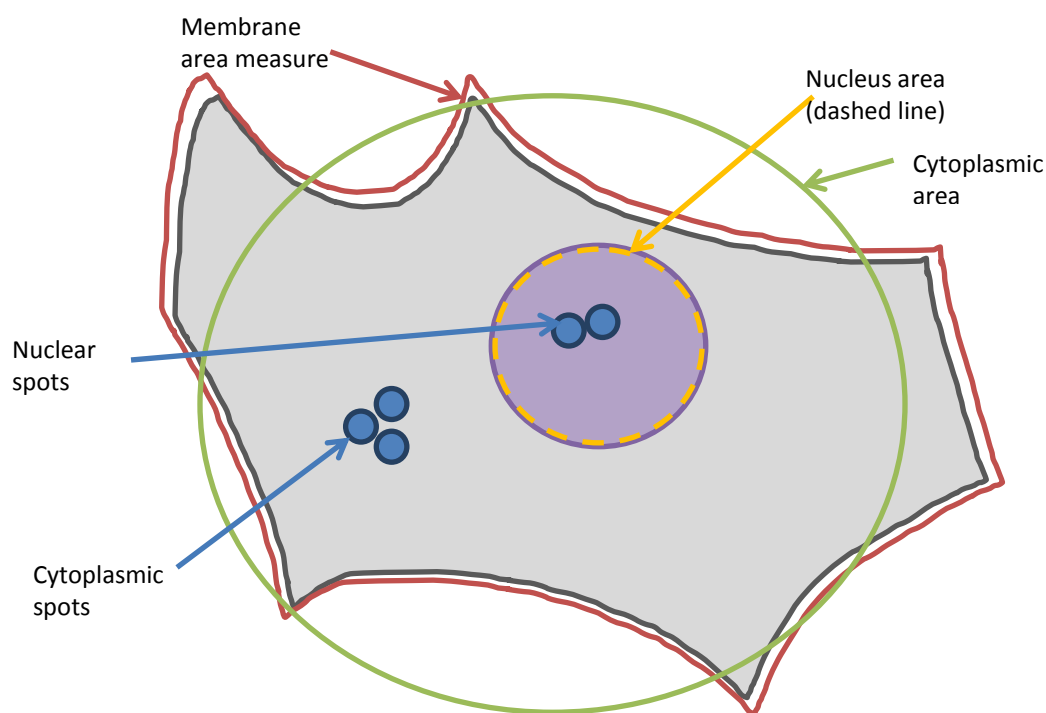


Figure 2.20 – Diagram representing the different parameters which can be measured using HCS imaging techniques. Cytoplasmic and nuclear spot intensities can be measured using a threshold to count cells as positive or negative for the biomarkers investigated.

2.12 Protein gel electrophoresis

No.	Preparation protocol	Sample used
1	IL8 in PBS 2000 pg/mL	
2a	IL8 2000 pg/mL plus TiO ₂ 1000 ppm in PBS incubated for 1 h at room temperature then centrifuged at 150 x 100 rpm for 5 min (Geneflow SciSPin Micro)	Supernatant
2b		TiO ₂ pellet washed in PBS and re-suspended
3a	TiO ₂ 1000 ppm in PBS incubated for 1hr at room temperature then centrifuged at 150 x 100 rpm for 5 min	Supernatant
3b		TiO ₂ pellet washed in PBS and re-suspended
4	IL8 added at 2000 pg/mL in 20% human serum	
5a	IL8 added at 2000 pg/mL in 20% human serum plus TiO ₂ 1000 ppm in PBS incubated for 1 h at room temperature then centrifuged at 150 x 100 rpm for 5 min	Supernatant
5b		TiO ₂ pellet washed in PBS and re-suspended

Table 2.17 – Gel electrophoresis sample preparation

For protein electrophoresis, 12% Bis-Tris protein gels (NuPAGE™ Novex™, Invitrogen, UK) were used. Samples were prepared as described in Table 2.17, then 500 µL of each preparation was concentrated using centrifuge filters (Amicon Ultra 0.5 mL 3K Ultracel membrane) and centrifuged at 14,000 rpm for 30 min. Samples containing TiO₂ NP particles (2b, 3b, 5b) were treated with reducing agent, and all samples were heated in sample buffer for 70°C for 10 min prior to electrophoresis in MES buffer for 20 min (all as per the manufacturer's protocol). Following electrophoresis, the gel was dyed using imperial protein stain (ThermoFisher Scientific, UK) for 1 h and washed in water twice. Images were captured using a digital camera (Canon S110 using standard settings).

Chapter 3

**Development and validation of *in vitro* models of
oral epithelium**

Synopsis

To study interactions between Ti implant degradation products and oral epithelial cells, a reproducible and representative *in vitro* model system was required.

H400 cell characterisation

H400 cells were selected for potential use in a model system. The choice of this specific cell line is discussed, along with the characteristics and assessment techniques of normal H400 growth and replication. It is important to remember that H400 cells are a cancer derived cell line, and although they have been previously used as a model for bacterial challenge of oral epithelium, findings cannot necessarily be extrapolated to primary cells. The first part of this chapter documents the growth characteristics and morphological appearance of H400 cells, then subsequently the markers of epithelial cell characteristics, such as cytokeratin expression are compared with those of primary oral epithelial cells. Cell line reproducibility, ease of growing and consistent culture characteristics were the key advantages of using H400 cells when compared with primary cells

Primary oral epithelial cell culture

Given the limitations of cell lines it was also important to have access to primary oral epithelial cells to supplement data generated from H400 cells. Methods used for culture of primary oral epithelial cells and their outcomes are described. A characteristic of primary cells in culture is the inability to generate long term continuous cultures of epithelial cells, however short term cultures produced sufficient cells to allow the necessary experiments to be performed. Primary cells were compared with H400 cells both morphologically and for cytokeratin expression using PCR.

Choice of Ti stimuli for model system

Ti species have been identified within the body in a number of forms in areas both adjacent to and in the tissues surrounding implanted Ti devices (Addison et al., 2012). Addison et al., describe the variety of Ti species located within biopsies of inflamed tissues excised from around failing Ti percutaneous implants (Bone Anchored Hearing Aids, BAHAs), which was found to include particles from nm sized up to >100 µm. Ti

was found to be scattered throughout the sample in a radial pattern, with the highest concentrations being closer to the implant surface. These Ti particles included a variety of forms such as metallic particles and oxides (including rutile and anatase) as identified by X-ray absorption spectroscopy. This work alongside supplementary measurements (Section 1.4.3) informed the choice of the most appropriate Ti stimuli as Ti oxide. A panel of Ti species was used (e.g. viability, NF kappa B activation) but anatase was chosen as the primary stimulus to reduce material variables in the experimental designs.

Potential interactions of nanoscale Ti products on known assays

NPs possess high surface energies favouring biomolecular adsorption (Horie et al., 2013) and whilst this is recognised in the literature, the impact upon data interpretation from NP exposure assays is frequently underestimated or ignored (Kroll et al., 2009). Therefore, it was important to identify whether established assays are affected by the presence of nanoscale Ti particles before they were used. Assays for cell viability and ELISAs were performed in the presence and absence of Ti. It was identified that a number of potentially useful experimental techniques such as ELISAs and certain viability assays were significantly confounded by the presence of Ti NPs, therefore highlighting the importance of validating each experimental technique in this model prior to use.

3.1 H400 cell growth and morphology

H400 cells are an epithelial cell line first described by Prime in 1990 (Prime et al., 1990). H400s are derived from a moderately well differentiated stage II squamous cell carcinoma of the alveolar process in a 55-year-old female. H400 cells have been used as an epithelial cell model in the periodontal literature in the context of responses to Nickel (Wylie et al., 2010); responses to periodontal pathogens including activation and nuclear translocation of NFκB and associated downstream inflammatory pathways (Milward et al., 2013, Milward et al., 2007); and cytokine responses including TNFα and IL8 production (Grant et al., 2010a). The table below outlines the known similarities and differences between H400 and primary oral epithelial cells.

Similarities between H400 cells and primary oral epithelial cells	Differences between H400 cells and primary oral epithelial cells
Similar expression of EGF receptors to normal keratinocytes (Prime et al., 1994)	H400 show a slightly increased sensitivity to epidermal growth factor (Prime et al., 1994)
Similar production of TNF α to normal keratinocytes (Prime et al., 1994)	H400 show a slightly lower number of EGF receptors compared with normal keratinocytes (Prime et al., 1994)
Similar nuclear:cytoplasmic ratio to cells of origin (Prime et al., 1990)	H400s are immortalised
Similar morphology when examined under light microscopy	H400 cells are all cloned therefore there will be no variability in DNA whereas primary oral epithelial cells will exhibit donor-donor variation
Similar cytokeratin expression to normal keratinocytes (Prime et al., 1994, Prime et al., 1990)	

Table 3.1 – similarities and differences between H400 cells and primary oral epithelial cells (keratinocytes).

3.1.1 *H400 morphology assessment*

Epithelial cells have a consistent, characteristic appearance, exhibiting:

- regular polygonal shape;
- tight junctions to other cells;
- growth in either islands, originating from a single cell or outwards from an established mass of cells.

When culturing primary epithelial cells from a tissue biopsy, cultures can become contaminated with connective tissue cells (mainly fibroblasts) which have a very different morphological appearance to epithelial cells:

- bi-polar or multi-polar;
- elongated shape;
- may not have regular tight junctions with other cells but can grow in more of a mass pattern with spaces between cells.

Light microscopy was used to assess the morphology and growth characteristics of H400 cells. The rate and pattern of H400 cell growth under standard culture conditions

was studied. Cells were cultured according to the methods detailed in Section 2.2 and seeded onto tissue culture treated plastic and incubated at $37 \pm 1^\circ\text{C}$ in 5% CO_2 . Cell counts were performed daily until H400 cells reached full confluence when viewed at x20 magnification by light microscopy (Primo Vert, Zeiss, Germany).

H400 growth quantification

Cell counts were carried out under standard growth conditions to quantify cell growth characteristics. As cell counts must be known to standardise data reporting, it was important to assess not only the growth characteristics of this cell line but also to verify cell count methods which can be used in experimental protocols and when re-seeding cells into cell culture vessels. Experimental protocols may involve cells being examined on an individual basis, for example to identify potential interactions with Ti products via microscopy techniques. Other methodologies required cells to be in a monolayer such as histocytochemistry. Experiments where H400 cells were exposed to Ti products were largely performed with H400 cells in a near confluent monolayer as previously discussed. Also the exposure of cells to Ti products will alter if cells are in single cell suspension compared with a monolayer, as cells grown to a confluent monolayer or within a tissue will have a reduced surface area expressing receptors than will cells that have been released from the substrate following trypsinisation.

Cell counting methods

Cell counts were performed after trypsinisation of the cell monolayer to produce a single cell suspension (see Section 2.2). A modified Neubauer haemocytometer was used for all cell counts. Cell counts were carried out prior to seeding into $12 \times 25 \text{ cm}^2$ flasks, then each day 3 randomly selected flasks were trypsinised (Section 2.2) and cell counts performed.

To count H400 cells in-situ, an eyepiece graticule fitted inside the microscope was employed to count cells at 10x magnification (Figure 3.2) using an inverted light microscope (Primo Vert, Zeiss, Germany). 25 cm^2 flasks (Corning, UK) were inoculated with 1×10^5 H400 cells in 5 mL supplemented DMEM as previously described, and incubated at 37°C 5% CO_2 for 4 days. Cell counts were performed in triplicate on 3 different flasks for both the above and below methods at the same time each day.

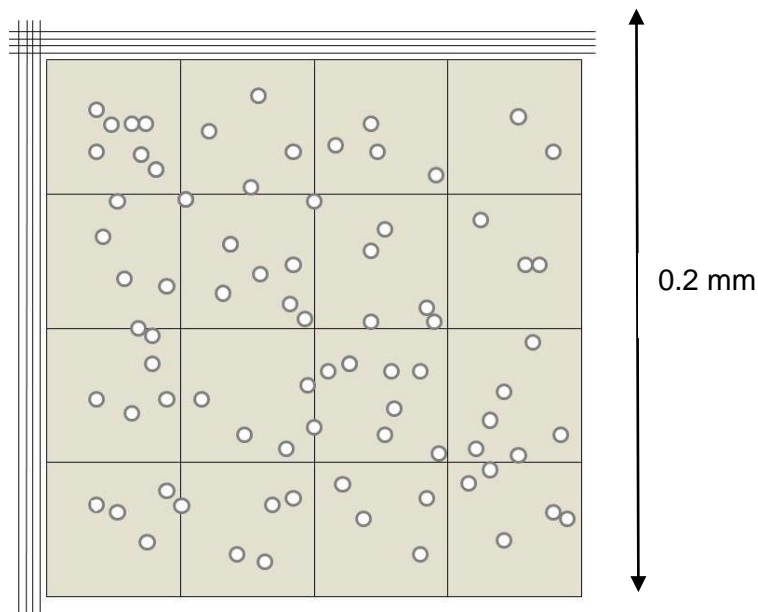


Figure 3.1 – Diagram representing a section of a modified Neubauer haemocytometer quadrant of 16 squares. To perform a cell count, four of these quadrants (16 small squares as shown) were counted and a mean cell count per quadrant was generated. This mean cell count per quadrant equates to the cell count $\times 10^4$ per mL within the sample examined. Cells positioned on a line were included in the box either to the left or below to ensure counts were not duplicated.

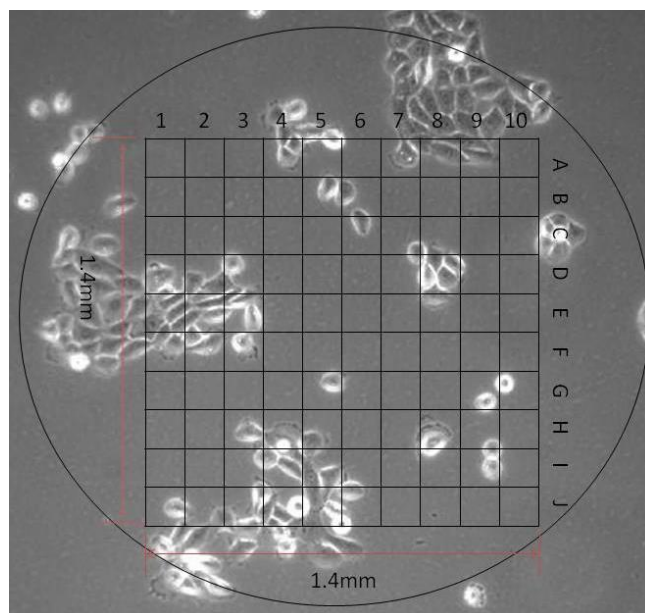


Figure 3.2 – Diagram showing eyepiece graticule superimposed over cells in situ (not to scale)

The number of cells visible was counted and this was then multiplied to give an approximate cell count in the cell culture vessel. To achieve reliable estimations of cell counts, Hunting curves were performed for each of the above methods in order to

establish the minimum number of counts which would give a valid approximation of cell number. Figure 3.6 shows the Hunting curves generated from each method.

3.1.2 *H400 morphology assessment – results*

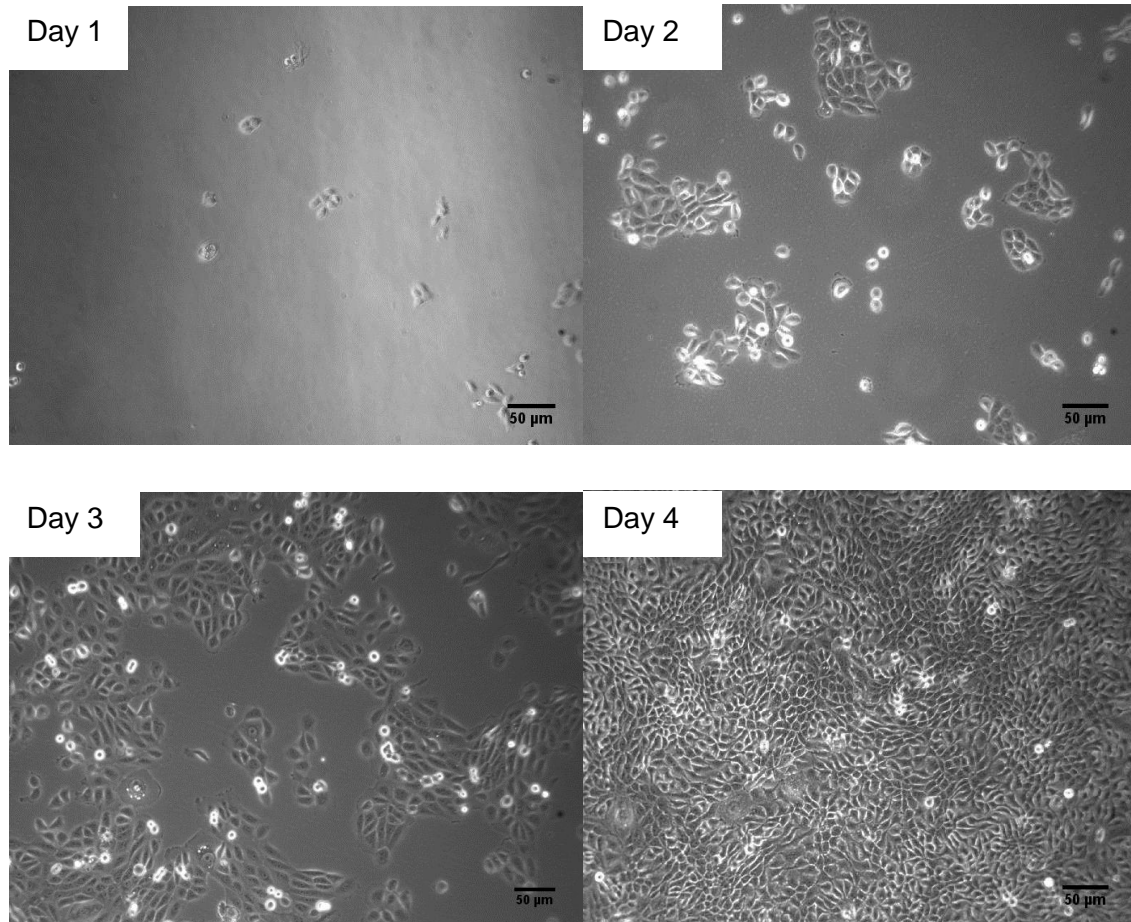


Figure 3.3 – Light microscopy images illustrating H400 cell growth from 1-4 days post seeding showing increasing growth to confluence. Note that as cells are confluent they become slightly compressed, appearing smaller than those on days 1-3 inclusive. This Figure is representative of the typical growth pattern of H400 cells as cultured according to the protocol in Section 2.2. A number of epithelial characteristics of growth are evident including outward growth from cell islands, regular non stellate shape, and formation of a confluent monolayer. No morphological changes were observed in cells from P4-P30.

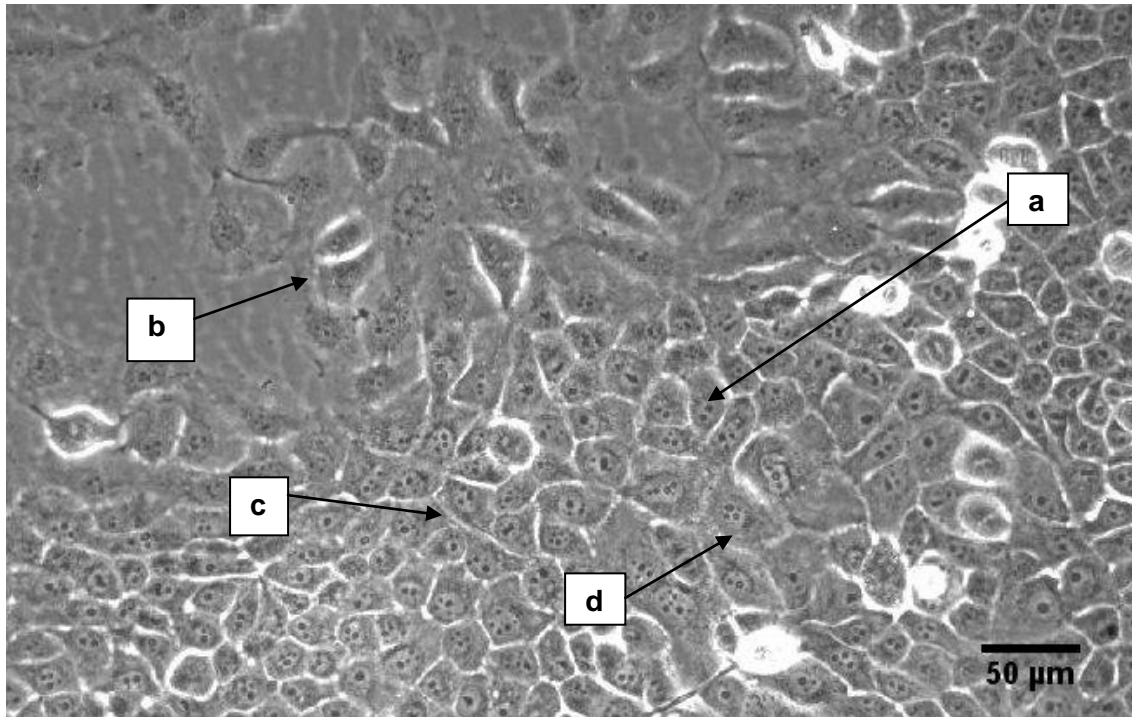


Figure 3.4 – H400 cells showing morphological features of epithelial cells. **a**=regular cobblestone appearance **b**=growth outwards from cell islands **c**=tight cell-cell junctions **d**=cuboidal, non-stellate shape (4 days post seeding).

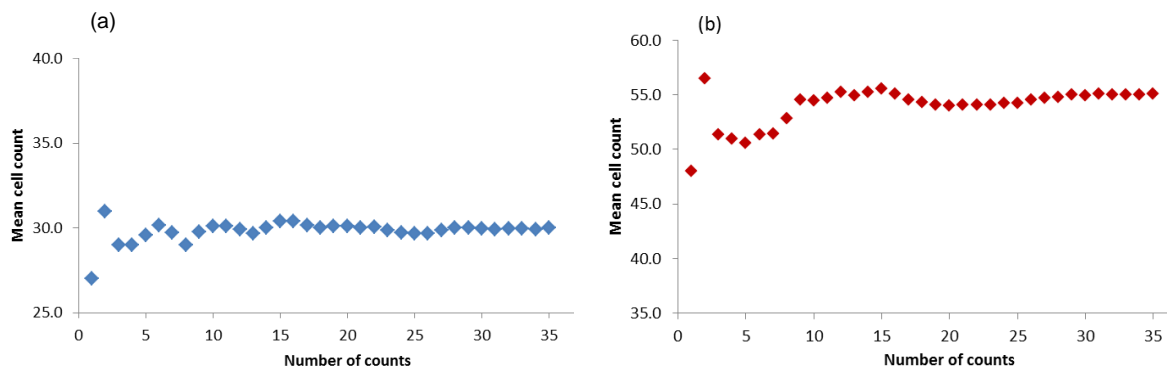


Figure 3.5 – Hunting curves for single cell suspension count using a haemocytometer (a) and in-situ count using an eyepiece graticule (b) showing that approximately 16 counts was adequate for both methods to achieve a reliable mean cell count. 16 was taken as a suitable number of counts for consistency.

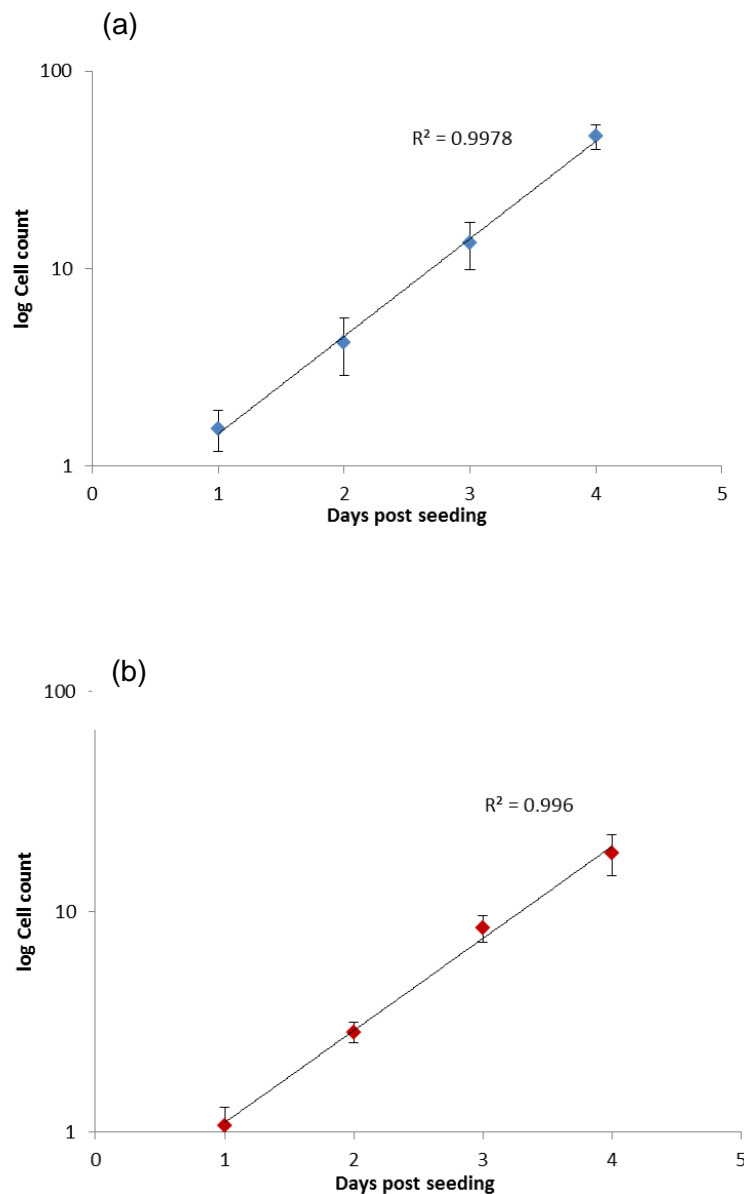


Figure 3.6 – Cell counts of single cell suspension using haemocytometer (a) and cell counts of in-situ cells within a monolayer using an eyepiece graticule (b) showing an exponential pattern of growth from each method up to 4 days post seeding when confluence was reached. $n=3$, mean and SD shown.

From Figure 3.6, it can be seen that both methods of cell counting identified the same pattern of growth, but the numbers of cells reported to be in each flask differed: the maximum cell count reached by day 4 was approximately 20×10^5 cells per flask using the trypsinised method and approximately 40×10^5 in the in-situ method.

Exponential growth patterns were identified using both methods. Cells were grown to 4 days as they were confluent at this time-point within the culture flasks, so continued culture would have required passage and re-seeding.

Two important factors to consider when accounting for the differences in cell numbers generated by the two methods are that trypsinising cells and counting them was likely to underestimate the number of cells in a flask, due to the fact that not all of the cells are detached from the cell culture surface. Trypsin is a proteolytic enzyme which breaks down the proteins responsible for cell attachment, but must be deactivated to prevent damage to cell surface proteins which could affect cellular function (Huang et al., 2010). A balance must be achieved between leaving the trypsin in the flask for sufficiently long to assist cellular dissociation from the culture treated surface and other cells in the monolayer, and avoiding leaving the trypsin in the flask so long that it adversely affects cell surface proteins. Flasks were trypsinised for the minimum possible time to prevent cellular damage whilst detaching the majority of adherent cells. The efficiency of this process is also dependent upon temperature and agitation, so trypsin solution was pre-warmed and flasks were kept in the incubator during detachment and were gently manually agitated halfway through trypsinisation.

The in-situ method may over-estimate viable cell counts, as areas at the edges of the flask are likely to be less confluent (confirmed by light microscopy), as well as the fact that any non-viable but still adherent cells are not excluded. However, cell viability cannot be assessed using cell counts in-situ, whereas it can be done using the trypsin method and Trypan blue staining as detailed previously.

3.1.3 *Conclusions from H400 growth characterisation and cell counts*

Figures 3.3 and 3.4 above confirmed that H400 cells had an epithelial appearance, and were simple to culture aseptically under the conditions described (Section 2.2). The approximate length of time between seeding density and confluence was established and served to inform future experimental methods.

H400 cells were reliably cultured under the conditions and seeding density described in Section 2.2, grew exponentially to confluence (approximately 4 days post seeding) and appeared to show the expected morphological features of epithelial cells when examined by light microscopy.

Once H400 cells have reached confluence on the available tissue culture treated surface, the rate of replication will slow. This is due to cells having no more available

space into which to divide. If culture medium is not refreshed then exhaustion of nutrients in the medium and acidification may occur, inhibiting cellular growth and division. When confluence is reached, if the flask is not trypsinised and cells re-seeded into a new vessel, the cells will become over confluent, leading to a lack of cell division and a higher percentage of non-viable cells. This happens at varying time points (>24 h) following confluence depending on the volume of the medium in a vessel and the cell count, however all exposure experiments reported in this study were carried out prior to cells reaching confluence.

3.2 Primary oral epithelial cell isolation and culture

It is accepted that H400 cells are an immortal cell line and their responses to stimuli and cellular behaviour *in vitro* may differ from epithelial cells *in vivo*. The literature indicates that cell lines and primary cells have differences, e.g. proteomic phenotype of hepatocytes (Pan et al., 2009) and phenotype of endothelial cells (Unger et al., 2002). However, it has also been highlighted that under the right conditions and with appropriate controls, immortalised cell lines can retain properties of the cells of origin (Masters, 2000). The H400 cell line was established with the use of a 3T3 cell feeder layer, with early passages being cytotoxic to mitomycin C-treated 3T3 cells, but in later passages the cells were not mesenchymal dependent (Prime et al., 1990). Normal (non-malignant) epithelial cells were shown to senesce at passages 3-4, highlighting the difficulty in establishing and successfully culturing primary epithelial cells.

H400 cells were compared with primary epithelial cells grown from either waste tissue from surgery or from biopsy samples taken as part of a clinical trial. Tissue samples were stored in transport media (Ham's F12 DMEM supplemented with 10% Fetal Calf Serum and 100 U/mL penicillin, 0.1 mg/mL streptomycin, Sigma-Aldrich, UK) for up to 24 h at 4°C as necessary before use. Primary epithelial cell culture was attempted using two methods. the first involved a "feeder layer" of 3T3 cells and the second used a direct explant method. The resulting cells were compared with H400 cells in terms of morphology and cytokeratin expression in order to establish the validity of H400s as an epithelial cell line in this work and also to establish a protocol for the use of primary oral epithelial cells.

3.2.1 Primary epithelial cell culture methods

Primary oral epithelial cell isolation and culture – “feeder layer” method

The use of a 3T3 cell feeder layer has been shown to facilitate the growth of primary epithelial cells (Gray et al., 1983, Taylor-Papadimitriou et al., 1977). A feeder cell layer was employed as epithelial cells in culture are thought to require growth factors produced by other cells *in vivo* (e.g. fibroblastic cells in this *in vitro* model). This protocol uses 3T3 cells to grow to approximately 1/3 confluence, then treated to arrest cell division, and for the epithelial biopsy to then be cultured alongside the non-dividing fibroblasts (see Section 2.4).

Primary oral epithelial cell isolation and culture – “explant” method

The explant method for isolating primary epithelial cells requires no feeder layer. This method has been described in detail in the literature (Groger et al., 2008) and is a less complex protocol with fewer stages where errors could be made. The protocol for the explant method is described in Section 2.4.2.

3.2.2 Results of primary epithelial cell culture

Initial cells cultured using the feeder layer method appeared to exhibit epithelial morphology when viewed under light microscopy.

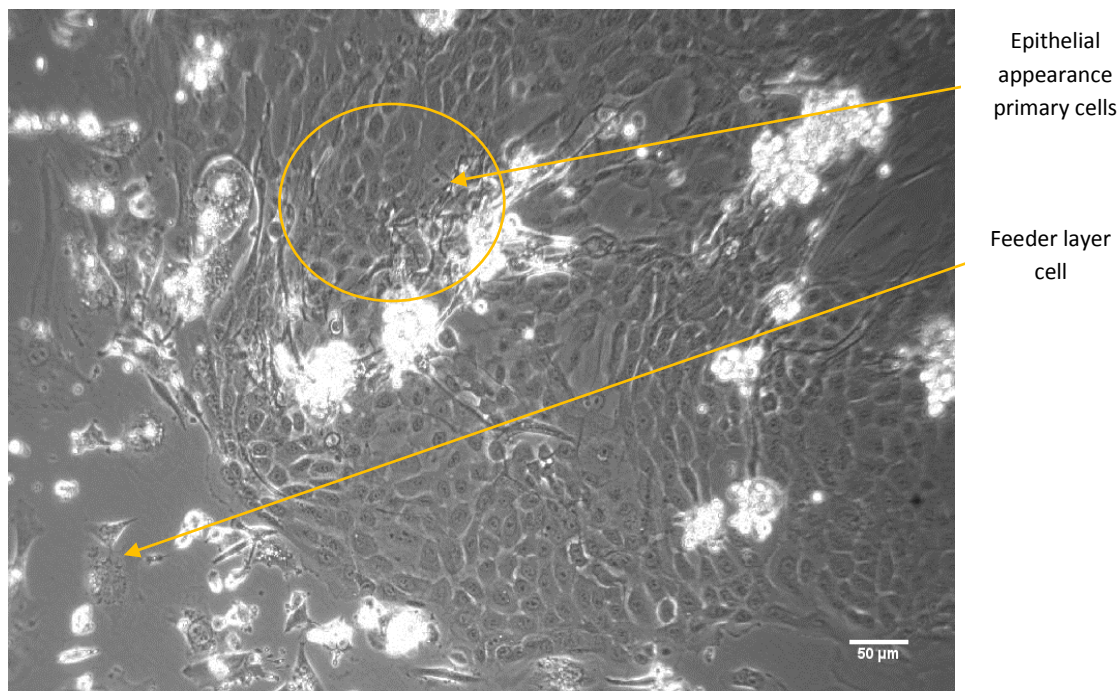


Figure 3.7 -Appearance of epithelial cells growing out from biopsy tissue on a 3T3 fibroblast feeder layer before passaging and reseeded.

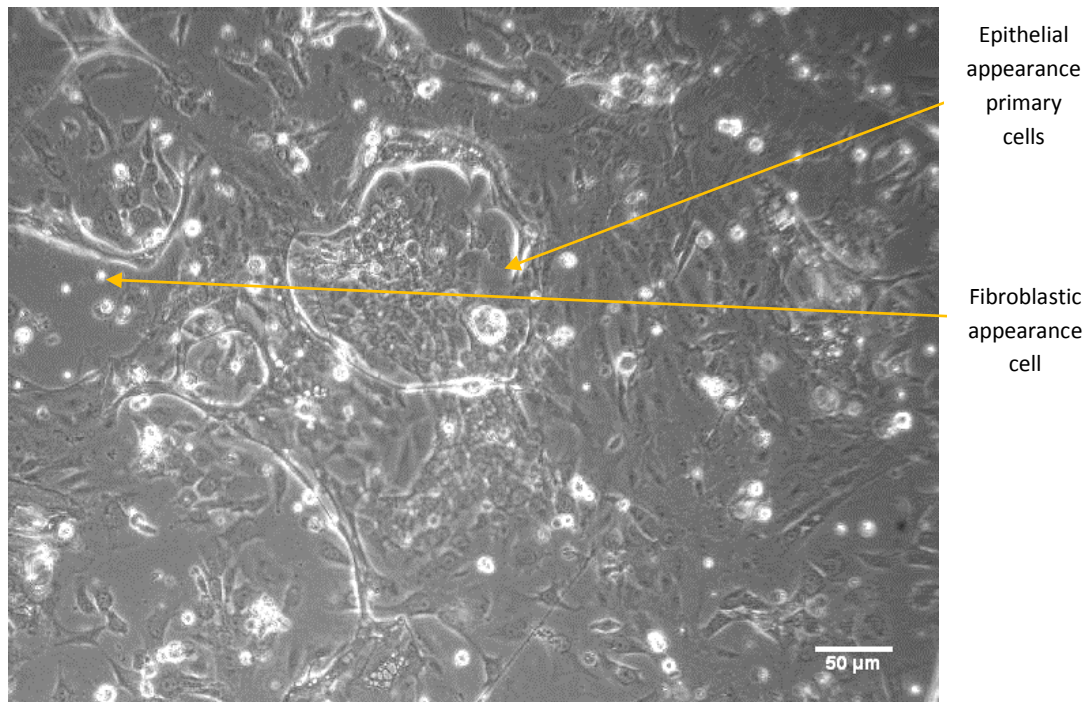


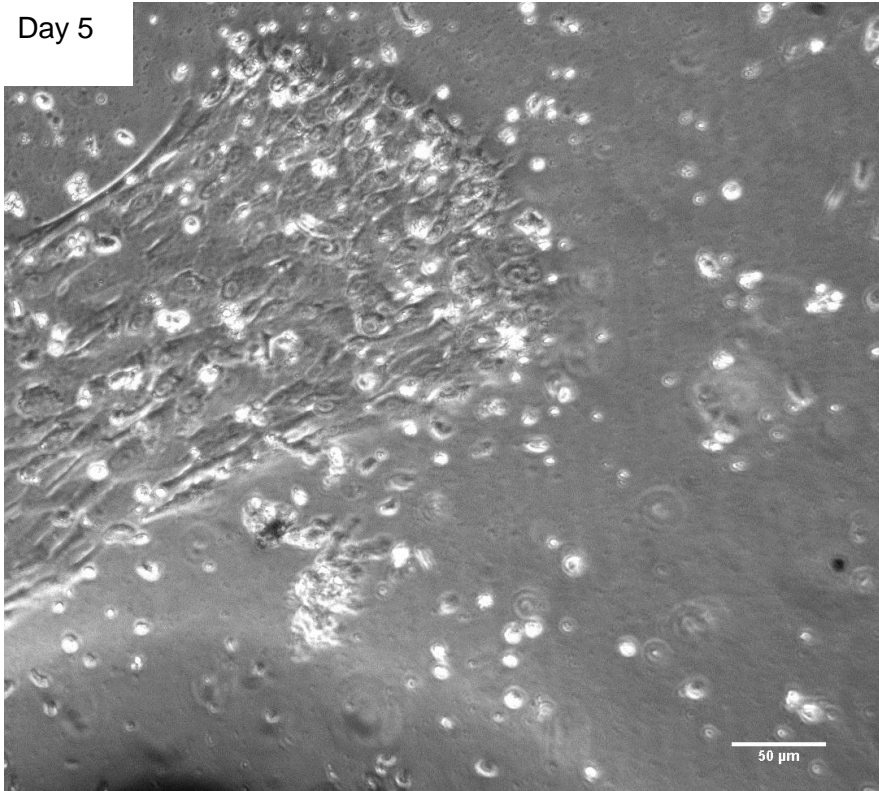
Figure 3.8 -Mixed epithelial and fibroblastic appearance of primary epithelial cells grown on a 3T3 feeder layer following cell passage

On following the protocol for passage and re-seeding of these epithelial cells (see Section 2.2), the morphology of the resulting re-seeded cells appeared to be fibroblastic as well as epithelial (Figure 3.8) with stellate shaped cells also present. This mixed morphology continued following re-seeding into a new culture vessel and until the vessel became confluent with mixed cells.

When the explant method was used, 50% of the tissue samples set up as described in Section 2.4.2 showed signs of growth at 21 days (n=20).

Figure 3.9 shows typical images taken on days 5 and 7 following inoculation of tissue samples into culture plasticware containing cell culture medium as described in chapter 2.

Day 5



Day 7

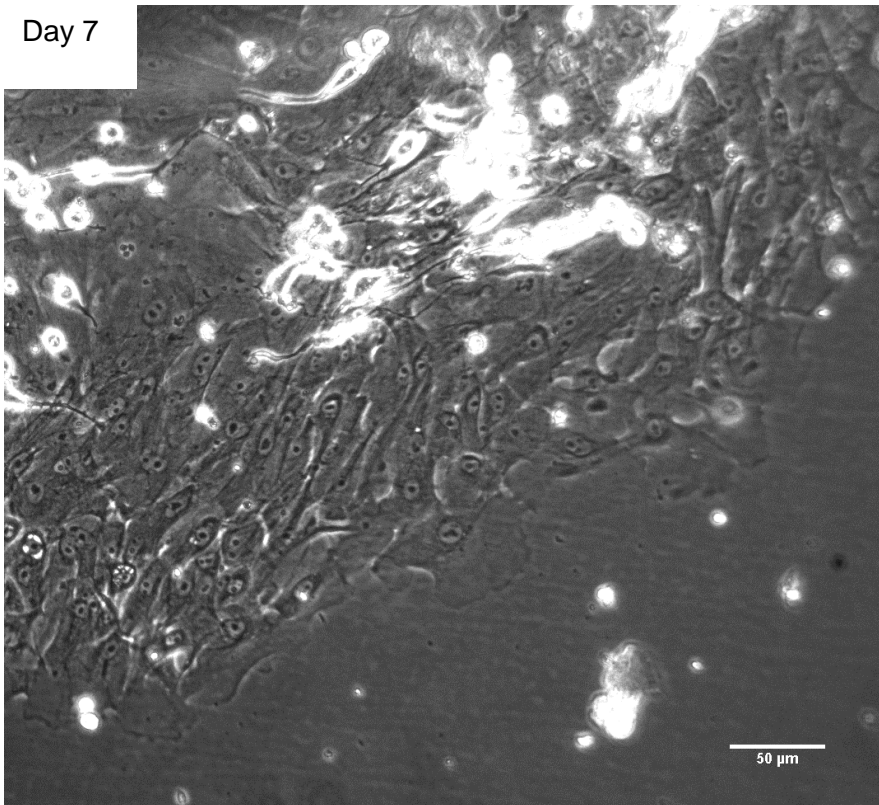


Figure 3.9 – Light microscopy images showing explanted oral epithelial tissue exhibiting epithelial appearance of primary cells growing outwards in a “cobblestone” formation from a tissue biopsy at 5 and 7 days post placement into a culture flask.

Within 15 – 21 days, a confluent area of cells exhibiting epithelial morphology can be seen (Figure 3.10).

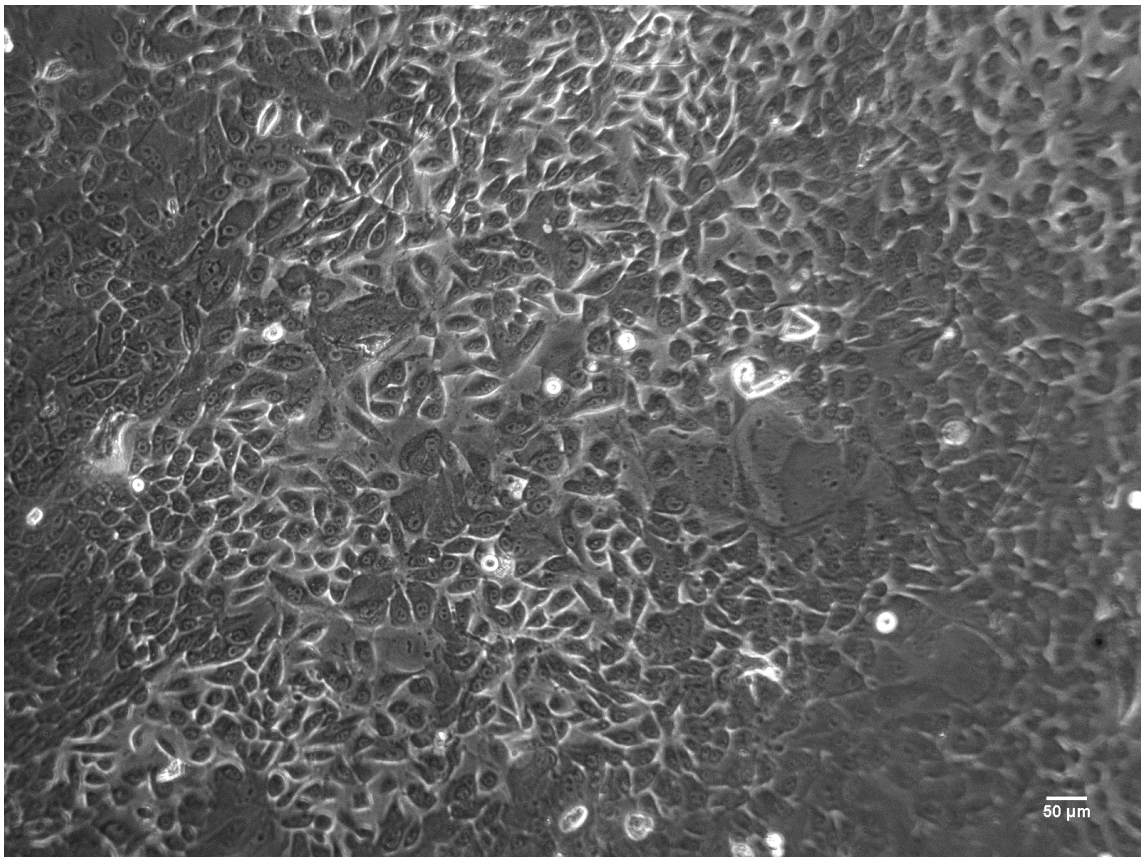


Figure 3.10 – Typical light microscopy image showing cells cultured from explanted epithelial tissue. A confluent area of cells exhibiting epithelial appearance can be seen 15 days post initial seeding of the explant.

However, similar issues to the feeder layer method arose in that the morphology appeared to shift to a more fibroblastic phenotype following initial cell passage. Despite repeated efforts, this shift in phenotype was a consistent finding. Figure 3.11 shows the morphology of cells 14 days after initial passage.

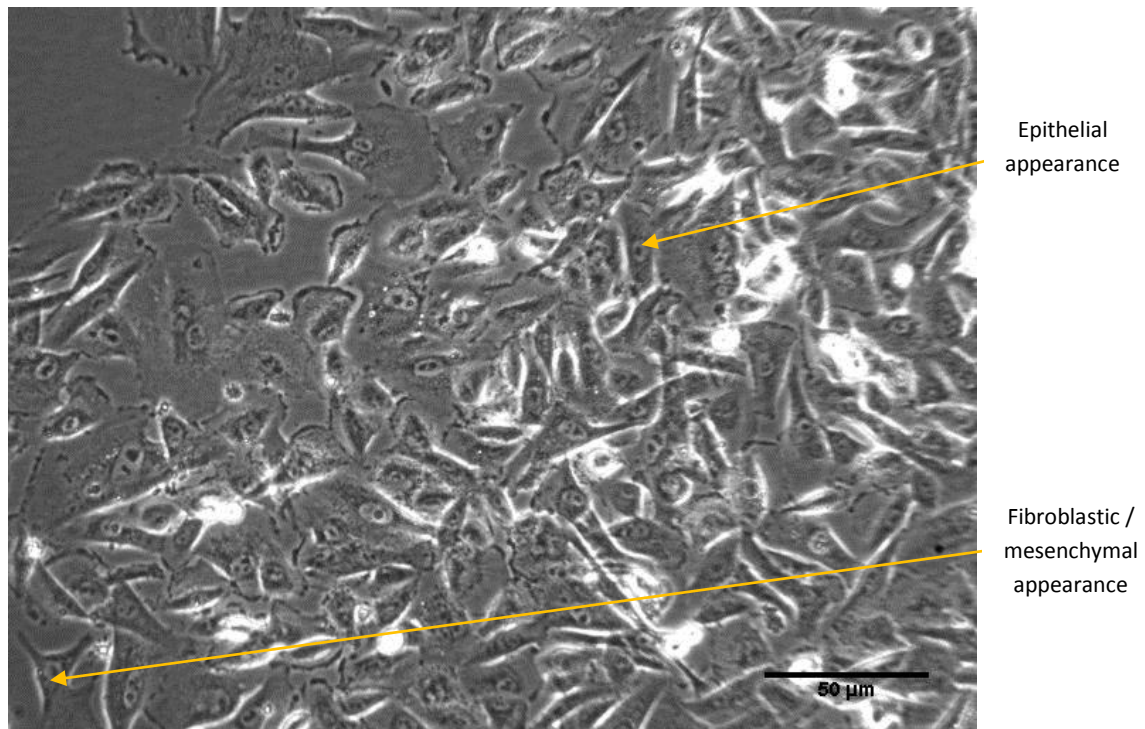


Figure 3.11 - Primary oral cells 14 days post passage showing a mixed morphology of epithelial and fibroblastic appearance

3.2.3 *Conclusions from primary oral epithelial cell culture*

The appearance of the cells cultured following the feeder layer method casts doubt over whether these cells are truly epithelial in nature. It was proposed that this was either due to fibroblastic contamination from the initial tissue sample, or that the 3T3 cells were not sufficiently inhibited from dividing and were contaminating the culture. This process was repeated 3 times with the same outcome.

The explant method seemed to produce a similar number of cells in a similar time to the “feeder layer” method, but with the convenience of not needing to prepare and culture fibroblast cells. However, there was a lower success rate for the explant method in terms of successful cell outgrowth from tissue of approximately 50% of biopsies from the explant method compared to approximately 80% for the feeder layer biopsies.

- The same issue occurred using both methods in that initial outgrowth had the morphological appearance of epithelial cells, but on examining the outgrowth following first cell passage this morphology did not remain consistent.

- For this reason, it was decided to characterise the cells that grew initially outwards from the tissue biopsy before passage, and to compare them to both H400 cells and fibroblasts.

3.2.4 *Characterisation of explant cellular outgrowth*

To validate the primary cell phenotype, indirect immunofluorescence (IF) (see Section 2.7 for methods) and RT-PCR (see Section 2.5 for methods) were used.

Indirect immunofluorescence staining of cellular outgrowth from biopsy tissue

Cytokeratins are proteins which form part of the filamentous protein structure in epithelial cells (Henzen-Logmans et al., 1987), and are considered to be phenotypic markers of epithelial cells. Vimentin is a filamentous protein which is expressed in mesenchymal and fibroblastic cells (Eckes et al., 1998), but not in epithelial cells. To characterise the cellular outgrowth from biopsy tissues, cells were stained using indirect immunofluorescence for vimentin and cytokeratin expression. A pan cytokeratin antibody (Monoclonal Anti-Cytokeratin PCK-26 produced in mouse, Sigma-Aldrich, UK) and anti-vimentin antibody (Monoclonal Anti-Vimentin VIM-13.2 produced in mouse, Sigma-Aldrich, UK) were used as primary antibodies, then secondary antibodies conjugated to FITC were used according to the protocol described in Section 2.7.

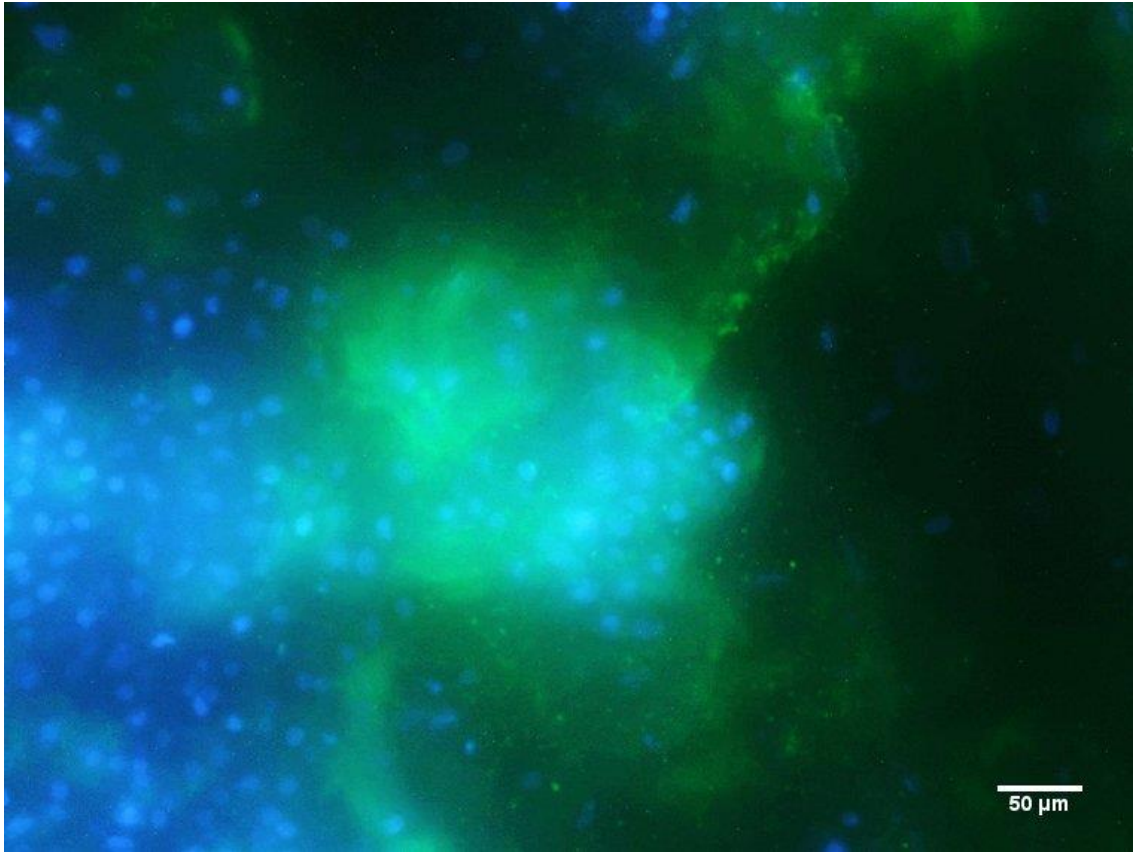


Figure 3.12 – Representative image of tissue outgrowth stained for cyokeratin expression (green) (Blue is DAPI) confirming that epithelial outgrowth has occurred from the biopsy. There is no stain for vimentin (red), therefore it can be concluded that the tissue has a significant epithelial component, in line with the PCR results shown in Section 3.3.4.

RT-PCR to assess cyokeratin and vimentin expression profiles for H400 cells, primary epithelial outgrowth from biopsies and fibroblasts

RT-PCR was performed on RNA extracted from half of the cell pellet from primary cells which were cultured as in Section 3.2.5, RNA was extracted and cDNA was synthesised (see Section 2.5).

Following synthesis of cDNA, RT-PCR was performed using primers for cyokeratins 1 and 5, which have been shown to be expressed in oral gingival epithelial cells (Mackenzie et al., 1991) and vimentin, a fibroblastic / mesenchymal cell marker. Primary epithelial cells (1°E) were compared with H400 cells (H) and primary fibroblast-like cells (1°F) (cells cultured to 6 passages post explant growth and more fibroblastic in appearance), and neutrophils (N) were included as a control cell as they should contain minimal amounts of cyokeratin and vimentin.

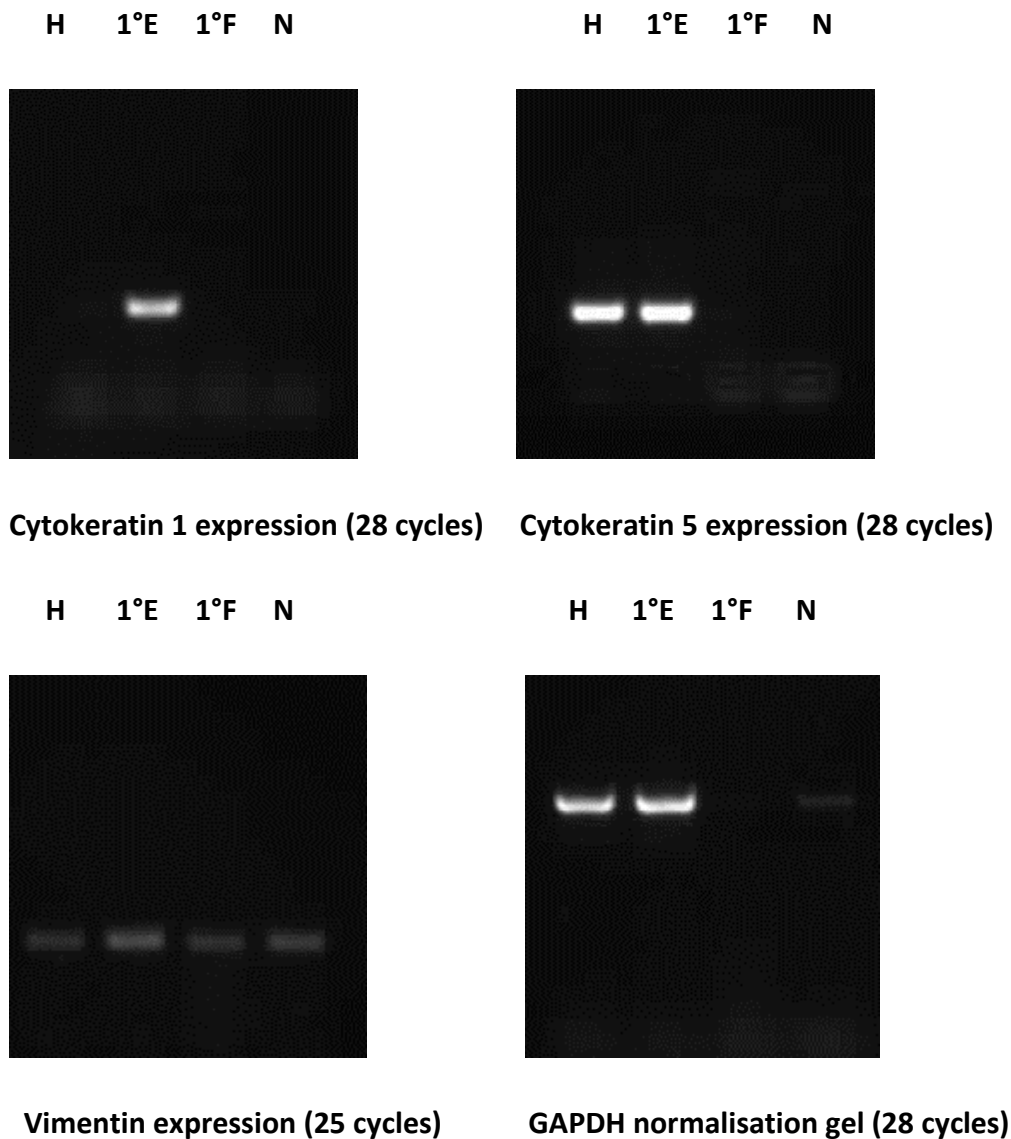


Figure 3.13 – Images of agarose gel showing expression of cytokeratins and vimentin in H (H400), 1°E (primary epithelial appearance), 1°F (primary fibroblastic appearance and N (neutrophil) cells.

These results clearly show that the primary epithelial cells express cytokeratins 1 and 5. The signal for vimentin expression from the fibroblastic cells appeared to be low, however following normalisation after further RT-PCR using a primer for glyceraldehyde 3-phosphate dehydrogenase (GAPDH), vimentin expression was shown, as was expected.

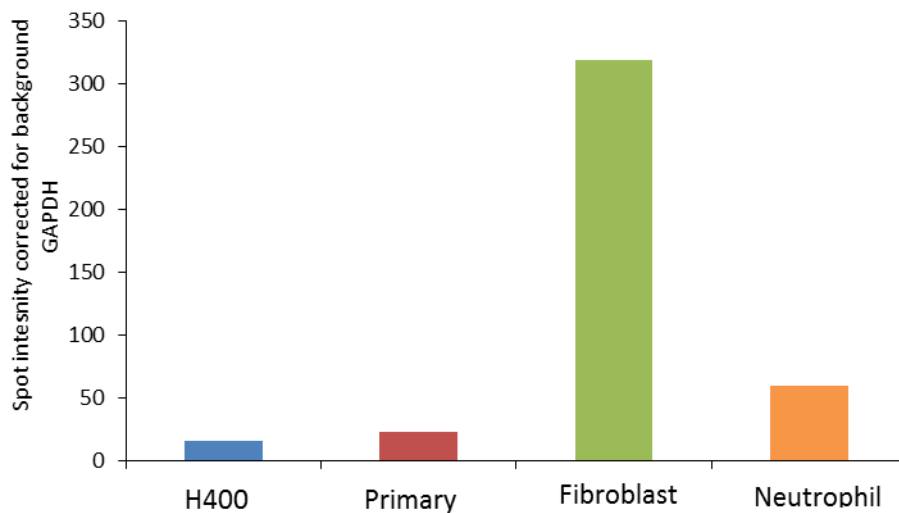


Figure 3.14 – Expression of vimentin in different cell types H400; primary (primary epithelial appearance cells), fibroblast (primary fibroblastic appearance cells) and neutrophil (neutrophils), adjusted for background expression of GAPDH, n=1. This result was consistent with previously published findings (Mackenzie et al., 1991).

3.2.5 *Conclusions of characterisation following culture of epithelial cells from gingival tissues*

It can be concluded that:

- H400 cells can be readily cultured and exhibit an exponential growth pattern until reaching confluence;
- H400 cells exhibit a classical epithelial morphology and cytokeratin expression profile;
- Early outgrowth from donor tissue initially produces well characterised epithelial cells using either the explant method or feeder cell layer method;
- The early outgrowth from donor tissue shows strong cytokeratin 1 and 5 expression and limited vimentin expression along with characteristic epithelial cell morphology, suggesting an epithelial cell phenotype;
- However, these primary epithelial cells lose their epithelial morphology and markers after the first passage, suggesting a loss of epithelial phenotype;
- Primary oral epithelial cells can be successfully isolated but long term culture and obtaining a reliable supply of these cells in the numbers required is problematic. There will also be inherent variability in cells from different

donors which will potentially compromise experimental design and subsequent results;

- For these reasons it was decided to use H400 cells for initial experimentation and then whenever possible verify results by using primary epithelial cells.

Based on the findings of initial studies it was decided to harvest primary epithelial cells via the “explant method” and use these cells for verification of H400 responses. The choice of the “explant method” for epithelial cell harvest was driven by the reduced time required and the lack of need for a feeder layer. Data generated in this study have highlighted the unreliability of extracting epithelial cells following passage with either of these techniques, therefore primary cells were grown out from explanted tissue and used immediately in experiments rather than following cell passage as the data demonstrated that passaged cells have a non-epithelial cytokeratin profile and also express vimentin.

3.3 Potential interactions of Ti NPs with known assays

The *in vitro* methods reported in published studies involve exposure of cells to a defined concentration of NPs within suspension. Given that NPs are insoluble and show a strong propensity for aggregation (Zhang, 2014), the exposure of each individual cell to NPs will not be uniform. Attempts to mitigate this have used sonication of suspensions as described by Taurozzi et al., prior to cell challenge (Taurozzi et al., 2013), however visual examination of samples after a few hours shows that agglomeration still occurs. For this reason, the sonicated powder was kept in water at stock concentration and added to the cell culture medium as required. When the stock suspension had been prepared for >48 h, it was re-sonicated to disperse any settled TiO₂ NPs (visual inspection showed settling of some powder in water after this time). Section 2.1.1 contains details of the sonication protocol used.

Conventional assays are commonly used to measure a range of outcomes such as cell viability, pro-inflammatory gene transcription factor activation and cytokine production. Many of these assays are multi-well plate-based assays and use a variety of chemistries to deliver a colour change or fluorescent signal which is in proportion to the quantity of specific analyte present. Conventional assays such as luminescent ATP

assays, MTT assays and LDH assays have been used to determine cell viability when exposed to NPs (Barillet et al., 2010, Gerloff et al., 2012, Fisichella et al., 2012). However, issues concerning the use of some of these assays in the presence of NPs have been highlighted (Kroll et al., 2009), and specific interactions between TiO₂ NPs and the MTT assay have been established (Holder et al., 2012). It is essential to ensure that NPs do not interfere with the chemistry of an assay system so that it can be reliably used in an experimental model.

3.3.1 *Cell Titer-Glo[®] verification with TiO₂*

Cell Titer-Glo[®] is an indirect luminescence assay which measures “viability” indirectly by quantifying the ATPase activity in a sample of cells. ATP is required for the conversion of the reagent into the end product, a process which produces light that can be quantified by a luminometer (see Section 2.3.1 for detail). This commercial assay is designed to work by being added to a sample of cells in serum supplemented medium, which will then be lysed and results in the generation of light proportional to the amount of ATP present in the sample. It is therefore more accurately a measure of metabolic activity as opposed to true cell viability. All experimental samples must be compared with control samples. Due to the number of steps involved in the assay, it is possible that the presence of TiO₂ NPs within the system may disrupt the assay chemistry and inhibit light production resulting in inaccurate results.

CellTiter-Glo[®] was used as detailed in Section 2.3.1. In cell free conditions, no interaction between TiO₂ NPs and RLU output were found at levels of 0-1000 ppm TiO₂ NPs.

3.3.2 *MTT ([3-(4,5-Dimethylthiazol-2-yl)-2,5-Diphenyltetrazolium Bromide]) Assay*

This is a colourmetric assay for assessing cell metabolic activity, as the reduction of the reagent to the product formazan is dependent upon the presence of NAD(P)H. This means that MTT is reduced in the mitochondria of living cells, therefore the amount of formazan present in a well following reduction should be proportional to the cell viability within that sample (Liu et al., 1997). Formazan has a purple colour, so the amount of end product can be determined by the quantification of light absorbance at a wavelength of 570 nm. The MTT assay has been used in the literature as a measure

of epithelial cell viability in the presence of TiO₂ NPs (Huang et al., 2009, Barillet et al., 2010). However due to the fact that it is a colourmetric assay it is reasonable to assume that assay output may be directly affected by the presence of TiO₂ NPs, not least because of TiO₂ being used widely as a pigment.

The MTT assay was tested under cell free conditions in the presence of up to 1000 ppm TiO₂ in cell culture medium as described in Section 2.1.1 and compared with wells containing media and H400 cells cultured under standard conditions. This was to assess if there was a significant interaction between TiO₂ NPs and the colour change as measured by the absorbance of the resulting solution at 570nm.

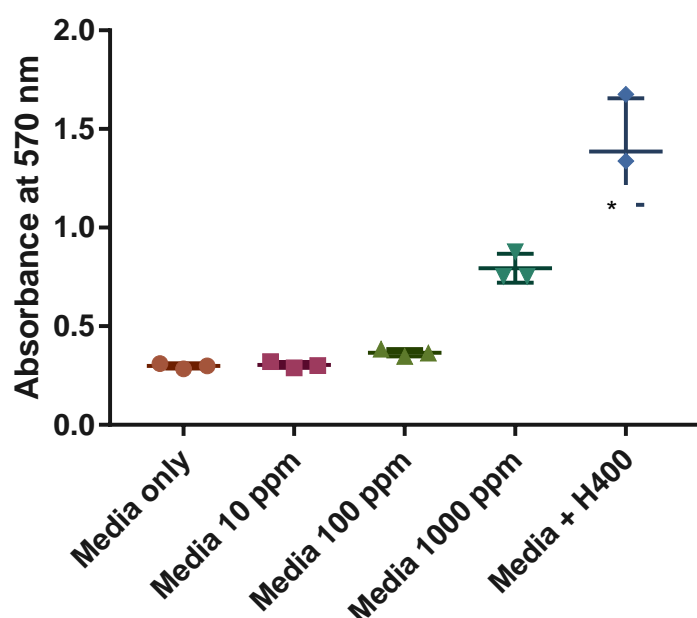


Figure 3.16 – Absorbance (Relative Absorbance Units) for cell culture media (M) containing 0-1000 ppm TiO₂ NPs and H400 cells (n=3). There appears to be a dose dependent interference from TiO₂ under cell free conditions, therefore this would potentially alter readings from cell containing wells. The asterisk shows a significant difference from media only when statistically tested using a one way ANOVA ($p < 0.001$).

MTT assay verification – conclusions

From the data presented, there is a clear interaction between TiO₂ NPs at concentrations that will be used in this work and the MTT assay making it unsuitable to measure cell viability/metabolic activity in the model system. The interaction (Figure 3.16) is to be expected due to the fact that TiO₂ is widely used as a pigment. Although

many other investigators have used the MTT assay with NPs, it was not used further in this experimental model and other measures of cell viability were investigated.

3.3.3 LDH assay

The LDH assay is a colourmetric assay used to determine cell viability. This assay uses cell supernatant to quantify levels of LDH. The assay measures the reduction of NADH via the conversion of lactate to pyruvate. Diaphorase then uses NADH in the reduction of the reagent to a red formazan product which can be measured. LDH is only present in cell culture medium if cells within the sample have damaged membranes, therefore are non-viable. LDH assays have been suggested to be unreliable when used in the presence of TiO₂ NPs (Chan et al., 2011), therefore it was essential to verify the assay in the context of the methods described in Chapter 2.

LDH assay verification – method

The CytoTox-ONE™ assay was used in this work and is a commercially available LDH assay kit. Cell free wells of a 96-well plate contained a range of TiO₂ NP concentrations from 0 to 1000ppm (see Section 2.2.2). 100 µL supernatant was removed from the wells and placed into a black, opaque bottomed plate for the LDH assay to be carried out (see Section 2.3.2). Known concentrations of LDH (positive control from CytoTox-ONE™ kit) were added to wells in order to assess the effect of the presence of TiO₂ NPs in the system.

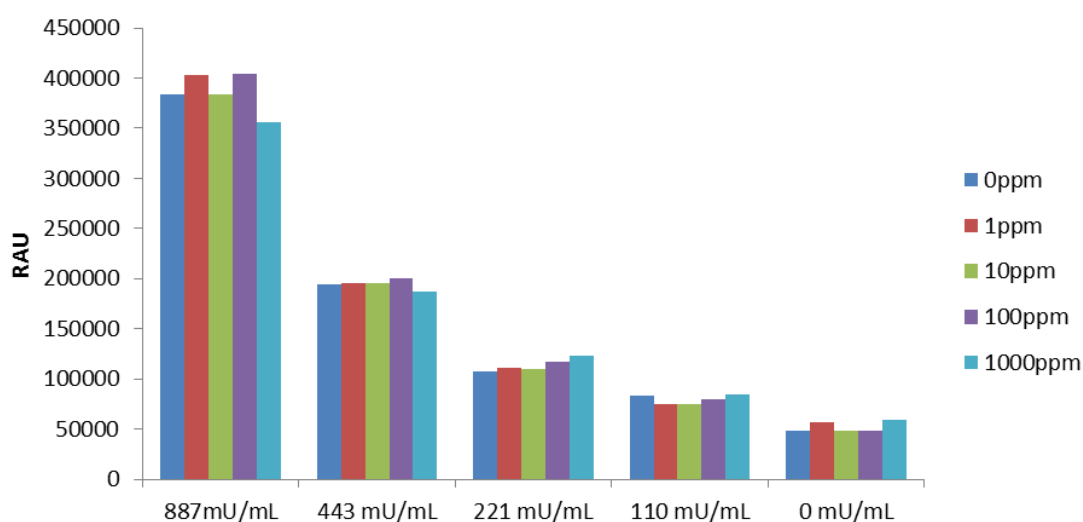


Figure 3.17 – Absorbance (RAU) of samples containing known concentrations of TiO₂ NPs and LDH. Interactions were not noted up to 887 mU/mL LDH and 1000 ppm TiO₂. n=1.

The initial data shown in Figure 3.17 suggest that the LDH assay is not significantly affected by the presence of TiO₂ NPs in the method described in Section 2.6.2. Further work to verify the LDH assay in terms of its sensitivity and other potential issues in the model system can be found in Section 5.1.2.

3.3.4 *CaspaseGlo® 3/7 assay*

The caspase enzymes are a group of enzymes essential for cellular apoptosis. Caspases 3 and 7 are effector caspases, which cleave proteins within a cell to initiate apoptosis. CaspaseGlo 3/7 is a commercially available luminescence assay which detects the presence of caspases 3 and 7 within a sample containing a cell population. The substrate is cleaved in the presence of caspases 3 and 7 to produce a substrate for luciferase used in the production of light (aminoluciferin). The reagent lyses the cells within a sample, and the amount of caspases 3 and 7 is proportional to the amount of light emitted, therefore indicating the proportion of cells within the sample which are apoptotic when compared with the control. It has been reported that TiO₂ NPs are capable of inducing apoptosis in a variety of human cells including human keratinocytes (Shukla et al., 2011a), human epidermal cells (Shukla et al., 2011b), human lung cancer line A549 (Srivastava et al., 2013), human embryonic kidney cells (Meena et al., 2012), cultured BEAS-2B cells (Park et al., 2008) and human liver cells (Shukla et al., 2013).

Cell free wells containing H400 cell culture medium as described in Section 2.2 with up to 1000ppm TiO₂ NPs were tested alongside wells containing control cells cultured according to the standard protocol (see Section 2.2.2) to investigate any interference between the TiO₂ NPs and the mechanism of action of the assay. As caspases are likely to be released over time, a selection of time-points up to 30 h was tested. No significant effect of the presence of up to 1000ppm TiO₂ NPs in a cell free system on the generation of light signal was observed.

3.3.5 *Conclusions from assay verifications*

It was concluded from this Section of work that cellular “viability” of H400 cells cultured as per the standard protocol and exposed to up to 1000 ppm TiO₂ (anatase,

<25 nm) may be assessed using the following assays; Cell Titer-Glo, LDH assay and CaspaseGlo 3/7.

It was decided not to use the MTT assay due to clear interference from the presence of TiO₂ in a cell free system. The results in general highlight the importance of validating known assays in a protocol involving nanoscale Ti products, and emphasise the need to validate each experimental protocol before interpreting any data produced.

3.4 Chapter conclusions

The conclusions from the work in this chapter which now lead on to further work are:

- H400 cells can be readily and reliably cultured according to the methods outlined in chapter 2.
- H400 cells are not completely representative of primary epithelial cell responses as they are an immortalised cell line, however they show good characterisation in terms of morphology, cytokeratin expression and growth characteristics in order to be used as an oral epithelial cell model to examine interactions between TiO₂ NPs and epithelial cells.
- While it was possible to culture primary epithelial cells from tissue in at least two ways, subsequent passage and reseeding of these cells produces a cell population with a reduced epithelial phenotype. The characterisation of these cells shows that epithelial markers are present in the initial outgrowth, however subsequent cell passages appear to show a more fibroblastic profile of markers. It was therefore decided to use initial outgrowth primary epithelial cells from biopsied tissue in experiments to ensure they are as pure a population of epithelial cells as possible. This in turn limits the availability of primary epithelial cells, therefore not all work was able to be carried out on both H400s and primary cells. It was decided that H400 cells would be used as the main cell model, and any significant findings validated by the use of primary oral epithelial cells where possible.
- TiO₂ NP dispersion in water produces a relatively homogeneously dispersed suspension, however on adding to cell culture medium, some settling out of TiO₂ occurs. This means that the concentrations of TiO₂ NPs added into each

system will be variable and hard to measure accurately. In addition, the actual local concentration adjacent to each cell is likely to vary considerably. However, this somewhat mimics the *in vivo* situation and was therefore acceptable in the model system used.

- The reported data have shown that TiO₂ NPs have potential to interact with a number of assays, so careful verification is required prior to use to ensure the validity of any results obtained. CellTiter-Glo[®], CytoTox-ONE[™] and CaspaseGlo[®] 3/7 all show insignificant confounding effects from the addition of TiO₂ NPs into the cell free model system.

Chapter 4

Imaging of interactions between TiO₂ NPs and oral epithelial cells

Synopsis

This chapter investigates the interactions between both H400 and primary epithelial cells with TiO_2 nanoparticles (TiO_2 NPs). Imaging potential interactions between epithelial cells and TiO_2 NPs is challenging, as conventional microscopy techniques (i.e. light microscopy) are limited in their ability to visualise NP agglomerations or individual NPs due a lack of resolution. In addition, conventional microscopy provides limited information on the 3D localisation of TiO_2 NPs in relation to epithelial cells i.e. are they located on the cell surface or intracellularly. Initially, light microscopy was used to gather an overview of features such as cell surface binding or intracellularisation of TiO_2 NPs by H400 cells. Subsequently TEM and reflectance microscopy were used to further elucidate how these particles associate with epithelial cells.

4.1 Light microscopy findings

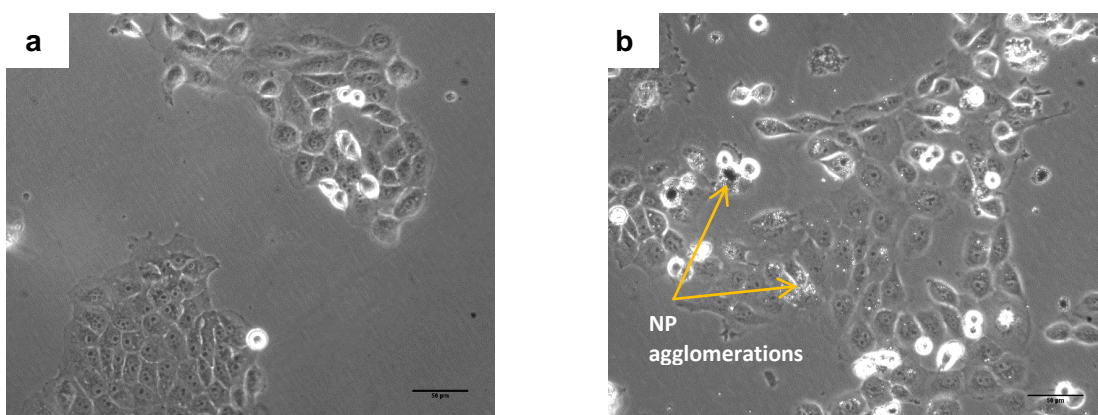


Figure 4.1 – A representative image of H400 cells cultured in a 25cm^2 cell culture flask without addition of TiO_2 NPs (a) and after the addition of 100 ppm TiO_2 NPs to cell culture medium for 24 h (b) showing potential association of NP agglomerations with cells but no apparent inhibition of growth at this stage (48 h post seeding) from a qualitative visual examination.

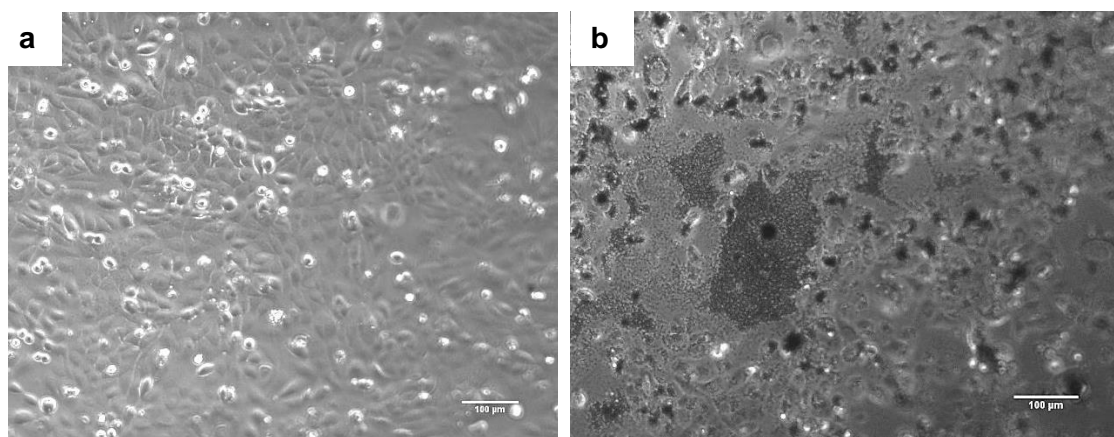


Figure 4.2 – A representative image of H400 cells cultured in a 25cm² cell culture flask without addition of TiO₂ NPs (**a**), and after the addition of 100 ppm TiO₂ NPs to cell culture medium for 48 h (**b**) showing potential association of NP agglomerations with cells and possible inhibition of growth at 72 h post seeding. Image (**a**) shows confluent cells while (**b**) shows an inconsistent monolayer with agglomerations of NPs visible.

Light microscopy suggested no clear inhibition of H400 cell growth at 24 h following the addition of TiO₂ NPs to the growth medium. At 48 h following TiO₂ NP addition, agglomerations of NPs were clearly visible in the flasks and appeared to prevent cells from adhering to the cell culture plate. Smaller agglomerations were associated with individual cells, potentially bound to the cell surface membrane or being intracellularly located. These features were consistent across multiple images. Complementary imaging techniques were performed to establish whether NPs were bound to cellular membranes, loosely associated with cell membranes or intracellularly located.

4.2 Transmission Electron Microscopy (TEM)

TEM was conducted on sectioned cells to confirm and add to the information gained from light microscopy. TEM provides a higher resolution than standard light microscopy due to the shorter equivalent wavelength of electron beams compared with that of visible light. Images can be acquired with subcellular resolution which is more suited to the investigation of NP interactions with cells and cellular substructures.

Sample preparation for TEM involves fixation of a sample in a solid matrix then sectioning into ultrathin (50 µm) sections. Sectioning allows intracellular structures to

be visualised, thereby enabling the location of intracellular agglomerations to be discerned from those associated with the cell membrane.

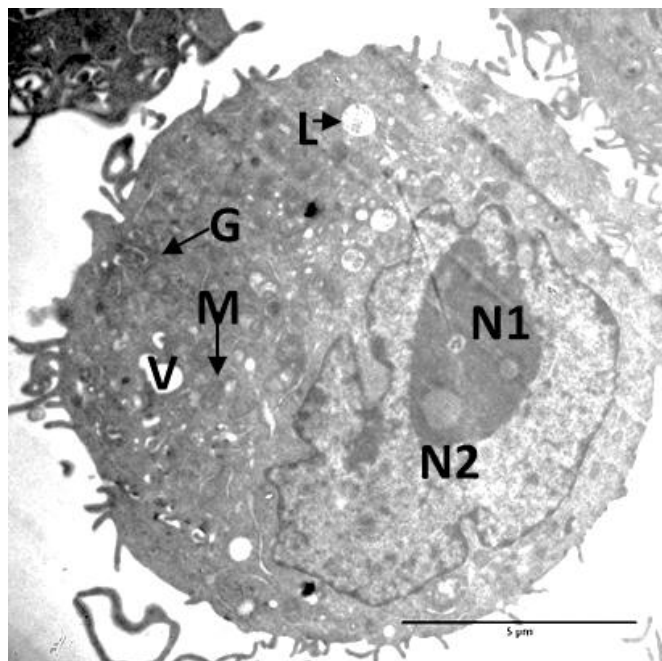


Figure 4.3 - a Section through a detached (trypsinised) and fixed H400 cell viewed using TEM. Labels are G= Golgi apparatus, L = lysosome, N1 = nucleolus, N2 = Nucleus, M= mitochondria and V = vacuole.

Cells for examination using TEM microscopy were prepared as per the protocol (Section 2.8.1) following culture and stimulation using a variety of conditions as listed below (all using H400 cells):

- Control cells: H400 cells cultured to 80-90% confluence under standard conditions (see Section 2.2);
- Washed with 100ppm medium: H400 cells cultured to sub confluence as in Section 2.2 then rinsed for <1 min with cell culture medium containing 100ppm TiO_2 NPs;
- Cultured for 24 h with 10 ppm TiO_2 NPs H400 cells cultured to 24 h prior to sub confluence then medium containing 10 ppm TiO_2 NPs added for 24 h;
- Cultured for 24 h with 100 ppm TiO_2 NPs: H400 cells cultured to 24 h prior to sub confluence then medium containing 100ppm TiO_2 NPs added for 24 h;
- Cultured for 24 h with 1000 ppm TiO_2 NPs: H400 cells cultured to 24 h prior to sub confluence then medium containing 1000ppm TiO_2 NPs added for 24 h.

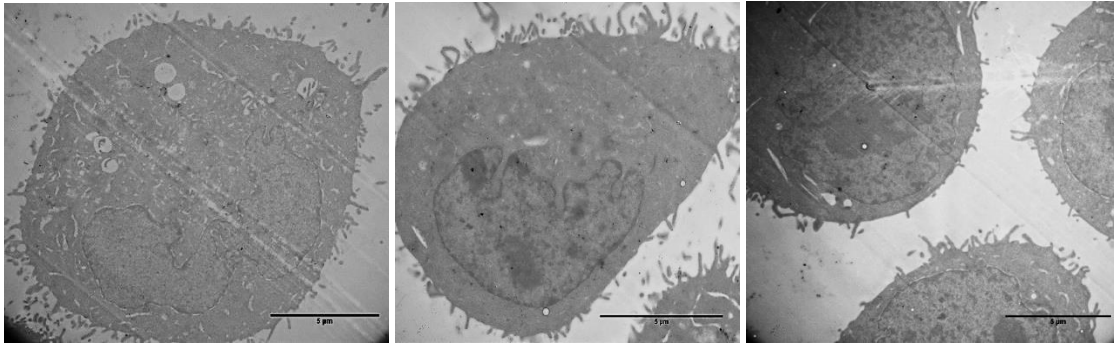


Figure 4.4 – Control (not exposed to TiO₂ NPs) H400 cells imaged using TEM. The non-uniform appearance of the cells is due to cell-cell variation and the level of sectioning through the cell which will alter the visible area of organelles. See Figure 4.3 for more organelle structure detail. Scale bar = 5 µm.

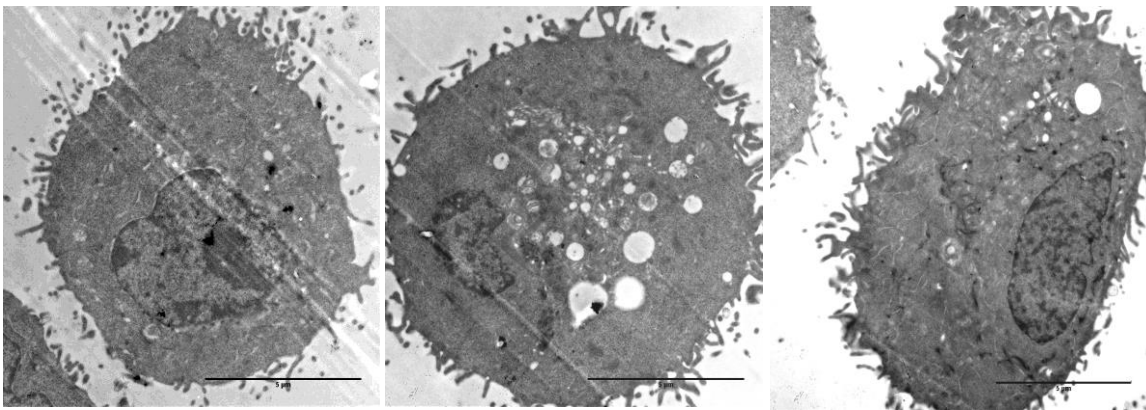


Figure 4.5 – H400 cells washed (<1 min) with cell culture media supplemented with 100ppm TiO₂ NPs to determine if NP agglomerations adhere to the cell membrane. Results indicated that no NP agglomerations were seen suggesting that immediate surface adherence is not a mechanism by which NP interact with H400 cells. Scale bar = 5 µm.

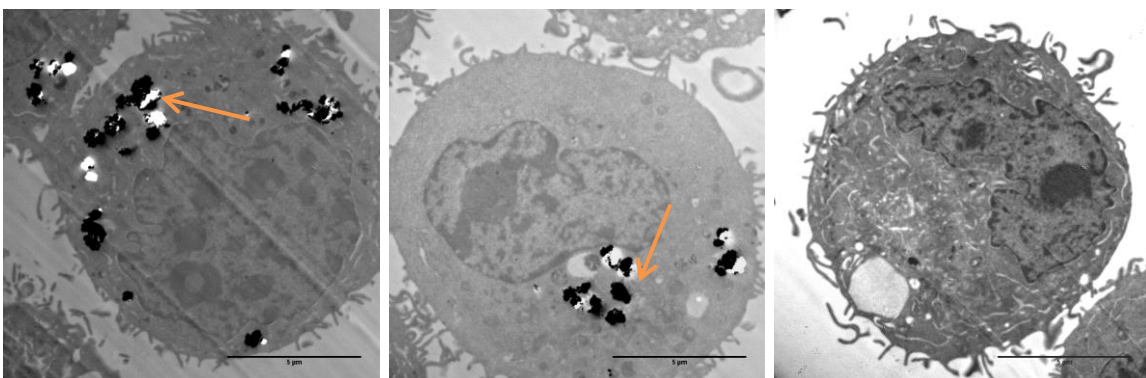


Figure 4.6 – H400 cells cultured with 10 ppm TiO₂ NPs in medium for 24 h showing varying numbers of NP agglomerations as marked by arrows seen as black or white features (charging in EM) associated with cells. Microscopic qualitative assessment showed that 30-50% cells had visible NPs agglomerations either intracellularly or associated with the cell membrane. The NP agglomerations appeared to be of the order of 0.5-2 µm diameter and within the cell cytoplasm. Scale bar = 5 µm.

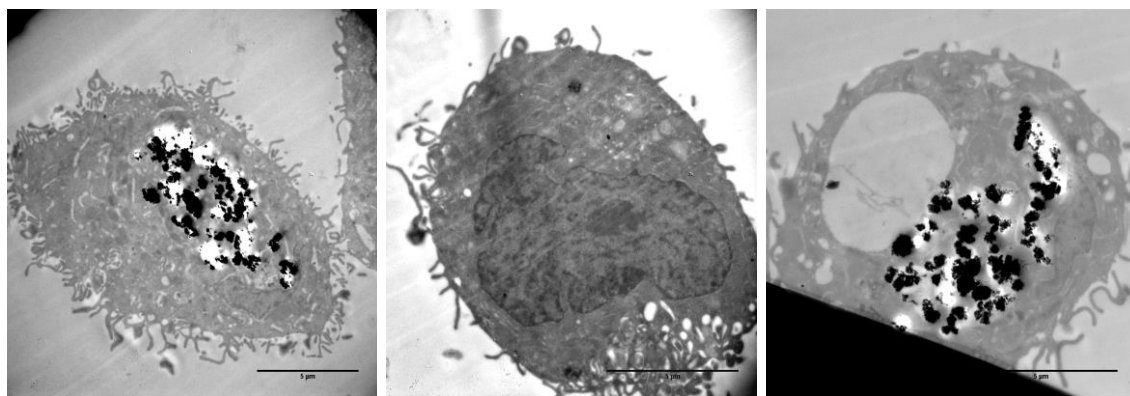


Figure 4.7 – H400 cells cultured for 24h in growth media containing 100ppm TiO₂ NPs. Results showed varying numbers of TiO₂ NP agglomerations associated with cells. 30-50% of cells appeared to have agglomerations visible intracellularly or associated with the cell membrane. The visible TiO₂ NP agglomerations visible appeared to be grouped into larger collections than at lower concentrations (10 ppm), with groups of agglomerations nearing 5 μm in diameter seen. Vesicle type structures appear in some images. TiO₂ NPs appear generally as agglomerations as opposed to being scattered throughout the cell. Scale bar = 5 μm.

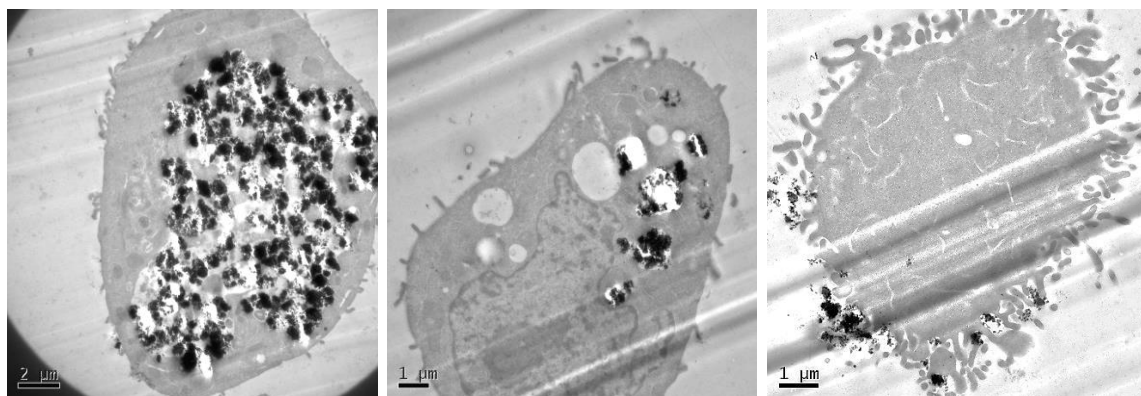


Figure 4.8 – H400 cells cultured with 1000ppm TiO₂ NP containing medium for 24h showing varying numbers of NP agglomerations associated with cells. 30-50 % of cells appeared to have NP agglomerations visible intracellularly or associated with the cell membrane from a qualitative visual assessment. The TiO₂ NP agglomerations appeared to be grouped into collections ranging from 0.5 μm to nearing the whole cell diameter (approx. 30 μm) in a non-uniform distribution. Scale bar = 2 or 1 μm.

This series of images demonstrates TiO₂ NP agglomerations. The amount of agglomerated NP within the cells increased with the exposure concentration; however accumulation was not consistent throughout the population of cells; 50-70 % cells appeared not to contain intracellular TiO₂ NPs. Higher exposure concentrations resulted in very large groups of agglomerations occupying a substantial proportion of

the cytoplasm of some cells, while other cells within the same sample appeared to have no visible intracellular agglomerations.

NPs have been shown to be present intracellularly in human lung epithelial cells (Singh et al., 2007) following exposure to ultrafine TiO₂ particles (using TEM and X-ray methods). TEM images from Singh et al., (Singh et al., 2007) showed small agglomerations of particles within lamellar bodies in lung epithelial cells as well as agglomerations of ultrafine particles within membrane bound vacuoles consistent with findings in this study. Singh et al., also noted a lack of uniformity in the intracellular number and location of ultrafine particles and proposed the uptake mechanism to be endocytosis (Singh et al., 2007). Polystyrene NP uptake into HeLa cells has also been reported (Dausend et al., 2008). Endocytosis is a process where cells actively uptake a molecule, particle or agglomeration by engulfing it within a membrane bound vesicle. Nanoparticle uptake into HeLa cells has been shown to occur, (Smith et al., 2012), and this intracellularisation was shown to be reduced but not entirely stopped by inhibition of the clathrin-mediated endocytosis pathway. These findings suggest that clathrin-mediated endocytosis is one mechanism of intracellularisation of carboxylate-modified polystyrene NPs into HeLa cells, but that multiple mechanisms may exist therefore accounting for some residual uptake once clathrin mediated endocytosis has been inhibited. Alternative mechanisms may include diffusion through pre-existing or induced perforations within the plasma membrane of the cell. From the findings of Smith et al., it is plausible that (clathrin mediated) endocytosis is one mechanism involved in the uptake of TiO₂ NPs into H400 cells.

4.2.1 *Limitations of TEM imaging*

Although these images appear to show intracellular agglomerations of TiO₂ NPs, there are alternative explanations which need to be ruled out before claiming that intracellularisation has occurred.

1. The particles may have been dragged during processing and may be superimposed over the cell sections rather than being located intracellularly. This is unlikely as the images appear to show membrane like structures

around agglomerations of nanoparticles, however it is not possible to exclude this scenario from these images alone.

2. The sample preparation for TEM imaging is complex, therefore some form of agglomeration of the nanoparticles may have arisen via mechanisms which are unrelated to epithelial cells themselves.

Therefore, the following two strategies were adopted to definitively identify whether the H400 cells contained intracellular TiO₂ NP agglomerations, and to further assess the TiO₂ NP agglomerations following alternative fixation methods.

1. To confirm endocytosis as a mechanism leading to TiO₂ NP intracellularisation, an endocytosis blocking agent was used to investigate whether this affected the apparent TiO₂ NP uptake.
2. In addition, an alternative imaging method (confocal microscopy) was used to confirm intracellular accumulation of TiO₂ NPs. Confocal microscopy enables visualisation of agglomerations within a cell without the need for cell sectioning and uses a less complex fixation protocol, mitigating the possibility of agglomerations being either caused by or introduced by the fixation and processing required for TEM.

Furthermore, reflectance confocal microscopy also allows visualisation of agglomerations and their association and distribution between cells to further investigate the non-uniform cell distribution.

4.2.2 *Treatment with an endocytosis inhibitor*

Dynasore hydrate is a cell permeable dynamin 1 and 2 GTPase activity inhibitor, and blocks endocytosis, which is dependent on dynamin for clathrin coated vesicle formation. Serum within cell culture medium is known to inhibit dynasore hydrate. For studies using dynasore, H400 cells were cultured in standard medium until just sub-confluent, then gently rinsed in warmed PBS and a serum free medium added (Section 2.2.1) with or without TiO₂ NPs as appropriate. To assess the effect of treating epithelial cells with dynasore hydrate, H400 cells were cultured with dynasore hydrate at a concentration of 80µM for 24 h in the presence of 100 ppm TiO₂ NPs. Control cells

were cultured with 0.1% DMSO (the vehicle for dynasore hydrate) and 100 ppm TiO₂ NPs.

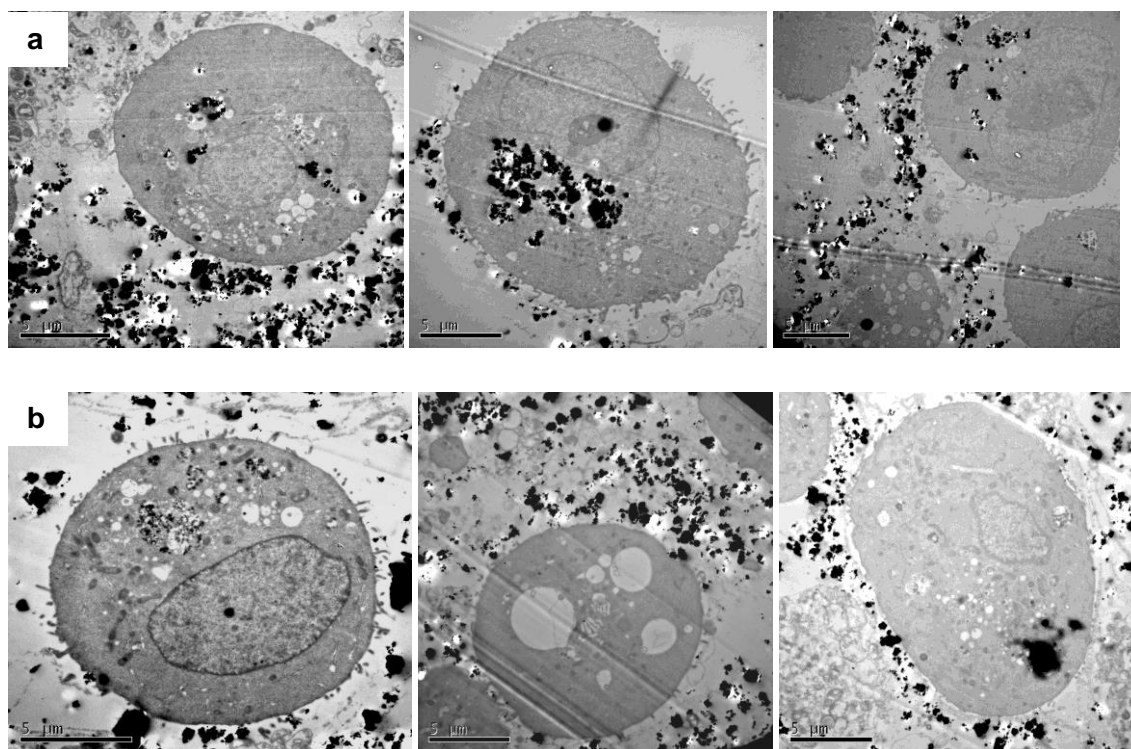


Figure 4.9 – H400 cells cultured with (a) 100 ppm TiO₂ NP containing medium for 24 h and 0.1% DMSO showing varying numbers of NP agglomerations associated with cells. Agglomerations are seen intracellularly in the size range of <1 µm to groups of agglomerations totalling >5µm. There was an enhanced amount of NP debris surrounding cells due to a number of possible reasons; either omission of serum means NPs will be more likely to associate with proteins within the cell membrane, or the protein corona which forms surrounding NPs in the presence of serum may make them more susceptible to washing off the monolayer prior to fixation. (b) Shows H400 cells cultured with 100 ppm TiO₂ NP containing medium for 24 h with 80 µM Dynasore Hydrate showing reduced numbers of NP agglomerations associated with cells as judged qualitatively by visual inspection. The agglomerations of NPs visible in the dynasore treated cells were smaller, and there appeared to be a higher proportion of cells with no visible NPs than in the control DMSO group although this cannot be reliably quantified in the sample size imaged. Scale bar = 5 µm.

TEM images showed a reduction in intracellular agglomerations of TiO₂ NPs, however subjective analysis of a limited number of cells did not enable quantification of any reduction in uptake. Some apparent intracellular TiO₂ NPs were still observed in dynasore treated cells and suggest that clathrin-mediated endocytosis was involved in uptake but that other mechanisms may also be operative and was consistent with previous findings (Smith et al., 2012).

4.3 Reflectance confocal microscopy

Reflectance confocal microscopy allows the visualisation of intracellular structures and was used to confirm intracellular agglomeration of TiO_2 NPs. For reflectance confocal microscopy, H400 cells were cultured on a glass coverslip and fixed using 4% paraformaldehyde before imaging. DAPI was used as a nuclear stain to enable cell visualisation in the fluorescence mode and to aid orientation. H400 cell preparation is detailed in Section 2.8.2.

For imaging, five randomly chosen areas on each coverslip were selected. The areas imaged were discounted if there were no visible cells present or if the cell layer appeared to have been damaged during fixation and mounting. The confocal stack of microscopy images was captured along with the reflectance confocal images of NP agglomerations. Images were analysed using FIJI (ImageJ, U. S. National Institutes of Health, Bethesda, Maryland, USA) software to maximise the visibility of organelles and to falsely colour the reflectance signal to enable location of the NP agglomerations within cells. Figures 4.10-12 show selected slices from the confocal stack of light microscopy images overlaid with the corresponding reflectance signal. These Sections were selected to include organelles to ensure they are intracellular images, and to exclude, as far as possible, surface associated agglomerations of NPs.

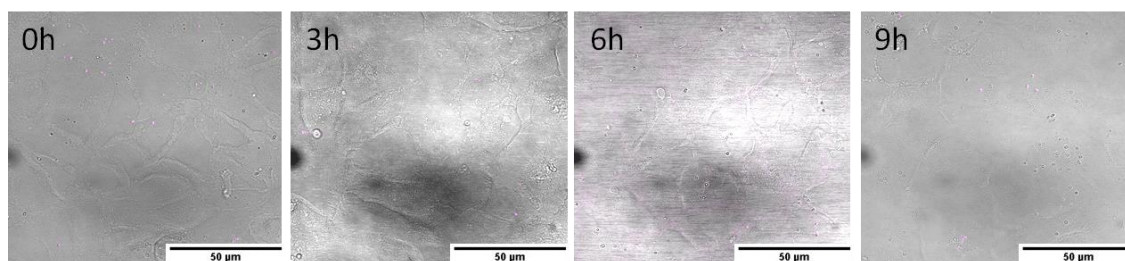


Figure 4.10 – H400 cells cultured with 1 ppm TiO_2 NPs for 0, 3, 6 and 9 h then fixed (Section 2.8.2) and viewed under reflectance microscopy. The violet colour was due to TiO_2 NPs overlaid on mid stack images from light microscopy images. A fairly broad scatter of violet points across the cell monolayer was observed, but due to the small size of agglomerations, visualisation of any specific agglomerations from these images is problematic.

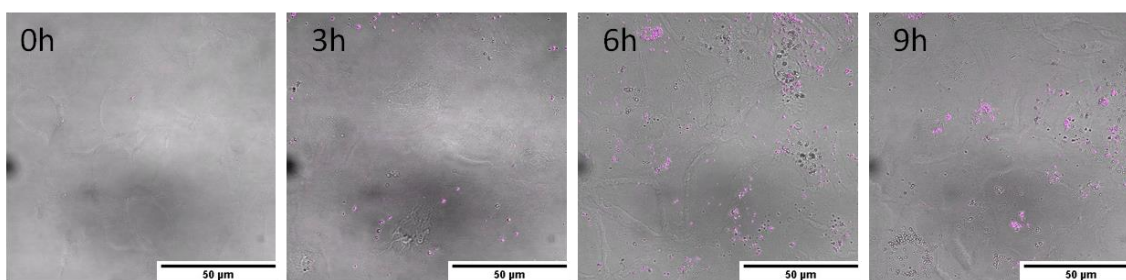


Figure 4.11 – H400 cells cultured with 10 ppm TiO_2 NPs for 0, 3, 6 and 9 h then fixed (Section 2.8.2) and viewed under reflectance microscopy. The violet colour was due to TiO_2 NPs overlaid on mid stack images from light microscopy images. Images show larger agglomerations found intracellularly with increasing time than in the 1ppm exposure sample shown in Figure 4.10. A non-uniform distribution of NP agglomerations within the cell population was observed.

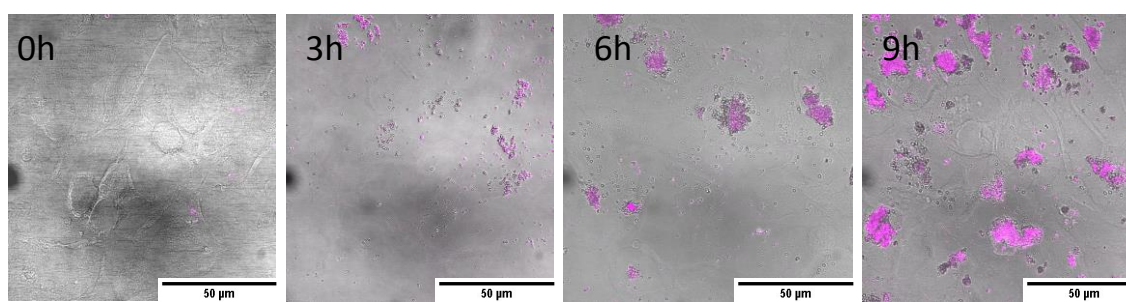


Figure 4.12 – H400 cells cultured with 100 ppm TiO_2 NPs for 0, 3, 6 and 9 h then fixed (Section 2.8.2) and viewed under reflectance microscopy. The violet colour was the signal from TiO_2 NPs overlaid on mid stack images from light microscopy images. Images show an increase in both the number of agglomerations over time and the size of these agglomerations within the cell monolayer when compared with lower concentrations of NPs. Again a non-uniform distribution was observed with certain cells producing a high signal from intracellular NPs compared with others showing very little or no signal at all.

Figures 4.10 – 4.12 demonstrated intracellular agglomerations of TiO_2 NPs from mid stack images. The magnitude of accumulation of intracellular TiO_2 NPs appears to be both dose and time dependent, and the agglomerations increase in size with higher exposure concentrations. A non-uniform distribution of uptake was seen at all exposure concentrations. The numbers of cells (approximately 34 cells per image) within 5 randomly selected images exhibiting NP agglomerations was quantified and correlated with time and exposure conditions (Figure 4.13).

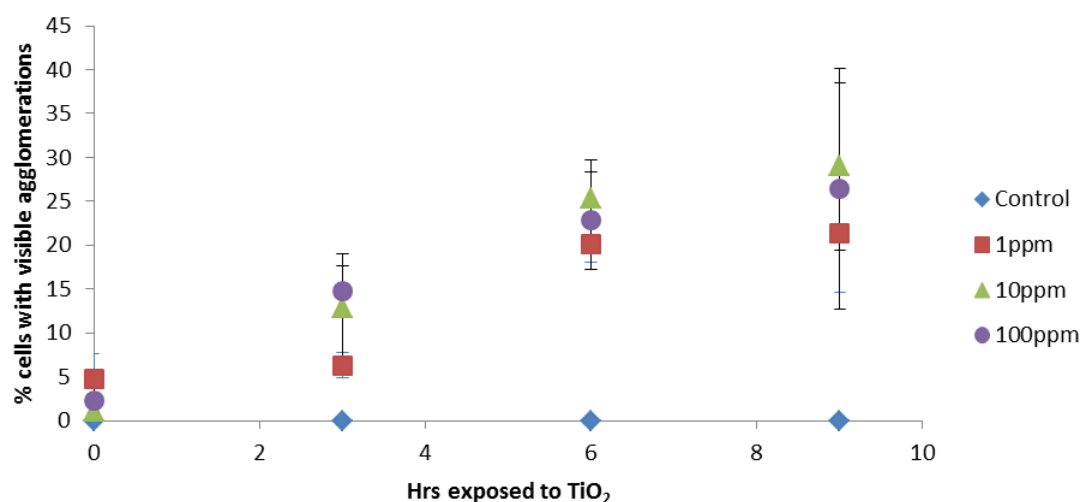


Figure 4.13 – Graph showing % cells with visible TiO₂ NP agglomerations following exposure to 0-100 ppm TiO₂ NPs for 0-9 h. Shows minimal differences in % cells with agglomerations, but images demonstrate that the agglomerations seen are larger at higher doses. n=5 images analysed, approximately 34 cells per image and 170 cells total. A two way ANOVA revealed no significant difference in the number of cells with TiO₂ NP agglomerations between the different exposure concentrations (p>0.05).

As the exposure concentration increased, the proportion of cells with visible intracellular agglomerations of NPs using reflectance microscopy did not increase significantly. Up to approximately 30% of cells exhibited visible agglomerations even when exposed to higher doses of NPs for longer time periods, and the images clearly demonstrated that the distribution of agglomerations was far from uniform within the cell population examined. Extended exposure time points (>9 h) were not performed due issues with cell confluency.

4.4 Imaging of TiO₂ NP accumulation in primary oral epithelial cells

The images of agglomerations of intracellular TiO₂ NPs in H400 cells suggest that this cell line has the capacity to intracellularise TiO₂ NPs. Reflectance microscopy was determined to be an efficient method to study TiO₂ NP accumulation and was employed to identify whether primary oral epithelial cells mirrored the pattern of uptake seen in the H400 cell line.

Primary epithelial cells were grown using the explant method and prepared (Sections 2.8.1 / 2.8.2) for imaging with both TEM and reflectance confocal microscopy. Due to the limitations of the isolation and culture of primary epithelial cells the numbers of

cells examined was lower than that for H400 cell imaging. As the adherence of primary cells to the culture glassware was less robust, cells were trypsinised prior to fixation for reflectance microscopy, and exhibited the more rounded appearance when compared with the images of the adhered confluent H400 cells seen previously. This was an experimental finding when growing primary epithelial cells on coverslips, often the primary cell monolayer was lost upon washing, compared with H400 cells, where the washing and fixing process did not seem to compromise the integrity of the cell layer. Therefore, it was decided to trypsinise and detach the primary cells from the cell culture surface prior to fixation, and to pipette the resulting suspension onto coverslips in order to prevent sample loss.

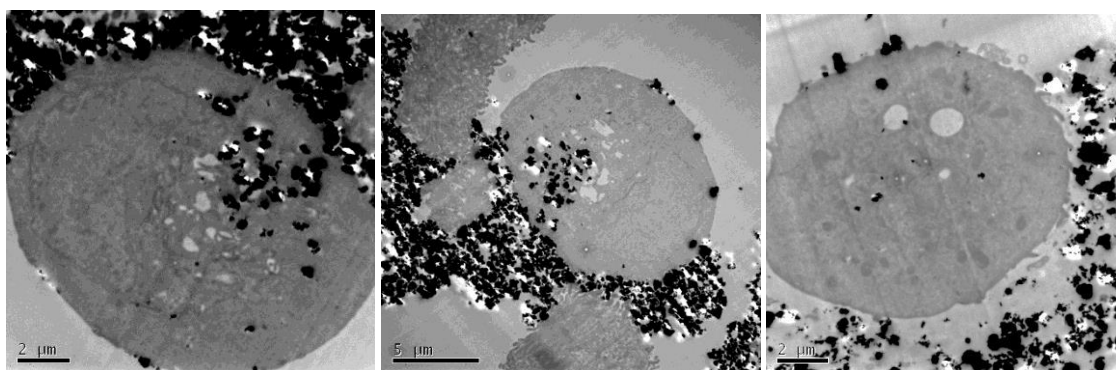


Figure 4.14 – TEM images showing primary human gingival epithelial cells exposed to TiO_2 100 ppm for 6 h. There is clear non-uniform intracellularisation in a similar manner to H400 cells, and NP agglomerations are visible intracellularly with a size range of 0.5 – 5 μm diameter.

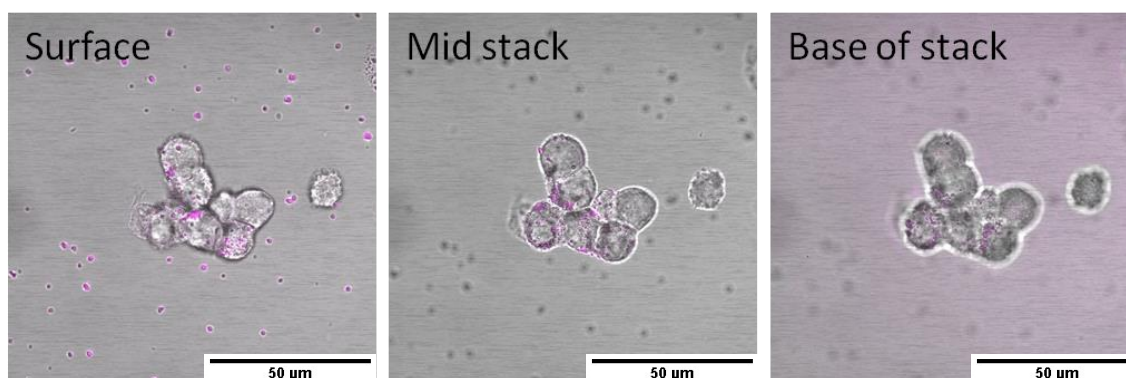


Figure 4.15 – Reflectance microscopy images of primary human gingival epithelial cells (clump of 7 cells plus single cell) exposed to 10ppm TiO_2 NPs for 6 h. Prepared after trypsinisation to increase ease of orientation on microscope compared with a monolayer. Images from cell surface, mid stack and base of stack showing clear intracellular NP agglomerations. As before violet false colour represents reflectance signal from TiO_2 NPs.

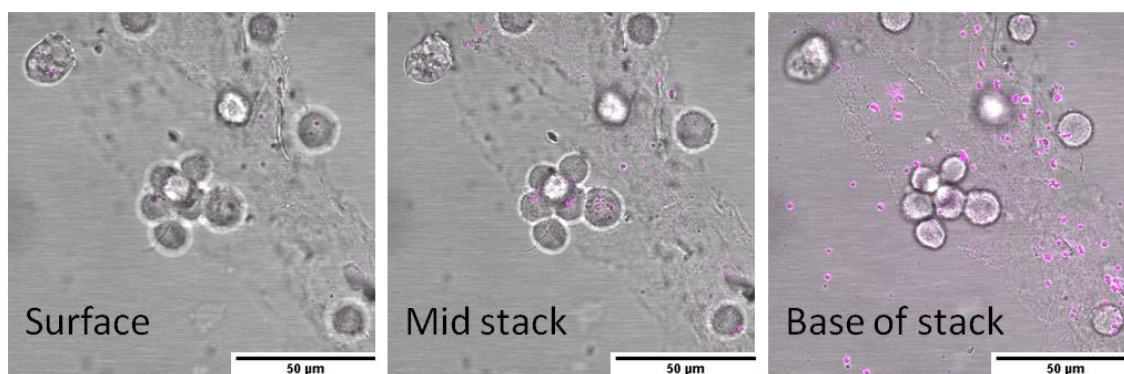


Figure 4.16 – Reflectance microscopy images of primary human gingival epithelial cells (clumps of cells plus single cells) exposed to 10 ppm TiO_2 NPs for 9 h. Prepared after trypsinisation to increase ease of orientation on microscope compared with a monolayer. Images from cell surface, mid stack and base of stack showing clear intracellular NP agglomerations. As before violet false colour represents reflectance signal from TiO_2 NPs.

Figures 4.15 and 4.16 show TiO_2 NP uptake in primary human oral epithelial cells. Although limited conclusions regarding the pattern of uptake can be drawn from these images due to the limited number of cells present, the presence of TiO_2 NPs within primary oral epithelial cells is evident.

Previously published work on the uptake of NPs by cancer cell lines (such as H400) and comparison with primary cells of a similar type is limited. Hepatocytes have been shown to take up NPs in both cancer cell lines and primary rat hepatocytes in similar amounts, but the uptake was highly dependent upon NP size and shape rather than simply cell type (Johnston et al., 2010). The specific uptake of NPs appears to depend upon both the NP studied (its coating, composition and shape) as well as the specific cell type involved and there are likely to be different uptake rates between cell lines and primary cells under certain conditions (Albanese et al., 2012). Again, multiple mechanisms of uptake are identified as being relevant in the uptake of polystyrene NPs by human alveolar epithelial cells including clathrin-mediated endocytosis (Kuhn et al., 2014). Surface charge also affects the likelihood of uptake by cells and through tissues; Bannunah et al., demonstrated positively charged NPs are more likely to be internalised by human colon epithelial cells than negatively charged NPs, a finding consistent across two sizes of NP examined (50 nm and 100 nm diameter) (Bannunah et al., 2014). It can be concluded that uptake of NPs by cells is a complex process which likely involves multiple mechanisms. Further work is required to fully characterise the processes involved.

4.5 Conclusions from cell imaging and justification for further investigation

A similar picture of intracellularisation and agglomeration of TiO₂ NPs appeared in primary gingival epithelial cells and H400 cells, therefore it can be assumed that the H400 model of interactions in this biological context has validity. The conclusions that can be drawn from the reported imaging work thus far are:

- Both H400 cells and primary epithelial cells appear to have the capacity to take up agglomerations of TiO₂ NPs in a dose and time dependent manner.
- Cells that have been exposed to larger doses of TiO₂ appear to take up larger amounts of TiO₂ NPs.
- TiO₂ NP uptake was not uniform across a cell population, and some cells remain free from visible agglomerations while others have significant amounts of TiO₂ NPs intracellularly.
- Cells which had intracellular agglomerations did not appear morphologically changed when compared with those without. This was supported by no apparent loss of viability in previously reported work (see chapter 3) at the above doses and timescales.

4.6 Synchrotron micro-focussed X-ray Fluorescence (SR-XRF)

2 dimensional micro-focussed SR-XRF is a method that can be used to measure concentration of elements at trace levels within a sample at a high spatial resolution. SR-XRF has been extensively used for biological imaging (Bacquart et al., 2007, Betz et al., 2007, Petibois et al., 2009) and Ti is an element in particular which can be imaged readily using this approach as its X-ray absorption energy (4.965 KeV) is distinct from native elements found in tissues (Mountjoy et al., 1999). Here SR-XRF was used to quantify, proportionally the number of cells within a sample exposure population that become associated with TiO₂ NPs. The proportion of cells within an exposure population actually interacting with the insoluble TiO₂ NPs stimulus will have a direct bearing on the interpretation of biological assays in the following chapters. SR-XRF has the capability to detect much smaller amounts of TiO₂ NPs than other imaging methods used to date in this work, alongside the far greater resolution of images.

4.6.1 *SR-XRF methods*

Sample preparation

H400 cells were cultured as previously described (Section 2.2.2) and exposed to TiO₂ NPs of varying concentrations (0 – 1000 ppm) for 0 – 24h. Following exposure, the cell monolayer was washed 3 times with warmed PBS and trypsinised to produce a cell suspension (see Section 2.2.2) and an equal volume of cell culture medium added to counteract the trypsin. The resulting cell suspension was then transferred aseptically to a sterile tube and centrifuged for 10 min at 1000 rpm. The resulting cell pellet was then re-suspended in ice cold methanol ($-20 \pm 2^{\circ}\text{C}$) to fix the cells, immediately mixed and pipetted at a relevant density (calculated from a cell count of the suspension before centrifugation) onto silicon nitride windows (membrane size 5.0 x 5.0 mm or 3.0 x 3.0 mm, Membrane thickness 500 nm, Silson, UK). Once air dried they were dipped into distilled water to remove crystalline artefacts from cell culture medium before being stored in a desiccator until use (up to 10 days). The above method for sample preparation is in line with current literature (Carter et al., 2010). The experimental samples produced were:

- Control cells – H400s cultured to just sub confluence then media changed for fresh medium for 24 h.
- 10 ppm - H400s cultured to 80-90% confluence then media changed for fresh medium containing 10 ppm anatase <25 nm as before for 24 h.
- 100 ppm - H400s cultured to just sub confluence then media changed for fresh medium containing 100 ppm anatase <25 nm as before for 24 h.

SR-XRF methods

2D SR-XRF was performed on the beamline ID21 at the European Synchrotron Radiation Facility (ESRF, Grenoble France) using an incident energy of 5.7 KeV and a beam footprint of $0.2 \times 0.7 \mu\text{m}^2$ and a $0.5 \mu\text{m}$ step-size. Detection limits for Ti were <1 parts per million.

4.6.2

Rr-XRF results

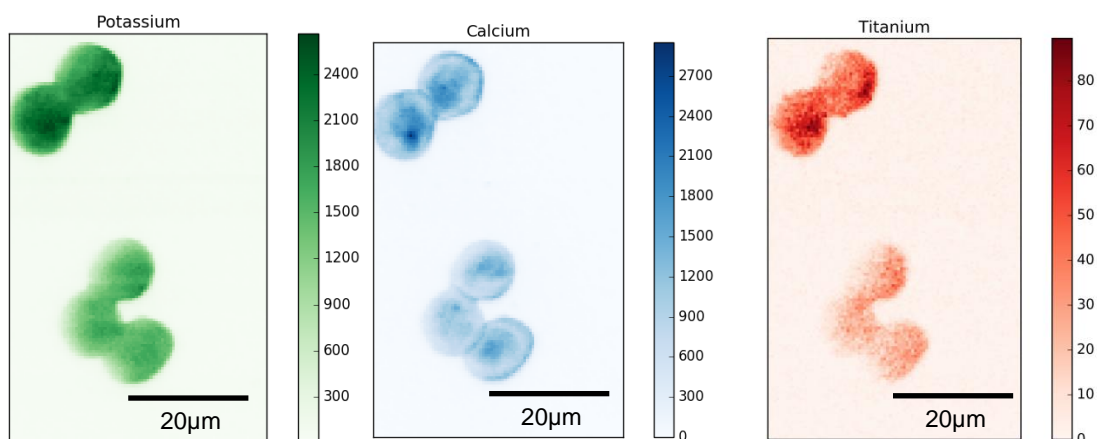


Figure 4.17 – Images showing relative fluorescence of Potassium, Calcium and Titanium in control H400 cells. The cells are not completely separated due to incomplete trypsinisation.

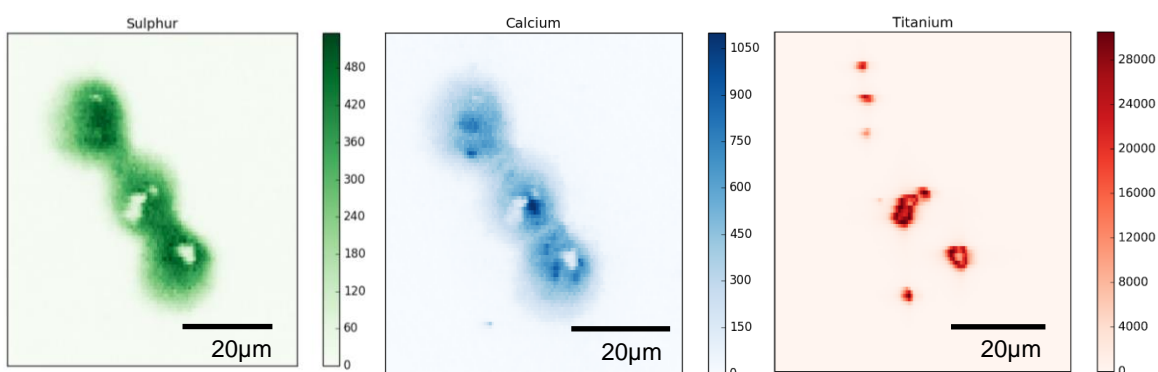


Figure 4.18 – A representative image of fluorescence of S or K, Ca and Ti in H400 cells exposed to TiO_2 10 ppm for 24h. Ti is seen within the confines of the cells in the area mapped. The white spots in all three signals are due to saturation of the signal from the large deposits of Ti leading to a loss of signal from the detector.

These initial results demonstrate a large accumulation of Ti present within the cell samples examined by SR-XRF in cells exposed to TiO_2 NPs when compared with control cells. There is saturation of the detector present (white spots) indicating that the actual concentration of Ti is higher than can be accurately recorded in some areas. The results also seem to show that Ti is present in agglomerations, concurrent with the other microscopy methods described in this chapter, and again that the distribution of Ti is non-uniform across the cell population.

To quantify the number of cells associated with Ti and in which manner, table 4.1 was constructed by counting the number of cells present, and recording if each cell was

associated with no Ti, “small” particles of Ti or “larger” particles of Ti. This table was produced using 10 ppm and 100 ppm exposed cell data. This was a qualitative assessment based on interpretation of images, where “small” particles were quantified as being signal spots <2 µm in diameter. 10 and 100 ppm data was included together to increase the amount of data and previous work has shown a lack of uniformity of association regardless of exposure concentration (see Section 4.2).

Cell count within image	Number associated with no Ti	Number associated with small particles of Ti	Number associated with large agglomerations of Ti
27	8	13	6
12	2	3	7
3	0	1	2
15	5	5	5
6	3	1	2
3	1	0	2
6	2	2	2
5	2	2	1
22	7	9	6
16	6	1	9
14	6	2	6
Totals: 129	42 (33 %)	39 (30 %)	48 (37 %)

Table 4.1 – table showing quantification of H400 cells associated with no Ti, small and large agglomerations. Approximately 2 out of 3 cells had some association with Ti after exposure to TiO₂ at 10 or 100 ppm for 24 h.

Co-localisation between Ti and Calcium (Ca)

A number of these images seem to show some co-localisation between Ti and Ca:

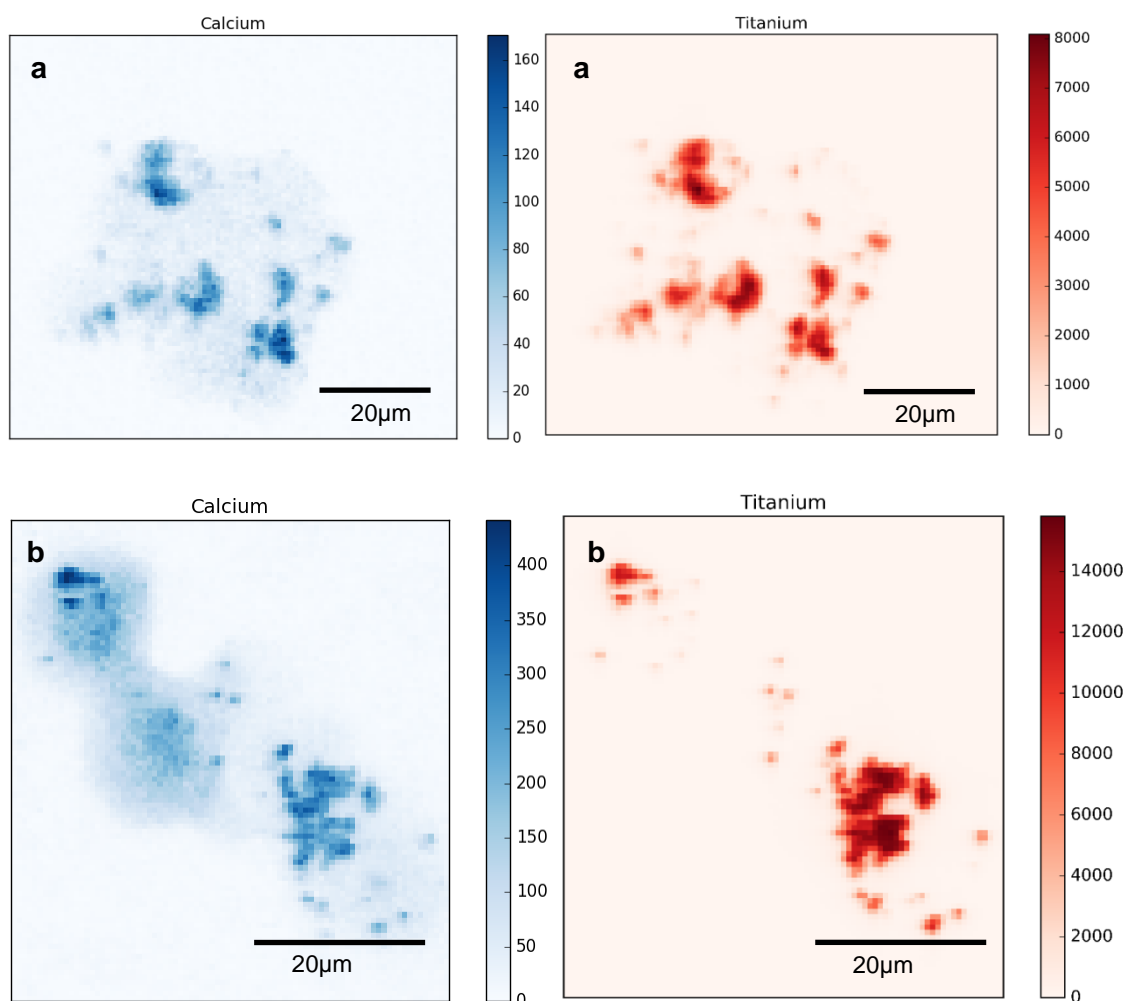


Figure 4.19 – X-ray fluorescence of Ca and Ti two groups (a and b) of H400 cells exposed to TiO_2 10 ppm for 24 h. The Ca and Ti signals from this group appear to show similar locations.

The potential co-localisation of Ca and Ti may be associated with the role Ca plays in lysosome formation, as Ca^{2+} has been reported to be essential for fusion of lysosomal membranes during uptake of target molecules (Luzio et al., 2007).

4.7 Chapter conclusions

- Intracellularisation of TiO_2 NPs by oral epithelial cells was clearly demonstrated.
- A variety of different imaging methods have shown an association of TiO_2 agglomerations with H400 epithelial cells. Further investigation shows that these agglomerations are indeed intracellular.
- Intracellularisation is not uniform within a cell population, and is dose and time dependent.

- There are no observable gross morphological changes in epithelial cells associated with TiO₂ NP intracellularisation.
- A similar pattern of intracellularisation was evident in primary oral epithelial cells in comparison to the H400 cell line.
- The lack of uniformity of uptake may be due to the lack of uniformity in local exposure to TiO₂ NPs of each cell. It has been shown that TiO₂ does agglomerate in cell culture medium. However, this is likely to be representative of the situation *in vivo*.
- Clathrin mediated endocytosis is partly, but not wholly, responsible for TiO₂ NP uptake by oral epithelial cells.

Further questions raised by this work include:

- Is this uptake of TiO₂ dependent on the cell cycle stage, thus accounting for the fact that only some cells in a population are seen to have agglomerations within them?
- What implications does TiO₂ NP intracellularisation have on epithelial cell biological responses both directly and on their interactions with other cell types?

Chapter 5

**Effects of interactions between TiO₂ NPs and oral
epithelial cells on cell viability, growth and
immune responses**

Synopsis

In Chapter 4 it was demonstrated that exposure of both H400 epithelial cells and primary oral epithelial cells to TiO₂ NPs leads to intracellular accumulation of agglomerations of particles after co-incubation. This chapter studies the consequences of these interactions on cell viability and on known inflammatory pathways within oral epithelial cells such as NFκB expression.

Epithelial cell viability has previously been reported to be affected by exposure to TiO₂ NPs. HaCaT (immortalised human keratinocytes) have been shown to internalise TiO₂ NPs and inhibition of HaCaT cell growth has been reported at TiO₂ NP concentrations of 10 – 300 ppm (Chan et al., 2011). Human A549 (lung epithelial cells) have been shown to produce an inflammatory response to TiO₂ NPs, including increased IL8 release alongside TiO₂ NP internalisation (Singh et al., 2007). The viability of other human cell types has been shown to be affected by the presence of TiO₂ including a monoblastoid cell line (Vamanu et al., 2008) and human embryonic kidney cells (Meena et al., 2012). In this chapter the effects on oral epithelial cell viability of exposure to a variety of concentrations of TiO₂ NPs is studied by conventional assay methods and high throughput techniques. Subsequently, the effects of TiO₂ NPs on epithelial cellular pathways (including NF kappa B activation, known to be important in inflammatory responses to pathogenic challenge) are investigated both in the presence and absence of microbial stimuli to simulate and identify any modification to normal oral epithelial cell responses to bacterial challenge from the oral microflora.

5.1 Conventional cell viability assays

As discussed in Section 3.6, and demonstrated by other investigators (Holder et al., 2012, Kroll et al., 2009) interactions between the insoluble TiO₂ NPs and a number of biological assays have been demonstrated. In this chapter assays employed were previously validated (see Section 3.6) for use in the presence of TiO₂ NPs. The suitability of each assay used is discussed alongside summary of findings from the combined assays in Section 5.1.4.

5.1.1

ATP activity measured by CellTiter-Glo®

CellTiter-Glo® (Promega, Wisconsin, USA) measures the ATP activity within a cell population and therefore measures viability indirectly (see Section 2.3.1).

H400 cells were cultured in 96-well plates (Section 2.2). TiO₂ NP dispersions were added to give final stimulation concentrations of 0 – 1000 ppm. After 0, 3, 6 and 24 h, plates were removed from the incubator and CellTiter-Glo® assays were performed (Section 2.3.1). Figure 5.1 shows the data for control cells compared with those treated with 1, 10, 100 and 1000 ppm TiO₂ NPs.

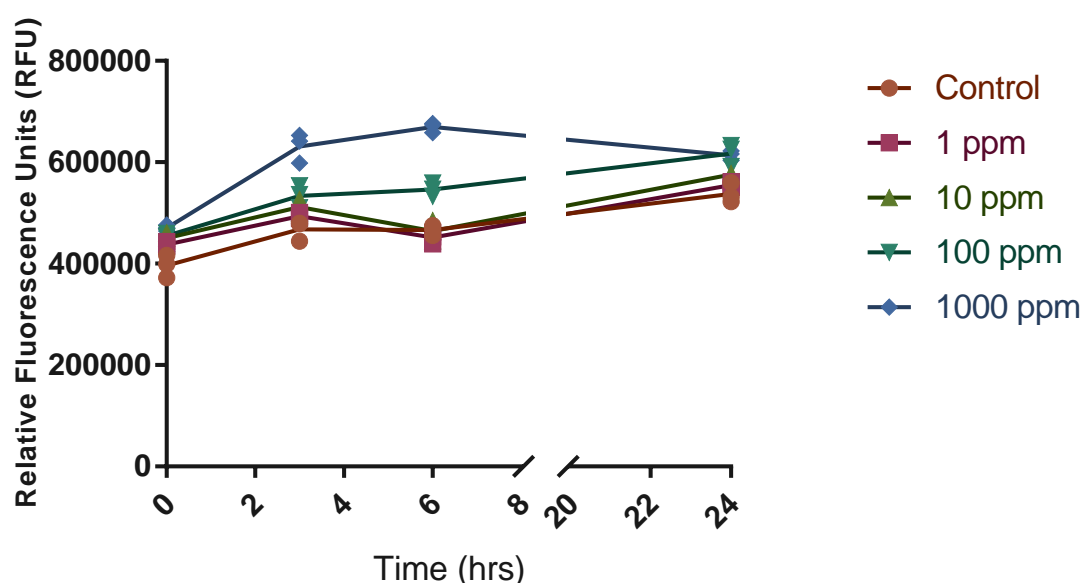


Figure 5.1 – CellTiter-Glo® luminescence (RFU) for H400 cells treated with 0, 1, 10, 100 and 1000 ppm TiO₂ NPs for 0, 3, 6 and 24 h (n=3, all data shown). ATPase activity is seen to be increased at 3 h and 6 h when compared with 0 h for all conditions. No reduction in ATPase measurement following exposures of up to 1000 ppm TiO₂ NPs was seen when compared with the respective controls.

CellTiter-Glo® assays showed an increase in the measured ATPase activity in all conditions at 3 and 6 h when compared with 0 h suggesting an overall increase in metabolic activity of the sampled H400 cell populations. Cells exposed to higher levels of TiO₂ NPs exhibited the greatest increases in ATPase activity at 3 and 6 h in particular, which may be attributable to an increased metabolic activity associated with their internalisation (or other interactions) with the Ti stimulus. Although there was no loss of ATP activity at any time point when compared with 0 h, the stimulation with TiO₂ NPs in comparison with a soluble stimulus is inhomogeneous and only a

proportion of the population become exposed. It is conceivable that the net measured ATPase activity is a combination of cells increasing in activity and possibly others reducing. The assay itself is not able to discriminate such behaviours and one indirect measurement of cell viability cannot be relied upon to give a true picture of the viability of a cell population. The results from using a conventional plate system and CellTiter-Glo® assay showed no loss of “viability” at the concentrations and timepoints tested, however the literature does report that epithelial cell death (apoptosis) as a result of exposure to TiO₂ NPs occurs (see also Table 1.5). To more robustly exclude cytotoxic effects of TiO₂ NPs on H400 cells in this system at varying time-points, additional assays and methods were used as detailed below.

5.1.2 *LDH concentration measured by CytoTox-ONE™*

The CytoTox-ONE™ assay detects LDH released extracellularly into cell culture medium due to cellular necrosis (Section 2.3.2).

Further verification of LDH assay

The LDH assay was verified for use in the presence of TiO₂ NPs in Chapter 3 (see Section 3.6.3), showing that the presence of up to 1000 ppm TiO₂ NPs did not affect the performance of this assay. To assess whether LDH remained stable in supernatant stored for a period of time, experiments were carried out to establish if any LDH released by cells could degrade over time. Figure 5.2 shows the stability of LDH (positive control from CytoTox-ONE™ Assay kit) in cell culture medium necessary for H400 growth and division stored for up to 42 h at room temperature (21 ± 2°C). The findings established acceptable storage parameters prior to assays being conducted.

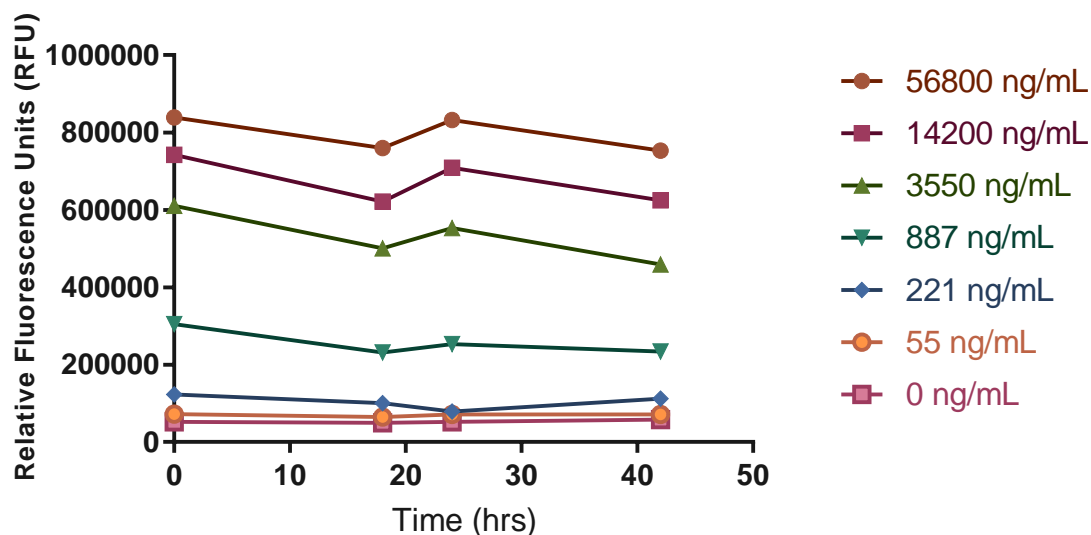


Figure 5.2 – Fluorescence (RFU) generated using CytoTox-ONE™ assay of known LDH concentrations (represented by each colour) added to cell free culture medium plotted against the time stored for at room temperature ($23 \pm 2^\circ\text{C}$) on the x axis. The differences between each concentration remain stable over time, therefore indicating that storage of medium for LDH quantification of multiple samples at one time would be a viable experimental design.

To establish the relationship between LDH release and H400 cell necrosis, cells were allowed to become over-confluent and the medium to become exhausted. As a result, there was increased H400 cell death due to lack of nutrition and acidification of the cell culture medium. To achieve a variety of degrees of confluence, a suspension containing 5×10^4 H400 cells in 200 μL was obtained and diluted with cell culture medium to achieve a range from 0 – 100 % (see Figure 5.3). DH levels in supernatant, caspase levels (as detected by CaspaseGlo 3/7, see Section 3.6.4) and staining with trypan blue (see Section 3.1.2) were all endpoints gathered from the same samples ($n=3$).

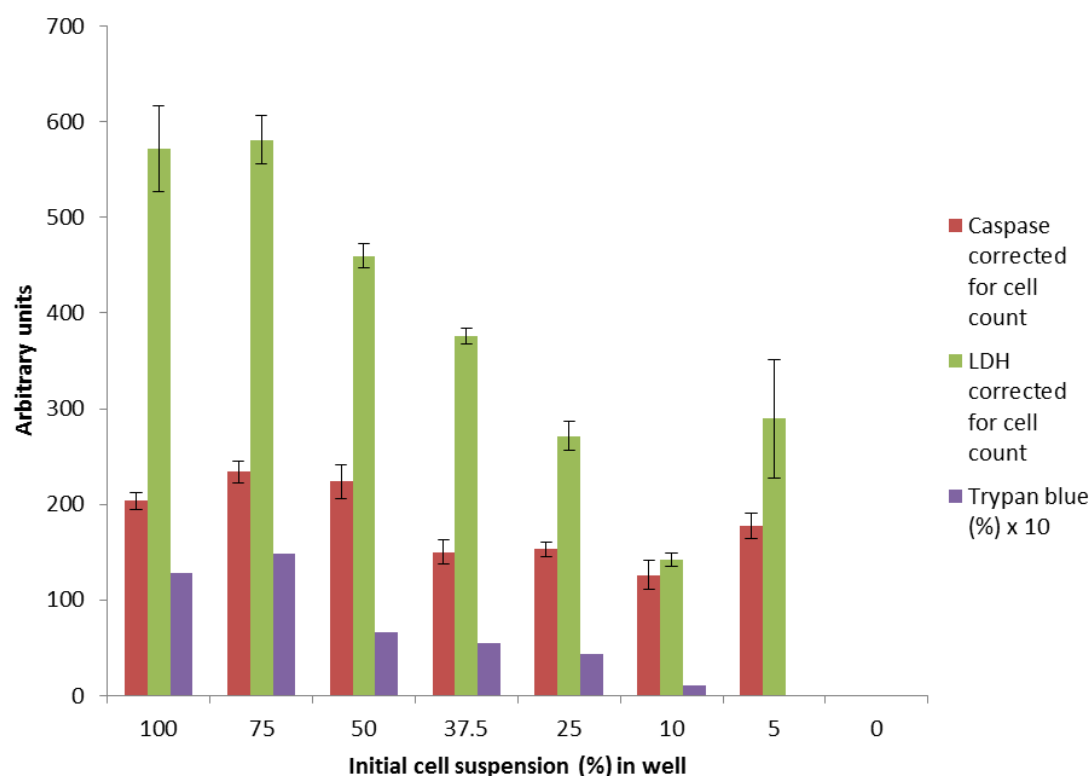


Figure 5.3 – LDH levels, Caspase 3 and 7 levels and percentage of cells positive for trypan blue stain within a 96-well plate (n=5, mean and SD shown) following incubation for 24 h. The data show that increased LDH levels were detected in cell populations containing higher proportions of non-viable cells, and the caspase levels appeared generally constant, indicating that necrotic H400 cells will release LDH at measurable levels. These data have been corrected for the cell counts present.

Allowing cells to become over-confluent was chosen as a mechanism of initiation of cell death as it does not rely on cytotoxic agents such as DMSO or heat, both of which were shown to interfere with the LDH assay in this application. Heat will denature the proteins present in LDH as it is an enzyme (Korzeniewski and Callewaert, 1983). It was concluded that the LDH assay was suitable for use in this experimental system, would detect necrosis of H400 cells within a population, and that the assay could be performed on supernatant removed from flasks and stored for up to 42 h. Furthermore, it was concluded that the main mechanism of cell death by over-confluence was necrosis, as there was a positive correlation between cells positively stained for Trypan blue and the LDH levels detected in the cell culture medium.

5.1.3 *CaspaseGlo® 3/7*

It has been reported that TiO₂ NPs are capable of inducing apoptosis in a variety of human cells (Shukla et al., 2011a, Srivastava et al., 2013, Meena et al., 2012, Park et

al., 2008, Shukla et al., 2013). Caspase-Glo® is an assay system designed to detect levels of caspase 3 and 7 within a cell population (see Section 2.3.3), and an increase in concentration of caspases 3 and 7 indicates that more apoptosis is occurring within a sample when compared with controls.

5.1.4 *Cell viability results from conventional assays*

Assays were performed in parallel to gain an overall view of the likely levels of viability, necrosis and apoptosis present in H400 samples exposed to up to 5000 ppm TiO₂ NPs.

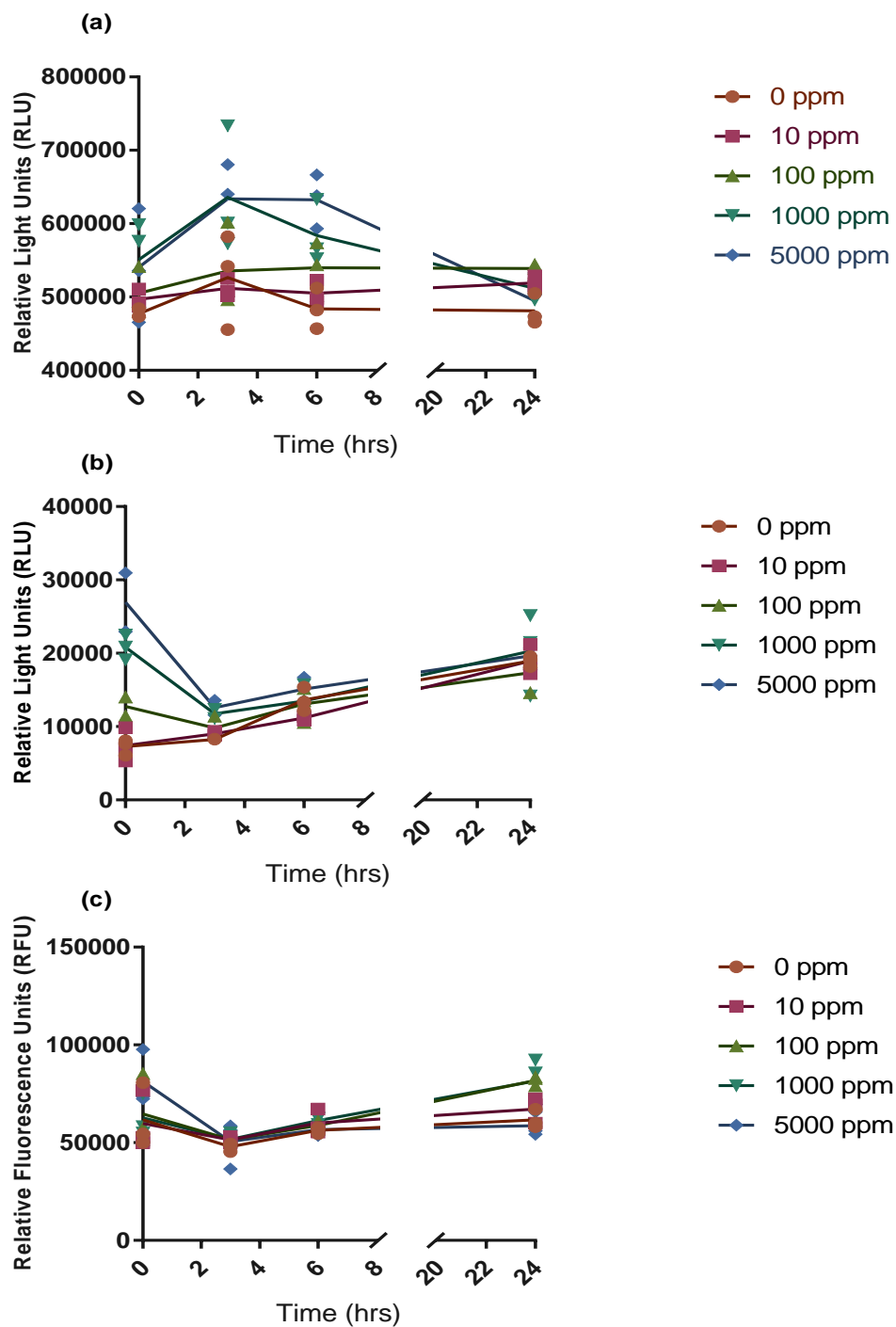


Figure 5.4 – Conventional viability assays performed at time-points up to 24 h on H400 cells exposed to up to 5000 ppm TiO₂ NPs (n=3, all data shown). **(a)** CellTiter-Glo®, **(b)** CaspaseGlo® 3/7, **(c)** CytoTox-ONE™. Plots show maintenance of ATPase activity following an initial peak at 3-6 h up to 1000 ppm **(a)** and an increase in both caspase activity **(b)** and necrosis **(c)** up to 24 h post exposure to TiO₂ NPs but the magnitude of changes over time appeared small. Figure **(a)** is a repeat of earlier data shown for comparison.

Figure 5.4 shows minimal differences in the measured responses of cell populations treated with 0-5000 ppm TiO_2 NPs using three different conventional assays. Key observations include:

- There is an apparent increase in metabolic activity shown by the increase in signal at 3-6 h from the CellTiter-Glo® data. This suggests there may be some increase in activity within the cells present, as a significant increase in the number of cells present within the well to account for this increased signal is unlikely.
- After the initial peak in Figure 5.4 (a), ATPase activity levelled off and remained constant in conditions up to 1000 ppm TiO_2 NP exposure, above which there was a reduction in the measurement of ATPase activity after 6 h.
- There was an apparent gradual increase in apoptotic markers over 24 h (Figure 5.7 (b)), but limited increase in the necrosis marker (LDH, Figure 5.4 (c)). The increases were not distinguishable from the control conditions.

Overall there is some evidence from the conventional assays of a minor loss of viability of H400 cells exposed to TiO_2 NPs. ATPase activity appeared reduced in H400 cells after 6 h following exposure to 1000 ppm and 5000 ppm concentrations of TiO_2 NPs when compared with controls, and there appeared to be an increase in Caspase activity and in the LDH concentration in medium after 6 h. However, the differences appeared small, and no assay showed a large reduction in cell 'viability' at the concentrations tested up to 24 h of co-culture with TiO_2 NPs. It is important to note that limitations of the assays conducted include:

- As concluded in Chapters 3 and 4, not all H400 cells in a population are exposed to an equal concentration of TiO_2 NPs. Therefore, the overall change in a light signal across an entire well of cells may be very small. It may therefore be that there are subtle changes in viability which are not identified using the assays described in this Section.
- The mechanism of cell death induced by TiO_2 NP exposure within epithelial cells is likely to be apoptosis, as published in the context of TiO_2 NPs and kidney cells (Park et al., 2008), human lung epithelium (Srivastava et al., 2013) and human liver cells (Shukla et al., 2013). If apoptosis is occurring in a small

subset of the population of H400 cells examined using these conventional assays, this may be in response to ROS activation, which will be discussed further.

- The issues surrounding using a nano-scale, insoluble stimulus means the local concentration of TiO_2 each cell is exposed to may vary widely. This in turn could mean that changes in the viability state of an overall population may be small but the effects on a number of individual cells may be significant.
- Changes in behaviour of individual cells may also affect the responses of neighbouring cells due to alterations in cell signalling mechanisms. These changes may be important but are not detected by the conventional assays above, and will be studied further in chapters 6 and 7.

5.1.5 *Sytox® green staining*

Sytox® green is a nucleic acid stain with a high affinity to DNA, which will readily stain the DNA content within the nuclei of non-intact cells. It can be used in two ways, firstly by measuring the amount of light output in a sample, for instance in a well plate seeded with cells of a known density, or by direct visualisation of a cell population. The method for staining H400 cells in this context is described in Section 2.3.4. The use of direct visualisation as opposed to quantifying light output was chosen due to the potential interferences discussed in Section 5.2.

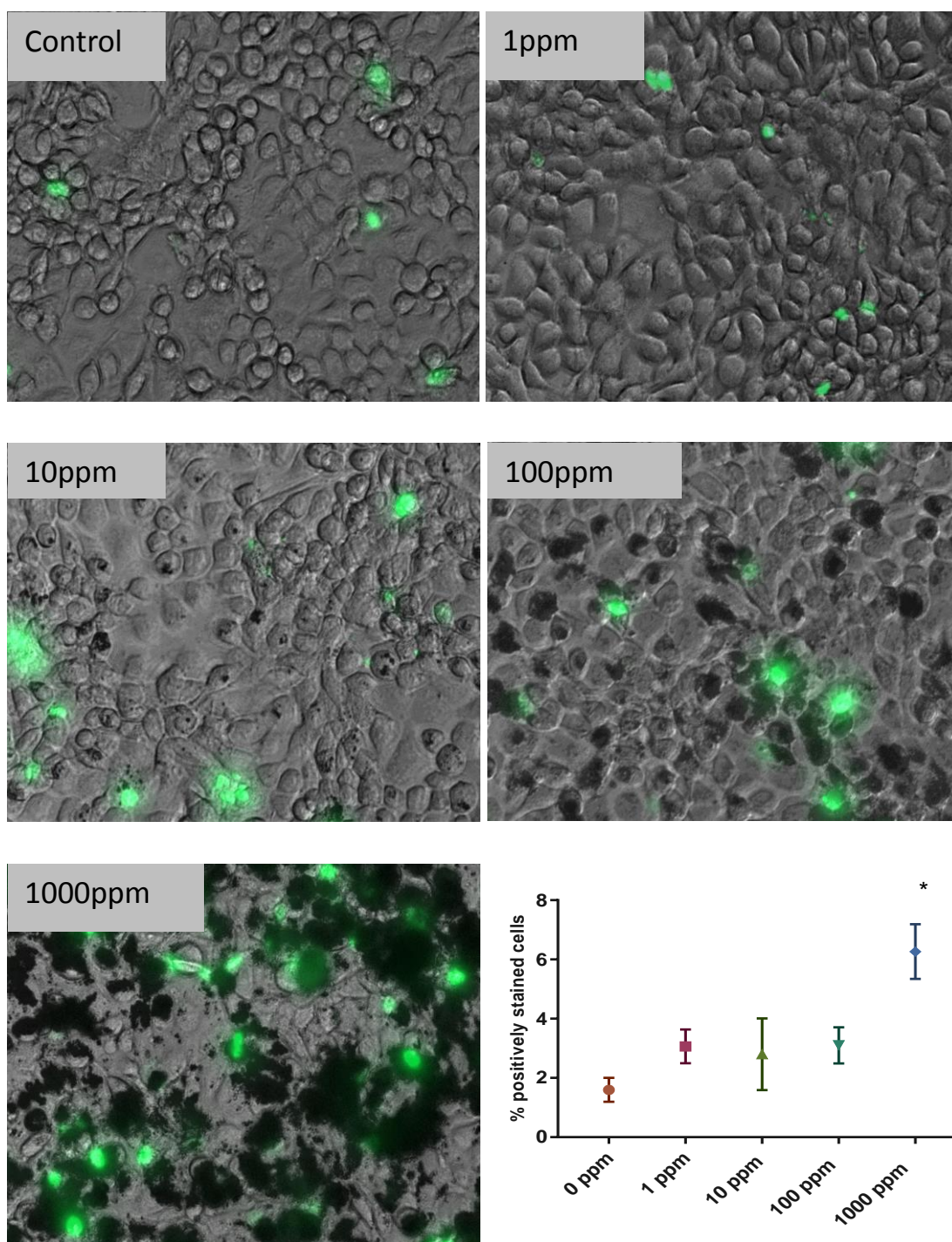


Figure 5.5 – Exemplar images showing Sytox® green stained cells in a population of H400 cells co cultured with TiO₂ NPs at concentrations of 0-1000 ppm and the proportion of positively stained cells within a number of images counted (n=3 image fields, approx. 250 cells per field). Asterisk shows significant increases in non-viable cells at 1000 ppm using one-way ANOVA (p<0.05) using total cell counts. The dark artefacts visible are TiO₂ NP agglomerations. This appears to show a dose dependent increase in non-viable cells from the images although only the largest concentration exposure was significant.

Figure 5.5 shows a significant increase in non-viable cells at exposure levels of 1000 ppm TiO₂, and there appears to be a correlation between the areas of TiO₂ NP

agglomeration and the non-viable cells. It is possible that there is therefore some effect on cell viability which is not clearly seen from the use of assays which average outputs across the entire cell population.

5.2 High Content Screening (HCS)

Ideally a homogeneous distribution of TiO₂ NPs would be achieved within a sample to ensure all cells encounter the same local TiO₂ NP concentration. Due to agglomeration of TiO₂ NPs, the localised concentration of TiO₂ NPs adjacent to each cell within a sample could differ largely within the experimental methods used for co-incubation. Therefore, HCS was used as an alternative method of assessing the cell population. The principles are the same as for conventional assays (reagents are added to cells which will generate light output or colour change in response to the generation or detection of a target molecule). However, the outcome is determined by the computer aided identification and analysis of relevant markers. This means that individual cells are labelled or stained for a particular target, then high numbers of cells are able to be individually analysed for a potentially large number of parameters depending on the markers used. The rationale for using this technique is that it may potentially overcome the limitations of conventional assay techniques in the experimental model used in this work and summarised below:

- Due to the issues surrounding the use of an insoluble stimulus which has been seen to agglomerate in cell culture medium, the individual exposure of each cell to TiO₂ NPs will potentially vary widely. Local concentration exposure of one cell may be in the multiples of thousands if adjacent to agglomerations, while other cells may experience no local exposure. Therefore, measuring the responses of a larger number of cells may show results which are so diluted in a small sample that they are not seen using conventional techniques.
- Viability assays using the conventional assays described in Section 5.1 rely on sacrificing a sample at each time-point or removing the supernatant from the sample. This is a limitation as it means continuous monitoring of the viability of the same cell population is not possible.

- A larger amount of data is gathered efficiently when using HCS when compared with conventional assays and allows for more robust statistical analysis.

All samples for processing by HCS were processed at Imagen Therapeutics (formerly Imagen Biotech, Alderley Edge, UK). H400 cells were cultured as described in Section 2.2 and stimulated and analysed as described by the specific protocol outlined in each section.

HCS assays

The following HCS assays were performed:

- Cell viability and cell death using DraQ7™ (Biostatus, UK)
- Cell count using Hoechst 33342, Trihydrochloride, Trihydrate - 10 mg/mL Solution in water (ThermoFisher Scientific, UK)
- Cell morphology using CellMask™ Green Stain (ThermoFisher Scientific, UK)
- Cell cycle markers using a histogram profile and computerised gate on Hoescht stained cells
- NFkappaB translocation using NFkB2 p100/p52 (18D10) Rabbit mAb (Cell Signalling Technology, Massachusetts, USA).

5.2.1 *Cell viability using HCS*

Draq7™ (Biostatus, UK) was used to assess the viability of cells using HCS. Draq7 is a red dye which will readily enter non-intact cells and hence stain the nuclei of non-viable cells. It is non-toxic to intact cells (Akagi et al., 2013). Draq7™ therefore has the advantage that it can be used repeatedly on the same sample to monitor viability over a time-course as opposed to using separate replicated wells to achieve an approximation of viability time. Draq7™ has been extensively tested to ensure compatibility with multi-stain experiments and for long term analysis (Akagi et al., 2013).

H400 cells were cultured as described previously. 24-48 h after seeding, cells were examined using light microscopy and 70-80 % confluent TiO₂ NPs were added as stimuli (Section 2.1.2) at a range of concentrations from 0-1000 ppm.

Generic HCS methods

Following exposures, H400 cells were fixed in 1 % formaldehyde and washed twice with PBS. Primary antibodies were diluted as appropriate according to the specific antibody used, and incubated with the cells in Digitonin (500 μ L/mL, Sigma-Aldrich, UK) to allow membrane permeabilisation. Primary antibodies were incubated for 1 h at room temperature ($21 \pm 2^{\circ}\text{C}$), following which the antibody was decanted and the plate was washed twice with PBS using a plate washer (Tecan UK Ltd, Reading, UK). Secondary antibodies were diluted as appropriate and again incubated for an hour at room temperature in conjunction with a Hoechst 3332 (Invitrogen, UK) to counterstain the nuclei. Following the second incubation the wells were again washed after removal of the secondary antibody mix. 100 μ L of PBS was added to each well for visualisation. Immunoreactivity staining for biomarkers was performed in triplicate for each experiment and triplicate readings were pooled.

HCS data capture and analysis

Biomarkers of interest were visualised and the intensity quantified using Cellomics ArrayScan[®] HCS reader: Compartmental Analysis Bio-Application (V2 Version, Thermo Scientific). Images of at least 5000 cells per well were captured in > 8 images taken in a spiral pattern outwards from the centre of each well. Each image was analysed through bio-application analysis protocols to identify the immunoreactivity fluorescence intensity for areas of interest for each individual cell. Areas of the cell were analysed along with sites within the cell depending on the specific area of interest (e.g. morphology scans assessed perimeter, area of cytoplasm and nucleus while NF κ B assay collected data on regions within the cell cytoplasm).

Within the relevant area of interest, threshold values were used to identify the sum of or mean intensity of areas showing fluorescence. The intensity was designated as relative light units (RLU). Cells which were immuno-positive for fluorescence values greater than the set thresholds were counted and reported as a percentage positive (% positive) relative to all those examined within the population.

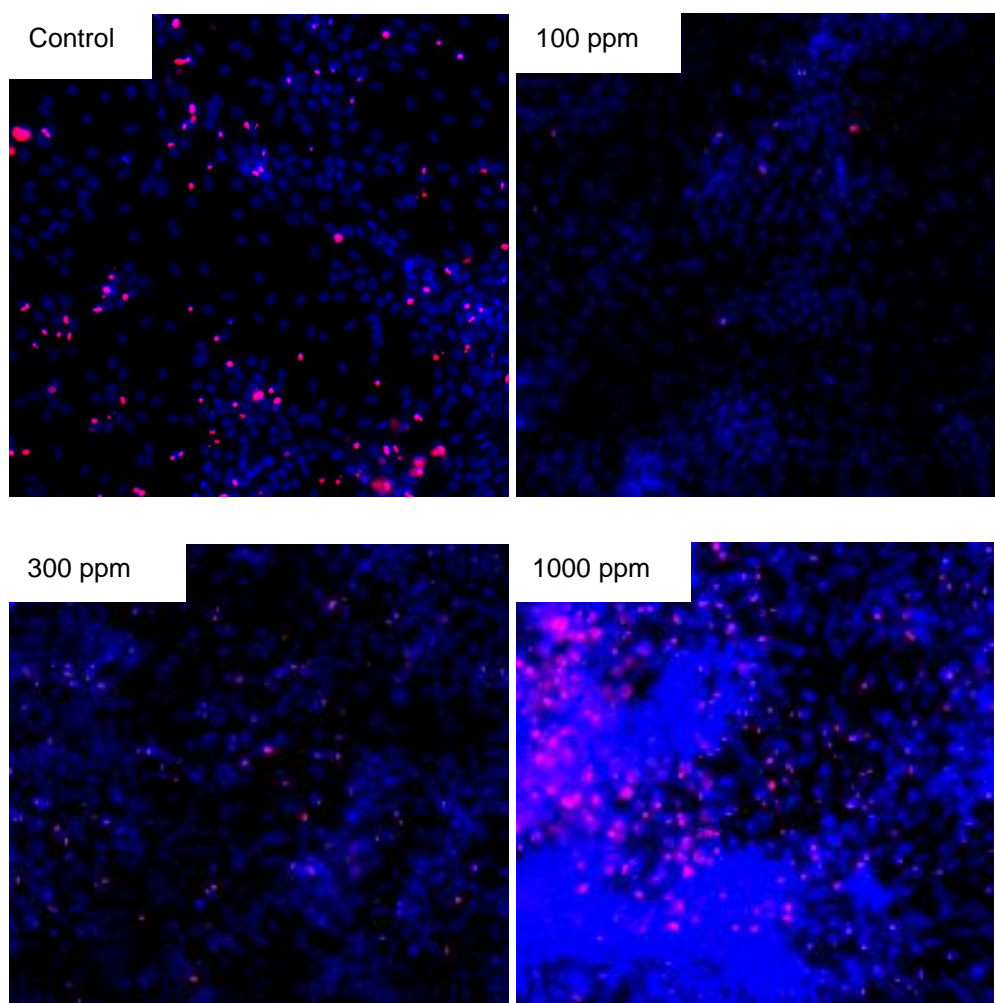
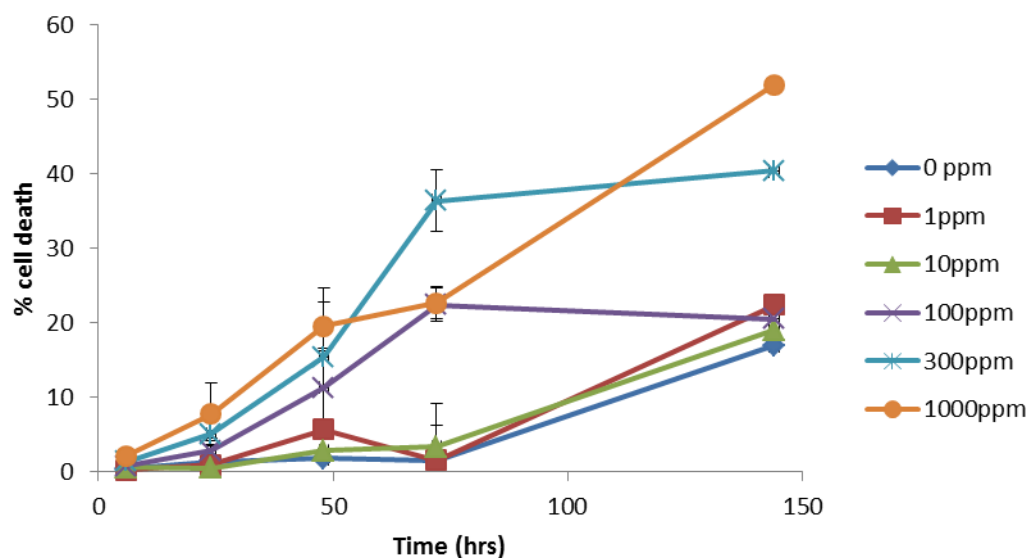


Figure 5.6 – Selected images showing cell viability 6 days following addition of TiO₂ NPs at concentrations shown. Draq7[™] positively stained cells are shown in red, cell nuclei are shown in blue. There appears to be an increased number of non-viable cells with an increase in TiO₂ NPs ppm from control to 1000 ppm. Lower concentration images were not made available from Imagen BioTech.

5.2.2 Cell count and cell death

(A)



(B)

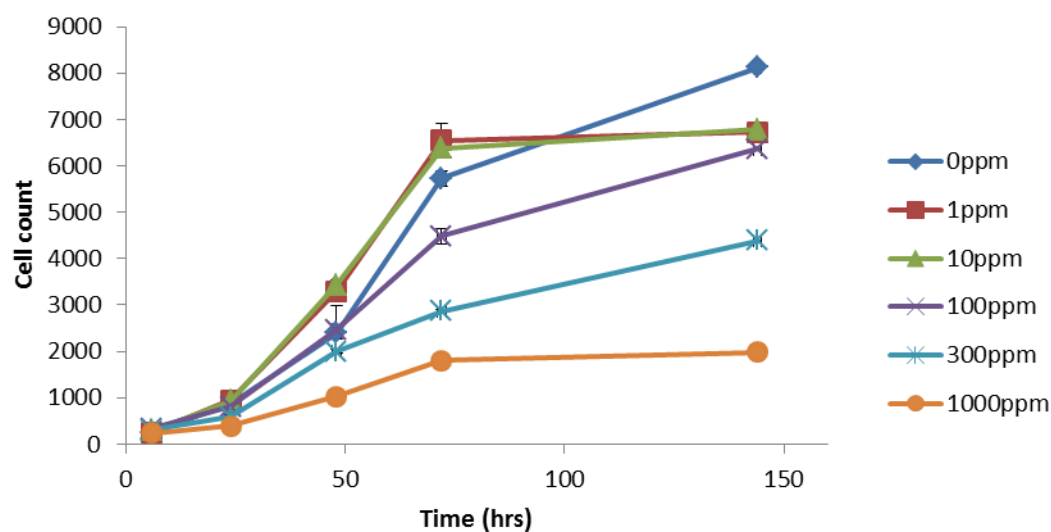


Figure 5.7 – Percentage cell death **(A)** and cell count of the whole population **(B)** as measured by HCS over 7 days (n=2, mean and SEM shown as supplied by Imagen Biotech). There is a clear dose dependent increase in percentage cell death at 300 ppm and 1000 ppm after 72 h, and a dose dependent reduction in cell count over time. However, the results may be influenced by the fact that the medium within the wells may well become exhausted at 72 h leading to an increase in cell death in all conditions, and a relative plateau of cell replication.

5.2.3 *Cell morphology*

As discussed in chapter 4, accurate measurements of cell size, shape and alterations in morphology following incubation with TiO₂ NPs have not been possible using TEM and light microscopy. Images captured using CellMask™, a fluorescent dye which will stain the plasma membrane, therefore representing the shape of the entire cell are shown in Figure 5.8. Cell nuclei are counterstained with DAPI (blue).

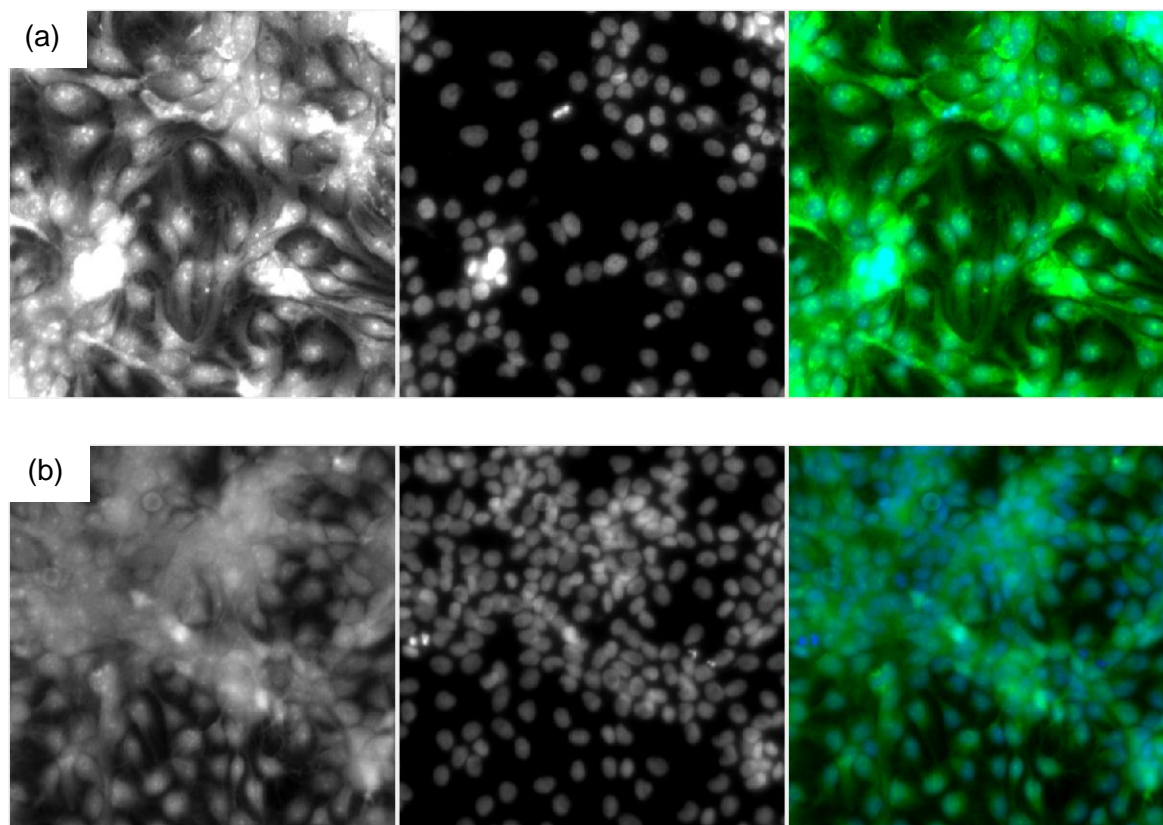


Figure 5.8 - H400 cells stained with CellMask plasma membrane stain (left), DAPI nuclear stain (centre) and combined image (right) at 6 days post exposure to 1000 ppm TiO₂ NPs (a) and control cells (b). The images show clear differences in cell morphology with H400s exposed to 1000 ppm TiO₂ NPs showing brighter plasma membrane signal and appearing more elongated in shape.

5.2.4 *Further work informed by HCS results*

High content screening generated some different results to the conventional assays described in Section 5.1. The HCS results are likely to be more robust as they use a higher number of samples, and therefore may be more representative. The initial results appear to show an increase in cell death and reduction in cell growth in response to an increase in TiO₂ NP ppm. There are also potential morphological

changes seen within cell populations associated with higher concentrations of TiO₂ NP exposures.

5.2.5 *Cell cycle as examined using HCS*

As discussed in Section 4.5, there was a non-uniform uptake of TiO₂ NPs within the populations of both H400 and primary oral epithelial cells examined. All methods used to image epithelial cells so far (light microscopy, TEM, FTIR techniques and confocal reflectance microscopy) showed the same pattern, namely that a sub-set of the cell population shows a large amount of associated NP agglomerations, while other cells within the population appear to not be associated with TiO₂ NP agglomerations. The pattern of association of agglomeration with cells may be due to non-uniform distribution within cell culture medium, but also could be affected by the cell cycle stage of each cell when exposed to TiO₂ NPs. According to the literature, endocytosis can occur at a variety of stages of the cell cycle, but may be more likely during G1 phase. Endocytosis is arrested at mitosis (Tuomikoski et al., 1989, Fielding et al., 2012). It has been shown that the concentration of NPs within a cell population varies, and that nanoparticles were present in higher concentrations at Gap 2/Mitosis>Synthesis>Gap 0/1 (Kim et al., 2012). It is therefore reasonable to expect that the cell cycle stage, which will be mixed within a growing cell population, may affect NP uptake in an epithelial cell population. What is also unknown is whether the cell cycle will be altered by the uptake of NPs into an epithelial cell. It has been shown that NPs are divided between daughter cells in A459 human lung epithelial cells (Kim et al., 2012), but that no dis-regulation of either viability markers or cell cycle stages were detected following NP internalisation in this particular study.

The stage of cell cycle was investigated using HCS. Conventional methods of cell cycle investigation, such as flow cytometry, were not used due to concerns that there could be potential interactions or issues with introducing nanoparticles into a flow cytometry system. The HCS system used was a similar methodology to those described in previous Sections, in that Hoersct stained fixed cells were imaged using a computerised histogram profile which 'gates' each phase.

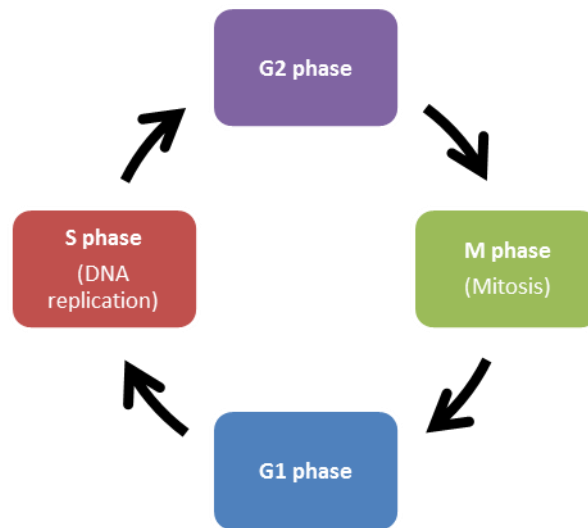


Figure 5.9 – Cell cycle diagram. Endocytosis is most likely to occur in the G1 phase of cell cycle (Quintart et al., 1979). Published data on endocytosis of nanoparticles in epithelial cells regarding cell cycle status the cell population are limited.

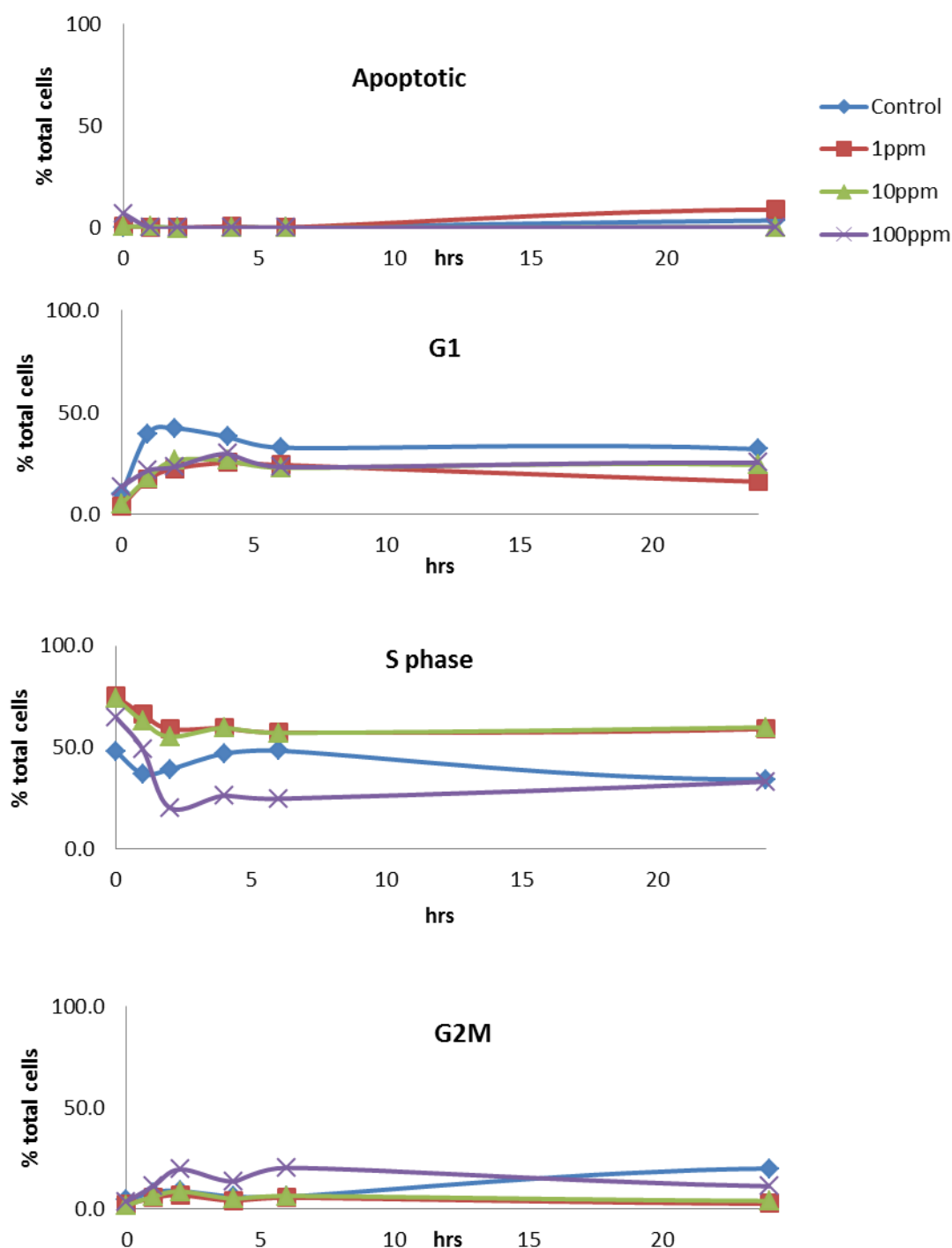


Figure 5.10 – HCS analysis of cell populations exposed to differing concentrations of TiO_2 NPs showing % cell population in a certain cell cycle point (y-axis) against time (x-axis). Figure 5.10 shows potential small alterations in cell cycle stages, therefore it can be assumed that the cell cycle stage, while it may initially determine which cells will uptake TiO_2 NPs, is unlikely to be affected by the presence of up to 1000 ppm TiO_2 NPs within the culture system.

5.2.6 Conclusions from HCS viability and initial assays

Alongside the differences discussed in Section 5.2.4, there are some similarities between the findings from conventional assays and HCS techniques when looking at

markers of viability within the H400 cell population when exposed to TiO₂ NPs. Both techniques show a potential dose dependent increase in cell death with increasing concentrations of TiO₂ NPs, however the magnitude of this appeared larger in HCS.

HCS techniques have also shown a number of features of TiO₂ NP interactions which were not identified by conventional methods. These were:

- Reduced cell counts in populations exposed to higher TiO₂ NP concentrations (over a longer time-course than examined by conventional methods)
- Potential morphological changes at higher concentrations as shown by the CellMask™ stain
- Minimal effects on cell cycle following incubation with TiO₂ NPs.

The HCS findings reinforce that conventional assay methods may not be the best way to examine cell populations where a non-homogeneous distribution of stimulus and potentially therefore heterogeneity in response is anticipated. It may be that conventional assays are not sensitive enough to distinguish the responses of a subset of cells in a population from the overall responses of the well as a whole when measures such as luminescence and fluorescence are used as end-points. Imaging techniques appear to give truer representation of epithelial cellular responses to TiO₂ NPs in this model system. It is therefore important to consider the use of HCS techniques in conjunction with conventional techniques wherever possible. The use of primary cells was not possible for HCS methods due to the number of cells required.

5.3 Effects of TiO₂ NPs on NFκB activation

It has been demonstrated that H400 epithelial cells will show an inflammatory response when challenged with relevant pathogenic stimuli (Milward et al., 2007). In the peri-implant situation, epithelial cells will interact not only with any implant derivatives present but also with peri-implant pathogens. Therefore, an important aspect of this work was to investigate how the interactions seen between epithelial cells and TiO₂ NPs could potentially influence cellular pathways known to be important in the response to pathogenic challenges.

5.3.1 *Activation of Nuclear Factor kappa-light-chain-enhancer of activated B cells (NFkB) in H400 cells*

Translation of NFkB from within the cytoplasm to the nucleus of epithelial cells is a characteristic feature of cells showing an inflammatory response. NFkB is a complex of proteins which are involved in the control of DNA transcription, cytokine production and cell survival and is found in most mammalian cell types (Makarov, 2000, Silverman and Maniatis, 2001). NFkB release is considered to be a key initial event in the inflammatory processes, particularly in chronic inflammatory conditions such as periodontitis (Milward et al., 2007, Milward et al., 2013), and potentially therefore peri-implantitis. NFkB is initially activated by stimuli such as oxidative stress and pathogenic challenge (Zhang and Ghosh, 2001). Once activated, the protein complex is not irreversibly bound within the nucleus, but can be moved back into the cytoplasm (Hayden and Ghosh, 2004) in its inactive form. Once bound within the nucleus, NFkB will activate transcription of DNA, production of cytokines to form an inflammatory response, and regulate cell survival. The recycling of NFkB can continue repeatedly, but it serves to ensure that the activation of NFkB is only transient within a cell. This mechanism is key in both acute and chronic inflammatory conditions.

The method used for staining H400 cells to show activation of NFkB is described in Section 2.6.1 and is a conventional staining approach where manual counts of stained cells were undertaken.

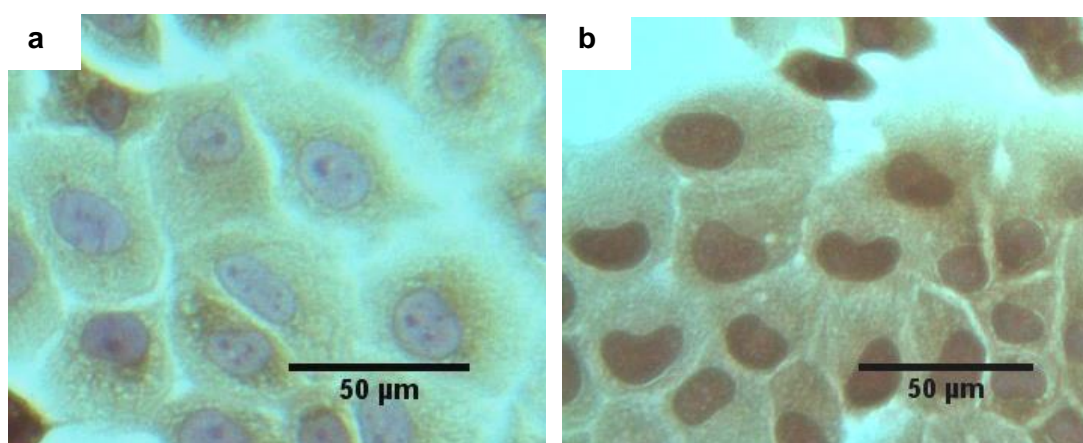
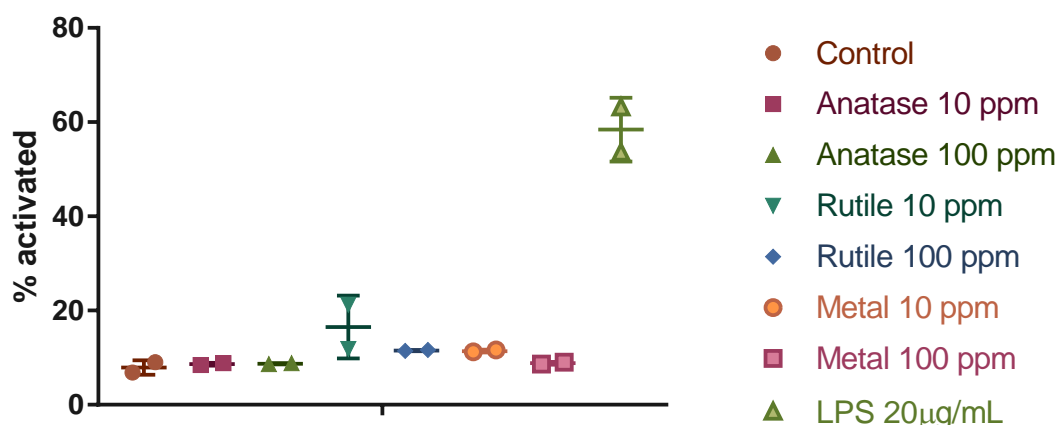


Figure 5.11 – H400 cells stained for the identification of NFkB translocation. Control cells (a) show the counterstained blue nucleus to be fairly free of the brown stained NFkB, while the activated cells (b) exposed to *E.coli* LPS 20 µg/mL for 1 h show translocation of NFkB to the nucleus.

The conditions for stimulation of H400 cells are explained in detail in Section 2.6.2, and quantification is described in 2.6.3.

Firstly, it was investigated whether TiO₂ NP exposure on H400 cells would lead to activation of NFκB. Figure 5.12 shows the percentage of activated cells within a population when exposed to a variety of Ti products along with a table detailing each stimulus. A wider panel of Ti species in the fine and ultrafine scale was used to assess the potential for other Ti stimuli to be pro-inflammatory to H400 cells by way of measuring NFκB translocation, and assess the relative inflammatory response to TiO₂ NPs as used before when compared with other potentially biologically relevant Ti products.



Name	Stimulus	Particle size	Concentration in medium	Supplier and code
Control	-	-	-	
Anatase 10	TiO ₂ (anatase)	<25 nm dia	10 ppm	637254 Sigma-Aldrich,
Anatase 100	TiO ₂ (anatase)	<25 nm dia	100 ppm	637254 Sigma-Aldrich,
Rutile 10	TiO ₂ (rutile)	~ 50 nm dia	10 ppm	1317802 Sigma-Aldrich,
Rutile 100	TiO ₂ (rutile)	~ 50 nm dia	100 ppm	1317802 Sigma-Aldrich,
Metal 10	Ti metal	~ 5 µm dia	10 ppm	Gift from Dr S Kalra
Metal 100	Ti metal	~ 5 µm dia	100 ppm	Gift from Dr S Kalra
LPS 20	<i>E.coli</i> LPS	-	20 µg/mL	L2630 Sigma-Aldrich

Figure 5.12 – graph showing activation of H400 cells exposed to the stimuli listed in the below table for 1 h (n=2, data and mean shown). This shows a limited activation of NFκB in H400 cells in response to Ti products using a conventional staining technique but a clear activation to the *E.coli* LPS as expected.

A HCS methodology was used in conjunction with the conventional assay above, where TiO_2 as anatase of 0-1000 ppm was used as the stimulus to investigate if there was an altered response in NF κ B activation of H400 cells. The HCS assay measured a number of features of each cell, not just the translocation of NF κ B as a “positive” or “negative” outcome as was recorded in the conventional assay. Due to the fact that the images where NF κ B was stained were captured digitally and analysed using specific software, the amount of NF κ B in the cytoplasm and the nucleus could be recorded. This was used to generate a nuclear:cytoplasmic ratio of NF κ B within cells, with a higher number indicating a higher amount of activated NF κ B. The other main difference in this technique compared with the conventional technique is that the HCS was carried out over a longer time period, allowing the investigation of the potential cycling of NF κ B into and back out of the nucleus of cells, a mechanism which may be important in chronic inflammatory conditions such as periodontitis and potentially peri-implantitis.

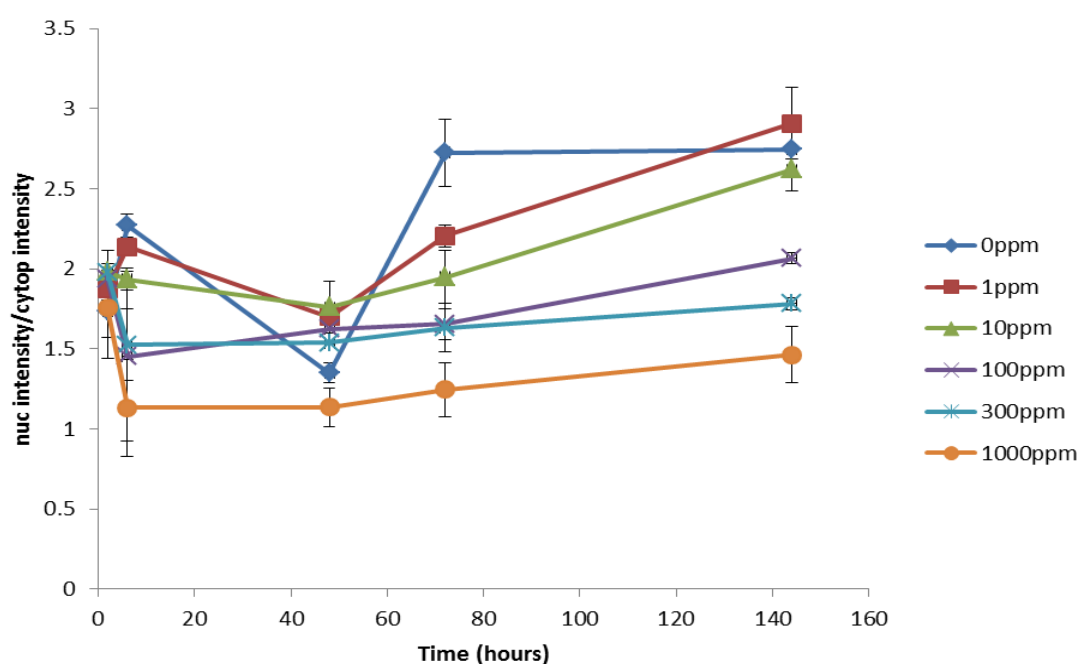


Figure 5.13 – Nuclear:cytoplasmic intensity of NF κ B stained with a flurophore of H400 cells exposed to 0-1000 ppm TiO_2 NPs (anatase, <25nm diameter). The higher the number, the more NF κ B is present in the nucleus. This appears to show a dose dependent suppression of background NF κ B activation post 72 h. An increase in background NF κ B activation would be expected in all conditions over time due to acidification of the medium eliciting a stress response within H400 cells.

The pattern of the control response over time in Figure 5.13 is as expected: An initial rise in NFκB activation as the cells are responding to being disturbed by a change in medium then a reduction as the cells are left to settle and grow normally, before a rise as the medium becomes exhausted. However, this pattern becomes disordered by the presence of TiO₂ NPs in a dose dependent manner to have an initial drop then less of a rise after medium exhaustion. This suggests that the presence of TiO₂ inhibits the activation of NFκB, possibly by binding to the NFκB or inhibiting its transport into the nucleus, or by blocking the receptors needed to activate the NFκB translocation.

5.4 TiO₂ NPs as a potential modifier of epithelial responses to bacteria

Responses of epithelial cells may be affected by the presence of TiO₂ NPs in a culture system. In the peri-implant environment *in vivo*, there will be exposure of the oral epithelial cells adjacent to an implant surface to a bacterial challenge. While it has been shown in this work that the exposure of oral epithelial cells (both H400s and primary epithelial cells) of TiO₂ NPs at up to 1000 pm concentration does not cause widespread viability changes in a population, it may be that the interactions between TiO₂ NPs and epithelial cells could impact on responses to bacterial challenge.

5.4.1 *NFκB responses of oral epithelial cells to bacterial LPS with and without pre-treatment with TiO₂ NPs – method*

Given that NFκB is a known pathway involved in the response of H400 cells to bacterial challenge (Milward et al., 2007), the effects of TiO₂ NPs as a co-exposure factor along with a pathogen on the activation of NFκB in response to bacteria was investigated. The method for NFκB activation detection is detailed in Section 2.6.1. The stimulus conditions were as follows:

Control cells	H400s cultured on glass slides in standard medium (see Section 2.2.2) until just sub confluent
LPS 20 mg/mL	H400 cells as control then stimulated with 20 mg/mL <i>E.coli</i> LPS for 1 h
LPS 40 mg/mL	H400 cells as control then stimulated with 40 mg/mL <i>E.coli</i> LPS for 1 h
TiO ₂	H400 cells as control then cultured with TiO ₂ NPs 10ppm for 18 h
TiO ₂ LPS 20mg/mL	H400 cells as control then cultured with TiO ₂ NPs 10ppm for 18 h then stimulated with 20 mg/mL <i>E.coli</i> LPS for 1 h
TiO ₂ LPS 40mg/mL	H400 cells as control then cultured with TiO ₂ NPs 10ppm for 18 h then stimulated with 40 mg/mL <i>E.coli</i> LPS for 1 h

Table 5.1 – H400 cell preparation prior to staining.

Triplicate slides were prepared and 500 cells counted from each condition.

5.4.2 *NFκB responses of oral epithelial cells to bacterial LPS with and without pre-treatment with TiO₂ NPs – results and discussion*

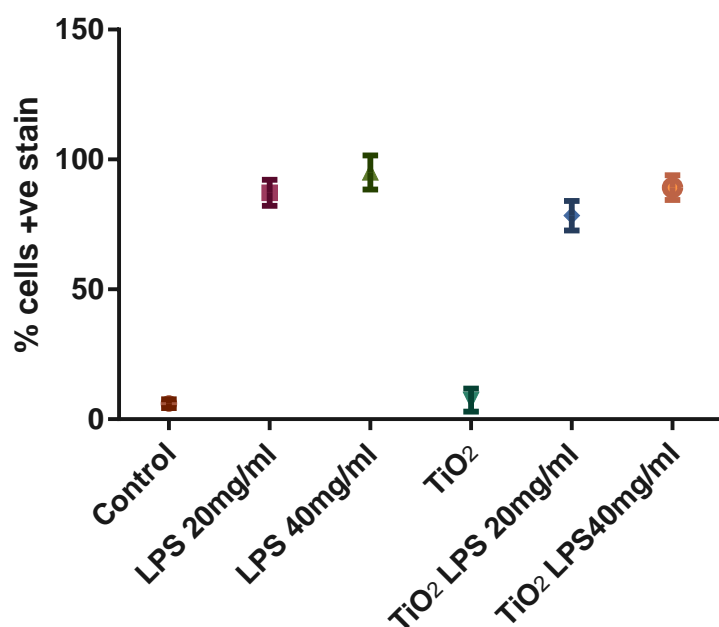


Figure 5.14 –NFκB activation in response to 20 mg/mL LPS when pre-treated with TiO₂ (n=10, mean and SD of counts shown) and LPS 40 mg/mL. Cells were either pre-treated for 18 h with 10 ppm TiO₂ or not. LPS was added for 1 h prior to washing and fixing.

The results from the conventional approach to staining show that there was a statistically significant down regulation in NFκB activation in cells pre-treated with TiO₂ however the effect size was small. This could be due to potential binding of LPS protein to TiO₂ NPs therefore reducing the effective concentration. Further investigation in this area is warranted.

5.4.3 Co-stimulation of H400 cells with heat killed *Fusobacterium nucleatum* and TiO₂ NPs

H400 cells were cultured on glass slides as in Section 2.2.2 and the staining protocol for NFκB activation is detailed in Section 2.6.1. Cells were stimulated as follows:

Control cells	H400s cultured on glass slides in standard medium (see Section 2.2.2) until just sub confluent
FN	H400 cells cultured in standard medium until just sub confluent then stimulated with heat killed FN at a concentration of 1×10^9 /mL for 1 h
TiO ₂ then FN	H400 cells cultured in standard medium until approx. 24 h prior to becoming just sub confluent then exposed to TiO ₂ 10ppm for 24 h then stimulated with heat killed FN at an MOI of 1×10^9 /mL for 1 h
FN/TiO ₂	H400 cells cultured in standard medium until just sub confluent then stimulated with TiO ₂ 10ppm and heat killed FN at an MOI of 1×10^9 /mL for 1 h concurrently.

Table 5.2 –H400 co-culture conditions prior to staining.

Triplicate slides of each condition were prepared and 500 cells were counted from each condition.

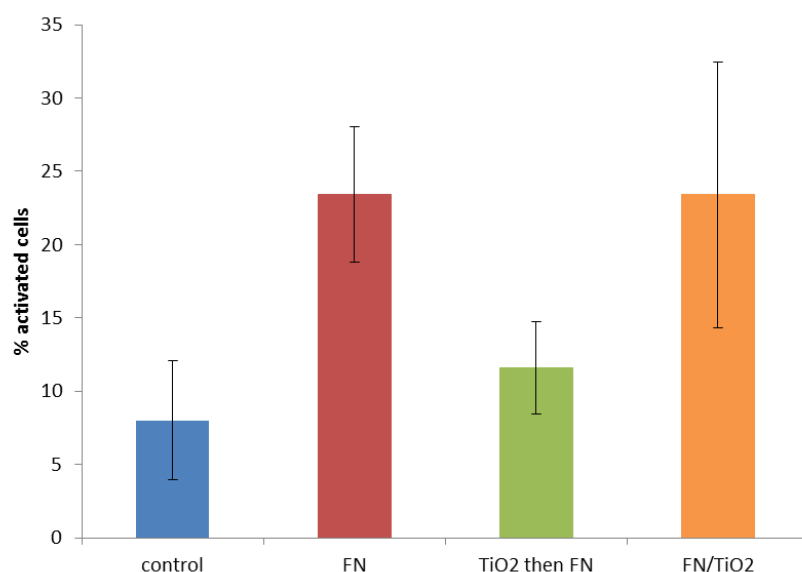


Figure 5.15 -The % activated H400 cells exposed to heat killed FN for 1 h +/- TiO₂ 10 ppm for 24 h previously or exposed to FN and TiO₂ concurrently for 1 h (n=5, mean and SD shown). A reduction in NFκB activation in response to FN when H400 cells have been previously exposed to TiO₂ compared with concurrent exposure or exposure to FN alone was observed.

5.4.4 *Co-stimulation of H400 cells with heat killed Fusobacterium nucleatum and TiO₂ NPs –discussion*

The results in Figure 5.15 suggest that pre-exposure to TiO₂ (a low concentration of 10 ppm) for 24 h seems to reduce the activation of NFκB in response to heat killed FN. TiO₂ NP itself has not been shown to stimulate NFκB translocation when measured by the same technique (see Section 5.3.1), therefore it is unlikely to be due to competitive stimulation of the epithelial cells. The fact that TiO₂ NPs have the capacity to modify epithelial responses to bacteria could be important clinically as epithelial cells are likely to be in contact with Ti species chronically. Therefore, potential inhibition of responses to bacteria would be an important *in vivo* consequence of the presence of Ti species in tissues adjacent to implants. To further investigate this potential modification of NFκB activation, HCS techniques were used.

5.4.5 *HCS investigation of NFκB responses to bacteria with and without TiO₂ NPs- method*

H400 cells were cultured according to Section 2.12 and after 24 h settling in wells, medium was changed for medium containing 0-100 ppm TiO₂ and cultured for a further 24 h. At this point, 10 μL of stimulus was added to each well, containing either heat killed FN (1x10⁹/mL), heat killed PG (1x10⁹/mL), *E.coli* LPS (20 mg/mL) or PBS (control). After 1 h incubation under standard cell culture conditions, cells were stained as appropriate, imaged, and analysed as appropriate (see also Section 5.2.1).

5.4.6 HCS investigation of NFκB responses to bacteria with and without TiO₂ NPs- results

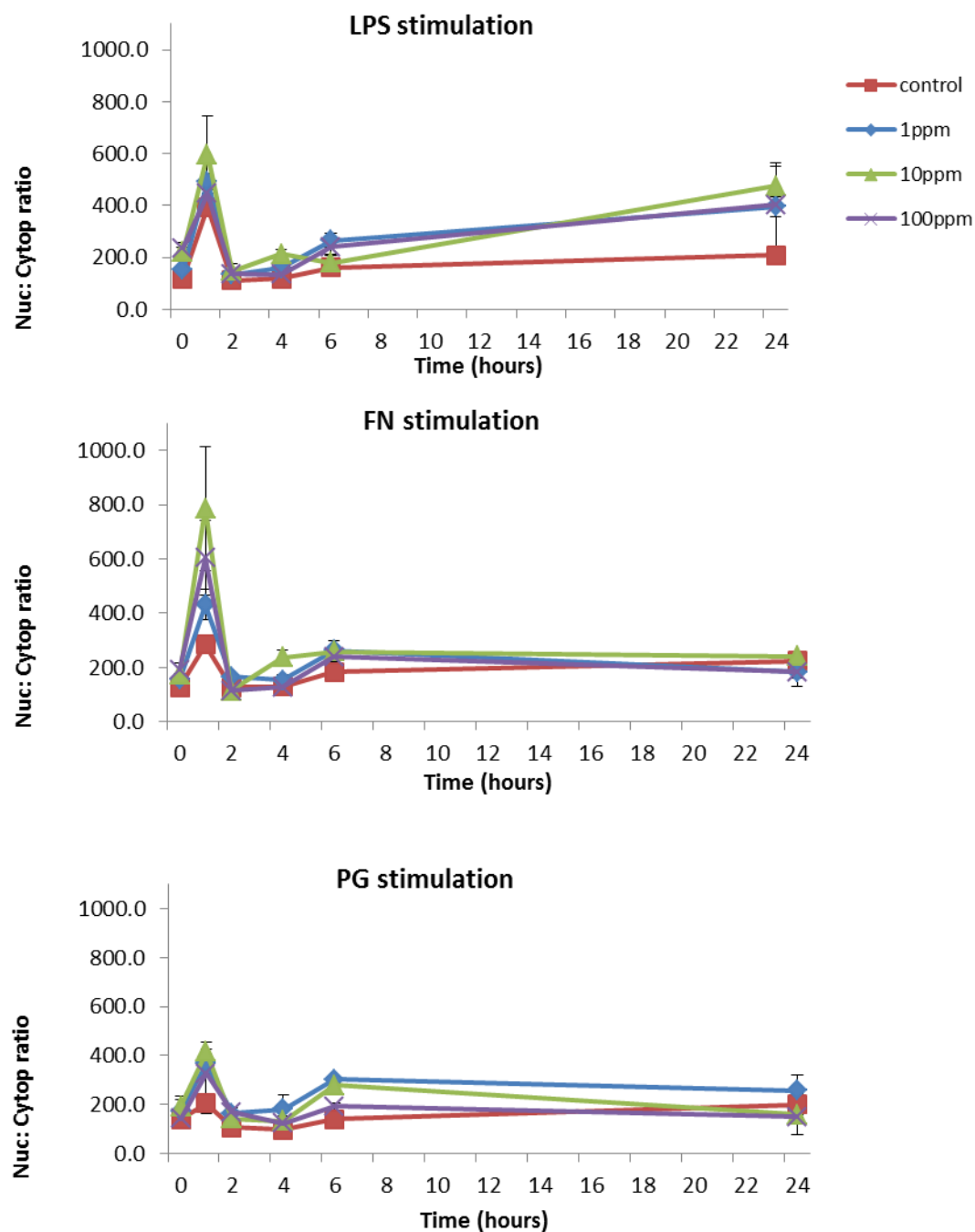


Figure 5.16 – Nuclear:cytoplasmic intensity ratio of fluorophore conjugated to NFκB in oral epithelial cells when stimulated with FN (*Fusobacterium nucleatum*), LPS (*E.coli* LPS) and PG (*Porphyromonas gingivalis*) over time. A small increase in activation of NFκB in cells pre-treated with TiO₂ was seen compared with those not pre-treated but the differences were small.

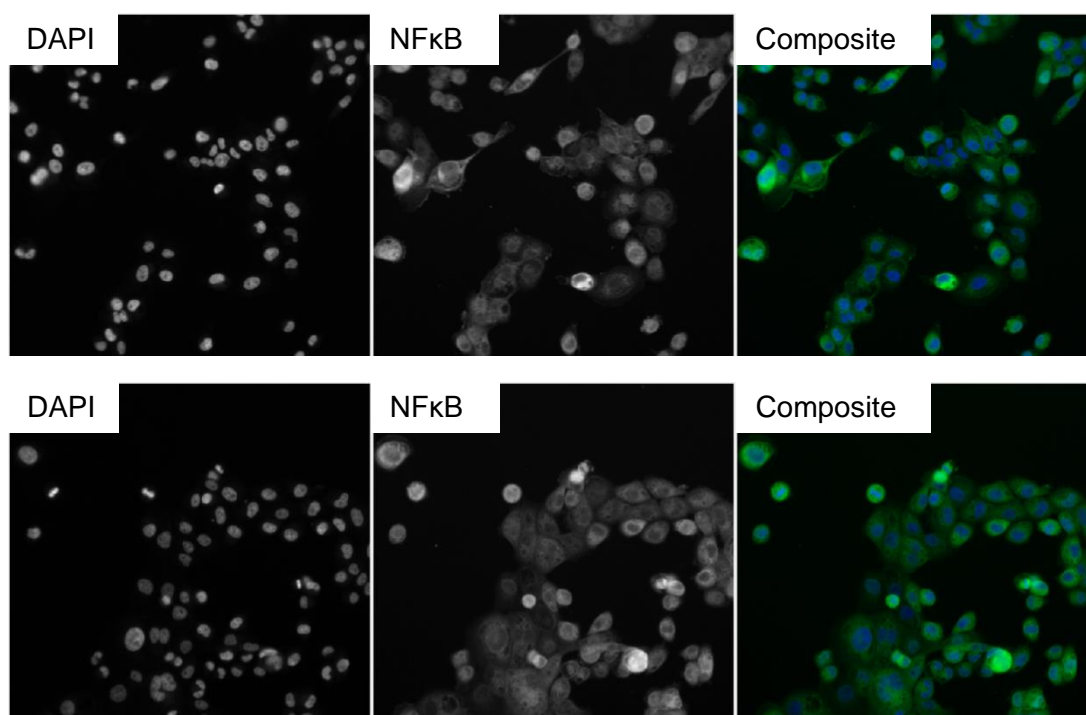


Figure 5.17 – Example images showing fluorescent signal from DAPI (left, nuclear stain), NFκB linked fluorophore (centre) and combined false colour image (right, DAPI blue and NFκB green) in H460 cells 1 h after being treated with PBS (control) showing minimal translocation of NFκB.

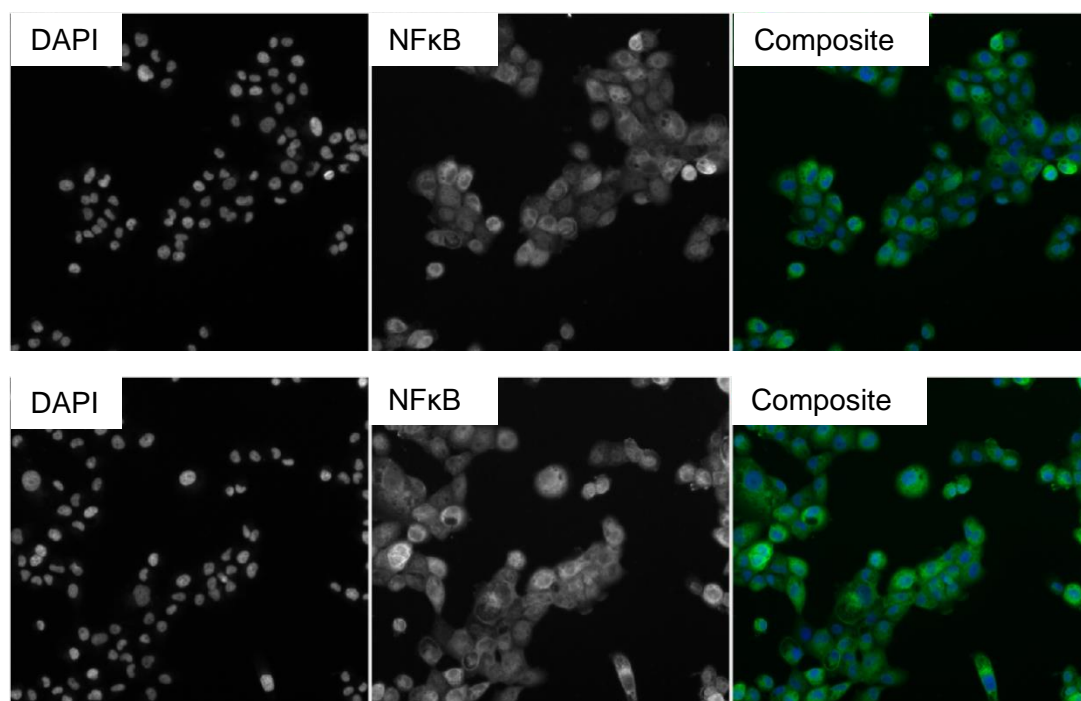


Figure 5.18 – Example images showing fluorescent signal from DAPI (left, nuclear stain), NFκB linked fluorophore (centre) and combined false colour image (right, DAPI blue and NFκB green) in H460 cells pre-treated with TiO₂ NPs at 10ppm for 24 h, 1 h after being treated with PBS (control) showing minimal translocation of NFκB.

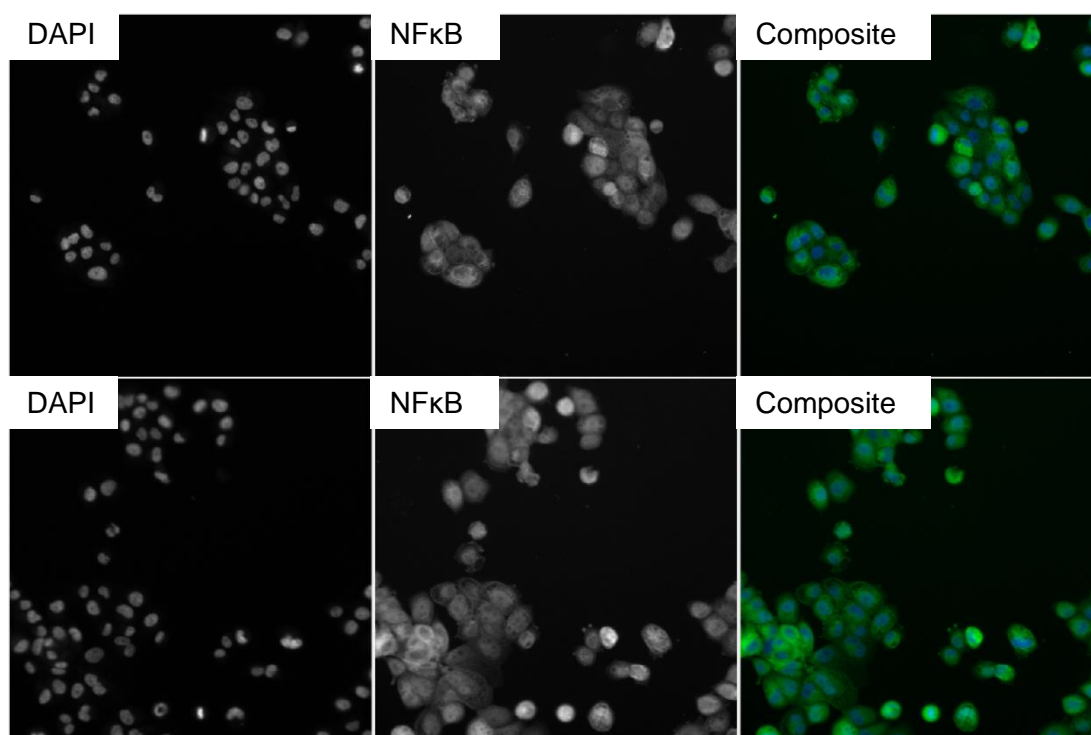


Figure 5.19 – Example images showing fluorescent signal from DAPI (left, nuclear stain), NFκB linked fluorophore (centre) and combined false colour image (right, DAPI blue and NFκB green) in H400 cells 1 h after being treated with *FN* showing a degree of translocation of NFκB.

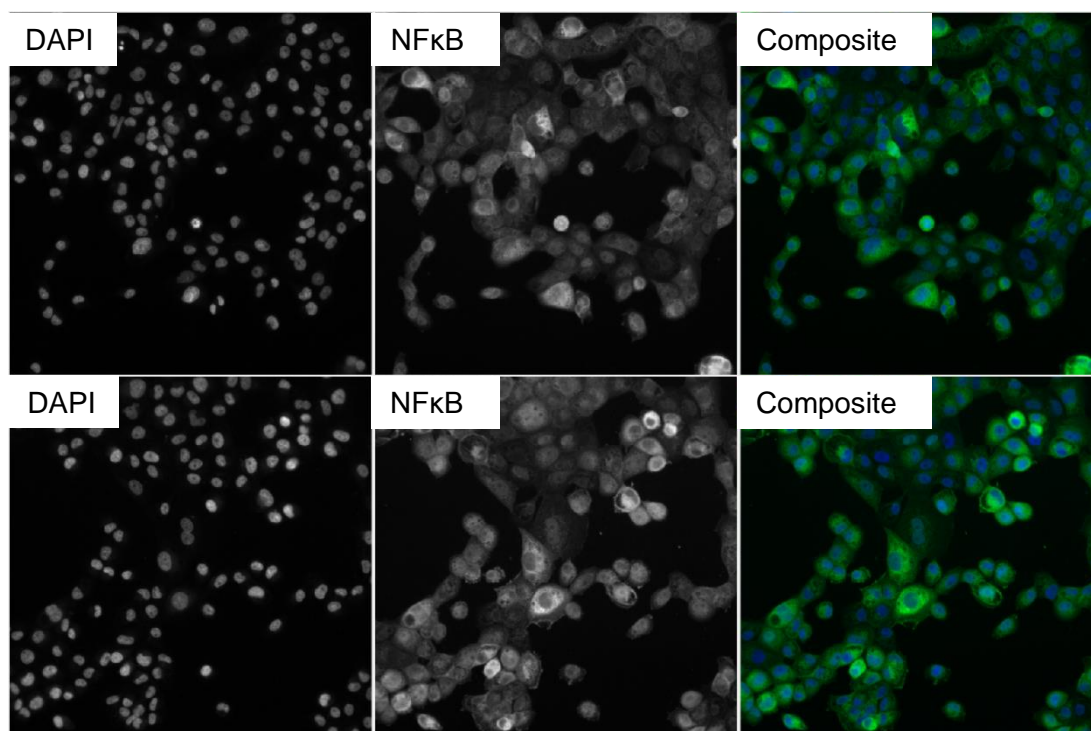


Figure 5.20 – Example images showing fluorescent signal from DAPI (left, nuclear stain), NFκB linked fluorophore (centre) and combined false colour image (right, DAPI blue and NFκB green) in H400 cells pre-treated with TiO₂ NPs at 10ppm for 24 h, 1 h after being treated with *FN* showing a degree of translocation of NFκB.

5.4.7 *HCS investigation of NFκB responses to bacteria with and without TiO₂ NPs- discussion*

Conventional staining and light microscopy showed only limited consequences of the presence of TiO₂ NPs on the NFκB translocation in H400 cells in the absence of other stimuli. However, when investigating the effects of the presence of TiO₂ NPs on NFκB translocation within cells in a co-stimulation model or using TiO₂ NP as a pre-treatment, there appeared to be small but statistical modifications in behaviour.

The results from the HCS investigation appear to show a different pattern to the conventional assay technique, in that there is a minimal difference in NFκB expression in H400 cells pre-treated with TiO₂ and those not pre-treated. There is a non-uniform distribution of TiO₂ within the cellular population due to insolubility and agglomeration within the cell culture system as previously discussed, so it may be that the HCS technique gives a truer picture of responses than the conventional approach to staining for NFκB which is limited to smaller sample numbers. HCS samples analyse at least 5000 cells in triplicate, so far higher numbers of cells are imaged and analysed than using conventional methods. Also using algorithms in the analysis of images in HCS means that cells are counted as positive or negative for certain parameters, as opposed to light output from a well as a whole being taken as a result. This means that it is less likely to have a dilution of positive cells in a sample.

5.5 Chapter conclusions

The direct effects on H400 cells following interactions with TiO₂ NPs are limited. Conventional assays showed an increase in ATPase activity at approximately 6 h, indicating cells are metabolically more active at this time-point, which ties in with the timescales of intracellularisation of NP agglomerations shown in Chapter 4. However conventional assays demonstrated only a small reduction in viability up to 24 h and with exposure concentrations ranging up to 1000 ppm TiO₂. Sytox green staining appeared to show an increase in the number of non-viable cells and these non-viable cells appeared to be located adjacent to NP agglomerations. There is evidence to show some reduced viability in longer term cultures at increasing concentrations from HCS data.

Known pathways in response to bacterial challenges such as NF κ B appear to be unaffected by pre-treatment with TiO₂ NPs when investigated using HCS techniques, however conventional staining appeared to show a small reduction in NF κ B activation in response to pre-treatment. The differences in results between HCS and conventional methods are likely to be due to the fact that each cell is not equally exposed or affected by the presence of TiO₂ NPs in this system. A number of factors which are important in both the *in vitro* and *in vivo* situations are relevant:

- TiO₂ is insoluble and agglomerates in cell culture mediums, therefore the local concentration in the immediate environ of each cell will not be uniform across the cell population.
- HCS techniques will reduce background noise, as cells are labelled individually as opposed to results being pooled across a whole cell population.
- It is possible that cell cycle stage of the cells determines whether or not an interaction is seen, however attempts to elucidate this using HCS techniques were inconclusive.

There appears to be a slight morphological change in H400 cells when stained with CellMask post TiO₂ NP exposure. LPS contamination is unlikely to be a significant issue in this model system, and any contamination may in fact be more representative of the clinical situation.

Chapter 6

**Effects of interactions between TiO₂ NPs and oral
epithelial cells on gene expression**

Synopsis

In Chapters 3 and 4 it was demonstrated that H400 cells and primary oral epithelial cells interact with TiO₂ NPs leading to NP intracellularisation. At concentrations of 1000 ppm of TiO₂ NPs and higher, a reduction in H400 viability was identified using conventional assays. A dose dependent reduction in cell viability and cell count was identified using HCS techniques. NFκB translocation in response to pathogenic stimuli was inhibited by the presence of TiO₂ NPs. Interactions such as intracellularisation and altered viability suggest that the responses of epithelial cells to TiO₂ NPs are likely to be complex and involve multiple cellular pathways and functions. In this chapter the gene expression profile of human oral epithelial cells when exposed to TiO₂ NPs is compared with non-exposed cells of the same type, and is investigated using DNA microarray and PCR techniques. Furthermore, relevant pathogenic stimuli are introduced into the co-culture model and their effects on gene expression and therefore potentially proteins expressed by oral epithelial cells are explored in the presence and absence of TiO₂ NPs.

6.1 DNA microarray

A DNA microarray is a device for a high throughput technique where a panel of DNA probes are presented to a DNA sample. In a microarray chip there are often many thousands of probes presented to the sample. Due to the specific sequences of the probes, complementary sections of DNA within the sample will bind to the probes, which are labelled with a reporter molecule. A higher signal from the specific label correlates with a greater expression of the target DNA sequence within that sample.

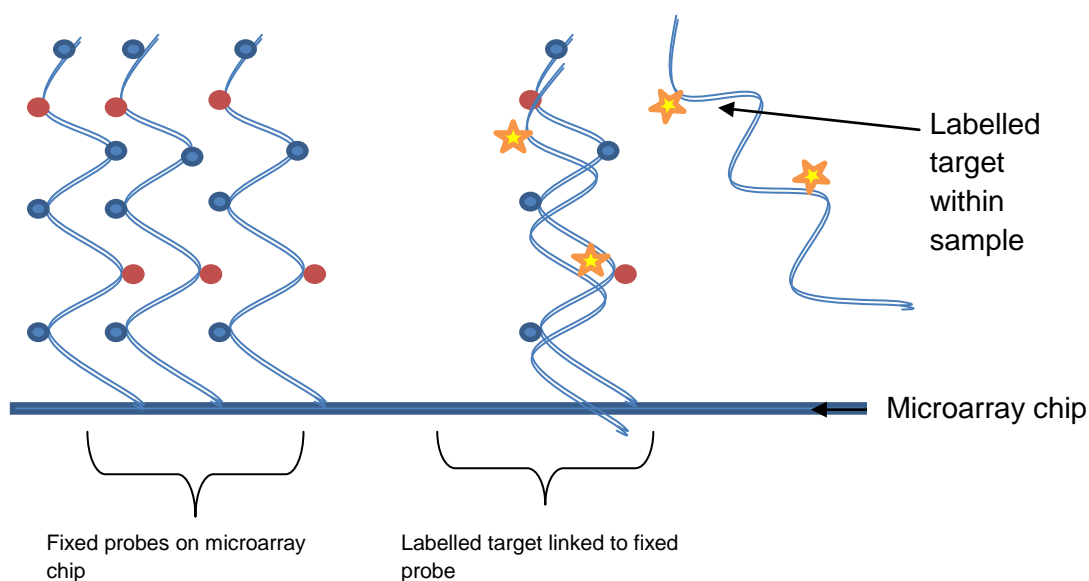


Figure 6.1 – Illustration of a DNA microarray chip.

DNA for the microarray assay is synthesised from RNA extracted from cells or tissue. The protocol for RNA extraction from epithelial cells grown in culture vessels is reported in Section 2.5.1. A DNA microarray approach was chosen as it is a non-presumptive technique, and the expression levels of thousands of genes can be generated, thus potentially allowing identification of novel genes that will enable a better understanding of the mechanisms underpinning the cellular effects of TiO₂ NP exposures. The interactions between oral epithelial cells and TiO₂ NPs have been shown to vary within cell populations, and involve a number of physiological processes. The objective was therefore to use a DNA micro-array approach as a screening tool with subsequent validation of findings performed using targeted and presumptive PCR techniques.

The Affymetrix Human Gene 1.0 ST Array was employed, which covers 36,079 total transcripts and 21,014 RefSeq (Entrez) genes, covering a wide range of potential cellular responses. Entrez Gene is a national database for gene-specific information, and records information from sequenced genomes (Maglott et al., 2011) and generated specific identifiers for genes known as GeneIDs. This allows quick identification of genes and the full Entrez Gene report allows access to a variety of gene specific information.

6.1.1 *Affymetrix GeneChip methods*

The microarray data using the Affymetrix GeneChip was generated at the University of Birmingham Institute of Cancer Sciences, as an assay service.

RNA sample preparation

H400 cells were cultured in 25 cm² cell culture treated flasks using standard growth conditions (Section 2.2.2). When the flasks had reached approximately 80 % confluence, determined visually using light microscopy, the growth medium was changed and supplemented with TiO₂ NPs according to the methods specified in Section 2.2.2. Subsequent to supplementation of the growth medium with TiO₂ NPs, flasks were incubated as described in Section 2.2.2. The culture medium was then removed and the cell monolayer was washed with warmed (37 ± 1°C) PBS three times. Flasks were then processed as described in Section 2.5.1. The process was completed three times on separate days to create full biological triplicates of each sample number. Samples were then processed separately and not pooled to enable sample comparison within conditions.

Sample number	Final concentration of TiO ₂ NPs in culture medium	Time from 0 h
1	0	6 h
2	0	24 h
3	100 ppm	6 h
4	100 ppm	24 h

Table 6.1 – H400 RNA sample preparation

The time points of 6 h and 24 h were chosen as intracellularisation was clearly evident in TEM images of H400 cells, 6 h post-TiO₂ NP exposure, and at 6 and 24 h post exposure a different set of genes may be activated. Gene expression changes have also been previously reported in H400 cells 24 h post-stimulation with periodontally relevant bacteria (Milward et al., 2007). Longer term cultures were avoided to reduce the risk of media exhaustion influencing cell responses. Shorter term cultures (< 2 h) were avoided to minimise the risk of disruption to cells from media supplementation affecting gene expression. The potential for TiO₂ NP interference with the microarray was minimised by avoiding high (> 100 ppm) TiO₂ NP exposures. The avoidance of higher TiO₂ NP concentrations may not have been necessary, but given the previously

reported effects of high TiO₂ NP concentrations with certain assays, a lower concentration was selected to reduce the risk of interference. This however, inevitably reduces the proportion of cells within the sample population that are directly exposed.

Sample preparation and microarray protocol

RNA samples were prepared (Section 2.5.1) and transferred to the Institute of Cancer Sciences (now the Institute of Cancer and Genomic Sciences) microarray service for processing. The processing briefly consisted of:

1. Synthesis of double stranded cDNA from RNA
2. Purification of double stranded cDNA
3. Synthesis of biotin labelled cRNA
4. Purification of biotin labelled cRNA
5. Fragmentation of cRNA
6. Target hybridisation and probe array wash and stain/label.

Following staining, arrays were scanned and analysed.

6.1.2 *GeneChip data analysis*

Images of microarray chips were scanned and then analysed using the Affymetrix GeneChip Command Console. The data analysis was completed by Dr Wenbin Wei at the University of Birmingham as part of the microarray service provided by the Institute of Cancer and Genomic Sciences. Probe level quantile normalisation (Bolstad et al., 2003) and robust multi-array analysis (Irizarry et al., 2003) was performed on the raw CEL files. The multi-array analysis was performed using the “Affy” package of the Bioconductor (<http://www.bioconductor.org>) project and custom Computable Document Format (cdf) HUGENE10ST_Hs_ENTREZG (version 17) (Dai et al., 2005). Gene annotation was based on the NCBI gene database downloaded on June 7, 2013. Differentially expressed genes were initially identified using Limma software (Bioconductor 3.3 open source software), with a fold change >1.5 and $p < 0.01$ (Smyth, 2004). Significance levels were not adjusted for multiple hypothesis testing.

6.1.3 *GeneChip results - DNA microarray data*

The tables below summarise the down-regulated and up-regulated genes at 6 h following TiO₂ NP exposure compared with 6 h control H400 cells. The fold changes at a significance of $p < 0.01$ are listed.

Symbol	Description	Fold Change
ID2	inhibitor of DNA binding 2, dominant negative helix-loop-helix protein	-8.44
SNORD116-8	small nucleolar RNA, C/D box 116-8	-2.82
ID1	inhibitor of DNA binding 1, dominant negative helix-loop-helix protein	-2.53
ID3	inhibitor of DNA binding 3, dominant negative helix-loop-helix protein	-2.14
SCARNA4	small Cajal body-specific RNA 4	-2.00
LOC100996467	metastasis-associated lung adenocarcinoma transcript 1-like	-1.95
BMI1	BMI1 polycomb ring finger oncogene	-1.86
MIR1247	microRNA 1247	-1.85
ANKRD36BP1	ankyrin repeat domain 36B pseudogene 1	-1.83
RHOBTB3	Rho-related BTB domain containing 3	-1.83
HIST1H2AH	histone cluster 1, H2ah	-1.78
TRAPPC2P1	trafficking protein particle complex 2 pseudogene 1	-1.73
RPL22	ribosomal protein L22	-1.71
RPSAP52	ribosomal protein SA pseudogene 52	-1.70
LSP1P3	lymphocyte-specific protein 1 pseudogene 3	-1.67
COX7B	cytochrome c oxidase subunit VIIb	-1.65
HIST3H2BB	histone cluster 3, H2bb	-1.63
HOXC13	homeobox C13	-1.58
RNU5B-1	RNA, U5B small nuclear 1	-1.58
TRGV3	T cell receptor gamma variable 3	-1.57
ORM1	orosomucoid 1	-1.53
GCNT4	glucosaminyl (N-acetyl) transferase 4, core 2	-1.52
CIITA	class II, major histocompatibility complex, transactivator	1.50
KRTAP5-5	keratin associated protein 5-5	1.51
ADAMTSL2	ADAMTS-like 2	1.54
FLJ44790	uncharacterized FLJ44790	1.54
NEDD9	neural precursor cell expressed, developmentally down-regulated 9	1.54
USP32P2	ubiquitin specific peptidase 32 pseudogene 2	1.55
TUBB8	tubulin, beta 8 class VIII	1.57
ZRSR2	zinc finger (CCCH type), RNA-binding motif and serine/arginine rich 2	1.57
HBB	hemoglobin, beta	1.57
LOC145757	uncharacterized LOC145757	1.68
OR10G9	olfactory receptor, family 10, subfamily G, member 9	1.68
MIR134	microRNA 134	1.74
IGKV1D-12	immunoglobulin kappa variable 1D-12	1.75
XAGE-4	XAGE-4 protein	1.93

ANAPC1P1	anaphase promoting complex subunit 1 pseudogene 1	2.00
FLJ45248	FLJ45248 protein	2.15
INS-IGF2	INS-IGF2 readthrough	2.25

Table 6.2 – Genes showing altered expression at 6 h in H400 cells exposed to TiO₂ NPs compared with control cells (fold change >1.5 and p < 0.001).

Symbol	Description	Fold Change
ID2	inhibitor of DNA binding 2, dominant negative helix-loop-helix protein	-8.03
ID3	inhibitor of DNA binding 3, dominant negative helix-loop-helix protein	-3.42
AKR1B10	aldo-keto reductase family 1, member B10 (aldose reductase)	-2.50
FABP4	fatty acid binding protein 4, adipocyte	-2.19
C10orf99	chromosome 10 open reading frame 99	-2.03
RHOBTB3	Rho-related BTB domain containing 3	-1.95
IGKV1D-12	immunoglobulin kappa variable 1D-12	-1.95
CLDN8	claudin 8	-1.91
KRTAP20-1	keratin associated protein 20-1	-1.82
ID1	inhibitor of DNA binding 1, dominant negative helix-loop-helix protein	-1.80
RIPK4	receptor-interacting serine-threonine kinase 4	-1.74
MGC21881	uncharacterized locus MGC21881	-1.70
TPTE2P6	transmembrane phosphoinositide 3-phosphatase and tensin homolog 2 pseudogene 6	-1.69
RFPL4AL1	ret finger protein-like 4A-like 1	-1.67
TMPRSS11E	transmembrane protease, serine 11E	-1.66
PTENP1	phosphatase and tensin homolog pseudogene 1	-1.65
TGM5	transglutaminase 5	-1.61
APOL1	apolipoprotein L, 1	-1.61
SNORA60	small nucleolar RNA, H/ACA box 60	-1.61
PSCA	prostate stem cell antigen	-1.57
CYP4F3	cytochrome P450, family 4, subfamily F, polypeptide 3	-1.56
KRT4	keratin 4	-1.55
HOXC13	homeobox C13	-1.54
AQP3	aquaporin 3 (Gill blood group)	-1.54
LY6D	lymphocyte antigen 6 complex, locus D	-1.53
POU5F1	POU class 5 homeobox 1	-1.52
OR1F2P	olfactory receptor, family 1, subfamily F, member 2	-1.52
ANKRD32	ankyrin repeat domain 32	1.50
ZNF443	zinc finger protein 443	1.50
MMS22L	MMS22-like, DNA repair protein	1.50
DEPDC1	DEP domain containing 1	1.51
TPRG1	tumor protein p63 regulated 1	1.51
FANCB	Fanconi anemia, complementation group B	1.51
CDCA7	cell division cycle associated 7	1.53
CENPK	centromere protein K	1.53
CEP128	centrosomal protein 128kDa	1.54
HNRNPA3	heterogeneous nuclear ribonucleoprotein A3	1.54
BRIP1	BRCA1 interacting protein C-terminal helicase 1	1.54

HMGCS1	3-hydroxy-3-methylglutaryl-CoA synthase 1 (soluble)	1.54
LYRM1	LYR motif containing 1	1.55
TNC	tenascin C	1.55
HELLS	helicase, lymphoid-specific	1.55
CDC7	cell division cycle 7	1.56
FAM111B	family with sequence similarity 111, member B	1.57
SNORD42B	small nucleolar RNA, C/D box 42B	1.57
IL1A	interleukin 1, alpha	1.57
CCL5	chemokine (C-C motif) ligand 5	1.58
WDHD1	WD repeat and HMG-box DNA binding protein 1	1.59
XRCC2	X-ray repair complementing defective repair in Chinese hamster cells 2	1.61
TRIM51	tripartite motif-containing 51	1.62
STC2	stanniocalcin 2	1.62
CENPH	centromere protein H	1.62
CLSPN	claspin	1.63
MND1	meiotic nuclear divisions 1 homolog (S. cerevisiae)	1.63
BRCA2	breast cancer 2, early onset	1.64
MYBL1	v-myb myeloblastosis viral oncogene homolog (avian)-like 1	1.64
MAD2L1	MAD2 mitotic arrest deficient-like 1 (yeast)	1.67
HSPA6	heat shock 70kDa protein 6 (HSP70B')	1.67
ATAD5	ATPase family, AAA domain containing 5	1.68
B4GALT6	UDP-Gal:betaGlcNAc beta 1,4- galactosyltransferase, polypeptide 6	1.68
ALG10B	ALG10B, alpha-1,2-glucosyltransferase	1.69
NT5E	5'-nucleotidase, ecto (CD73)	1.69
DDX11L2	DEAD/H (Asp-Glu-Ala-Asp/His) box helicase 11 like 2	1.71
OCM2	oncomodulin 2	1.77
ANAPC1P1	anaphase promoting complex subunit 1 pseudogene 1	1.98
CXCL10	chemokine (C-X-C motif) ligand 10	2.06
TPPP3	tubulin polymerization-promoting protein family member 3	2.30
PDIA3	protein disulfide isomerase family A, member 3	2.65
TRAV8-3	T cell receptor alpha variable 8-3	2.73
ALG10B	ALG10B, alpha-1,2-glucosyltransferase	1.69
NT5E	5'-nucleotidase, ecto (CD73)	1.69
DDX11L2	DEAD/H (Asp-Glu-Ala-Asp/His) box helicase 11 like 2	1.71
OCM2	oncomodulin 2	1.77
ANAPC1P1	anaphase promoting complex subunit 1 pseudogene 1	1.98
CXCL10	chemokine (C-X-C motif) ligand 10	2.06
TPPP3	tubulin polymerization-promoting protein family member 3	2.30
PDIA3	protein disulfide isomerase family A, member 3	2.65
TRAV8-3	T cell receptor alpha variable 8-3	2.73

Table 6.3 - Genes showing altered expression at 24 h in H400 cells exposed to TiO₂ NPs compared with control cells (fold change >1.5 and p < 0.01).

6.1.4 *GeneChip results - DNA microarray data interpretation and discussion - Ontological grouping*

Ontological grouping was used to manage the complex data sets generated by microarray techniques. Ontological grouping can be useful to identify potential causes of certain genes being up- or down-regulated, as genes are grouped according to cellular functions. The technique takes lists of genes showing altered expression and databases provide information on the functions of these genes (if known), to produce groups of genes relevant to defined cellular processes. For the datasets in Figures 6.2 and 6.3, the PANTHER classification system was used (Mi et al., 2010, Mi et al., 2013) and the PANTHER tool used for generating outputs (Thomas et al., 2006). The molecular function of each gene showing altered expression was matched to the categories within the Panther GO-Slim molecular function database of 20972 genes and 14830 function hits. The parent categories were:

- antioxidant activity
- binding
- catalytic activity
- channel regulator activity
- receptor activity
- signal transducer
- structural molecule activity
- translation regulator activity
- transporter activity

Each parent category consists of a number of child categories which are listed where relevant.

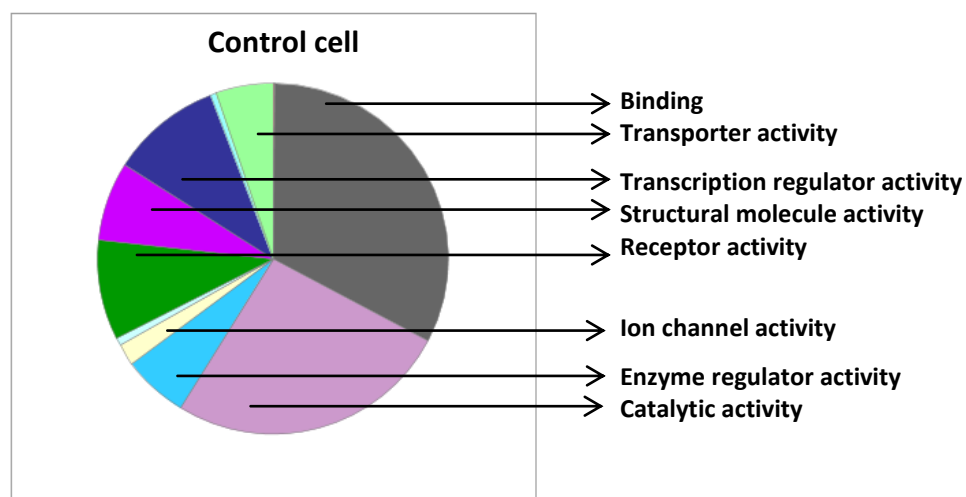
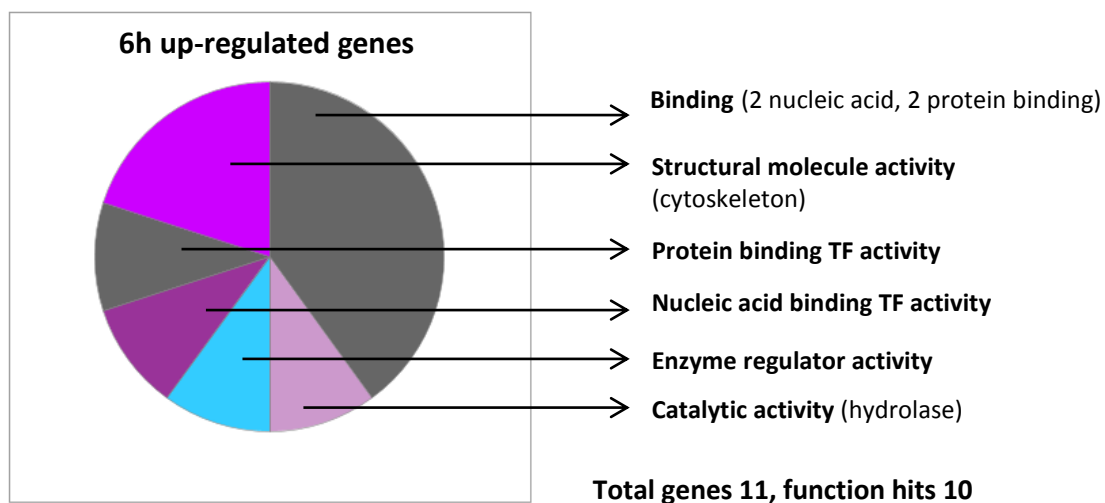
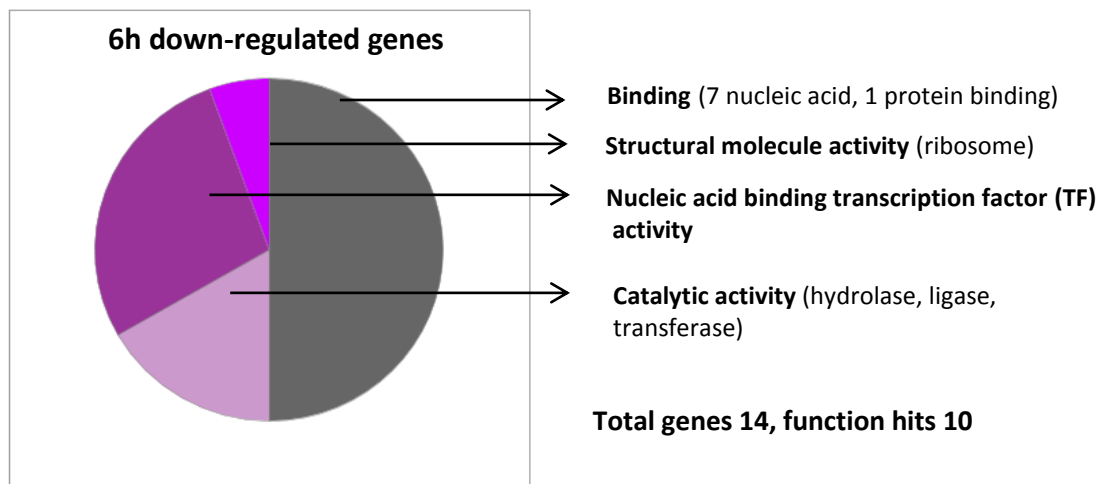


Figure 6.2 – diagrams showing ontological grouping by function of genes with altered expression as labelled in H400 cells exposed to TiO₂ NPs 100 ppm for 6 h compared with a control cell sample. Generated using PANTHER tool (Mi and Thomas, 2009). The largest changes were observed in “binding” genes.

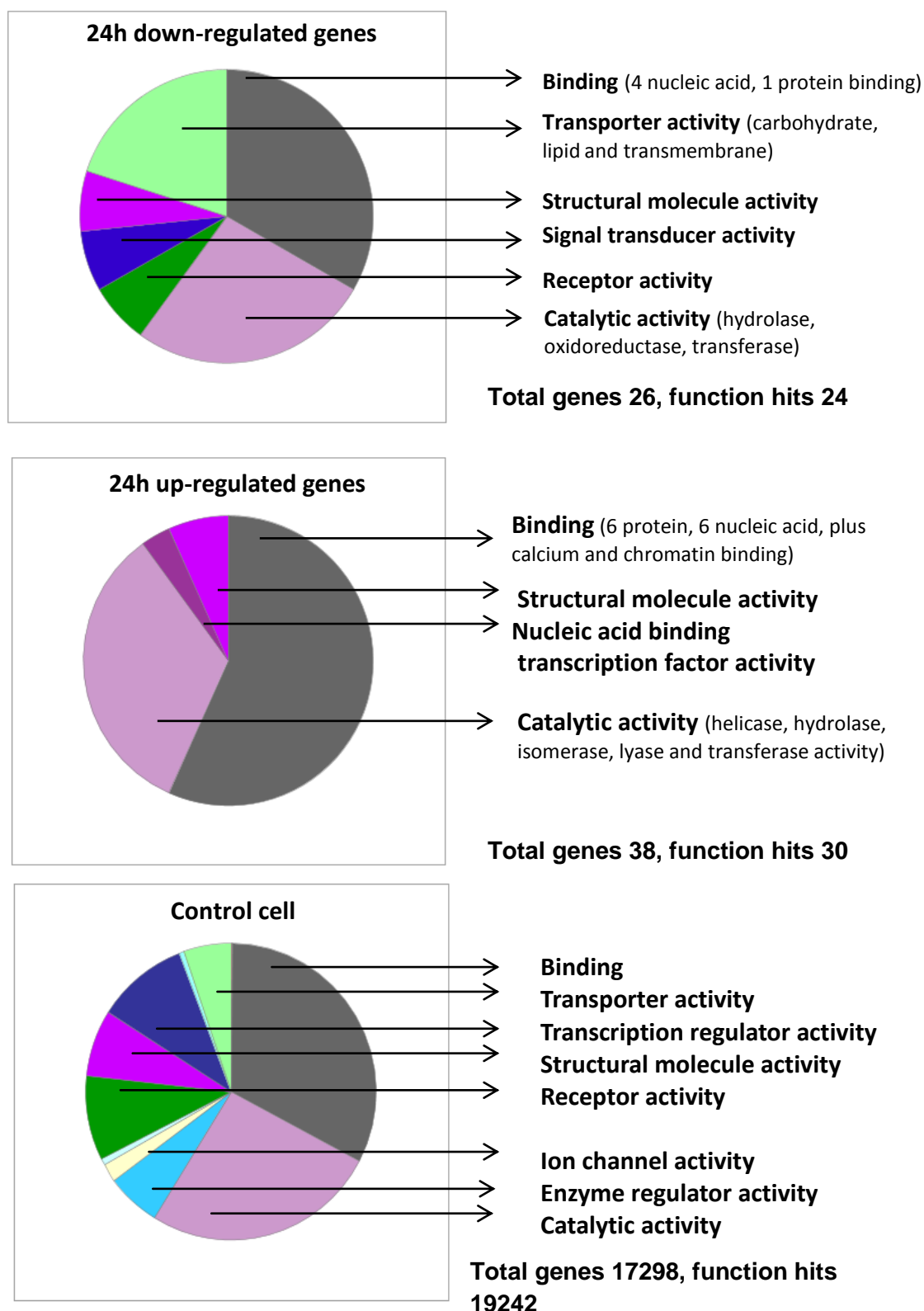


Figure 6.3 – diagrams showing ontological grouping by function of genes with altered expression as labelled in H400 cells exposed to TiO₂ NPs 100 ppm for 24 h compared with a control cell sample. Generated using PANTHER tool (Mi and Thomas, 2009). Shows transporter genes are down-regulated at 24 h, possibly following intracellularisation of TiO₂ NPs.

Up-regulated and down-regulated genes common in both 6 h and 24 h exposures to TiO₂ NPs were in the ontological group 'binding'. These genes fall into a variety of sub-categories, and mainly demonstrate that nucleic acid binding genes are down-regulated and both protein binding and some nucleic acid binding genes are up-regulated. Both nucleic acid and protein binding are complex gene groups with a large number of functions. Therefore, the information presented here is inadequate to gain a comprehensive understanding of the specific alterations to cell processes in response to TiO₂ NP exposures. However, there are indications that intracellularisation is occurring by endocytosis at or before 6 h (as discussed in chapter 4) in that transporter activity is down-regulated at 24 h. Cytoskeleton reorganisation is also likely to be occurring due to the changes in regulation of structural protein coding genes specific to the cytoskeleton. These findings are discussed further in Section 6.1.5.

6.1.5 *GeneChip results - DNA microarray data interpretation and discussion – Common genes between 6 h and 24 h samples*

To identify if there was a consistent elevation or downregulation due to the exposure of TiO₂ NPs to H400 cells, results were analysed to identify genes that were in common as being up- or down-regulated in both the 6 h and 24 h data sets when compared with their respective controls (fold change >1.5 and $p < 0.01$).

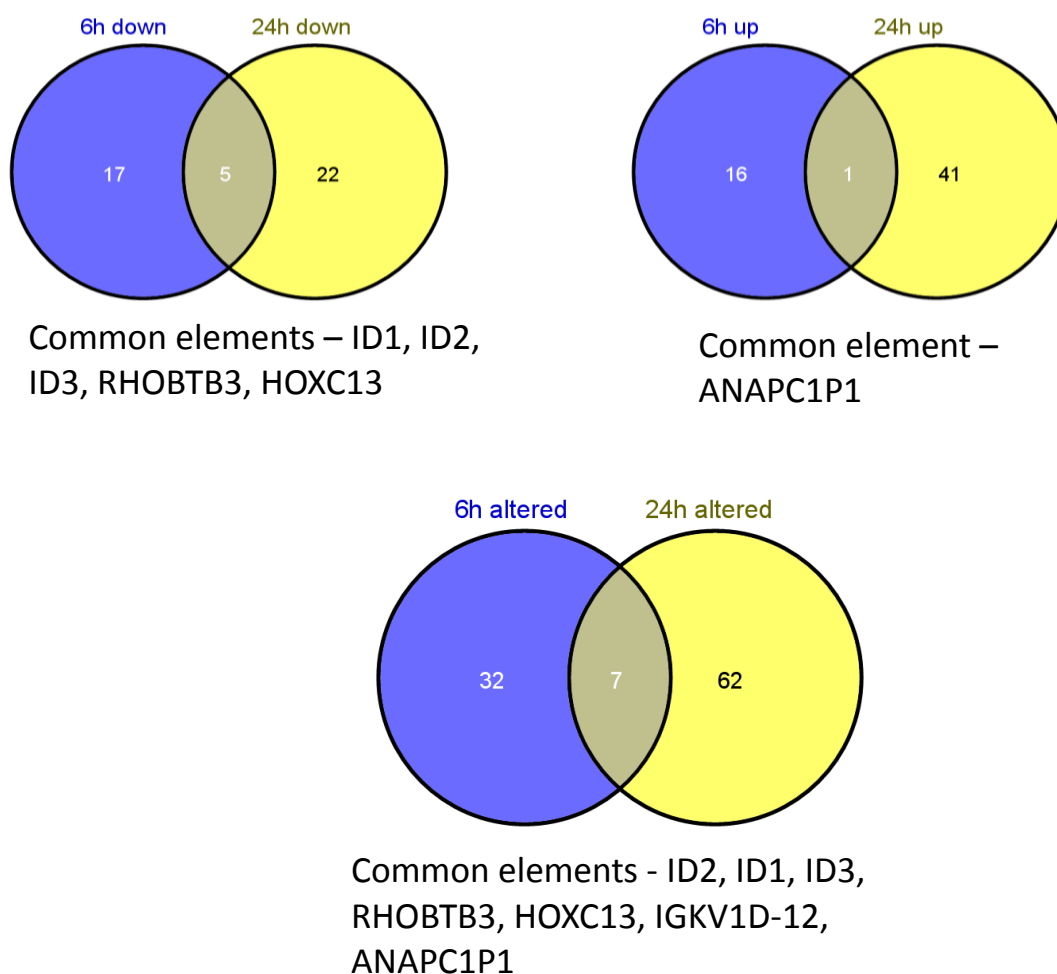


Figure 6.4 – Venn diagrams showing down-regulated, up-regulated and altered expression of genes in H400 cells at 6 h (blue) and 24 h (yellow) TiO₂ exposure at 100 ppm compared with respective control cells as detected by the AffyChip.

ID1, ID2, ID3:

These helix-loop-helix (HLH) transcription factors are three of a family of four genes. ID1, ID2 and ID3 were all significantly downregulated in both conditions with the biggest fold change being for ID2 (>-8.00 fold change). ID1, ID2 and ID3 genes codes for ID1, ID2 and ID3 proteins, respectively. All ID proteins are thought to play a role in negatively regulating cell differentiation; therefore, suppression of these proteins could lead to an increase in cell differentiation.

Transcription factors can be broadly categorised into:

- | | |
|----------------|--|
| Superclass I | – those containing basic domains |
| Superclass II | – those containing zinc co-ordinated DNA binding domains |
| Superclass III | – those containing helix-turn-helix domains |
| Superclass IV | – those containing β -scaffold factors. |

Superclass I can be divided further into subcategories depending on the specific motifs present (e.g. basic HLH or bHLH). bHLH transcription factors all share a highly conserved HLH region which mediates protein-protein interactions, and also a basic DNA binding region (Forrest and McNamara, 2004). The ID class of HLH proteins are dominant-negative regulators of class I and class II bHLH proteins (Benezra et al., 1990). ID proteins probably mediate communication between pathways that regulate cellular growth and differentiation, and ID expression is upregulated after mitosis triggering.

Inhibition of any of the ID genes is sufficient to inhibit fibroblastic proliferation stimulated by serum (Barone et al., 1994). Physiological processes ID proteins (IDs) are known to be involved in include, the regulation of cyclin-dependent kinase (cdk) inhibitors (which regulate the cell cycle). ID2 specifically appears to inactivate the retinoblastoma protein (pRb), promoting cellular growth (Lasorella et al., 2000).

IDs can also act as cellular differentiation inhibitors; therefore, downregulation would imply an inhibition of the prevention for cell differentiation. Ectopic ID expression inhibits cell differentiation in epithelial cells, and expression of ID genes is significantly reduced on terminal differentiation of different cells. It has been suggested that ID1 renders cells refractory to differentiation signals and receptive to growth signals by inactivating one or more basic HLH proteins that co-ordinate growth and differentiation in the mammary epithelium of mice (Desprez et al., 1995). The ID proteins are also thought to play a role in vascular lesion formation (Forrest and McNamara, 2004).

ID1, 2 and 3 are expressed in multiple tissues during murine embryological development and tissue morphological changes, but thereafter ID2 is the only member of this family expressed in epithelium, while ID1 and ID3 are found in the surrounding mesenchyme (Coppe et al., 2003). This family of proteins is also often over-expressed in malignancy. ID1 can facilitate the phenotypic transition from resting, sessile keratinocytes to mobile, migrating and proliferating keratinocytes during wound healing (Schaefer et al., 2001). There is evidence to suggest that different ID proteins

can play opposing roles in the same tissue, as well as the same ID playing a different role in a different tissue.

Cell lines derived from squamous cell carcinomas (SCCs), such as H400 cells, express ID 123 mRNA at high levels. Cell lines derived from head and neck SCCs have shown high expression of ID1. Knockdown of ID1 inhibits the metastatic potential of breast cancer cells (Fong et al., 2003). It is therefore not surprising that high levels of ID genes are present, but each sample exposed to TiO₂ NPs was compared with the respective control, therefore the change in expression remains valid, and ID genes should not be discounted as being falsely elevated in cell line samples.

ID1 and TiO₂ NPs

Lee et al., (Lee et al., 2009) reported that ID1 was down-regulated in lung cancer cells exposed to TiO₂ NPs (15-350 nm diameter), while cells exposed to extracellular ID1 appeared to undergo less apoptosis and proliferated more. They hypothesised this was due to ID 1 modulating an intracellular signalling pathway and protecting against apoptosis as well as enhancing proliferation. It is possible that ID1 plays a role in the TiO₂ induced repression of cell viability. IDs 1-3 are unlikely to be relevant proteins in the process of intracellularisation of TiO₂ NPs, and the altered expression of the IDs are more likely to be due to effects of TiO₂ NPs on the cell. Changes in motility, proliferation and apoptosis are likely to be occurring due to the downregulation of these genes and apparent reduction in levels of the ID proteins in affected cells.

HOXC-13

HOXC-13 was downregulated in all samples (>-1.54 fold change). HOXC-13 codes for the protein HOXC13, which belongs to the homeobox family of genes, a highly conserved family of transcription factors which play an important role in morphogenesis in all multicellular organisms. There are four gene clusters: HOXA, HOXB, HOXC and HOXD. HOXC13 is in a cluster of HOXC genes located on chromosome 12 and may have an important role in keratin production.

RhoBTB3

RhoBTB3 was downregulated in all samples (>-1.83 fold change). RhoBTB3 codes for the RhoBTB3 protein which is a member of a family of Rho GTPases and is localised to the trans-golgi network. Knockout mice have been shown to exhibit a decreased body length and males had abnormal tooth morphology. RhoGTPases are key regulators of the actin-based cytoskeleton, and RhoBTB3 has also been shown to interact directly with Rab9 GTPase to function in protein transport from endosomes to the Golgi network (Espinosa et al., 2009). RhoBTB3 interacts with other proteins (TIP47) on membranes, and it is hypothesised that its function may be to release this cargo selection protein from vesicles to allow fusion at the Golgi (Espinosa et al., 2009). It is therefore possible that the down-regulation of RhoBTB3 may be associated with the intracellularisation of TiO₂ NPs via clathrin-mediated endocytosis (see also Section 4.2.2).

ANAPC1P1

ANAPC1P1 codes for a protein involved in promotion of anaphase. Its function is not yet well characterised.

IGKV1D-12

IGKV1D has not been well characterised yet.

Overall the number of genes that are up- or down-regulated is small, implying minimal changes within the gene expression of H400 cells when exposed to 100 ppm TiO₂ NPs for 6 and 24 h respectively. There is no strong trend from the data to suggest any specific ontological groups are altered compared with any others. The overall conclusions of this work will be discussed at the end of this chapter.

6.1.6 *GeneChip results - DNA microarray data interpretation and discussion – robustness of microarray data*

To validate the microarray data, confirmatory PCR was performed (see Section 6.2). Samples were analysed according to their agreement between replicates; an example graph of this is shown in Figure 6.5.

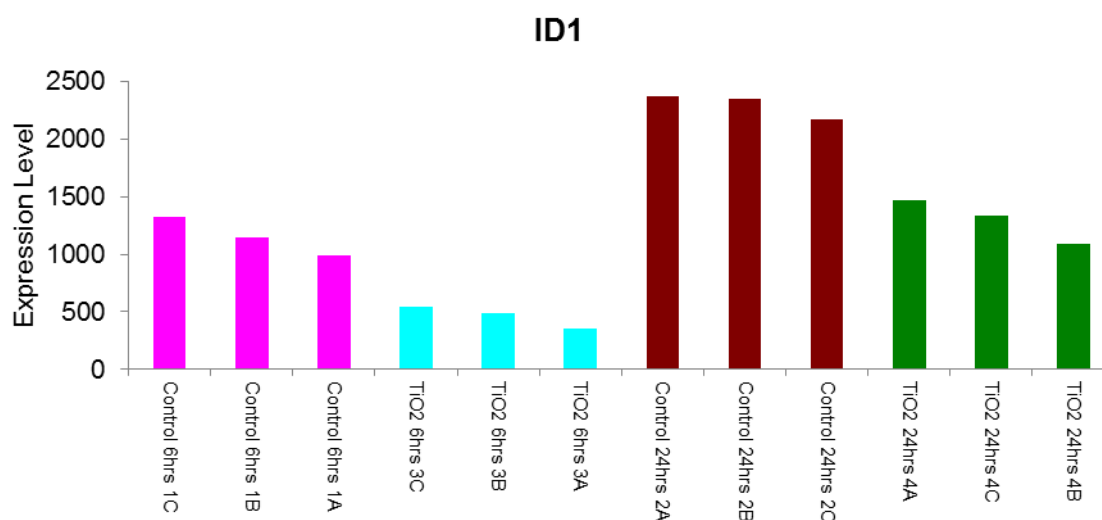


Figure 6.5 – Example graph of the levels of expression of ID1 in each sample replicate. Samples were not pooled in order to eliminate errors in one replicate altering the overall data. The graph above shows good trend replication in each set of samples.

6.2 Confirmatory PCR

To confirm the accuracy of the microarray data, PCR was performed. A selection of genes was chosen including those significantly up-or down-regulated according to the microarray results.

6.2.1 Confirmatory PCR – methods

Confirmatory semi quantitative PCR was performed (Section 2.5.6) on duplicate H400 RNA samples generated at the same time as those used for the microarray.

6.2.2 *Confirmatory PCR – results and conclusion*

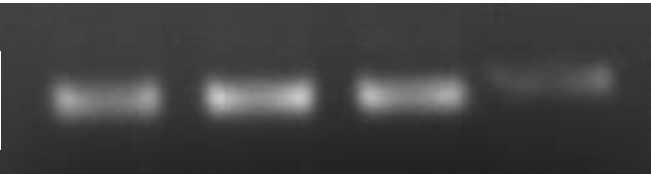
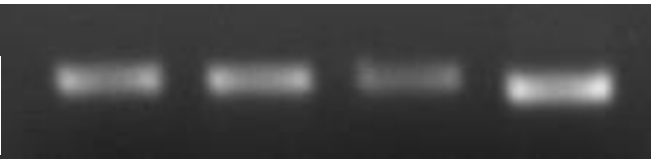
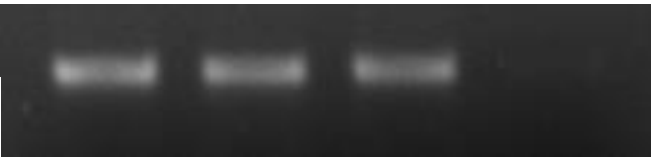
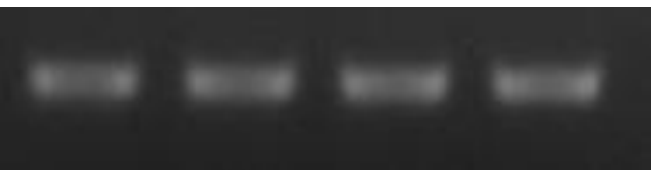
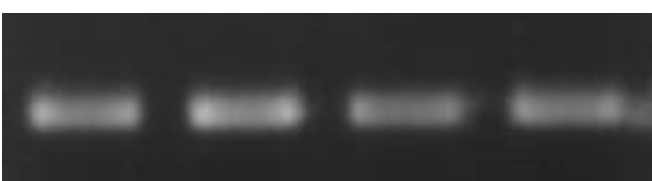
	Control 6 h	TiO ₂ 6 h	Control 24 h	TiO ₂ 24 h	Agreement with microarray?
ID1					Yes
ID2					Yes
ID3					Yes
CXCL10					Yes
RHOB- TB3					Yes

Figure 6.6 – Images of agarose gels showing agreement of up- or down- regulation between PCR and microarray data on a selection of genes. Although the degree of change is different in most samples, PCR is only semi-quantitative, therefore the fold changes are unlikely to be numerically accurate.

These data demonstrate that the microarray data appeared to be representative of gene expression changes in H400 cells as described in this chapter.

6.2.3 *Confirmatory PCR – Primary oral epithelial cells –aim and methods*

The same methods as described in Section 2.5.6 were used to perform semi quantitative PCR on primary oral epithelial cells, to establish if H400 cells are likely to be an appropriate model for the behaviour of oral epithelial cells in this context. Due to issues outlined in chapter 3, PCR was only performed on a small selection of genes.

6.2.4 *Confirmatory PCR – Primary oral epithelial cells –results and conclusions*

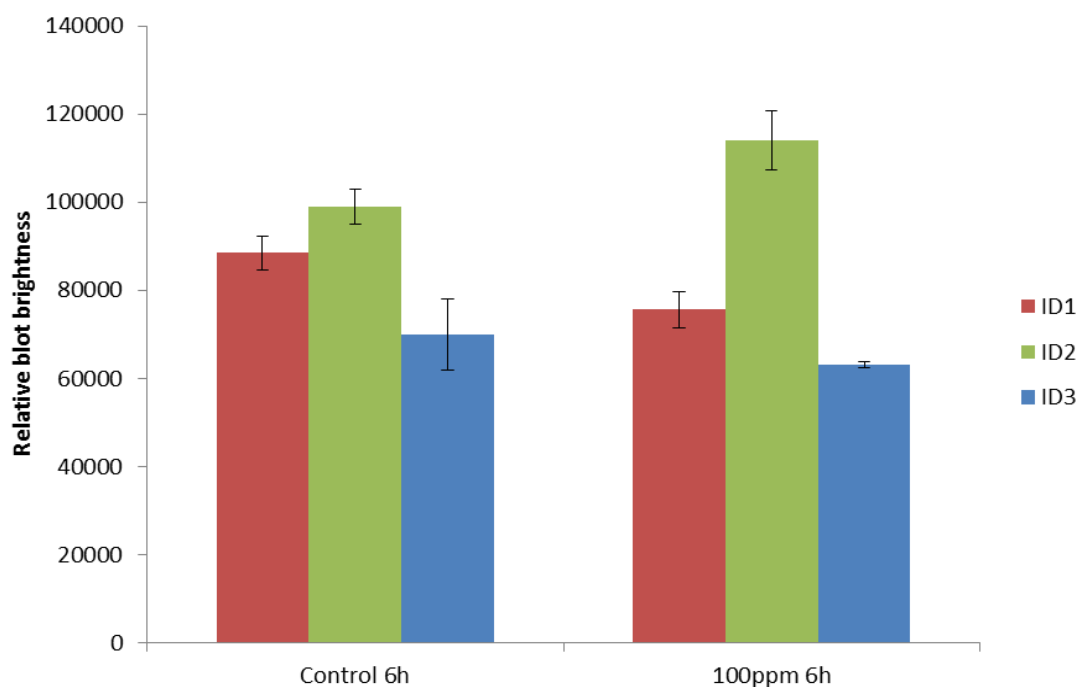


Figure 6.7 - Primary epithelial cell semi-quantitative PCR data showing a down-regulation of ID1 and 3 in cells exposed to TiO₂ for 6h and an up-regulation of ID2 (n=3, error bars show SD). This was in contrast to data from H400 cells where ID1, ID2 and ID3 were all downregulated. Therefore, H400 cells may not be an accurate model for ID gene expression in epithelial cells.

Primary cells showed a different gene expression profile to H400 cells when stimulated with TiO₂ NPs. This implies that the microarray data may not be translatable to oral epithelial cells in the clinical situation.

Immortalised cells such as H400 cells are, as discussed in chapter 3, used as a substitute for primary cells in many experiments. In the microarray data presented here, H400 cells were used for the following reasons:

- Availability of cells to ensure a good quantity of high quality RNA was produced;
- Consistency, as multiple donors would potentially have been needed in order to produce a sufficient number of epithelial cells. This intra-donor variation in cell phenotype may have led to a lack of clarity of gene expression changes as each donor's cells may have produced different baseline gene expressions;
- Financial – each microarray assay is expensive, so it was not feasible to run microarrays on multiple samples. Ideally, multiples of paired control-matched

microarrays would have been performed on primary cells from a set of donors, and the results combined and analysed.

The results described above gives an indication of the gene expression changes within immortalised epithelial cells, and the PCR data in Figure 6.7 indicates that these responses may not be applicable to primary oral epithelial cells. However, the magnitude and number of changes in gene expression shown by the microarray is lower than was anticipated; for instance Milward et al., (2007) noted significantly altered expression of upwards of 400 genes when examining the interactions between H400 cells and periodontal pathogens (Milward et al., 2007). While the response of H400 cells to TiO₂ NPs is likely to be far less inflammatory than the response to pathogenic bacteria, it seems surprising that the microarray data did not disclose higher magnitude fold changes in more genes. The possible reasons for this are discussed in Section 6.4.

6.3 Co-stimulation qPCR (Quantitative Real Time PCR)

6.3.1 *Co-stimulation qPCR - aims*

Sections 6.1 and 6.2 demonstrated minimal effects of exposure to TiO₂ NPs in isolation on the gene expression profile of H400 cells at 6 h or 24 h. In the clinical situation, there is likely to be a bacterial challenge present in the peri-implant tissues. It is therefore relevant to investigate whether previous exposure to, or coincident exposure to TiO₂ NPs alongside pathogenic bacteria may produce an altered cellular response to a purely pathogenic stimulation. This was examined using qPCR (Section 6.3.2).

6.3.2 *Co-stimulation qPCR - methods*

H400 cells were cultured in 6-well plates as described in Section 2.2.2. Once cells were judged to be just sub-confluent by light microscopy, samples were exposure to bacteria (heat killed *FN* or *Pg*, see Section 2.9.5) with or without TiO₂ NPs as a modifier (Table 6.4)

Sample	TiO₂ NP exposure	Bacterial exposure
Control	None	none
TiO₂ 1 h	100 ppm 1 h	none
TiO₂ 24 h	100 ppm 24 h	none
FN 1 h	None	FN (MOI 100:1) for 1 h
TiFN 1 h	100 ppm 1 h coincident with bacteria	FN (MOI 100:1) for 1 h
Ti 24 h FN 1 h	100pm 24 h pre-treatment prior to bacteria	FN (MOI 100:1) for 1 h
PG 1 h	None	PG (25:1) for 1 h
TiPG 1h	100 ppm 1 h coincident with bacteria	PG (25:1) for 1 h
Ti 24h PG 1h	100pm 24 h pre-treatment prior to bacteria	PG (25:1) for 1 h

Table 6.4 – H400 plating conditions prior to qPCR

Following exposures (or control conditions), samples were washed three times using warmed PBS to remove bacteria and TiO₂ NPs. Subsequently samples were trypsinised and prepared for RNA extraction (Section 2.5.1). Following RNA extraction, cDNA was synthesised using the protocol described in Section 2.5.4. qPCR was performed as detailed in Section 2.5.7.

6.3.3 Co-stimulation qPCR - results

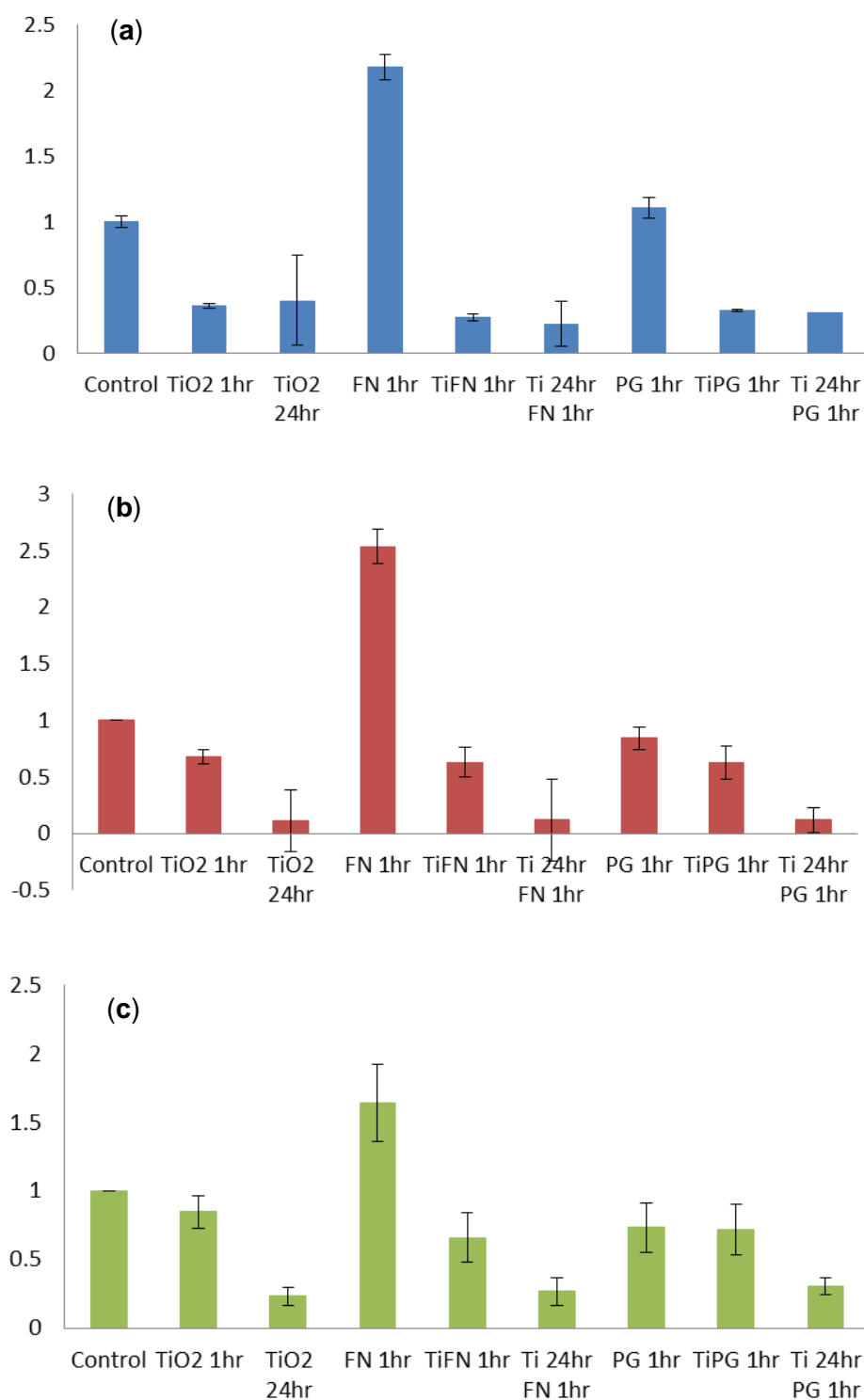


Figure 6.8 – Histograms showing ID1 (a), ID2 (b) and ID3 (c) expression using qPCR of H400 samples (n=4, mean data and SD shown). Graphs show a reduction in ID 1, 2 and 3 expression following TiO₂ NP treatment, as seen in the microarray data.

6.3.4 Co-stimulation qPCR - discussion

Co-stimulation qPCR showed that the addition or pre-treatment of H400 cells with TiO₂ in conjunction with bacteria significantly changes the expression of ID genes when compared with stimulation with bacteria alone. This suggests that TiO₂ has the potential to act as a modifier to H400 responses to bacteria. In ID1, 2 and 3 the expression of the gene is reduced markedly under conditions where cells were exposed to TiO₂ prior to exposure to bacteria as well as, to a lesser degree, when the cells were stimulated by bacteria and TiO₂ concurrently. Published work on the possible link between TiO₂ and the ID genes is scant, however Lee et al., highlighted that ID1 expression “attenuates the degree of TiO₂ induced cytotoxicity in lung cells” (Lee et al., 2009), a statement which may also be true for oral epithelial cells.

6.4 Chapter conclusions

This chapter has demonstrated that a DNA microarray is a robust method of examining gene expression changes in H400 cells when exposed to TiO₂ NPs, as confirmed by both PCR and qPCR. The gene expression profile of H400 cells in response to TiO₂ NPs at 100ppm for 6 h and 24 h did not change as much as anticipated; there are a number of factors which may be important in explaining this finding:

- As shown in previous work, only a minority of cells will interact with TiO₂ NPs (see also Chapter 4). There will therefore be a “dilution” effect of cells showing potentially altered gene expression by other cells that may exhibit an unchanged gene expression profile due to the heterogeneous response of the cell population.
- TiO₂ may simply have a minimal effect on the gene expression of H400 cells at all time-points, or 6 h and 24 h may miss peaks in gene expression changes that occur at different time-points. 6 h and 24 h should however show intracellularisation as demonstrated by other microscopy methods (see chapter 4) and 24 h should show some effects on cell viability (see chapter 5).
- As reported in Chapter 4, H400 cells take up TiO₂ NP agglomerations by 6 h. There may be minimal changes occurring after this intracellularisation.

However, more genes show altered expression at 24 h, suggesting there may be further changes later on in the exposure time-course.

- There is some crossover in H400 gene expression changes at 6 h and 24 h, mainly in a family of genes important in cell differentiation and replication (ID genes).
- Primary cells appear to show a different expression pattern of ID genes compared with controls than H400 cells, therefore H400s may not offer an accurate model of epithelial gene expression in the context of interaction with TiO₂ NPs and examination by microarray.
- TiO₂ NPs appear to have the potential to act as a modifier in gene expression changes in H400 cells when responding to bacterial challenges.

The subsequent chapter will investigate cell to cell interactions involving epithelial cells in the presence and absence of TiO₂ NPs.

Chapter 7

**Effects of the presence of TiO₂ NPs on cell to cell
signalling processes**

Synopsis

In chapters 4 to 6, TiO₂ NPs were shown to interact with oral epithelial cells in culture, becoming intracellularised and leading to alterations in cell morphology. TiO₂ NP exposures had some effects on oral epithelial cell viability and led to changes in gene expression and potentially functional changes in response to pathogenic bacteria. The overall effects on the cell population in terms of viability were however limited.

It has been established that epithelial cells (including oral epithelium) play an important role in a number of cell-cell signalling pathways, particularly in the presence of a pathogenic challenge, producing signalling molecules to recruit other cell types and initiating and propagating an immune response (Yilmaz et al., 2003, Krisanaprakornkit et al., 2000, Milward et al., 2007). Many of the pathways by which oral epithelial cells interact with other cell types in response to a pathogenic challenge have been well characterised. Based on preliminary findings in previous chapters it was hypothesised that oral epithelial cells exposed to TiO₂ NPs may exhibit perturbed responses to known stimuli. The effect of TiO₂ NP exposures on the NFκB intracellular signalling pathway was previously investigated and a potential reduction in NFκB activation was demonstrated with increasing concentrations of TiO₂ NPs when co-stimulated with a bacterial pathogen. Following on from this observation, this chapter investigates whether TiO₂ NPs can also impact upon extracellular signalling involved in epithelial cell responses, including ROS production as a downstream consequence, cytokine expression and interactions with polymorphonuclear leukocytes (neutrophils) cells.

7.1 Cytokine release from H400 cells as detected using ELISAs

ELISAs offer a sensitive method of detecting and quantifying cytokine release from cells in culture. A broad panel of ELISAs for the detection of relevant proteins of acquired immune responses and also inflammatory processes were chosen to investigate cytokine release from H400 cells in culture in the presence and absence of TiO₂ NPs. Specific antibodies are attached to a surface to bind a target antigen. An enzyme is then linked to the antibody-antigen complex and a colour changing reporter enzyme substrate is added. The degree of subsequent colour change reflects the

concentration of the target antigen within the sample. In this work a sandwich ELISA was employed. In a sandwich ELISA, a specific antibody is bound to the substrate surface and any non-specific binding sites are blocked. The sample and any target antigen contained within will bind to the antibody on the surface. The specific enzyme linked antibody is then applied prior to the reporter substrate. The term “sandwich” is used as the target is between the antibody on the ELISA plate surface and the enzyme-linked antibody. The sandwich ELISA system is described further in Section 2.10.

ELISAs (IL8 (CXCL8)), Interferon-gamma (IFN- γ), Interleukin 1-Beta (IL-1 β), TNF α , and Interleukin-6 (IL-6)) were performed using DuoSet ELISA kits (R&D systems, Bio-technie, UK) according to the manufacturer’s instructions. Each ELISA was tested against standards of known concentrations to obtain a standard curve. This exercise was repeated in both the presence and absence of TiO₂ NPs due to concerns regarding potential interactions between TiO₂ NPs and the cytokine or antibody (see also Section 3.6.5).

Previously, where NPs have been shown to induce or fail to induce cytokine expression measured by ELISAs, it is important to recognise that the assay result can be affected by any binding between the NPs and the ELISA target or components of the assay system (Irshad et al., 2013). To date, only a small number of studies have acknowledged this issue. The presence of NPs has been shown to disrupt ELISAs with carbon NPs shown to adsorb to IL8 (Monteiro-Riviere and Inman, 2006, Hsiao and Huang, 2011) and TiO₂ NPs to adsorb to IL-6 (Veranth et al., 2007).

Investigators have reported that TiO₂ NP exposure will stimulate the release of IL8 (as identified by use of ELISAs) from a variety of cell types including human endothelial cells (Peters et al., 2004) and human lung epithelial cells (Wilson et al., 2012). However, no consideration was given to the potential interaction between IL8 and TiO₂ NPs themselves. IL8 (CXCL8) is a pro-inflammatory chemokine and potent chemoattractant produced by a variety of cell types, specifically targeting neutrophils (Bickel, 1993). IL8 is key in the initiation and propagation of the acute inflammatory response. Previous studies using ELISA techniques to identify IL8 release in

experiments where TiO₂ NPs are present have dismissed or ignored the potential for IL8-TiO₂ NP interactions (Singh et al., 2007, Peters et al., 2004).

7.1.1 *ELISA standard curves in the presence and absence of TiO₂ NPs - methods*

The cytokine panel selected consisted of IL8, IFN- γ , IL-1 β , TNF α and IL-6. The rationale for choosing these cytokines was that they have previously been found at elevated levels in fluid exudate from inflamed tissue surrounding percutaneous Ti implants when compared with clinically healthy peri-implant tissues by our group (Grant et al., 2010b). Inflammatory responses from the host immune system are essential in maintaining peri-implant health and indeed pro-inflammatory cytokines are present in fluid exudate collected from around failed Ti implants (Grant et al., 2010b). However, disordered or excessive host immune responses have been shown to produce tissue damage in periodontitis (Matthews et al., 2007), a similar clinical condition to peri-implantitis.

For each cytokine, manufacturer supplied standards were prepared in reagent diluent with 100ppm TiO₂ NP supplementation, then incubated for 1 h and centrifuged at 150 x 100 rpm for 5 min before making up standards in serial dilutions. Data were gathered as detailed in Section 2.10.1.

7.1.2 ELISA standard curves in the presence and absence of TiO_2 NPs – results (Figure 7.1)

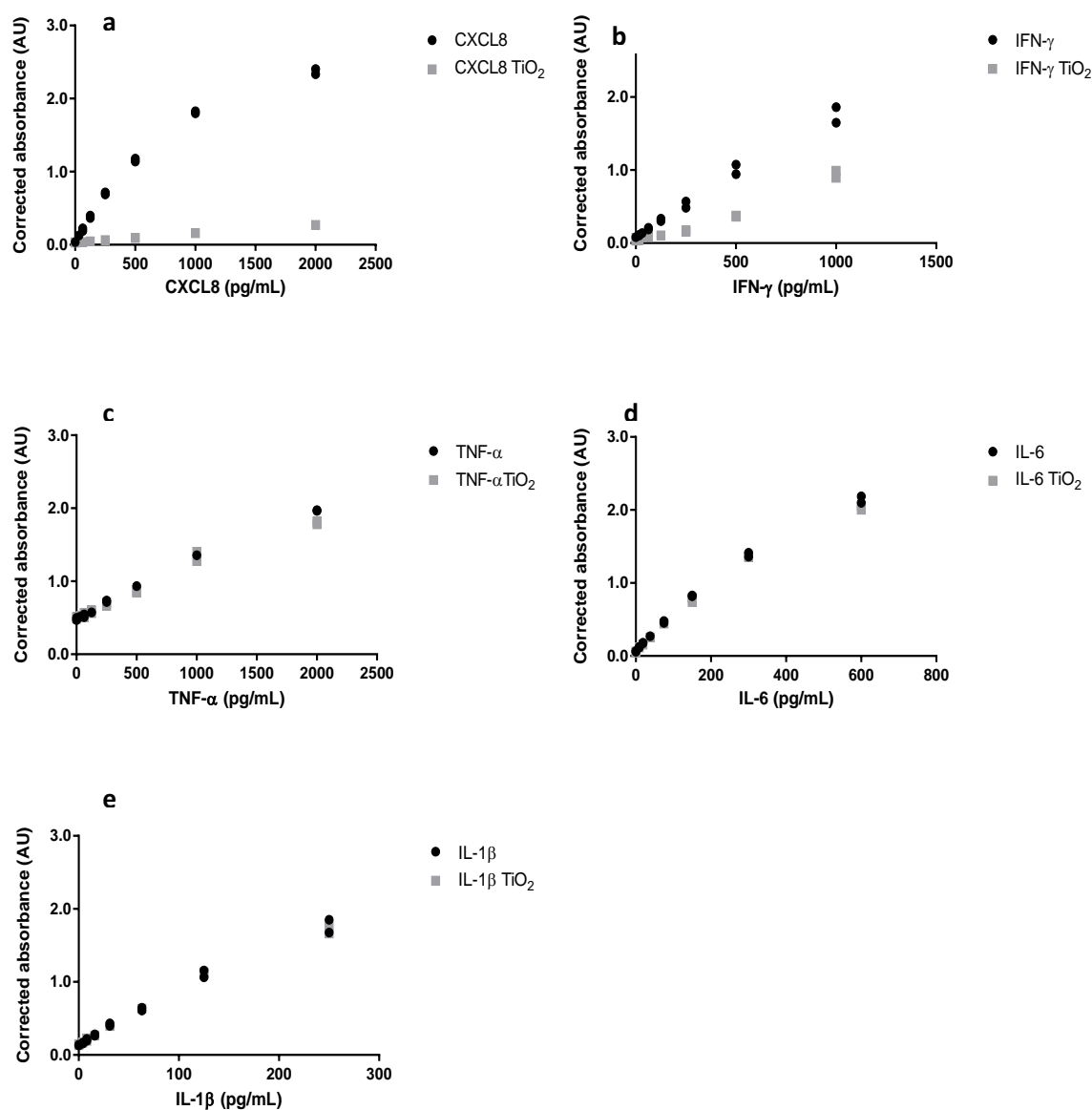


Fig. 7.1 (a-e) – A plot of cytokine concentration (replicate points shown) against absorbance (arbitrary units, AU) derived from ELISA ($n=2$) for the serially diluted specific standard and for the serially diluted specific standard following exposure to 100ppm TiO_2 NPs for 24 h and centrifugation to remove insoluble contents.

7.1.3 ELISA standard curves in the presence and absence of TiO_2 NPs – conclusions

In the absence of TiO_2 NPs, the standard curves show a linear (IFN- γ , TNF α , IL-1 β) and a log-linear (IL8, IL-6) relationship showing the concentrations of target cytokine. IL8 and IFN- γ exhibited a reduction in reading in the presence of TiO_2 NPs (discussed further in Section 7.2).

7.1.4 *ELISAs performed on supernatants from H400 cells - aims*

The aim of this study was to establish the nature of inflammatory cytokine production from H400 cells stimulated by TiO₂ NPs, pathogenic bacteria, and their combination. It has been established that TiO₂ NPs may be pro-inflammatory as reported previously in lung epithelial cells (Singh et al., 2007). The same behaviour could be elicited from H400 cells, and the peri-implant situation involves a pathogenic bacterial challenge to which epithelial cells will respond. Exposure either previously or concurrently to TiO₂ NPs has the potential to modify any oral epithelial responses to pathogenic bacteria.

7.1.5 *ELISAs performed on supernatants from H400 cells - methods*

ELISA kits were used as per the manufacturer's instructions. Supernatants were prepared using 25 cm² flasks to culture H400 cells to sub-confluence as in Section 2.2.2 (where applicable) then treated as follows:

Cell free control:	Cell culture medium only
H400 control:	H400 cells cultured in standard medium
H400 plus TiO ₂ :	H400 cells cultured in standard medium then exposed to TiO ₂ 100ppm for 24 h
Cell free FN:	Heat killed FN at an equivalent MOI of 100:1 (determined by previous work by a colleague)
H400 plus FN:	H400 cells cultured in standard medium then exposed to heat killed FN at an equivalent MOI of 100:1 for 4 h
H400 plus TiO ₂ pre-treatment then FN	H400 cells cultured in standard medium then exposed to TiO ₂ 100ppm for 24 h then heat killed FN at an equivalent MOI of 100:1 for 4 h
H400 plus TiO ₂ and FN:	H400 cells cultured in standard medium then exposed simultaneously to TiO ₂ 100ppm and heat killed FN at an equivalent MOI of 100:1 for 4 h
Cell free PG:	Heat killed PG at an equivalent MOI of 25:1 (Grant et al., 2010a)
H400 plus PG:	H400 cells cultured in standard medium then exposed to heat killed PG at an equivalent MOI of 25:1 for 4 h
H400 plus TiO ₂ pre-treatment then PG:	H400 cells cultured in standard medium then exposed to TiO ₂ 100ppm for 24 h then heat killed PG at an equivalent MOI of 25:1 for 4 h
H400 plus TiO ₂ and PG:	H400 cells cultured in standard medium then exposed simultaneously to TiO ₂ 100ppm and heat killed PG at an equivalent MOI of 25:1 for 4 h

Table 7.1 – ELISA sample preparation

All supernatants were aseptically aspirated from triplicate flasks, pooled and centrifuged at 15000 rpm for 5 min in order to remove TiO₂ NPs as far as practically possible. FN = *Fusobacterium nucleatum*, PG = *Porphyromonas gingivalis* (see Section 2.9.5). Supernatants were stored at 4 ± 1°C and allowed to equilibrate to room temperature before use.

7.1.6 ELISAs performed on supernatants from H400 cells - results

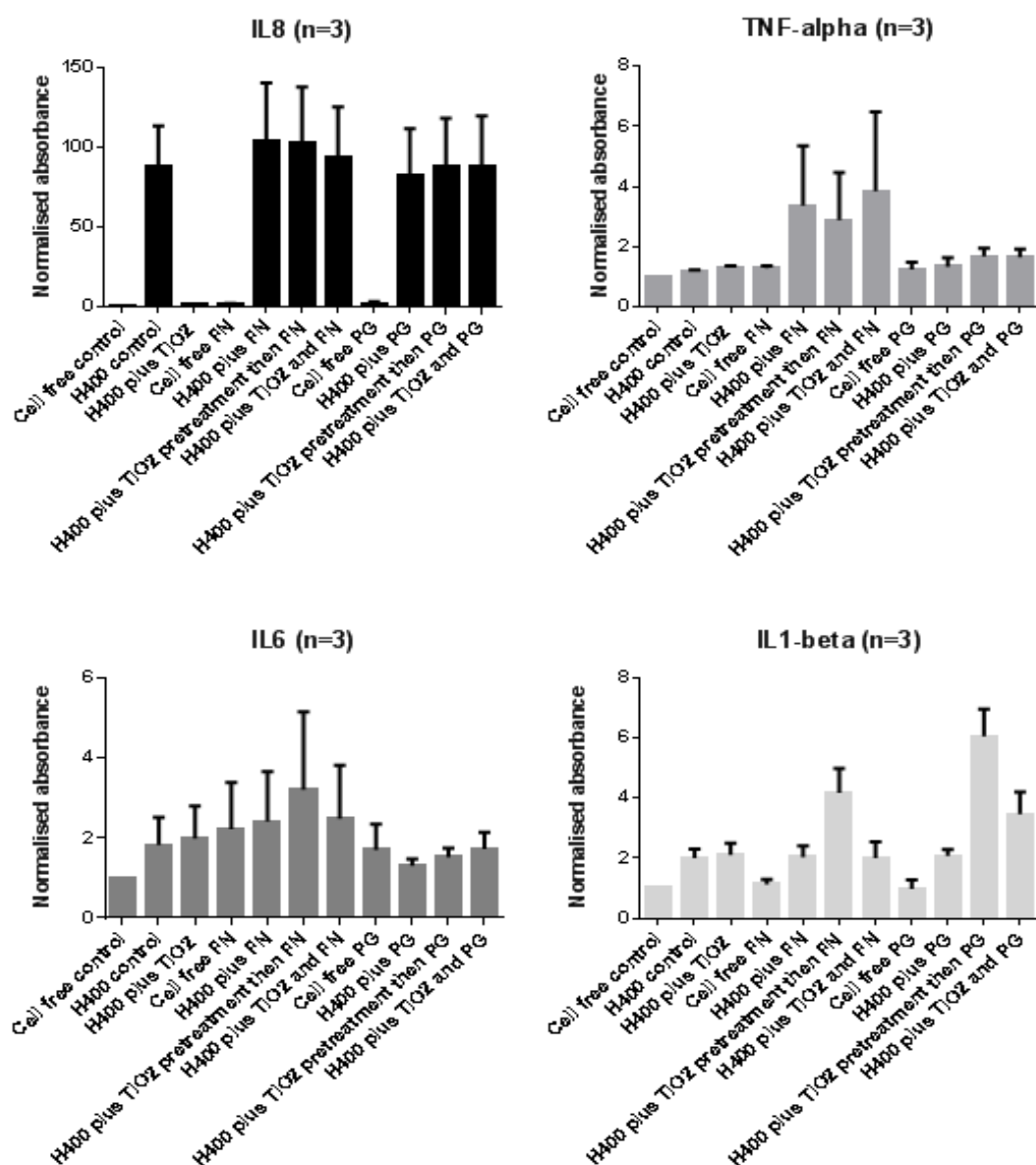


Figure 7.2 – ELISA data showing absorbances representing cytokine concentration in supernatants as detailed in Section 7.1.5. Results from IL8 and IFN- γ were accounted for by interference of TiO₂ NPs in the ELISA. Data from IL8 ELISA is shown for interest purposes only.

Condition	IL8	TNF α	IFN- γ	IL-6	IL-1 β
H400 control	+++	ns	ns	ns	+++
H400 plus TiO ₂	ns	ns	ns	ns	+++
Cell free FN	ns	ns	ns	ns	ns
H400 + FN	+++	ns	ns	ns	+++
H400+TiO ₂ then FN	+++	ns	ns	ns	+++
H400 +TiO ₂ /FN	+++	ns	ns	ns	ns
Cell free PG	ns	ns	ns	ns	ns
H400 + PG	+++	ns	ns	ns	+++
H400+TiO ₂ then PG	+++	ns	ns	ns	+++
H400 +TiO ₂ /PG	+++	ns	ns	ns	+++

Table 7.2 – table of ELISA data shown in Figure 7.2 summarised. +++ = significant elevation, ns = non-significant difference compared with cell free control (two tailed t-test assuming equal variances, $p < 0.05$)

Figure 7.2 shows cytokines produced by H400 cells in response to treatment with relevant bacteria and / or TiO₂ NPs. The results for IL8 are, as previously mentioned, shown for interest rather than being taken as accurate due to the potential interaction between TiO₂ NPs and IL8. TNF α was elevated significantly when FN was used as a stimulus either with or without TiO₂ NPs when compared with all other conditions. This agrees with published data that FN induces production of human beta defensin 2 (hBD-2) in oral epithelial cells via the production of TNF α (Krisanaprakornkit et al., 2000). Small variations are seen in the expressions of IL6 and IL1- β , however the patterns appear inconsistent and the magnitude of changes is minor.

7.1.7 *ELISAs performed on supernatants from H400 cells - conclusions*

An important observation was the interaction between IL8 (and to a lesser extent IFN- γ) and TiO₂ NPs. The magnitude of expression of IL8 is large even as a background signal from H400 (as found by other researchers within the institution) but this decreases to cell free levels when TiO₂ NPs were added.

7.2 Interaction between TiO₂ NPs and IL8 / IFN γ

The interaction between TiO₂ NPs and both IL8 and IFN- γ can be noted in Figure 7.1 where the detection of IL8 was depleted considerably after exposure to TiO₂. IFN- γ detection was similarly affected although to a lesser extent. Other cytokines were

unaffected, therefore it can be concluded that there is a possibly a specific interaction taking place between the TiO₂ NPs used and IL8 / IFN- γ . Due to the extent to which this occurs with IL8 and the fact that IL8 is such an important pro-inflammatory cytokine, an interaction with TiO₂ could have clinical implications.

To establish the likely nature of this interaction, a number of experiments were carried out which will be detailed in this Section. Binding between IL8 and TiO₂ NPs has been reported in the literature (Horie et al., 2013), but not fully investigated beyond concluding that there is an association. ELISA use has been shown in this study to be inappropriate in detecting IL8 in the presence of TiO₂ NPs, however this methodology has been used to quantify IL8 in the presence of TiO₂ by multiple authors (Singh et al., 2007, Wilson et al., 2012, Haleem-Smith et al., 2012).

7.2.1 *Interaction between TiO₂ NPs and IL8 –ELISA investigation method*

To investigate whether the interaction between TiO₂ NPs and IL8 is dependent upon the dose of TiO₂ used, IL8 detection ELISAs were run on standard samples exposed to differing concentrations of TiO₂ for 1 h at room temperature before centrifugation and serial dilution (see Section 2.1. for detailed ELISA methodology). NPs have a high surface free energy, therefore will adsorb biomolecules readily (<0.5 min) on contact with, for instance, biological fluids (Tenzer et al., 2013), therefore a 1 h incubation is more than adequate to allow an association to form. The resulting protein coating is known as the protein corona, and has shown to be reversible in part therefore allowing partial replacement of proteins already bound to the nanoparticle (Lundqvist et al., 2011). This means that the binding of IL8 and IFN γ within the protein corona surrounding TiO₂ NPs may be partially, but crucially is unlikely to be fully, reversible. It may also be possible that IL8 and IFN γ would replace other proteins in a protein corona.

To further test the specificity of IL8 adsorption to the TiO₂ NPs the NPs were pre-exposed to human serum to establish whether the avidity of IL8 to NP binding was affected by other proteins present in tissue fluids *in vivo*. Human serum was isolated from blood collected in a lithium-heparin containing 6 mL tube from a healthy volunteer with informed consent and ethical approval (number 10/H1208/48). Briefly,

the serum was isolated by incubating the tube at RT for 30 min then at 4 °C for 30 min. The tube was then centrifuged at 1000 rcf for 30 min at 4°C before aspirating the serum from the top of the tube. The serum was diluted 1 in 10 with sterile PBS to avoid saturating the ELISA plate with target. The resulting diluted serum was then used as a diluent for the high ELISA standard and exposed to TiO₂ of differing concentrations and centrifuged before dilution as reported previously. The serum samples were compared with standard reagent diluent for reference.

Interaction between TiO₂ NPs and IL8 -ELISA results

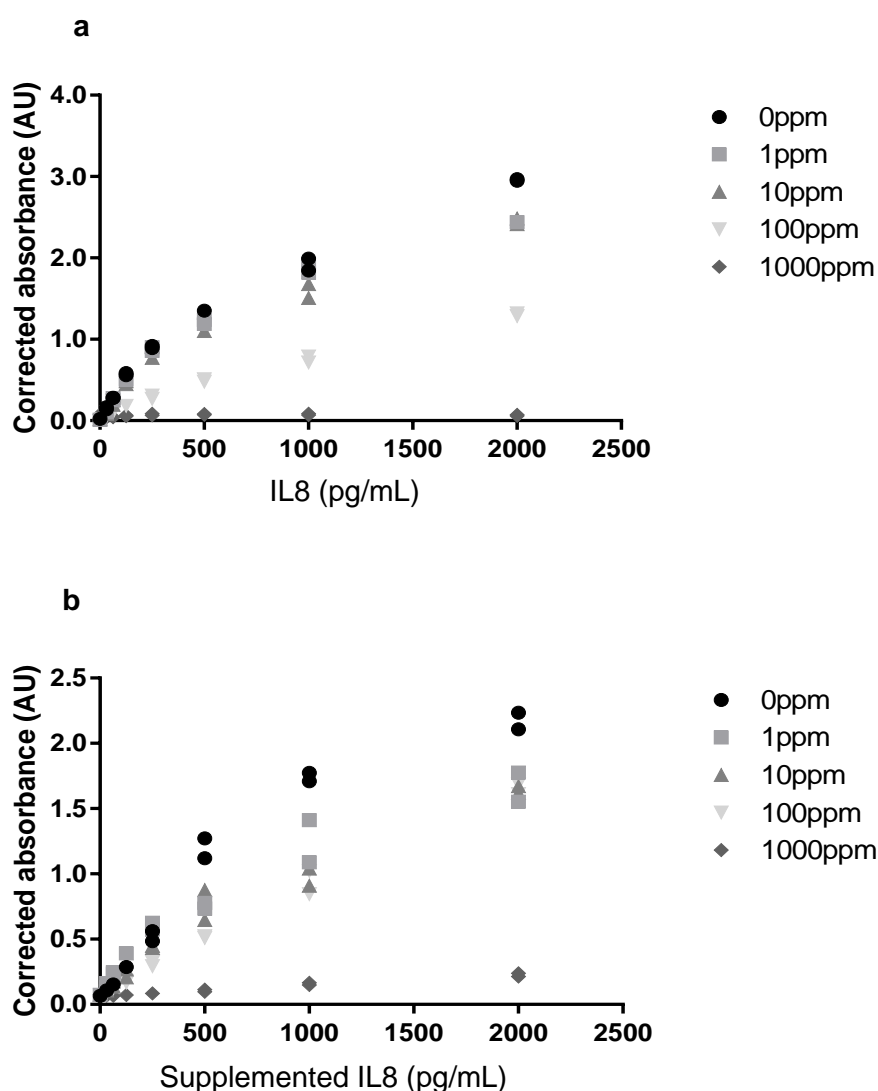


Figure 7.3 – A plot of IL8 concentration (mean and SEM) against absorbance (arbitrary units) derived from ELISA (n=3) for the IL8 standard (0 ppm) serially diluted in standard reagent diluent (**a**) and human serum (1 in 10) (**b**) and for the IL8 standard following exposure to 1, 10, 100 and 1000 ppm of TiO₂ NPs for 1 h then serially diluted in reagent diluent or human serum (1 in 10), respectively before centrifugation to remove insoluble contents. Replicate data points shown, n=2.

Interaction between TiO₂ NPs and IL8 – conclusions

The reported data shows a clear dose response, therefore concluding there is likely to be a specific binding between TiO₂ and IL8 taking place. This fits with the results shown by Horie et al., 2013, where smaller NPs were shown to bind more IL8 than larger particles, therefore implying the surface area of TiO₂ NPs available within a system will give its binding capacity for IL8. However, Horie et al., also reported that the protein corona of a NP is partially reversible, therefore in a physiological environment, where there will be a significantly more varied protein complex available, this binding between IL8 and TiO₂ NPs may either be inhibited initially or other proteins may partially replace IL8 within the corona of the NP (Horie et al., 2013).

A dose dependent reduction in signal occurred in the presence of a more complex protein field for both IL8 and IFN γ , confirming that there is a specific affinity to bind IL8 and IFN γ to TiO₂ NPS in preference to other proteins.

7.2.2 *Demonstration of IL8 / TiO₂ NP binding*

To further confirm whether IL8 binds to TiO₂ NPs a protein gel electrophoresis technique was employed. This technique will qualitatively demonstrate whether any IL8 was bound to TiO₂ particles once centrifuged, and if there was depletion of the IL8 signal in samples where the supernatant was tested post-centrifugation. Section 2.13 describes the methodology for this in detail, however in brief a panel of samples was prepared and summarised in Table 7.3.

No.	Preparation protocol	Sample used
1	IL8 in PBS 2000 pg/mL	
2a	IL8 2000 pg/mL plus TiO ₂ 1000 ppm in PBS incubated for 1 h at room temperature then centrifuged at 150 x 100 rpm for 5 min (Geneflow SciSPin Micro)	Supernatant
2b		TiO ₂ pellet washed in PBS and re-suspended
3a	TiO ₂ 1000 ppm in PBS incubated for 1hr at room temperature then centrifuged at 150 x 100 rpm for 5 min	Supernatant
3b		TiO ₂ pellet washed in PBS and re-suspended
4	IL8 added at 2000 pg/mL in 20% human serum	
5a	IL8 added at 2000 pg/mL in 20% human serum plus TiO ₂ 1000 ppm in PBS incubated for 1 h at room temperature then centrifuged at 150 x 100 rpm for 5 min	Supernatant
5b		TiO ₂ pellet washed in PBS and re-suspended

Table 7.3 – Protein gel sample preparation

Following the sample concentration as detailed in Section 2.13, protein gel electrophoresis was performed in order to identify the presence of IL8 in the samples.

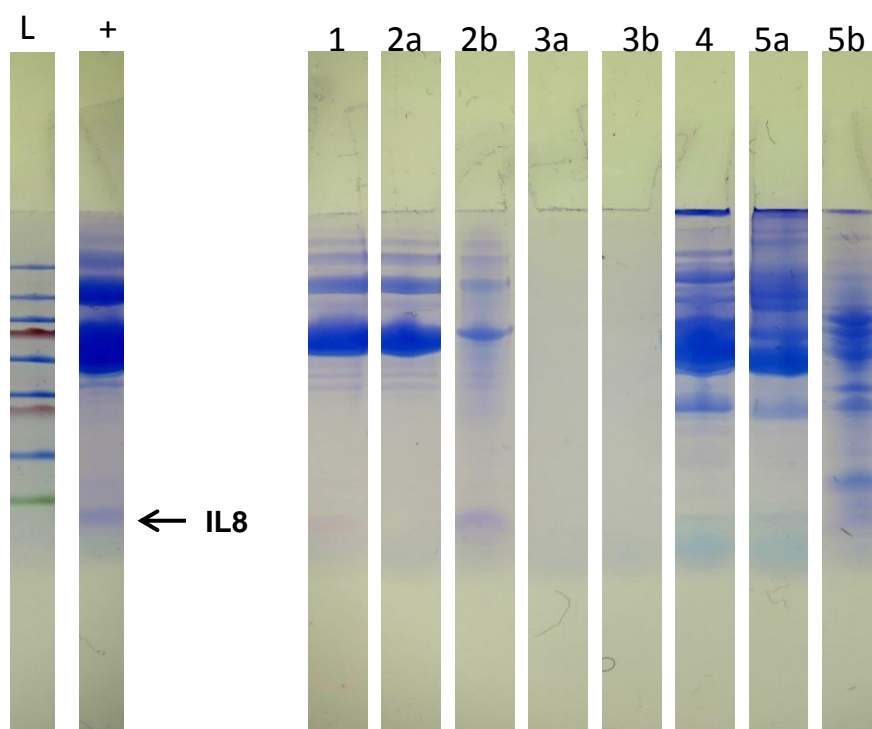


Figure 7.4 – Sections taken from an imperial Blue stained protein gel. 1= IL8 2000 pg/mL in PBS (high standard used on ELISA)

2a= Supernatant (SN) from IL8 2000 pg/mL in PBS plus 1000ppm TiO₂ incubated overnight then centrifuged out

2b=TiO₂ particles centrifuged out and washed in PBS from 2a

3a= SN from TiO₂ in PBS only prepared as above

3b= TiO₂ particles centrifuged out and washed in PBS from 3a

4= IL8 2000 pg/mL in 20% human serum, 80% PBS

5a= SN from IL8 2000 pg/mL in 20% human serum plus TiO₂ 1000ppm prepared as above

5b= TiO₂ particles centrifuged and washed in PBS from 5a

L= ladder

+ = Positive control = IL8 at 100 ng/mL

Samples showing the presence of IL8 (Figure 7.4) were the positive control, Lane 2b (where TiO₂ NPS exposed previously to IL8 were separated by centrifugation and washed in PBS before electrophoresis) and Lane 5b (where TiO₂ particles exposed previously to IL8 in 20% human serum were separated by centrifugation and washed in PBS before electrophoresis). The results support the ELISA data showing depletion of IL8 present in any supernatants where TiO₂ NPs were introduced and then removed by centrifugation. This strongly implies that the IL8 is bound to TiO₂ NPs and is removed

from the supernatant during centrifugation. The functional consequences of IL8 depletion by TiO₂ NPs were subsequently considered by studying the chemotaxis of human neutrophils.

7.2.3 *Chemotaxis assay as a functional measure of IL8 activity in the presence and absence of TiO₂ – aims and method*

One of the principal functions of IL8 is to act as a chemoattractant for peripheral blood neutrophils (PBNs or neutrophils). This chemoattractant capability can be visualised and quantified using an assay for neutrophil chemotaxis. The method is described in detail in Section 2.9.6, but in brief involves exposing freshly isolated PBNs to a gradient of substrate being tested, and tracking the movement of the PBNs. Movement towards the stimulus implies the substrate is a chemoattractant, and the speed and velocity (movement towards the stimulus) of cell movement can be used to generate a measure of the strength of the chemoattractant, known as the Chemotactic Index (CI) (Roberts et al., 2015).

Chemotaxis assays were run using freshly isolated PBNs from healthy volunteers and the substrates tested for their chemoattractant properties were as follows:

RPMI – negative control.

fMLP – a known strong chemoattractant 10 nm in 1% BSA PBS – positive control

IL8 – Interleukin 8 at a concentration of 200 ng/mL in 1% BSA PBS

IL8 supernatant – IL8 as above incubated with 100 ppm TiO₂ for 1 h then centrifuged at 1500 rpm for 5 min. The supernatant was aspirated and formed this sample.

TiO₂ – TiO₂ NPs (anatase <25nm, Sigma-Aldrich, UK) sonicated in water and added to 1% BSA PBS at a concentration of 100 ppm

TiO₂ spun and washed – TiO₂ pellet left from the preparation of IL8 supernatant sample washed twice in PBS and centrifuged as before then re-suspended at a concentration of approximately 100ppm in 1% BSA PBS.

For each PBN sample, a video of responses to each substrate was captured and analysed as described in Section 2.9.7. 15 cells per video were manually tracked and the co-ordinates used to generate data on their speed and directional movement towards the stimulus. Results were pooled (n=6). The second data set is from

chemotaxis assays investigating to what extent dose dependence plays a role in affecting the chemoattractant properties of IL8 (200ng / mL) when exposed to TiO₂ NPs in 1% BSA PBS at a concentration on 0-1000ppm. This was repeated using PBNs from different volunteers.

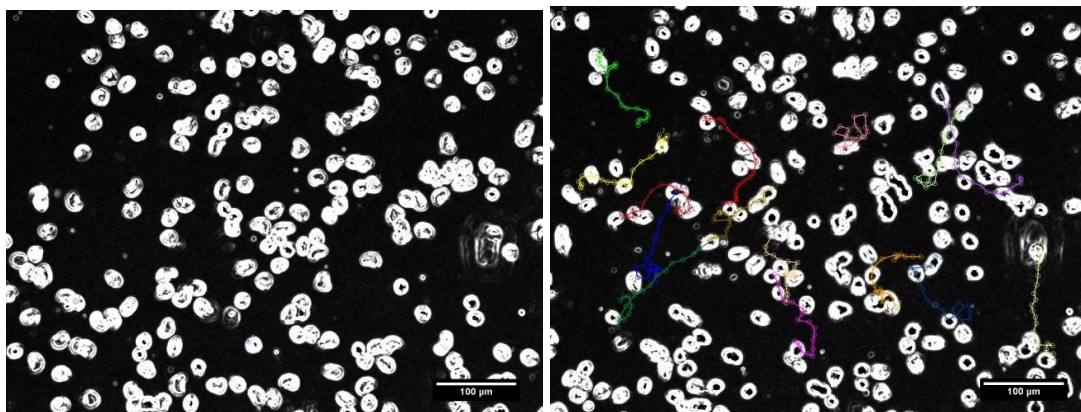


Figure 7.5 – examples of first (left) and last (right) frames of 40 frames of a chemotaxis video showing the coloured lines where a selection of randomly chosen cells were tracked. The coordinates of this movement were pooled and used to generate the subsequent dataset. 20 points were generated from each video.

7.2.4 Chemotaxis assay as a functional measure of IL8 activity in the presence and absence of TiO_2 – results

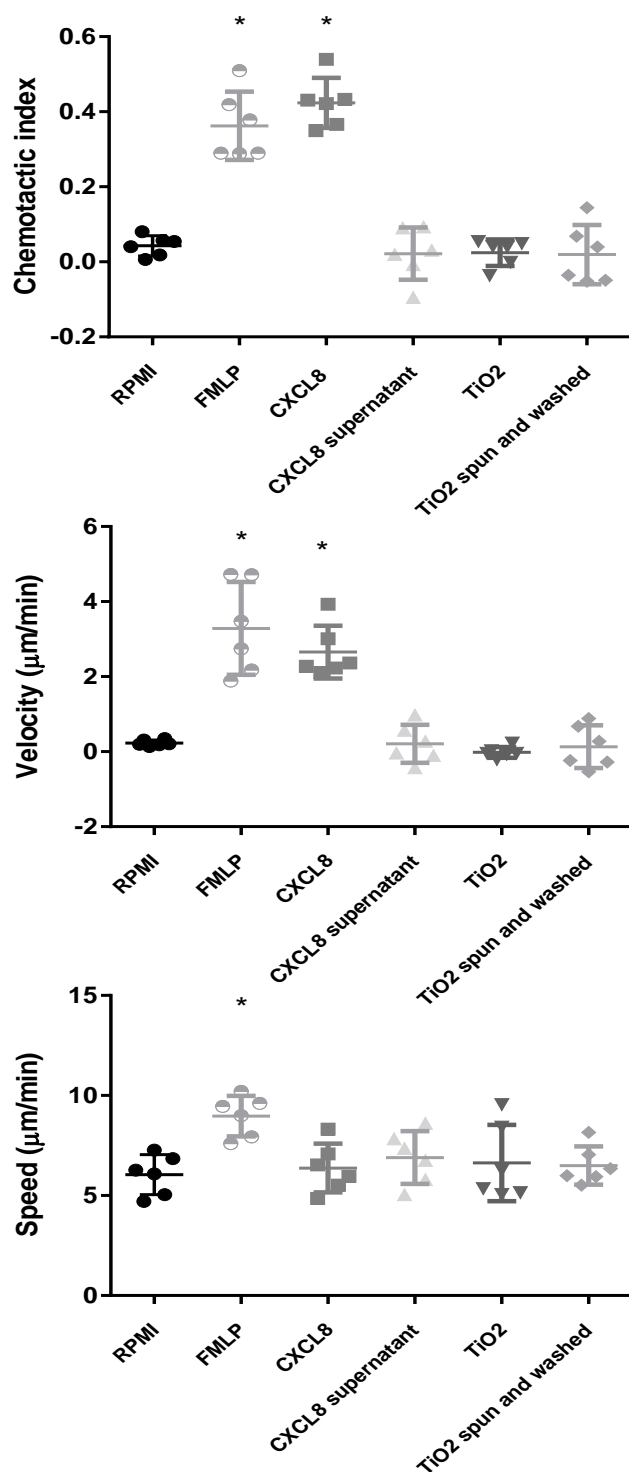


Figure 7.6 – Box-whisker plots showing data points plus mean and SD for Speed, Velocity and Chemotactic Index of PBNs ($n=6$ donors) exposed to the positive (FMLP) and negative (RPMI) control chemoattractant and to the experimental chemoattractants. * indicates significant differences ($\alpha=0.05$) from RPMI as determined using one-way ANOVA.

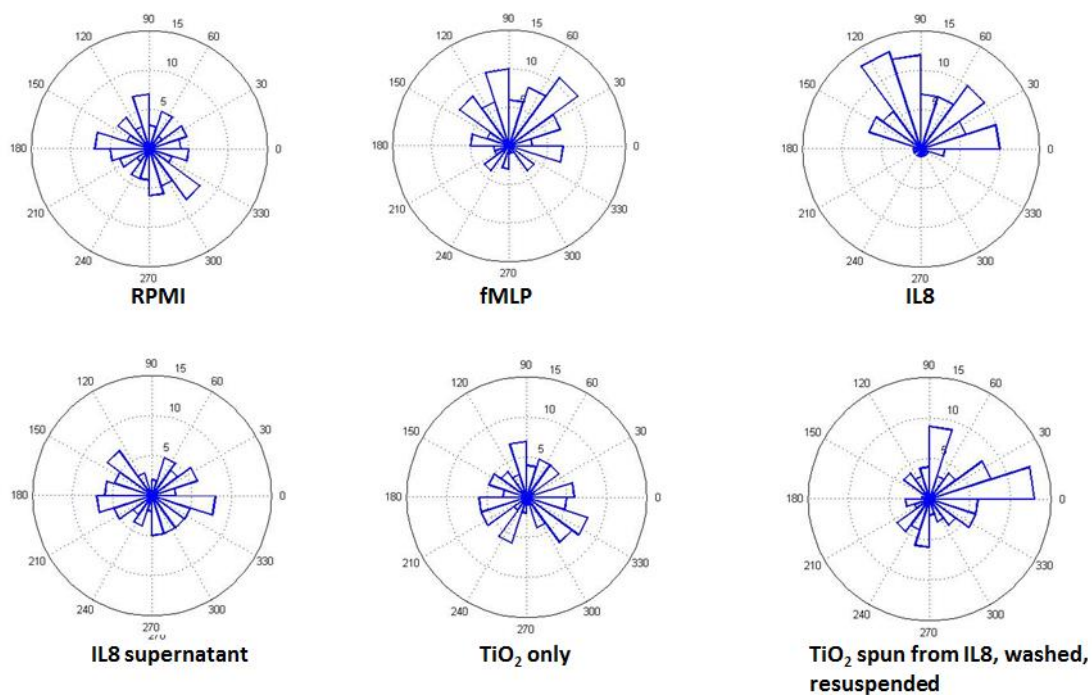


Figure 7.7 - Chemotaxis vector plots showing the proportion and directionality of movement of cells in each segment during the observation period. The larger the segment, the more cells moved preferentially in that direction. The inner numerical notation shows radially the distance moved and circumferential numerical notation the movement angle where the chemoattractant gradient is normal to 90 degrees. Clear directional movement towards the chemoattractant is observed for fMLP and IL8 by the more vertical direction of the segments.

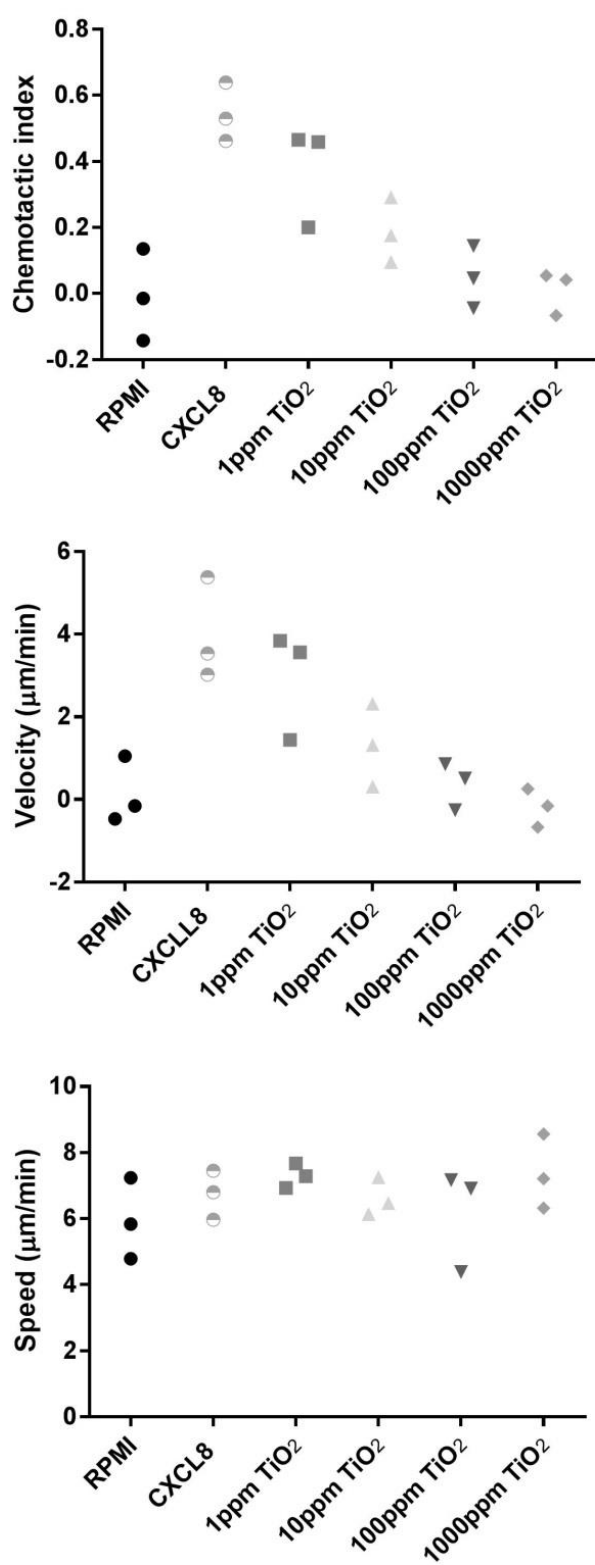


Figure 7.8 – Data plots (n=3 donors, all data shown) showing data points, mean and SD of data for Speed, Velocity and Chemotactic Index of neutrophils exposed to the positive (fMLP) and negative (RPMI) control chemoattractant and to the experimental chemoattractants (IL8 at initially 200 ng/mL exposed to 1, 10, 100, 1000 ppm of TiO₂ NPs for 1 h before centrifugation to remove the insoluble NPs.

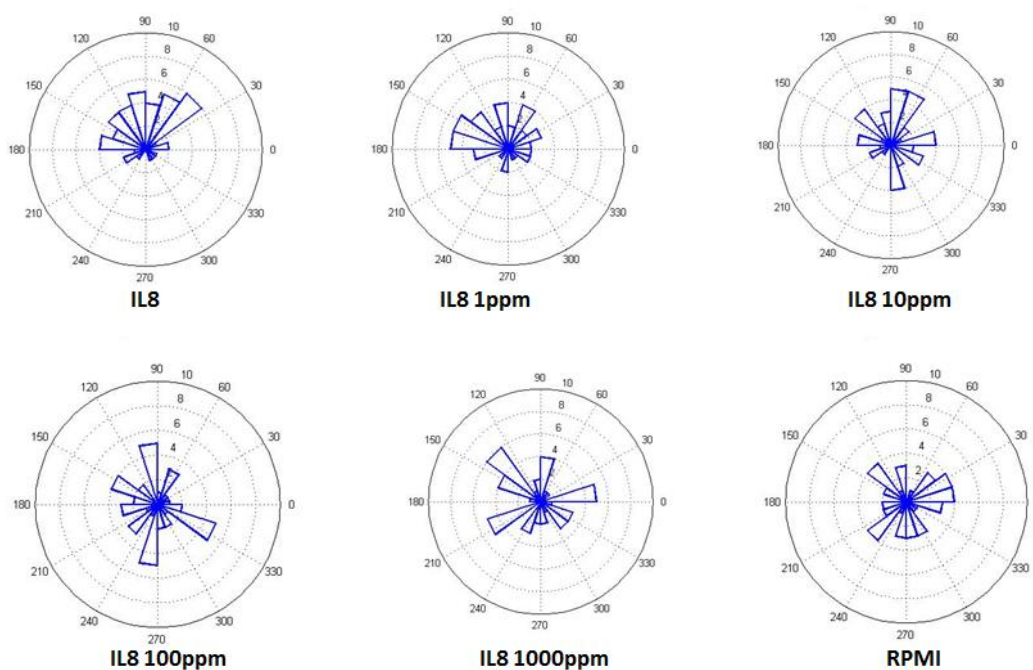


Figure 7.9- Chemotaxis vector plots showing the proportion and directionality of movement of cells in each segment during the observation period. The inner numerical notation shows radially the distance moved and circumferential numerical notation the movement angle where the chemoattractant gradient is normal to 90 degrees. Clear directional movement towards the chemoattractant is observed for fMLP and for IL8 however >1ppm TiO_2 exposure results in non-preferential directional movement.

7.2.5 Chemotaxis assay as a functional measure of IL8 activity in the presence and absence of TiO_2 – conclusion

Figures 7.6 and 7.7 demonstrate the altered chemoattractant properties of IL8 once exposed to TiO_2 NPs. Figures 7.8 and 7.9 indicate the loss of directional movement towards the supernatant remaining after the addition of TiO_2 NPs to IL8 and centrifugation to remove insoluble material, indicating further that the IL8 is bound to the NPs. Once the NPs were re-suspended they did not act as a chemoattractant, therefore indicating that the association with IL8 is somewhat robust. The chemotactic index and velocity shown in Figures 7.8 and 7.9 demonstrate a dose dependent reduction in movement of neutrophils towards the chemoattractant with increasing amounts of TiO_2 being present. Speed of neutrophils was not affected suggesting that the random movement of cells remained consistent but directional accuracy of this movement was lost. This is potentially a highly important finding, as *in vivo*, neutrophil recruitment into tissues is dependent upon directional movement in response to

chemoattractant gradients. If this ability is lost or perturbed, the immune response will be altered.

7.3 ROS production

Aside from chemotaxis, ROS release from neutrophils, once at the site of tissue injury or infection represents another important biological function. A variety of ROS exists including peroxides, superoxide and hydroxyl radicals. ROS are produced by cells as a natural by-product of oxygen metabolism but are produced in excess when cells are stressed (Battino et al., 1999). Cellular stress can be caused by a number of stimuli such as heat and ultraviolet light exposure (Cho et al., 2009), and exposure to chemical stimuli of pathogenic or other origins (Tschopp and Schroder, 2010). Excess of ROS can generate a state known as oxidative stress and can result in significant cellular damage, mutagenicity and tumorigenesis (Aruoma, 1998, Forsberg et al., 2001). However ROS are also known to act as an intracellular signalling system involved in cellular processes such as inflammation, cell cycle progression and apoptosis (Wang et al., 2010), so the balance and control of ROS production is critical for correct cellular function. Endogenous ROS are produced through multiple mechanisms including mitochondrial leakage and in particular within neutrophils via the NADPH⁺ oxidase pathway (Holmstrom and Finkel, 2014). Other cell types such as epithelial cells produce ROS at a much lower concentration to modulate certain inflammatory processes such as regulation of NFκB (Chapple, 1996, Chapple, 1997). ROS can also be generated from exogenous sources. In the context of oral epithelium exposures to tobacco smoke, drugs or pollutants are relevant.

Neutrophils constitute the majority of circulating white blood cells (WBCs). Neutrophils are often known as the “first responders” to sites of infection or tissue damage, and can be recruited by host- derived components such as chemokines or by bacterial products (Kobayashi et al., 2005). Neutrophils are recruited to the site of infection or injury by the generation of a chemoattractant gradient, where the highest concentration of a chemoattractant (e.g. a cytokine such as IL8) released by cells is in the vicinity of the injury. Chemoattractants attract neutrophils from the circulating blood to move to the site of injury via diffusion through tissues and cellular movement

known as chemotaxis (Bagorda and Parent, 2008). Once at a site of infection, neutrophils may phagocytose, kill and digest bacteria and fungi (Nauseef, 2007). Neutrophils are capable of producing an oxidative burst of ROS via the NADPH⁺ oxides which is important in phagocytosis and pathogen killing. Released ROS are damaging to pathogenic organisms, but can also cause bystander damage to the host tissues and cells. The mechanisms of damage by ROS include peroxidation of lipids, oxidation of proteins, damage to nucleic acids and activation of cell death pathways (Bergamini et al., 2004). ROS damage to host structures has been demonstrated in the context of acute lung injury, inflammatory conditions such as rheumatoid arthritis, and possibly more pertinently in periodontal disease (Battino et al., 1999, Moraes et al., 2006, Matthews et al., 2007, Wright et al., 2010, Grommes and Soehnlein, 2011). Therefore, ROS turnover and activation is a process which must be closely regulated in order to maintain protection from pathogenic organisms whilst limiting excess ROS damage to host tissues. It is therefore important to assess whether ROS production is altered or stimulated in response to signalling molecules which may be produced by H400 cells, a process which could be perturbed by the presence of TiO₂.

7.3.1 *ROS generation by neutrophils in response to stimulation by H400 supernatants - method*

Due to the close relationship both mechanistically and anatomically between the oral epithelium and neutrophil function in the context of periodontal and peri-implant disease, (Tribble and Lamont, 2010) the effects of supernatants from H400 cells cultured with and without TiO₂ NPs and periodontal pathogens on ROS production by neutrophil cells were investigated. Epithelial cells may produce cytokines when stimulated by TiO₂ NPs which could in turn cause neutrophils to produce ROS in response, and an interaction between TiO₂ NPs and epithelial cells could therefore influence the response of peripheral blood neutrophils to pathogens present in the peri-implant environment. This hypothesis was tested using the assay methods described in detail in Section 2.9.

In summary, fresh neutrophils were isolated from the venous blood of healthy volunteers. Luminol and Isoluminol were used to detect intracellular and extracellular ROS respectively. Wells containing neutrophils, luminol/isoluminol and RPMI were

placed in a 96-well plate reading luminometer to create a background reading. This methodology was validated by using known ROS production stimulants PMA (phorbol 12-myristate 13-acetate) and bacteria (see Section 2.9.5 for bacterial stimulus preparation).

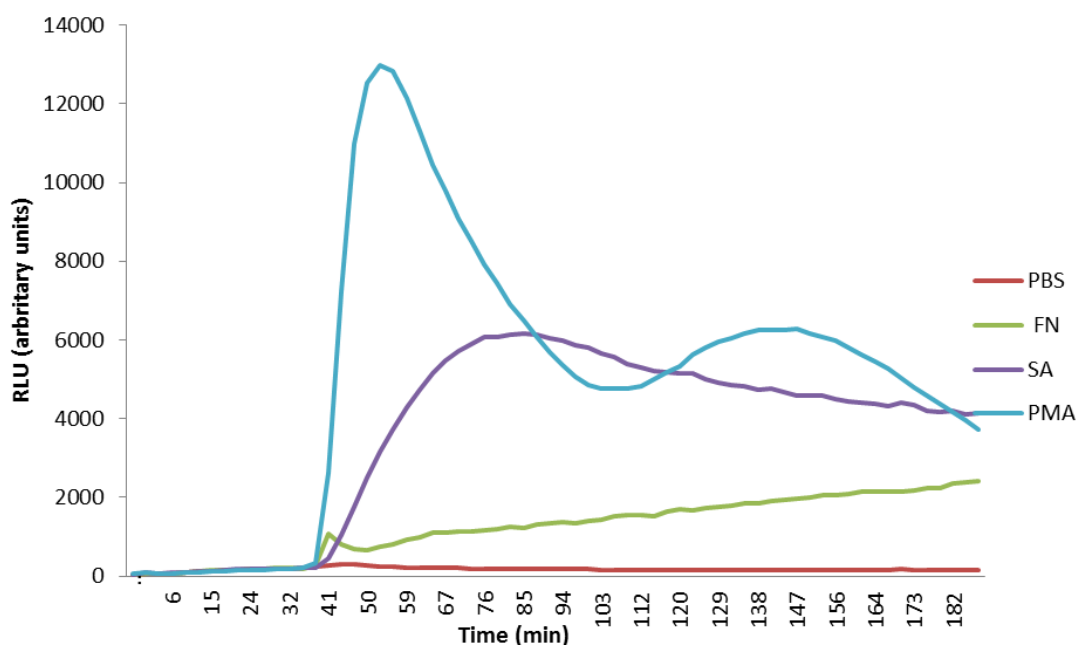


Figure 7.10 – Plot showing verification of use of Luminol and assay described in Section 2.9 to detect oxidative burst (n=3, line shown is mean data). FN stimulates to a lesser degree when compared with opsonised *S. aureus* and PMA due to the different receptor pathways by which ROS production is activated (*S. aureus* via FcYR and FN via TLRs 2 and 4). However, given that the amount of ROS generation in response to supernatants in the next experiment is likely to be low, FN was used as a positive control.

For preparation of supernatant samples used to stimulate neutrophils, H400 cells were cultured as detailed in Section 2.2.2. TiO₂ NPs were added to the culture medium at the concentrations and times indicated:

- H400 in cell culture medium (SN control)
- H400 cells in cell culture medium (SN 1000ppm 4h)
- H400 cells in cell culture medium (SN 10ppm 4h)
- Cell free cell culture medium (Media)
- Cell free PBS (negative control) (PBS)
- FN (MOI 150) (positive control) (FN)

7.3.2 *ROS generation by neutrophils in response to stimulation by H400 supernatants – results and conclusions*

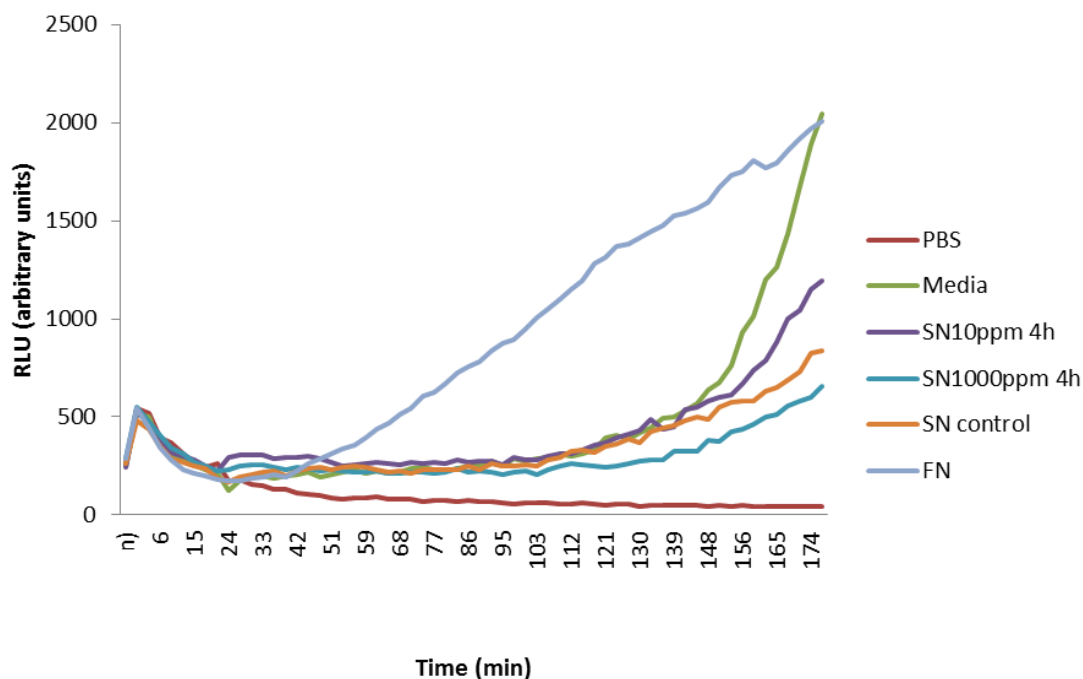


Figure 7.11 – ROS curve showing RLU generated by addition of supernatants as listed to wells containing neutrophils and luminol over time. Shows an unexpected rise in light production over time for some supernatants alongside the expected rise following addition of FN (n=1, typical pattern shown compared with repeated experiments).

No significant ROS production was observed in response to stimulation of neutrophils with supernatants from H400 culture. However, an increase in light output after approximately 100 min is indicative of interaction between the contents of cell culture medium and assay components. This may be due to the presence of proteins within the cell culture medium. To study the potential interactions between the ROS assay and cell culture media, cell free wells containing luminol in a range of cell culture media to which 0.5% H_2O_2 was added to produce a simulation ROS burst were subjected to the same assay as before.

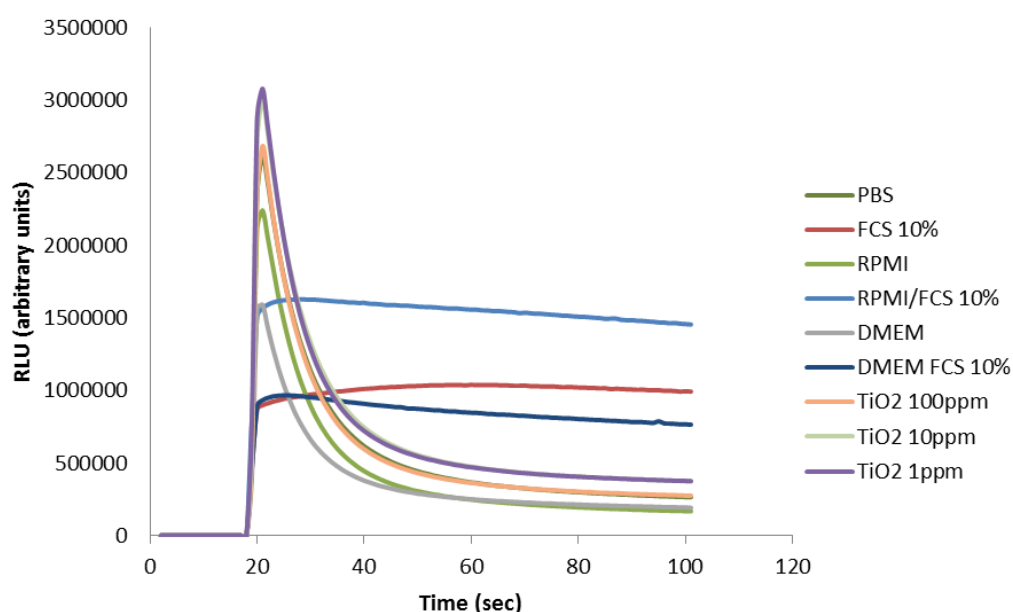


Figure 7.12 – Cell free simulated ROS burst generated by H_2O_2 addition to wells containing luminol and media as listed, TiO_2 was suspended in water. Suggests interaction of ROS occurring in media containing foetal calf serum (FCS) ($n=3$, mean data shown).

Wells containing no protein (absence of FCS) showed the expected pattern of a peak in light output following peroxide addition then a reduction to baseline levels as the H_2O_2 was exhausted. Wells containing FCS showed both a reduced ROS peak and then a constant signal which indicates quenching of luminol by the presence of protein, an interaction which has previously been described (Lundqvist et al., 1995). Protein free medium was therefore used as in the previously described method.

7.3.3 *H400 growth in RPMI (Roswell Park Memorial Institute) medium*

RPMI is a composition of medium traditionally used for certain types of cell culture (ion particular cells from lymphoid tissue). RPMI was piloted as a possible FCS free growth medium for H400 cells in order to obtain supernatants containing released cytokines, but no FCS to affect the ROS assay.

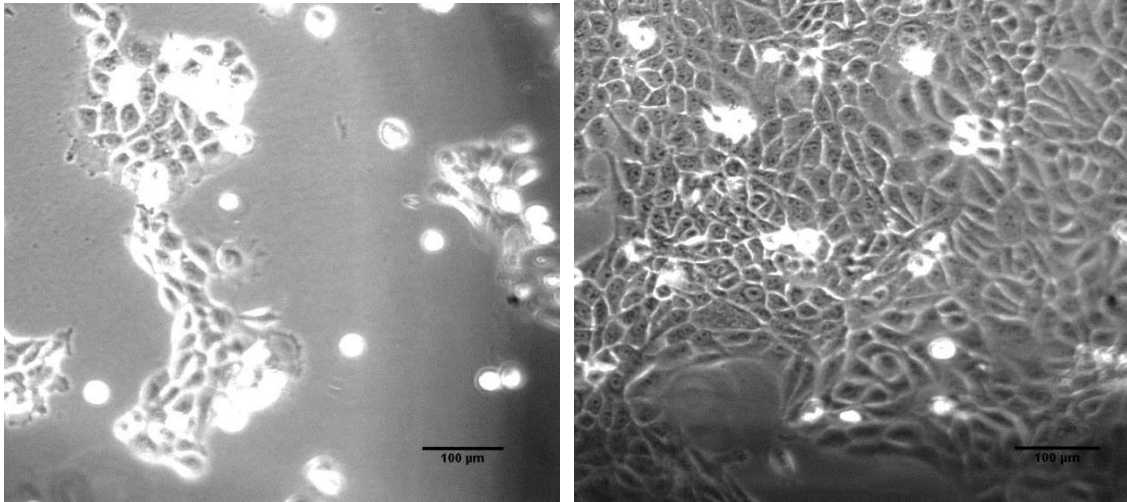


Figure 7.13 – A typical optical micrograph illustrating the growth of H400 cells at 24 h (left) and 48 h (right) post seeding at 2×10^5 cells in standard H400 cell culture medium. Images show the typical growth as observed and detailed in Chapter 3.

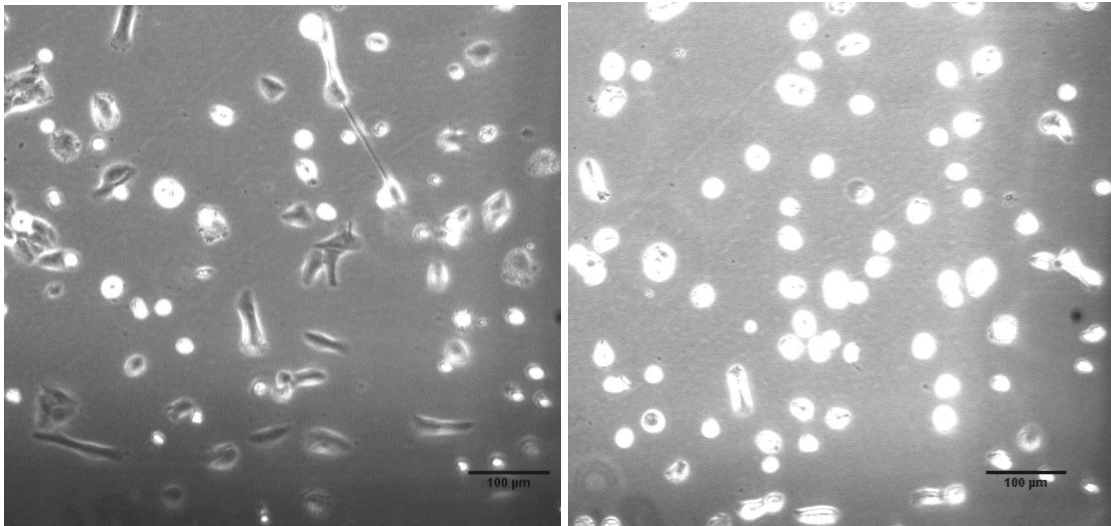


Figure 7.14 – A typical optical micrograph illustrating the growth of H400 cells at 24 h (left) and 48 h (right) post seeding at 2×10^5 cells in RPMI medium. Images show altered morphology, reduced adherence, potential loss of viability and limited growth.

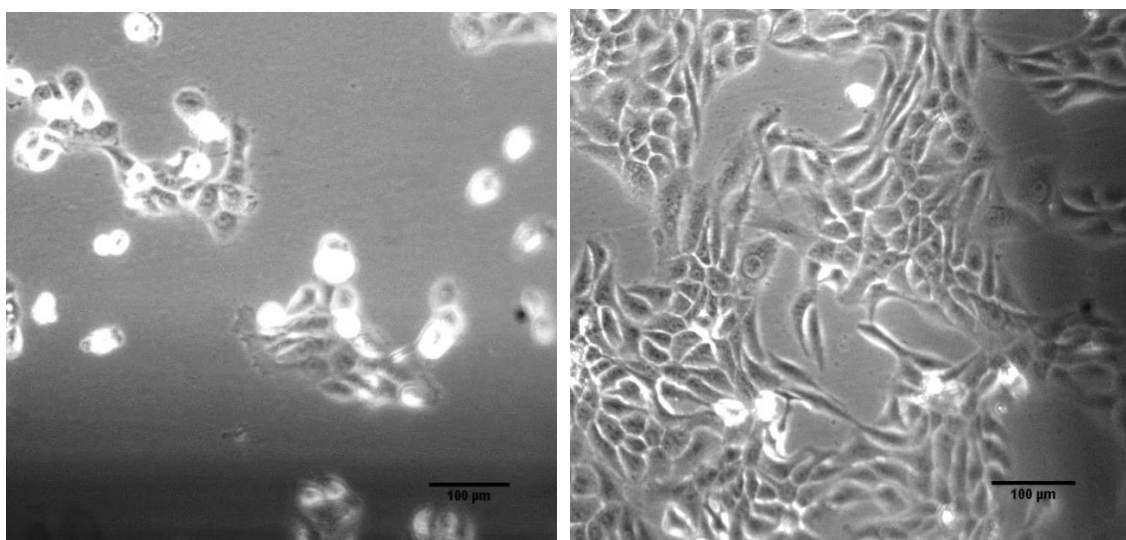


Figure 7.15 – A typical optical micrograph illustrating the growth of H400 cells at 24 h (left) and 48 h (right) post seeding at 2×10^5 cells initially in standard H400 cell culture medium, then exchanging medium post 24 h to RPMI, therefore 24 h post seeding image is immediately post medium exchange and 48 h post seeding image is 24 h post medium change to RPMI. Appears to show normal morphology and growth in cells.

Due to the visible growth inhibition and morphological changes seen in Figure 7.14 when culturing H400 cells without FCS supplementation, cells were cultured in DMEM medium supplemented with FCS according to previously described methods until sub confluent. This was then exchanged for RPMI containing the appropriate stimulus. The medium change may have caused an alteration in cellular responses, however cell growth and morphology remained normal as examined by light microscopy within the time frame stated.

7.3.4 *ROS assay using supernatants from H400 cell culture as priming agents to freshly isolated neutrophils*

Due to issues with interference in the assay from the addition of cell culture medium containing FCS, the following supernatants were prepared by aseptically aspirating cell culture medium from a 25 cm² flask and centrifuged at 15000 rpm for 5 min (Geneflow SciSPin Micro) to largely remove TiO₂ NPs. 10 µL of the centrifuged supernatant was then added to each well after a background reading was established (see Section 2.9 for full method for ROS generation assay). No stimulation of neutrophils was seen when using supernatants as stimulants (data not shown). The same supernatants were then used as priming agents (added 20 µL to wells for 20 min prior to stimulation with opsonised *Sa* (ops *Sa*)).

- Cells and medium - H400 in RPMI (SN control)
- As control plus 1000 ppm TiO₂ for 4 h (SN 1000ppm 4h)
- As control plus 10 ppm TiO₂ for 4 h (SN 10ppm 4h)
- Cell free RPMI(Media)
- Cell free PBS (negative control) (PBS)
- As control plus FN (MOI 150) (positive control) (FN).

7.3.5 ROS assay using supernatants from H400 cell culture as priming agents to freshly isolated neutrophils – results

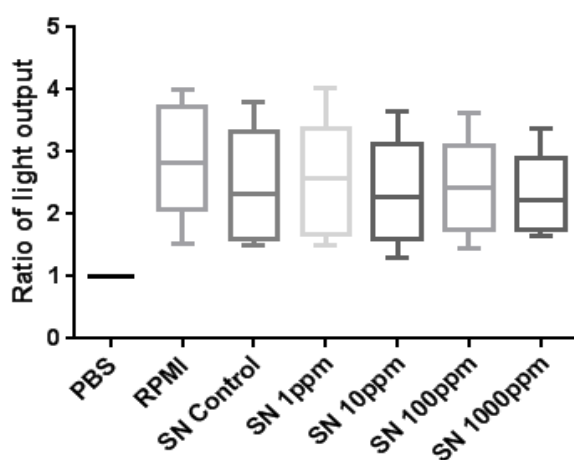


Figure 7.16 - Box and whisker plot (n=5) to show relative oxidative burst responses of neutrophils stimulated with ops *Sa* when primed with RPMI based supernatant from H400 cells normalised to PBS. No evidence of any priming effects of H400 supernatant on neutrophils compared with controls. Data are normalised to PBS

7.3.6 ROS assay using supernatants from H400 cell culture as priming agents to freshly isolated neutrophils – conclusions

The data presented in Figure 7.16 show that there is unlikely to be significant cytokine release from H400 cells when stimulated by TiO₂ NPs at concentrations up to 1000ppm to either subsequently influence neutrophil function. Therefore, it is unlikely that stimulation of H400 cells by TiO₂ NPs alone will cause significant effects on neutrophil function via the mechanism of stimulation of a ROS response either by stimulation of ROS production or priming of neutrophils.

7.3.7 *Effect of TiO₂ NPs on the priming action of IFN γ*

An interaction between TiO₂ NPs and IFN γ was observed in an ELISA assay. IFN γ is a known primer of neutrophils for enhanced activity upon secondary activation (Ellis and Beaman, 2004). Therefore, if the activity of IFN γ is inhibited in part by the presence of TiO₂ NPs to which it becomes bound, this may inhibit the enhancement of a neutrophil response within tissues. To assess if there is a functional impairment of IFN γ by binding to TiO₂, further ROS assays were performed (see Section 2.9). PBNs were primed with either:

- TiO₂ NPs alone (50 ppm)
- IFN γ alone (110 units)
- Both TiO₂ and IFN γ
- No primer

and were then stimulated with PMA or PBS (control) and oxidative burst measured.

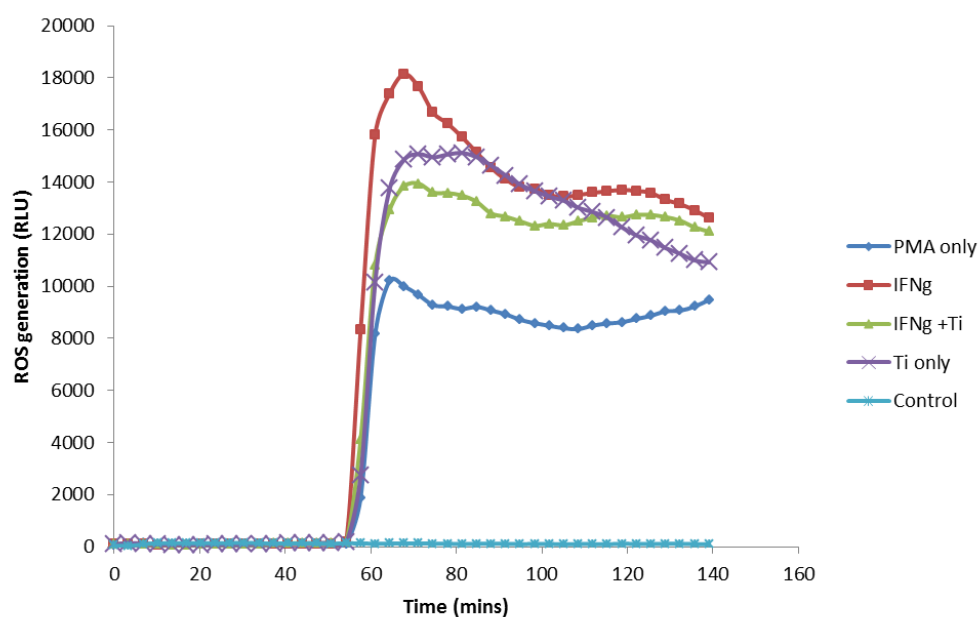


Figure 7.17 – ROS generation of neutrophils primed with 110 units of IFN γ +/- TiO₂ NPs (50ppm) then stimulated with PMA compared with control cells (no primer or stimulation) and cells primed with PBS then stimulated with PMA. Shows a reduction in the ROS peak when TiNPs are added to IFN γ , therefore showing a functional assay where a known priming cytokine is being affected by the presence of TiO₂ NPs in the system. n=1 shown here but representative data.

Figure 7.17 shows that the priming action of IFN γ is reduced upon the addition of TiO₂ NPs to levels below that of either TiO₂ or IFN γ alone. However, TiO₂ NPs alone show

some priming ability. This confirms the potential in an *in vivo* situation for the potential alteration of priming of neutrophils within tissues if Ti species are present and come into contact with certain chemokines.

7.4 Chapter conclusions

The results reported in this chapter show that TiO₂ NPs can preferentially bind IL8 and to a lesser extent IFN γ when compared with other cytokines. It can be concluded that the mechanism of binding between TiO₂ NPs and IL8 or IFN γ has some specificity. If IL8 is rendered inactive by binding to TiO₂ NPs then this could also have important implications for the recruitment of neutrophils at a site infection or injury. If structural cells are generating IL8 as a pro-inflammatory cytokine into tissues but this is inactivated by the presence of TiO₂ NPs, the inflammatory response may be compromised. IL8 also induces processes important in host defences such as phagocytosis, therefore this process could also be adversely affected by the presence of TiO₂ NPs within tissues. The impairment of IL8 as a chemoattractant by the addition of TiO₂ NPs is not a phenomenon widely discussed in the literature. TiO₂ NPs have been shown to cause increased inflammation resulting in increased chemotactic responses (Renwick et al., 2004) and also to impair the chemotactic and phagocytic ability of alveolar macrophages (Liu et al., 2010). While this study has concentrated on the interaction between TiO₂ NPs and IL8 due to the extent of the knockdown in detection of IL8 in the presence of TiO₂, it is important to note that IFN γ also appears to selectively bind to TiO₂ NPs to a lesser extent. The functions of IFN γ could also therefore be affected by the presence of TiO₂ NPs within tissues, further hampering host immune responses. It has been demonstrated that IFN γ is less efficient at priming PBN cells when in the presence of TiO₂ NPs and is further evidence of a potential immunomodulatory role in an extra-cellular context.

Chapter 8

Discussion, conclusions and further work

Introduction

8.1 Discussion

8.1.1 *Epithelial function and structure*

The primary function of epithelium is to provide a structural barrier to prevent injury to the underlying tissues from a variety of sources, including physical, chemical, and biological damage. The structure of epithelium is ideally suited to these roles as it consists of adherent (Wertz and Squier, 1991) cells with tight cell-cell junctions, therefore inhibiting intracellular ingress of pathogens or other noxious stimuli (Wertz and Squier, 1991). Furthermore, epithelium is stratified and layers are able to be shed constantly, allowing healing of, and mechanical protection for, underlying structures, (Nanci, 2013). Epithelial tissues vary in their complexity and structural functions throughout the body, dependent on their specific site; for instance, alveolar epithelial lining secretes mucous to the apical areas of constituent cells in order to entrap pathogens or irritants, while the epithelia which line the small intestine secrete digestive enzymes (Rieux et al., 2005).

The oral epithelium is specialised to provide multi-layered protection to associated tissues such as connective tissues, muscle and alveolar bone. Mechanically, the stratified squamous structure seen in masticatory epithelium is protective against the forces and potential injury generated during mastication (Squier and Kremer, 2001b). This epithelium is keratinised in areas of high masticatory load such as the dorsum of the tongue, hard palate and the attached gingivae (Nanci, 2013). Areas of the mouth which are required to be elastic in order to accommodate speech and mastication such as the unattached gingivae are non-keratinised (Wertz and Squier, 1991). The stratification of epithelium is more complex than simply comprising layers of identical cells, and exhibits distinct layers of cells with variations of differentiation between the surface layers and basal membrane (Squier and Kremer, 2001b, Nanci, 2013). In addition to mechanical and chemical protection due to its structure, the oral epithelium exhibits a diverse array of functions when exposed to bacterial challenge producing chemokines and cytokines relevant to initiating and promoting an inflammatory response (Philpott et al., 2001, Milward et al., 2007). In the peri-implant

situation, there are differences between the periodontal tissues and peri-implant tissues, which include:

- the absence of the complex sub-epithelial architecture adjacent to implanted devices than is seen in the periodontal tissues (Palmer, 1999, Lang et al., 2011);
- no periodontal ligament (PDL) is present adjacent to implanted devices, and osseointegration means, by definition, there should be direct contact between the implant surface and osseous cells (Palmer, 1999, Carlsson et al., 1986);
- Gingival fibres do not insert into the implanted Ti device as they would into the cementum of a periodontally healthy tooth, as in a peri-implant situation ligament fibres are predominantly circular, affording less resistance to pocket probing (Lang et al., 2011).

It has been argued that there is limited evidence to support the theory that structural differences in the tissues surrounding implants and teeth affects disease initiation and progression (Lang et al., 2011). However the same authors also report that the *“detailed molecular aspects of the (implant) adhesion of the connective tissue are not known”* (Lang et al., 2011). Given the complex disease processes which continue to be characterised in the periodontium, the statement that structural differences do not affect the host response in peri-implant tissues seems likely to be an oversimplification. Authors have reported a variety of findings when discussing the keratinisation of peri-implant tissues; however the literature has also identified considerable variation in the width and amount of keratinised epithelium present adjacent to implants (Chung et al., 2006).

8.1.2 *Implant derivatives within oral epithelial cells and associated tissues*

Derivatives of Ti implants, in multiple Ti speciations, have been identified within tissues adjacent to implanted devices which have been identified as insoluble particles in a variety of size, composition and cellular associations. Addison et al., described the scattering of Ti based species from the nano-scale up to micron scale located within epithelium excised from inflamed transmucosal Ti devices (Addison et al., 2012). Ti and Fe species were also identified using synchrotron X-ray spectroscopy in hard and soft

tissue samples taken from patients exhibiting clinical features of peri-implantitis (Fretwurst et al., 2016). Olmedo et al., described metallic particle distribution from cytology samples surrounding implants to be increased (2.44 ppb in sample sediment) with clinical signs of peri-implantitis when compared with clinically healthy Ti implants (0.88 ppb in sample sediment) and controls with no implants (0 ppb) (Olmedo et al., 2012). These pieces of evidence suggest that inflamed or infected mucosa surrounding Ti implants is more likely to contain higher amounts of Ti debris than do healthy tissues; is this a causative issue or reactive? It has been established that the corrosion behaviour of Ti is adversely affected by lower pH (Duffo et al., 1999), so there may be a cyclic effect of acidification and particle release.

The effect within oral peri-implant tissues of the presence of metallic species is an area in which there is a lack of published data. Much of the current literature involving the interactions between epithelium and small scale metal or metal-oxide particles is related to respiratory epithelium. A synopsis of this literature can be found in Chapter 1, but below are some key findings pertinent to TiO₂ NPs and interactions observed with human epithelial cells.

- TiO₂ NPs have been shown to be internalized by human alveolar epithelial cells, but in contrast to other metal oxide NPs such as copper oxides, they did not induce cell death (Moschini et al., 2013). These findings are entirely consistent with the results described within this thesis and are probably due to the chemical stability of TiO₂ compared with other metal oxides such as CuO (see Section 5.1).
- TiO₂ NPs were reported to produce a dose and time dependent decrease in cell viability in a lung cancer cell line (Lee et al., 2009). Other studies have also reported dose dependent cytotoxic effects of TiO₂ NPs on human alveolar epithelial cell lines involving both necrotic and apoptotic pathways (Kim et al., 2010) and at relatively low concentrations (30 ppm) have shown an increase in ROS production by alveolar cells at 4 h (Limbach et al., 2007). ROS were also found to be elevated by Singh et al., (Singh et al., 2007), in common with previously mentioned publications; however this paper also reports the use of ELISA detection of IL8 release post TiO₂ exposure in alveolar epithelium, a

finding which may not be valid in light of issues identified with the binding between IL8 and TiO₂ discussed within this thesis (see Section 7.2).

- Srivastava et al., have also highlighted the potential for TiO₂ NPs to be genotoxic in human lung cancer cell lines as well as apoptotic (Srivastava et al., 2013). However apoptotic states were not noted as being increased within H400 cell populations exposed to a variety of concentrations of TiO₂ NPs compared with controls when examined using HCS (Section 5.2.5).

It can therefore be surmised that many previous authors have found TiO₂ NPs to have significant cytotoxic potential to certain epithelial cells. The literature in the context of oral epithelial cells specifically is limited, however it seems unlikely from both the findings within this thesis and the clinical picture of epithelium surrounding implanted Ti devices that Ti implant derivatives will themselves significantly influence oral epithelial cell viability. However, it is more plausible that implant derived species within tissues surrounding implants may influence cell-cell signalling and the complex pathways which are known to take place during inflammation in response to bacterial challenge or mechanical injury.

The inflammatory exudate immediately adjacent to inflamed peri-implant tissues has been demonstrated to contain a range of inflammatory cytokines including IL8 and IFN- γ (Grant et al., 2010b). Therefore, the interactions between Ti implant derivatives and inflammatory mediators may be potentially clinically relevant within these tissues. IL8 and IFN- γ have been shown within this work to interact with TiO₂ NPs however only a narrow range of cytokines were explored. Due to the complex nature of cell to cell signalling and the wide variety of cytokines and chemokines produced *in vivo* both by and in response to epithelial cells, there is potential for wide ranging interactions with metal derived species located within tissues. Furthermore, the movement of implant derived particles once within tissues may take a variety of paths. Intracellularisation of TiO₂ NPs by oral epithelial cells has been shown within this thesis. What the fate of these intracellular particles is following cellular replication and eventual epithelial shedding is an area where further research is warranted. It could be that particles persist in daughter cells, and localised accumulation of metallic particles is an ongoing

process, or it may be that these particles are shed within cells once they are exfoliated from the epithelial surface.

Due to the process of liberation of Ti debris from implant surfaces being a likely consequence of MACC, physiochemical corrosion, and cellular-gated corrosion mechanisms (Cadosch et al., 2009a) it can be assumed that the entry of these products into tissues will be a continuous process, potentially leading to accumulation of metallic particles within the epithelium. Figures 1.3 and 1.4 in Section 1.4.3 demonstrate a sub-epithelial accumulation of Ti debris within tissue samples and relative accumulation may be considered due to epithelial shedding. Whether these particles would remain fixed in location within tissues or be transported, passively or actively, by different cell types, is an area where further enquiry is needed, as each outcome has implications for the longer term effects of the presence of these species within tissues.

8.1.3 *Effects of TiO₂ NPs on the viability of oral epithelial cells*

Conventional assays which measure ATPase activity, LDH levels and Caspase 3/7 activity as markers of epithelial cell viability all showed minimal changes in the presence of TiO₂ NPs of up to 1000 ppm. However, contrasting evidence from HCS methods suggested some reduced viability in both long term cultures (>24 h) and at increasing exposure concentrations.

It is difficult to clearly define the effects of TiO₂ NPs on the viability of oral epithelial cells given the differences in results presented in this work. Previously published literature suggests there is the potential for viability to be compromised in certain cell lines at higher NP exposure concentrations (Section 5.1). However, limited evidence for this was found here, with the exception of HCS results. Sytox green staining showed an increase in the number of non-viable cells and these non-viable cells appeared to be located adjacent to NP agglomeration; however, data quantification using the methods described in Section 5.1.5 is difficult, and using a well format to measure total light output with this assay as opposed to imaging individual cells may well lead to a loss of discrimination of the signal. HCS techniques overcome this problem by imaging a large number of cells and computationally generating an average from this complex 2D

image rather than arriving at an average at the point of detection. The use of HCS techniques as opposed to more simple conventional techniques when investigating the problem of a heterogeneous response to non-uniform exposures is discussed further in Section 8.1.5.

From a clinical perspective, the results showing that viability of oral epithelial cells is relatively unaffected by clinically relevant concentrations of TiO₂ NPs, is entirely consistent with the clinical presentation of the peri-implant tissues. Epithelium does not appear to slough away from implant sites with even advanced peri-implantitis lesions. Peri-implant mucositis, where inflammation is clearly present within the epithelial tissues surrounding an implant, is not consistently associated with deeper levels of tissue destruction affecting underlying bone (Lindhe and Meyle, 2008). A more complex picture of disease initiation and progression rather than simply disruption of the viability of epithelial cells in response to implant metal debris within tissues is much more plausible.

8.1.4 *Intracellularisation of TiO₂ NPs by epithelial cells*

Imaging the interactions between TiO₂ NPs and oral epithelial cells is challenging for a number of reasons. The size of the TiO₂ NPs used in the majority of experiments in this thesis was nominally <25 nm diameter, although agglomeration of NPs always occurs when in cell culture medium. This means that simple light microscopy even at relatively high magnifications can only be used to detect larger agglomerations of TiO₂ NPs.

Both TEM and confocal reflectance microscopy showed that there were intracellular agglomerations of NPs within both H400 and primary oral epithelial cells. However, extrapolating the number of cells in a population which appeared to have intracellular TiO₂ NPs becomes difficult to determine from methods with such narrow fields of views. An estimation of the proportion of cells with clearly visible agglomerations was approximately 1/3 of an exposed H400 cell population. Currently the literature on the intracellularisation of NPs in epithelial cells is not extensive. Polystyrene NPs have been shown to accumulate in HeLa cells (Smith et al., 2012), however in their paper the signal of fluorescence from NPs was taken as the measure of intracellular NPs so

the proportion of the cell population containing NPs was not quantified. The fact that oral epithelial cells will uptake NPs is discussed in a paper by Chan et al., (Chan et al., 2011), and TEM imaging was used to demonstrate this process, however the proportion of cells which showed intracellular NPs was again not clarified. Here, the use of SR-XRF mapping allowed further discrimination of the number of cells interacting with TiO₂ NPs. This technique provides significantly higher discriminatory ability than optical microscopy and revealed that the proportion of cells interacting was much higher at approximately 2/3 of a H400 cell population. This finding is important insofar that the results of biological assays should be interpreted with the knowledge that one third of the exposed population interacted with large agglomerations, one third with small agglomerations or individual NPs and the remaining third appears to be unstimulated. This informs the approach to future studies as it shows that not all cells are either exposed to or likely to be responding equally to the NPs, and furthermore that the local concentration of NPs in the space immediately surrounding each cell may be vastly different.

While the uptake of TiO₂ NPs was imaged in H400 cells and primary epithelial cells, due to limitations in the number of primary cells available for processing and imaging there were fewer cells imaged than H400 cells (this is fully discussed in chapter 3). Other considerations when using primary cells would be the variation between donors, and the likelihood that a cell population harvested and cultured from oral tissues may not be purely epithelial in phenotype. For this reason, it would be experimentally challenging to produce robust data using only primary tissue harvested epithelial cells.

8.1.5 *Dose responses of epithelial cells to TiO₂ NPs*

TiO₂ is insoluble and agglomerates in cell culture mediums. Therefore, the local concentration in the immediate environment of each cell within a population will not be uniform. The non-uniform distribution of TiO₂ NPs within the specific experimental model used in this thesis is likely to lead to a variety of responses from cells within a population, a feature which may lead to blurring or loss of results if a measure of the whole population is made (for example, the microarray techniques detailed in chapter 6). The likelihood of gaining a more representative result is increased when using methods such as HCS which will reduce background noise, as cells are labelled

individually as opposed to results being pooled. This was demonstrated by the apparent differences between epithelial cell 'viability' post exposure to TiO₂ NPs when investigated using conventional vs HCS techniques, as discussed in Section 5.2.6.

The implications of this variation in response are important both in the *in vitro* study of NP-cell interactions and the appreciation of the likely variability of cell responses to NPs *in vivo*. This work strongly suggests that HCS techniques may be more appropriate than conventional techniques when examining the effects of NPs within cell culture medium on cell responses. Also it is important to realise that *in vivo*, cells will be exposed to a wide variety of 'local' concentrations, so a biologically relevant concentration of NPs is difficult if not impossible to define (Addison et al., 2012). Deciding on what constitutes a clinically relevant dose is complex and the exact exposure of an individual cell within the model systems used in this thesis was impossible to define.

Future work would be to further qualify and characterise the pattern of NP uptake to include more primary cell investigations, and to investigate the effect on the pattern of uptake variables such as NP size, NP species and particle shape may have alongside concentration and duration of exposure. It was not possible to concentrate on the responses of a small number of cells adjacent to particles within the cell culture model used within this work, therefore the results gained from biological assays of whole populations are likely to provide both an underestimation and a combination of responses to different events.

8.1.6 *Interference of TiO₂ NPs in suspension with known assays and difficulties of using conventional assays only*

As outlined in Chapter 3, insoluble TiO₂ NPs were distributed evenly in water post-sonication, however on being added to cell culture medium, some agglomeration inevitably occurs. This leads to an uneven distribution of NP stimulus and also a change in optical density of the cell culture medium which may influence colourmetric or light emitting assays. It is therefore essential to verify assay performance prior to use. A variety of assays were judged to be significantly influenced by the NP stimulus, despite

data from equivalent assays being regularly reported in the NP literature. For example, the MTT assay is colourimetric, and the altered optical density spectral absorbance of the resulting solution is altered significantly by the addition of TiO₂ NPs. Also IL8 appeared to be bound by TiO₂ NPs, negating the results of ELISA testing for this cytokine (see Section 7.2), and to a lesser extent IFN- γ . Therefore, it is imperative to rigorously test assays for use in conjunction with exposure stimuli prior to use. This issue has been only previously discussed briefly by a limited number of investigators (Holder et al., 2012, Kroll et al., 2009).

8.1.7 *Effects of TiO₂ on inflammation involving oral epithelial cells*

Known pathways that are stimulated in epithelial cells in response to bacterial challenges such as the translocation of NF κ B were investigated using conventional and HCS techniques. A small reduction in NF κ B activation in response to pre-treatment with TiO₂ NPs before exposure to relevant periodontal pathogens was found when using conventional staining, however this was not clear from the HCS techniques used. The fact that TiO₂ NPs will bind to IL8 (and to a lesser extent IFN γ , as discussed in chapter 7) may well affect the inflammation process *in vivo*. It has been shown that IFN γ is less efficient at priming PMNLs when in the presence of TiO₂ NPs, meaning that the inflammatory process may be further disrupted in by other mechanisms other than the binding of IL8.

Within the clinical picture, the concept that Ti implant derived particles could act as islands within tissues which are capable of binding cytokines is potentially very interesting. If cells are responding to inflammation by producing pro-inflammatory cytokines, such as IL8 and these are being bound to particles within tissues then this may have the capacity to disorder the immune response. Furthermore, it is unknown if the IL8 is inactivated by being bound to TiO₂ NPs, or if this process is reversible. There is potential for the perturbation of immune responses via this mechanism by a wide range of particles and involving a wide range of targets; expanded from the small panel looked at within this thesis, IFN γ and IL8 both appear to interact with TiO₂. The ramifications of this from a clinical point of view could be far reaching, potentially causing the inactivation of some attempts by cells to mount an inflammatory response, or if pro-inflammatory cytokines are still active when bound, potential to deflect

More pertinent to the clinical situation of peri-implant disease is the potential of Ti species being present within tissues to act as a modifying factor in the complex host – bacterial imbalance which is known to produce significant inflammation and tissue destruction in peri-implant disease. Current research on the presence of cytokines in peri-implant disease highlights Interleukin 12 (IL-12) and TNF α as being prevalent in severe peri-implantitis compared with health or mucositis (Duarte et al., 2009) and IL8 and MIP1- α as significantly elevated chemokines in advanced peri-implantitis when compared with early peri-implantitis (Petković et al., 2010). Extensive research into potential biomarkers for peri-implant disease has been published (Heitz-Mayfield, 2008), where peri-implant fluid and saliva have been tested for markers of soft tissue inflammation and bone resorption. Clinically, the processes occurring during advanced peri-implantitis will involve bone resorption and therefore osteoclastic activity, therefore it is expected that osteoclastic markers will be elevated in tissues surrounding implants which are ‘failing’ (Grant et al., 2010b). The inflammatory process within gingival tissues is complex with multiple cell signalling molecules involved in periodontal disease (King, 2008, Darveau, 2010), and any of these processes could potentially be altered by the presence of Ti debris in some form in the peri-implant situation. From the data presented in this thesis, it is therefore important to appreciate that Ti products within tissues have the potential to affect cell-cell signalling in terms of biological processes such as inflammation as demonstrated by the dose dependent inactivation of IL8 when exposed to TiO₂ NPS, and a similar process may occur involving other markers of inflammation or bone resorption.

It is not being suggested that the presence of metallic particles within tissues are potentially causing peri-implant diseases, but the presence of these particles may have the capacity to modify other risk factors for peri-implantitis. Probably the greatest risk factor for the development of both peri-implantitis and periodontitis is poor oral hygiene (Heitz-Mayfield and Lang, 2010, Feloutzis et al., 2003). Poor oral hygiene will ensure a persistent bacterial challenge, with increasing virulence over time as the composition of the biofilm changes (Hajishengallis et al., 2011, van Winkelhoff et al., 2002). Destruction of the periodontal tissues occurs in periodontitis as a result of the host response to the bacterial challenge; a process which is regulated by the secretion

of cytokines and other cell signalling molecules. In the situation where periodontal pathogens or their products are present within tissues, the presence of implant derived species could once again form interferences in the cell-cell signalling processes which occur within tissues via perturbation of either the free movement of cytokines, or by potentially inactivating released cytokines.

A history of, or indeed the concurrent presence of, periodontitis is a known risk factor for loss of osseointegration (Heitz-Mayfield, 2008). Patients who suffer with chronic periodontitis have been shown to exhibit neutrophil hyper-reactivity in response to IL8 (Ling et al., 2015), therefore if implant derived species within tissues are inhibiting the presence or directionality of the concentration gradient of IL8 within tissues, a disordering of inflammation may occur. It has been shown that patients with a 'thin' mucosal biotype are at higher risk of peri-implantitis than those with a 'thick' biotype (Aguirre-Zorzano et al., 2013). Thin biotype is associated with looser connective tissue than the 'thick' biotype (Abraham et al., 2014). This has potential significance when considering the presence of implant derived particles within the tissues. Implant derived particles could potentially enter and move through tissue layers more readily in patients exhibiting a 'thin' biotype, therefore the potential for the presence and perhaps amount of metal species present could be higher in these patients. This thesis has shown specific binding capacity for IL8 to TiO₂ NPs even within a serum containing environment, meaning within a complex protein panel TiO₂ NPs appear to preferentially bind and deactivate IL8. The variety of metallic species which could be present within tissues adjacent to implanted Ti devices is large, not just in speciation but in size and shape, which are factors which have been shown to influence binding characteristics (Albanese et al., 2012).

8.3 Overall conclusions

There are a number of issues surrounding the use of an insoluble NP stimulus within a biological system. These include:

- TiO_2 NPs have been shown to interfere with results gained from some types of assay, e.g. the MTT assay (see Section 3.3). This factor has limited the variety of assay techniques which were used within this thesis, but has also highlighted that previously published work may not be accurate due to the lack of attention paid to this phenomenon;
- The dose of stimulus which each cell was exposed to within the model system, developed in Chapter 3 is impossible to quantify accurately. Agglomeration of TiO_2 NPs within the culture system means that the localised concentration adjacent to some cells may be many multiples of the exposure concentration. This has implications for the study of NPs within biological systems on a wider scale;
- High Content Screening (HCS) techniques may give a more accurate representation of cellular responses, due to the loss of background 'noise' due to the categorisation of each cell rather than looking at overall cellular product output across a population;
- The viability of both H400 cells and primary oral epithelial cells is unaffected by the presence of TiO_2 NPs at concentrations of up to 100ppm. This is to be expected when the clinical picture of an implanted device is considered, as epithelial destruction and sloughing is not seen adjacent to implanted Ti devices.

Intracellularisation of TiO_2 NPs occurs in both H400 cells and primary oral epithelial cells following co-culture:

- The pattern of uptake appeared to be both time and dose dependent;
- Intracellularisation of TiO_2 NPs was not consistent across a cell population. A subset of the cell population appears to take up TiO_2 NPs, whilst other cells appear to not intracellularise NPs;

- Intracellularisation of TiO₂ NPs by oral epithelial cells is partly, but not wholly, due to clathrin mediated endocytosis.

The gene expression changes expressed by H400 cells exposed to TiO₂ NPs compared with control cells at 6h and 24 h exposure appear to be limited:

- Data are clearly limited by a lack of knowledge of the exposure concentration and inconsistency in the nature of exposures to individual cells within a population;
- Primary oral epithelial cells express ID genes differently to H400 cells. Therefore, the gene expression findings for H400 cells may not be representative of the behaviours of primary oral epithelial cells;
- When oral epithelial cells are exposed to a bacterial challenges, the addition of TiO₂ NPs appear to potentially modify gene expression changes.

TiO₂ NP species on the nanoscale have the potential to bind to biomolecules:

- IL8 and IFN γ have both been shown be depleted in the presence of TiO₂ NPs;
- IL8 has been shown to selectively bind to TiO₂ NPs even in the presence of a complex protein environment;
- IL8 as a chemoattractant is inhibited in a dose dependent manner by the addition of TiO₂ NPs.

These points are of potential clinical relevance.

The null hypothesis that *“Ti species similar to those released from implanted Ti devices do not elicit significant biological responses from oral epithelial cells”* has been disproved.

8.4 Future work

This thesis has been a wide ranging, diverse piece of work which has looked at numerous techniques, and has provided the starting point for many potential avenues of research.

There are a number of areas presented within this thesis where repetitions and modifications of experiments would be of benefit. Initially, a repeat of the microarray at different time-points and a repeat with exposure to known periodontal pathogens in the presence and absence of TiO₂ NPs would help to elucidate the potential modification of epithelial cellular responses in this context.

Also the HCS data gathered was limited due to practicalities of transporting viable cell cultures at different time points to an external assay provider. However, the results were interesting and investigation of co-culture models involving pathogens and TiO₂ NPs across a panel of other inflammatory markers would be valuable.

A further area which would be highly informative would be to investigate the mechanism in more detail of the binding shown between IL8 and TiO₂ NPs. A number of questions are still unknown with regard to this interaction:

- Is the binding exhibited reversible? If so, under which conditions?
- Is the binding capacity affected by NP shape and size, and to what extent?
- Does IL8 remain active when bound, or are certain receptor sites blocked?
- Does any inactivation continue once released if binding is reversible?

Investigation (both by ELISA and functional assays) of a wider panel of cytokines involved in the immune response would give more information on potential interactions between cytokines and metallic particles. Furthermore, the TiO₂ NPs stimulus was limited to anatase particles of a specific shape and size throughout this work; it is important to appreciate that a variety of species have been identified within tissues adjacent to implanted Ti devices, so widening the panel of stimuli will enable investigation of other potential interactions.

References

- ABOSTONSMILE.COM (online). 2012.. *Implants-Part 1-Why are implants important?* Available at: <http://www.abostonsmile.com/blog/2012/07/19/implants-part-1-why-are-85782> (accessed 12 April 2017).
- ABRAHAM, S., DEEPAK, K. T., AMBILI, R., PREEJA, C. & ARCHANA, V. 2014. Gingival biotype and its clinical significance – A review. *The Saudi Journal for Dental Research*, 5, 3-7.
- ADDISON, O., DAVENPORT, A. J., NEWPORT, R. J., KALRA, S., MONIR, M., MOSSELMANS, J. F., PROOPS, D. & MARTIN, R. A. 2012. Do 'passive' medical titanium surfaces deteriorate in service in the absence of wear? *Journal of the Royal Society Interface*, 9, 3161-4.
- ADELL, R., LEKHOLM, U., ROCKLER, B. & BRANEMARK, P. I. 1981. A 15-year study of osseointegrated implants in the treatment of the edentulous jaw. *International Journal of Oral Surgery*, 10, 387-416.
- AFFYMETRIX. *GeneChip Human Gene ST Arrays* [Online]. Available at: http://www.affymetrix.com/estore/browse/products.jsp?navMode=34000&productId=131453&navAction=jump&ald=productsNav#1_1 (Accessed 5 April 2017).
- AGUIRRE-ZORZANO, L. A., VALLEJO-AISA, F. J. & ESTEFANÍA-FRESCO, R. 2013. Supportive periodontal therapy and periodontal biotype as prognostic factors in implants placed in patients with a history of periodontitis. *Medicina Oral, Patología Oral y Cirugía Bucal*, 18, e786-e792.
- AISENBERG, M. S. 1952. Histology and physiology of the supporting structures. *Journal of the American Dental Association*, 44, 628-32.
- AKAGI, J., KORDON, M., ZHAO, H., MATUSZEK, A., DOBRUCKI, J., ERRINGTON, R., SMITH, P. J., TAKEDA, K., DARZYNKIEWICZ, Z. & WLODKOWIC, D. 2013. Real-time cell viability assays using a new anthracycline derivative DRAQ7 (R). *Cytometry Part A*, 83A, 227-234.
- ALBANESE, A., TANG, P. S. & CHAN, W. C. W. 2012. The Effect of Nanoparticle Size, Shape, and Surface Chemistry on Biological Systems. *Annual Review of Biomedical Engineering*, 14, 1-16.
- ALBREKTSSON, T. O., JOHANSSON, C. B. & SENNERBY, L. 1994. Biological aspects of implant dentistry: osseointegration. *Periodontology 2000*, 4, 58-73.
- AN, N., RAUSCH-FAN, X., WIELAND, M., MATEJKA, M., ANDRUKHOV, O. & SCHEDULE, A. 2012. Initial attachment, subsequent cell proliferation/viability and gene expression of epithelial cells related to attachment and wound healing in response to different titanium surfaces. *Dental Materials*, 28, 1207-14.
- ANDREW, N. & INSALL, R. H. 2007. Chemotaxis in shallow gradients is mediated independently of PtdIns 3-kinase by biased choices between random protrusions. *Nature Cell Biology*, 9, 193-200.

- ARUOMA, O. I. 1998. Free radicals, oxidative stress, and antioxidants in human health and disease. *Journal of the American Oil Chemists Society*, 75, 199-212.
- ARYS, A., PHILIPPART, C., DOUROV, N., HE, Y., LE, Q. T. & PIREAUX, J. J. 1998. Analysis of titanium dental implants after failure of osseointegration: combined histological, electron microscopy, and X-ray photoelectron spectroscopy approach. *Journal of Biomedical Materials Research*, 43, 300-12.
- ATIEH, M. A., ALSABEEHA, N. H., FAGGION, C. M., JR. & DUNCAN, W. J. 2013. The frequency of peri-implant diseases: a systematic review and meta-analysis. *Journal of Periodontology*, 84, 1586-98.
- AVILA, G., MISCH, K., GALINDO-MORENO, P. & WANG, H.-L. 2009. Implant Surface Treatment Using Biomimetic Agents. *Implant Dentistry*, 18, 17-26.
- BACQUART, T., DEVES, G., CARMONA, A., TUCOULOU, R., BOHIC, S. & ORTEGA, R. 2007. Subcellular speciation analysis of trace element oxidation states using synchrotron radiation micro-X-ray absorption near-edge structure. *Analytical Chemistry*, 79, 7353-9.
- BAGGIOLINI, M., WALZ, A. & KUNKEL, S. L. 1989. Neutrophil-activating peptide-1/interleukin 8, a novel cytokine that activates neutrophils. *Journal of Clinical Investigation*, 84, 1045-9.
- BAGORDA, A. & PARENT, C. A. 2008. Eukaryotic chemotaxis at a glance. *Journal of Cell Science*, 121, 2621-2624.
- BALAJI, S. M. 2013. Direct v/s Indirect sinus lift in maxillary dental implants. *Annals of Maxillofacial Surgery*, 3, 148-153.
- BANNUNAH, A. M., VLLASALIU, D., LORD, J. & STOLNIK, S. 2014. Mechanisms of nanoparticle internalization and transport across an intestinal epithelial cell model: effect of size and surface charge. *Molecular Pharmaceutics*, 11, 4363-73.
- BARILLET, S., SIMON-DECKERS, A., HERLIN-BOIME, N., MAYNE-L'HERMITE, M., REYNAUD, C., CASSIO, D., GOUGET, B. & CARRIERE, M. 2010. Toxicological consequences of TiO₂, SiC nanoparticles and multi-walled carbon nanotubes exposure in several mammalian cell types: an in vitro study. *Journal of Nanoparticle Research*, 12, 61-73.
- BARONE, M. V., PEPPERKOK, R., PEVERALI, F. A. & PHILIPSON, L. 1994. Id proteins control growth induction in mammalian cells. *Proceedings of the National Academy of Sciences of the United States of America*, 91, 4985-8.
- BATTINO, M., BULLON, P., WILSON, M. & NEWMAN, H. 1999. Oxidative injury and inflammatory periodontal diseases: the challenge of anti-oxidants to free radicals and reactive oxygen species. *Critical Reviews in Oral Biology and Medicine*, 10, 458-76.
- BENEZRA, R., DAVIS, R. L., LOCKSHON, D., TURNER, D. L. & WEINTRAUB, H. 1990. The protein Id: a negative regulator of helix-loop-helix DNA binding proteins. *Cell*, 61, 49-59.

- BERGAMINI, C. M., GAMBETTI, S., DONDI, A. & CERVELLATI, C. 2004. Oxygen, reactive oxygen species and tissue damage. *Current Pharmaceutical Design*, 10, 1611-1626.
- BERGLUNDH, T., GISLASON, O., LEKHOLM, U., SENNERBY, L. & LINDHE, J. 2004. Histopathological observations of human periimplantitis lesions. *Journal of Clinical Periodontology*, 31, 341-7.
- BERGLUNDH, T., LINDHE, J., ERICSSON, I., MARINELLO, C. P., LILJENBERG, B. & THORSEN, P. 1991. The soft tissue barrier at implants and teeth. *Clinical Oral Implants Research*, 2, 81-90.
- BERTRAND, E., GLORANT, T., GORDIN, D. M., VASILESCU, E., DROB, P., VASILESCU, C. & DROB, S. I. 2010. Synthesis and characterisation of a new superelastic Ti-25Ta-25Nb biomedical alloy. *Journal of the Mechanical Behavior of Biomedical Materials*, 3, 559-564.
- BETZ, O., WEGST, U., WEIDE, D., HEETHOFF, M., HELFEN, L., LEE, W.-K. & CLOETENS, P. 2007. Imaging applications of synchrotron X-ray phase-contrast microtomography in biological morphology and biomaterials science. I. General aspects of the technique and its advantages in the analysis of millimetre-sized arthropod structure. *Journal of Microscopy*, 227, 51-71.
- BIDRA, A. S. 2012. No reliable evidence suggesting what is the most effective interventions for treating peri-implantitis. *Evidence Based Dentistry*, 13, 50-1.
- BOLSTAD, B. M., IRIZARRY, R. A., ASTRAND, M. & SPEED, T. P. 2003. A comparison of normalization methods for high density oligonucleotide array data based on variance and bias. *Bioinformatics*, 19, 185-193.
- BOSSHARDT, D. D. & LANG, N. P. 2005. The Junctional Epithelium: from Health to Disease. *Journal of Dental Research*, 84, 9-20.
- BOYER, R., WELSCH, G. & COLLINGS, E. W. 2004. Materials Properties Handbook - Titanium Alloys. Metals Park, Ohio: ASM International.
- BRAINARRAY. *University of Michigan Molecular and Behavioural Neuroscience Institute* [Online]. Available: <http://brainarray.mbni.med.umich.edu/Brainarray/Database/CustomCDF/CDFdownload.asp#v17> (Accessed 02 August 2013).
- BRANEMARK, P. I. 1959. Vital microscopy of bone marrow in rabbit. *Scandinavian Journal of Clinical and Laboratory Investigation*, 11 Supp 38, 1-82.
- BRANEMARK, P. I. 1983. Osseointegration and its experimental background. *Journal of Prosthetic Dentistry*, 50, 399-410.
- BRANEMARK, R., BRANEMARK, P. I., RYDEVIK, B. & MYERS, R. R. 2001. Osseointegration in skeletal reconstruction and rehabilitation: a review. *Journal of Rehabilitation Research and Development*, 38, 175-81.
- BRINKMANN, V., REICHARD, U., GOOSMANN, C., FAULER, B., UHLEMANN, Y., WEISS, D. S., WEINRAUCH, Y. & ZYCHLINSKY, A. 2004. Neutrophil extracellular traps kill bacteria. *Science*, 303, 1532-5.

- CADOSCH, D., CHAN, E., GAUTSCHI, O. P. & FILGUEIRA, L. 2009a. Metal is not inert: role of metal ions released by biocorrosion in aseptic loosening--current concepts. *Journal of Biomedical Materials Research A*, 91, 1252-62.
- CADOSCH, D., CHAN, E., GAUTSCHI, O. P., SIMMEN, H.-P. & FILGUEIRA, L. 2009b. Bio-corrosion of stainless steel by osteoclasts—in vitro evidence. *Journal of Orthopaedic Research*, 27, 841-846.
- CARLSSON, L., ROSTLUND, T., ALBREKTSSON, B., ALBREKTSSON, T. & BRANEMARK, P. I. 1986. Osseointegration of titanium implants. *Acta Orthopaedica Scandinavica*, 57, 285-9.
- CARTER, E. A., RAYNER, B. S., MCLEOD, A. I., WU, L. E., MARSHALL, C. P., LEVINA, A., AITKEN, J. B., WITTING, P. K., LAI, B., CAI, Z., VOGT, S., LEE, Y.-C., CHEN, C.-I., TOBIN, M. J., HARRIS, H. H. & LAY, P. A. 2010. Silicon nitride as a versatile growth substrate for microspectroscopic imaging and mapping of individual cells. *Molecular Biosystems*, 6, 1316-1322.
- CASWELL, C. W, CLARK, A.E. (1991). *Dental Implant Prosthodontics*. Philadelphia, Pennsylvania: Lippincott.
- CHAN, J., YING, T., GUANG, Y. F., LIN, L. X., KAI, T., FANG, Z. Y., TING, Y. X., XING, L. F. & JI, Y. Y. 2011. In vitro toxicity evaluation of 25-nm anatase TiO₂ nanoparticles in immortalized keratinocyte cells. *Biological Trace Element Research*, 144, 183-96.
- CHAPPLE, I. L. 2006. Oxidative stress, nutrition and neutrogenomics in periodontal health and disease. *International Journal of Dental Hygiene*, 4 Suppl 1, 15-21; discussion 50-2.
- CHAPPLE, I. L. & MATTHEWS, J. B. 2007. The role of reactive oxygen and antioxidant species in periodontal tissue destruction. *Periodontology 2000*, 43, 160-232.
- CHAPPLE, I. L. C. 1996. Role of free radicals and antioxidants in the pathogenesis of the inflammatory periodontal diseases. *Journal of Clinical Pathology-Clinical Molecular Pathology Edition*, 49, M247-M255.
- CHAPPLE, I. L. C. 1997. Reactive oxygen species and antioxidants in inflammatory diseases. *Journal of Clinical Periodontology*, 24, 287-296.
- CHO, S., SHIN, M. H., KIM, Y. K., SEO, J. E., LEE, Y. M., PARK, C. H. & CHUNG, J. H. 2009. Effects of Infrared Radiation and Heat on Human Skin Aging in vivo. *Journal of Investigative Dermatology Symposium Proceedings*, 14, 15-19.
- CHUNG, D. M., OH, T. J., SHOTWELL, J. L., MISCH, C. E. & WANG, H. L. 2006. Significance of keratinized mucosa in maintenance of dental implants with different surfaces. *Journal of Periodontology*, 77, 1410-20.
- COOK, S. D., THOMAS, K. A., KAY, J. F. & JARCHO, M. 1988. Hydroxyapatite-coated titanium for orthopedic implant applications. *Clinical Orthopaedics and Related Research*, 225-43.
- COPPE, J. P., SMITH, A. P. & DESPREZ, P. Y. 2003. Id proteins in epithelial cells. *Experimental Cell Research*, 285, 131-45.

- CRUBZY, E., MURAIL, P., GIRARD, L. & BERNADOU, J.-P. 1998. False teeth of the Roman world. *Nature*, 391, 29-29.
- DAI, M. H., WANG, P. L., BOYD, A. D., KOSTOV, G., ATHEY, B., JONES, E. G., BUNNEY, W. E., MYERS, R. M., SPEED, T. P., AKIL, H., WATSON, S. J. & MENG, F. 2005. Evolving gene/transcript definitions significantly alter the interpretation of GeneChip data. *Nucleic Acids Research*, 33, e175.
- DARVEAU, R. P. 2010. Periodontitis: a polymicrobial disruption of host homeostasis. *Nature Reviews Microbiology*, 8, 481-490.
- DAUSEND, J., MUSYANOVYCH, A., DASS, M., WALTHER, P., SCHREZENMEIER, H., LANDFESTER, K. & MAILANDER, V. 2008. Uptake mechanism of oppositely charged fluorescent nanoparticles in HeLa cells. *Macromolecular Bioscience*, 8, 1135-1143.
- DESPREZ, P. Y., HARA, E., BISSELL, M. J. & CAMPISI, J. 1995. Suppression of mammary epithelial cell differentiation by the helix-loop-helix protein Id-1. *Molecular and Cellular Biology*, 15, 3398-404.
- DIAS, I. H., CHAPPLE, I. L., MILWARD, M., GRANT, M. M., HILL, E., BROWN, J. & GRIFFITHS, H. R. 2013. Sulforaphane restores cellular glutathione levels and reduces chronic periodontitis neutrophil hyperactivity in vitro. *PloS One*, 8, e66407.
- DOHAN EHRENFEST, D. M., COELHO, P. G., KANG, B. S., SUL, Y. T. & ALBREKTSSON, T. 2010. Classification of osseointegrated implant surfaces: materials, chemistry and topography. *Trends in Biotechnology*, 28, 198-206.
- DONARUMA, L. G. 1988. Definitions in biomaterials, D. F. Williams, Ed., Elsevier, Amsterdam.
- DONLAN, R. M. 2002. Biofilms: microbial life on surfaces. *Emerging Infectious Diseases*, 8, 881-90.
- DUARTE, P. M., DE MENDONCA, A. C., MAXIMO, M. B. B., SANTOS, V. R., BASTOS, M. F. & NOCITI, F. H. 2009. Differential cytokine expressions affect the severity of peri-implant disease. *Clinical Oral Implants Research*, 20, 514-520.
- DUFFO, G., BARREIRO, M., OLMEDO, D., CROSA, M., GUGLIELMOTTI, M. B. & CABRINI, R. L. 1999. An experimental model to study implant corrosion. *Acta Odontologica Latinoamericana*, 12, 3-10.
- ECKES, B., DOGIC, D., COLUCCI-GUYON, E., WANG, N., MANIOTIS, A., INGBER, D., MERCKLING, A., LANGA, F., AUMAILLEY, M., DELOUVEE, A., KOTELIANSKY, V., BABINET, C. & KRIEG, T. 1998. Impaired mechanical stability, migration and contractile capacity in vimentin-deficient fibroblasts. *Journal of Cell Science*, 111 (Pt 13), 1897-907.
- EFFAH, E. A., BIANCO, P. D. & DUCHEYNE, P. 1995. Crystal structure of the surface oxide layer on titanium and its changes arising from immersion. *Journal of Biomedical Materials Research*, 29, 73-80.

- EICK, S., REISSMANN, A., RODEL, J., SCHMIDT, K. H. & PFISTER, W. 2006. Porphyromonas gingivalis survives within KB cells and modulates inflammatory response. *Oral Microbiology and Immunology*, 21, 231-7.
- ELIAS, C. N. 2008. Biomedical applications of titanium and its alloys. *Journal of the Minerals, Metals & Materials Society*, 60, 46-49.
- ELLIS, T. N. & BEAMAN, B. L. 2004. Interferon- γ activation of polymorphonuclear neutrophil function. *Immunology*, 112, 2-12.
- ESPINOSA, E. J., CALERO, M., SRIDEVI, K. & PFEFFER, S. R. 2009. RhoBTB3: a Rho GTPase-family ATPase required for endosome to Golgi transport. *Cell*, 137, 938-48.
- ESPOSITO, M., GRUSOVIN, M. G., MAGHAIREH, H. & WORTHINGTON, H. V. 2013. Interventions for replacing missing teeth: different times for loading dental implants. *Cochrane Database Systematic Reviews*, Cd003878.
- ESPOSITO, M., THOMSEN, P., MOLNE, J., GRETZER, C., ERICSON, L. E. & LEKHOLM, U. 1997. Immunohistochemistry of soft tissues surrounding late failures of Branemark implants. *Clinical Oral Implants Research*, 8, 352-66.
- FELOUTZIS, A., LANG, N. P., TONETTI, M. S., BURGIN, W., BRAGGER, U., BUSER, D., DUFF, G. W. & KORNMAN, K. S. 2003. IL-1 gene polymorphism and smoking as risk factors for peri-implant bone loss in a well-maintained population. *Clinical Oral Implants Research*, 14, 10-17.
- FIELDING, A. B., WILLOX, A. K., OKEKE, E. & ROYLE, S. J. 2012. Clathrin-mediated endocytosis is inhibited during mitosis. *Proceedings of the National Academy of Sciences of the United States of America*, 109, 6572-7.
- FILIPI, K., HALACKOVA, Z. & FILIPI, V. 2011. Oral health status, salivary factors and microbial analysis in patients with active gastro-oesophageal reflux disease. *International Dental Journal*, 61, 231-7.
- FISICHELLA, M., BERENGUER, F., STEINMETZ, G., AUFFAN, M., ROSE, J. & PRAT, O. 2012. Intestinal toxicity evaluation of TiO₂ degraded surface-treated nanoparticles: a combined physico-chemical and toxicogenomics approach in caco-2 cells. *Particle and Fibre Toxicology*, 9.
- FONG, S., ITAHANA, Y., SUMIDA, T., SINGH, J., COPPE, J. P., LIU, Y., RICHARDS, P. C., BENNINGTON, J. L., LEE, N. M., DEBS, R. J. & DESPREZ, P. Y. 2003. Id-1 as a molecular target in therapy for breast cancer cell invasion and metastasis. *Proceedings of the National Academy of Sciences of the United States of America*, 100, 13543-8.
- FORREST, S. & MCNAMARA, C. 2004. Id family of transcription factors and vascular lesion formation. *Arteriosclerosis, Thrombosis, and Vascular Biology*, 24, 2014-20.
- FORSBERG, L., DE FAIRE, U. & MORGENSTERN, R. 2001. Oxidative stress, human genetic variation, and disease. *Archives of Biochemistry and Biophysics*, 389, 84-93.

- FRETWURST, T., BUZANICH, G., NAHLES, S., WOELBER, J. P., RIESEMEIER, H. & NELSON, K. 2016. Metal elements in tissue with dental peri-implantitis: a pilot study. *Clinical Oral Implants Research*, 27, 1178-86.
- FRITSCHI, B. Z., ALBERT-KISZELY, A. & PERSSON, G. R. 2008. Staphylococcus aureus and other bacteria in untreated periodontitis. *Journal of Dental Research*, 87, 589-93.
- GERLOFF, K., FENOGLIO, I., CARELLA, E., KOLLING, J., ALBRECHT, C., BOOTS, A. W., FORSTER, I. & SCHINS, R. P. 2012. Distinctive toxicity of TiO₂ rutile/anatase mixed phase nanoparticles on Caco-2 cells. *Chemical Research in Toxicology*, 25, 646-55.
- GERMANIER, Y., TOSATTI, S., BROGGINI, N., TEXTOR, M. & BUSER, D. 2006. Enhanced bone apposition around biofunctionalized sandblasted and acid-etched titanium implant surfaces. *Clinical Oral Implants Research*, 17, 251-257.
- GOLDBERG, N. I. & GERSHKOFF, A. 1949. The implant lower denture. *Dental Digest*, 55, 490-4.
- GRANT, M. M., KOLAMUNNE, R. T., LOCK, F. E., MATTHEWS, J. B., CHAPPLE, I. L. & GRIFFITHS, H. R. 2010a. Oxygen tension modulates the cytokine response of oral epithelium to periodontal bacteria. *Journal of Clinical Periodontology*, 37, 1039-48.
- GRANT, M. M., MONKSFIELD, P., PROOPS, D., BRINE, M., ADDISON, O., SAMMONS, R. L., MATTHEWS, J. B., REID, A. & CHAPPLE, I. L. 2010b. Fluid exudates from inflamed bone-anchored hearing aids demonstrate elevated levels of cytokines and biomarkers of tissue and bone metabolism. *Otology & Neurotology*, 31, 433-9.
- GRAY, T., THOMASSEN, D., MASS, M. & BARRETT, J. C. 1983. Quantitation of cell proliferation, colony formation, and carcinogen induced cytotoxicity of rat tracheal epithelial cells grown in culture on 3T3 feeder layers. *In Vitro*, 19, 559-570.
- GROGER, S., MICHEL, J. & MEYLE, J. 2008. Establishment and characterization of immortalized human gingival keratinocyte cell lines. *Journal of Periodontal Research*, 43, 604-14.
- GROMMES, J. & SOEHNLEIN, O. 2011. Contribution of neutrophils to acute lung injury. *Molecular Medicine*, 17, 293-307.
- HAJISHENGALLIS, G., LIANG, S., PAYNE, M. A., HASHIM, A., JOTWANI, R., ESKAN, M. A., MCINTOSH, M. L., ALSAM, A., KIRKWOOD, K. L., LAMBRIS, J. D., DARVEAU, R. P. & CURTIS, M. A. 2011. Low-abundance biofilm species orchestrates inflammatory periodontal disease through the commensal microbiota and complement. *Cell Host Microbe*, 10, 497-506.
- HALEEM-SMITH, H., ARGINTAR, E., BUSH, C., HAMPTON, D., POSTMA, W. F., CHEN, F. H., RIMINGTON, T., LAMB, J. & TUAN, R. S. 2012. Biological responses of human mesenchymal stem cells to titanium wear debris particles. *Journal of Orthopaedic Research*, 30, 853-63.

- HAYDEN, M. S. & GHOSH, S. 2004. Signaling to NFkappaB. *Genes and Development*, 18, 2195-224.
- HEIT, B., LIU, L., COLARUSSO, P., PURI, K. D. & KUBES, P. 2008. PI3K accelerates, but is not required for, neutrophil chemotaxis to fMLP. *Journal of Cell Science*, 121, 205-14.
- HEITZ-MAYFIELD, L. J. 2005. Disease progression: identification of high-risk groups and individuals for periodontitis. *Journal of Clinical Periodontology*, 32 Suppl 6, 196-209.
- HEITZ-MAYFIELD, L. J. A. 2008. Peri-implant diseases: diagnosis and risk indicators. *Journal of Clinical Periodontology*, 35, 292-304.
- HEITZ-MAYFIELD, L. J. A. & LANG, N. P. 2010. Comparative biology of chronic and aggressive periodontitis vs. peri-implantitis. *Periodontology 2000*, 53, 167-81.
- HENZEN-LOGMANS, S., MULLINK, H., RAMAEKERS, F. S., TADEMA, T. & MEIJER, C. L. M. 1987. Expression of cytokeratins and vimentin in epithelial cells of normal and pathologic thyroid tissue. *Virchows Archiv A*, 410, 347-354.
- HIRSCH, E., KATANAIEV, V. L., GARLANDA, C., AZZOLINO, O., PIROLA, L., SILENGO, L., SOZZANI, S., MANTOVANI, A., ALTRUDA, F. & WYMAN, M. P. 2000. Central role for G protein-coupled phosphoinositide 3-kinase gamma in inflammation. *Science*, 287, 1049-53.
- HOLDER, A. L., GOTH-GOLDSTEIN, R., LUCAS, D. & KOSHLAND, C. P. 2012. Particle-induced artifacts in the MTT and LDH viability assays. *Chemical Research in Toxicology*, 25, 1885-92.
- HOLMSTROM, K. M. & FINKEL, T. 2014. Cellular mechanisms and physiological consequences of redox-dependent signalling. *Nature Reviews: Molecular Cell Biology*, 15, 411-21.
- HORIE, M., KATO, H. & IWAHASHI, H. 2013. Cellular effects of manufactured nanoparticles: effect of adsorption ability of nanoparticles. *Archives of Toxicology*, 87, 771-781.
- HSIAO, I. L. & HUANG, Y. J. 2011. Improving the Interferences of Methyl Thiazolyl Tetrazolium and IL8 Assays in Assessing the Cytotoxicity of Nanoparticles. *Journal of Nanoscience and Nanotechnology*, 11, 5228-5233.
- HUANG, H.-L., HSING, H.-W., LAI, T.-C., CHEN, Y.-W., LEE, T.-R., CHAN, H.-T., LYU, P.-C., WU, C.-L., LU, Y.-C., LIN, S.-T., LIN, C.-W., LAI, C.-H., CHANG, H.-T., CHOU, H.-C. & CHAN, H.-L. 2010. Trypsin-induced proteome alteration during cell subculture in mammalian cells. *Journal of Biomedical Science*, 17, 36.
- HUANG, S., CHUEH, P. J., LIN, Y.-W., SHIH, T.-S. & CHUANG, S.-M. 2009. Disturbed mitotic progression and genome segregation are involved in cell transformation mediated by nano-TiO₂ long-term exposure. *Toxicology and Applied Pharmacology*, 241, 182-94.
- IRIZARRY, R. A., BOLSTAD, B. M., COLLIN, F., COPE, L. M., HOBBS, B. & SPEED, T. P. 2003. Summaries of affymetrix GeneChip probe level data. *Nucleic Acids Research*, 31.

- IRSHAD, M., SCHERES, N., CRIELAARD, W., LOOS, B. G., WISMEIJER, D. & LAINE, M. L. 2013. Influence of titanium on in vitro fibroblast-*Porphyromonas gingivalis* interaction in peri-implantitis. *Journal of Clinical Periodontology*, 40, 841-9.
- J PHILPOTT, D., E GIRARDIN, S. & J SANSONETTI, P. 2001. Innate immune responses of epithelial cells following infection with bacterial pathogens. *Current Opinion in Immunology*, 13, 410-416.
- JEPSEN, S., BERGLUNDH, T., GENCO, R., AASS, A. M., DEMIREL, K., DERKS, J., FIGUERO, E., GIOVANNOLI, J. L., GOLDSTEIN, M., LAMBERT, F., ORTIZ-VIGON, A., POLYZOIS, I., SALVI, G. E., SCHWARZ, F., SERINO, G., TOMASI, C. & ZITZMANN, N. U. 2015. Primary prevention of peri-implantitis: managing peri-implant mucositis. *Journal of Clinical Periodontology*, 42 Suppl 16, S152-7.
- JOHNSTON, H. J., SEMMLER-BEHNKE, M., BROWN, D. M., KREYLING, W., TRAN, L. & STONE, V. 2010. Evaluating the uptake and intracellular fate of polystyrene nanoparticles by primary and hepatocyte cell lines in vitro. *Toxicology and Applied Pharmacology*, 242, 66-78.
- JOLIVET, J. P., CASSAIGNON, S., CHANEAC, C., CHICHE, D., DURUPHY, O. & PORTEHAULT, D. 2010. Design of metal oxide nanoparticles: Control of size, shape, crystalline structure and functionalization by aqueous chemistry. *Comptes rendus Chimie*, 13, 40-51.
- JONAS, L., FULDA, G., RADECK, C., HENKEL, K. O., HOLZHUTER, G. & MATHIEU, H. J. 2001. Biodegradation of titanium implants after long-time insertion used for the treatment of fractured upper and lower jaws through osteosynthesis: element analysis by electron microscopy and EDX or EELS. *Ultrastructural Pathology*, 25, 375-83.
- JUNKER, R., DIMAKIS, A., THONEICK, M. & JANSEN, J. A. 2009. Effects of implant surface coatings and composition on bone integration: a systematic review. *Clinical Oral Implants Research*, 20, 185-206.
- KASEMO, B. 1983. Biocompatibility of titanium implants: surface science aspects. *Journal of Prosthetic Dentistry*, 49, 832-7.
- KEDICI, S. P., AKSUT, A. A., KILICARSLAN, M. A., BAYRAMOGLU, G. & GOKDEMIR, K. 1998. Corrosion behaviour of dental metals and alloys in different media. *Journal of Oral Rehabilitation*, 25, 800-8.
- KIKKERT, R., LAINE, M. L., AARDEN, L. A. & VAN WINKELHOFF, A. J. 2007. Activation of toll-like receptors 2 and 4 by gram-negative periodontal bacteria. *Oral Microbiology and Immunology*, 22, 145-51.
- KIM, I.-S., BAEK, M. & CHOI, S.-J. 2010. Comparative Cytotoxicity of Al₂O₃, CeO₂, TiO₂ and ZnO Nanoparticles to Human Lung Cells. *Journal of Nanoscience and Nanotechnology*, 10, 3453-3458.
- KIM, J. A., ABERG, C., SALVATI, A. & DAWSON, K. A. 2012. Role of cell cycle on the cellular uptake and dilution of nanoparticles in a cell population. *Nature Nanotechnology*, 7, 62-8.

- KING, G. L. 2008. The Role of Inflammatory Cytokines in Diabetes and Its Complications. *Journal of Periodontology*, 79, 1527-1534.
- KLOKKEVOLD, P. R. & NEWMAN, M. G. 2000. Current status of dental implants: a periodontal perspective. *The International Journal of Oral & Maxillofacial Implants*, 15, 56-65.
- KLOKKEVOLD, P. R., NISHIMURA, R. D., ADACHI, M. & CAPUTO, A. 1997. Osseointegration enhanced by chemical etching of the titanium surface. A torque removal study in the rabbit. *Clinical Oral Implants Research*, 8, 442-447.
- KOBAYASHI, S. D., VOYICH, J. M., BURLAK, C. & DELEO, F. R. 2005. Neutrophils in the innate immune response. *Archivum Immunologiae et Therapiae Experimentalis*, 53, 505-17.
- KOPPRASCH, S., PIETZSCH, J. & GRAESSLER, J. 2003. Validation of different chemilumigenic substrates for detecting extracellular generation of reactive oxygen species by phagocytes and endothelial cells. *Luminescence*, 18, 268-73.
- KORZENIEWSKI, C. & CALLEWAERT, D. M. 1983. An enzyme-release assay for natural cytotoxicity. *Journal of Immunological Methods*, 64, 313-320.
- KRISANAPRAKORNKIT, S., KIMBALL, J. R., WEINBERG, A., DARVEAU, R. P., BAINBRIDGE, B. W. & DALE, B. A. 2000. Inducible expression of human beta-defensin 2 by *Fusobacterium nucleatum* in oral epithelial cells: multiple signaling pathways and role of commensal bacteria in innate immunity and the epithelial barrier. *Infection and Immunity*, 68, 2907-15.
- KROLL, A., PILLUKAT, M. H., HAHN, D. & SCHNEKENBURGER, J. 2009. Current in vitro methods in nanoparticle risk assessment: limitations and challenges. *European Journal of Pharmaceutics and Biopharmaceutics*, 72, 370-7.
- KUHN, D. A., VANHECKE, D., MICHEN, B., BLANK, F., GEHR, P., PETRI-FINK, A. & ROTHEN-RUTISHAUSER, B. 2014. Different endocytotic uptake mechanisms for nanoparticles in epithelial cells and macrophages. *Beilstein Journal of Nanotechnology*, 5, 1625-36.
- KUMAR, P. S., MASON, M. R., BROOKER, M. R. & O'BRIEN, K. 2012. Pyrosequencing reveals unique microbial signatures associated with healthy and failing dental implants. *Journal of Clinical Periodontology*, 39, 425-33.
- LAMONT, R. J. & JENKINSON, H. F. 1998. Life below the gum line: pathogenic mechanisms of *Porphyromonas gingivalis*. *Microbiology and Molecular Biology Reviews*, 62, 1244-63.
- LANG, N. P., BERGLUNDH, T. & WORKING GROUP 4 OF SEVENTH EUROPEAN WORKSHOP ON, P. 2011. Periimplant diseases: where are we now?--Consensus of the Seventh European Workshop on Periodontology. *Journal of Clinical Periodontology*, 38 Suppl 11, 178-81.
- LASORELLA, A., NOSEDA, M., BEYNA, M. & IAVARONE, A. 2000. Id2 is a retinoblastoma protein target and mediates signalling by Myc oncoproteins. *Nature*, 407, 592-598.

- LAZZARA, R. J. 1993. Managing the soft tissue margin: the key to implant aesthetics. *Practical Periodontics and Aesthetic Dentistry*, 5, 81-88.
- LEE, Y. S., YOON, S., YOON, H. J., LEE, K., YOON, H. K., LEE, J. H. & SONG, C. W. 2009. Inhibitor of differentiation 1 (Id1) expression attenuates the degree of TiO₂-induced cytotoxicity in H1299 non-small cell lung cancer cells. *Toxicology Letters*, 189, 191-9.
- LEVIN, L. 2013. Editorial: peri-implantitis: the disease of the future. *Quintessence International*, 44, 643.
- LI, L.-H., KONG, Y.-M., KIM, H.-W., KIM, Y.-W., KIM, H.-E., HEO, S.-J. & KOAK, J.-Y. 2004. Improved biological performance of Ti implants due to surface modification by micro-arc oxidation. *Biomaterials*, 25, 2867-2875.
- LI, Y., WONG, C., XIONG, J., HODGSON, P. & WEN, C. 2010. Cytotoxicity of Titanium and Titanium Alloying Elements. *Journal of Dental Research*, 89, 493-497.
- LIMBACH, L. K., WICK, P., MANSER, P., GRASS, R. N., BRUININK, A. & STARK, W. J. 2007. Exposure of engineered nanoparticles to human lung epithelial cells: influence of chemical composition and catalytic activity on oxidative stress. *Environmental Science & Technology*, 41, 4158-4163.
- LINDHE, J., LANG, N. P. & KARRING, T. 2008. *Clinical Periodontology and Implant Dentistry*, Oxford, Blackwell Munksgaard.
- LINDHE, J. & MEYLE, J. 2008. Peri-implant diseases: Consensus Report of the Sixth European Workshop on Periodontology. *Journal of Clinical Periodontology*, 35, 282-5.
- LING, M. R., CHAPPLE, I. L. & MATTHEWS, J. B. 2015. Peripheral blood neutrophil cytokine hyper-reactivity in chronic periodontitis. *Innate Immunity*, 21, 714-25.
- LINKOW, L. I. & DORFMAN, J. D. 1991. Implantology in dentistry. A brief historical perspective. *New York State Dental Journal*, 57, 31-5.
- LIU, X., CHU, P. K. & DING, C. 2004. Surface modification of titanium, titanium alloys, and related materials for biomedical applications. *Materials Science and Engineering: R: Reports*, 47, 49-121.
- LIU, Y., PETERSON, D. A., KIMURA, H. & SCHUBERT, D. 1997. Mechanism of cellular 3-(4,5-dimethylthiazol-2-yl)-2,5-diphenyltetrazolium bromide (MTT) reduction. *Journal of Neurochemistry*, 69, 581-93.
- LUNDQVIST, H. & DAHLGREN, C. 1996. Isoluminol-enhanced chemiluminescence: a sensitive method to study the release of superoxide anion from human neutrophils. *Free Radical Biology and Medicine*, 20, 785-92.
- LUNDQVIST, H., KRICKA, L. J., STOTT, R. A., THORPE, G. H. G. & DAHLGREN, C. 1995. Influence of Different Luminols on the Characteristics of the Chemiluminescence Reaction in Human Neutrophils. *Journal of Bioluminescence and Chemiluminescence*, 10, 353-359.
- LUZIO, J. P., PRYOR, P. R. & BRIGHT, N. A. 2007. Lysosomes: fusion and function. *Nature Reviews Molecular Cell Biology*, 8, 622-632.

- MACKENZIE, I. C., RITTMAN, G., GAO, Z., LEIGH, I. & LANE, E. B. 1991. Patterns of cytokeratin expression in human gingival epithelia. *Journal of Periodontal Research*, 26, 468-78.
- MAGLOTT, D., OSTELL, J., PRUITT, K. D. & TATUSOVA, T. 2011. Entrez Gene: gene-centered information at NCBI. *Nucleic Acids Research*, 39, D52-7.
- MAKAROV, S. S. 2000. NFkappaB as a therapeutic target in chronic inflammation: recent advances. *Molecular Medicine Today*, 6, 441-8.
- MASTERS, J. R. 2000. Human cancer cell lines: fact and fantasy. *Nature reviews Molecular Cell Biology*, 1, 233-6.
- MATTHEWS, J. B., WRIGHT, H. J., ROBERTS, A., LING-MOUNTFORD, N., COOPER, P. R. & CHAPPLE, I. L. 2007. Neutrophil hyper-responsiveness in periodontitis. *Journal of Dental Research*, 86, 718-22.
- MEENA, R., RANI, M., PAL, R. & RAJAMANI, P. 2012. Nano-TiO₂-induced apoptosis by oxidative stress-mediated DNA damage and activation of p53 in human embryonic kidney cells. *Applied Biochemistry and Biotechnology*, 167, 791-808.
- MI, H., DONG, Q., MURUGANUJAN, A., GAUDET, P., LEWIS, S. & THOMAS, P. D. 2010. PANTHER version 7: improved phylogenetic trees, orthologs and collaboration with the Gene Ontology Consortium. *Nucleic Acids Research*, 38, D204-10.
- MI, H., MURUGANUJAN, A., CASAGRANDE, J. T. & THOMAS, P. D. 2013. Large-scale gene function analysis with the PANTHER classification system. *Nature Protocols*, 8, 1551-66.
- MI, H. & THOMAS, P. 2009. PANTHER pathway: an ontology-based pathway database coupled with data analysis tools. *Methods in Molecular Biology*, 563, 123-40.
- MILWARD, M. R., CHAPPLE, I. L., CARTER, K., MATTHEWS, J. B. & COOPER, P. R. 2013. Micronutrient modulation of NFkappaB in oral keratinocytes exposed to periodontal bacteria. *Innate Immunity*, 19, 140-51.
- MILWARD, M. R., CHAPPLE, I. L., WRIGHT, H. J., MILLARD, J. L., MATTHEWS, J. B. & COOPER, P. R. 2007. Differential activation of NFkappaB and gene expression in oral epithelial cells by periodontal pathogens. *Clinical and Experimental Immunology*, 148, 307-24.
- MISCH, C. E. 1999. *Contemporary Implant Dentistry*, St. Louis, Missouri: Mosby.
- MISCH, C. E., PEREL, M. L., WANG, H. L., SAMMARTINO, G., GALINDO-MORENO, P., TRISI, P., STEIGMANN, M., REBAUDI, A., PALT, A., PIKOS, M. A., SCHWARTZ-ARAD, D., CHOUKROUN, J., GUTIERREZ-PEREZ, J. L., MARENZI, G. & VALAVANIS, D. K. 2008. Implant success, survival, and failure: the International Congress of Oral Implantologists (ICOI) Pisa Consensus Conference. *Implant Dentistry*, 17, 5-15.
- MOLLINEDO, F., BORREGAARD, N. & BOXER, L. A. 1999. Novel trends in neutrophil structure, function and development. *Immunology Today*, 20, 535-537.
- MOMBELLI, A. & DÉCAILLET, F. 2011. The characteristics of biofilms in peri-implant disease. *Journal of Clinical Periodontology*, 38, 203-213.

- MONTEIRO-RIVIERE, N. A. & INMAN, A. O. 2006. Challenges for assessing carbon nanomaterial toxicity to the skin. *Carbon*, 44, 1070-1078.
- MORAES, T. J., ZURAWSKA, J. H. & DOWNEY, G. P. 2006. Neutrophil granule contents in the pathogenesis of lung injury. *Current Opinion in Hematology*, 13, 21-7.
- MOSCHINI, E., GUALTIERI, M., COLOMBO, M., FASCIO, U., CAMATINI, M. & MANTECCA, P. 2013. The modality of cell-particle interactions drives the toxicity of nanosized CuO and TiO₂ in human alveolar epithelial cells. *Toxicology Letters*, 222, 102-16.
- MOUNTJOY, G., PICKUP, D. M., WALLIDGE, G. W., ANDERSON, R., COLE, J. M., NEWPORT, R. J. & SMITH, M. E. 1999. XANES study of Ti coordination in heat-treated (TiO₂)_x(SiO₂)_(1-x) xerogels. *Chemistry of Materials*, 11, 1253-1258.
- MUINONEN-MARTIN, A. J., VELTMAN, D. M., KALNA, G. & INSALL, R. H. 2010. An improved chamber for direct visualisation of chemotaxis. *PloS One*, 5, e15309.
- NAKAGAWA, M., MATSUYA, S., SHIRAIISHI, T. & OHTA, M. 1999. Effect of fluoride concentration and pH on corrosion behavior of titanium for dental use. *Journal of Dental Research*, 78, 1568-72.
- NAGATA, T., KANSHA, M., IRITA, K. & TAKAHASHI, S. 2001. Propofol inhibits FMLP-stimulated phosphorylation of p42 mitogen-activated protein kinase and chemotaxis in human neutrophils. *British Journal of Anaesthesia*, 86, 853-8.
- NANCI, A. 2013. *Ten Cate's Oral Histology; Development, Structure and Function*, St Louis, Missouri: Elsevier Inc.
- NANCI, A. & TEN CATE, A. R. O. H. 2008. *Ten Cate's oral histology : development, structure, and function*, St. Louis, Missouri: Mosby.
- NAUSEEF, W. M. 2007. How human neutrophils kill and degrade microbes: an integrated view. *Immunological Reviews*, 219, 88-102.
- NISAPAKULTORN, K., SUPHANANTACHAT, S., SILKOSESSAK, O. & RATTANAMONGKOLGUL, S. 2010. Factors affecting soft tissue level around anterior maxillary single-tooth implants. *Clinical Oral Implants Research*, 21, 662-670.
- NOCITI, F. H., JR., CESCO DE TOLEDO, R., MACHADO, M. A., STEFANI, C. M., LINE, S. R. & GONCALVES, R. B. 2001. Clinical and microbiological evaluation of ligature-induced peri-implantitis and periodontitis in dogs. *Clinical Oral Implants Research*, 12, 295-300.
- OLATE, S., LYRIO, M. C. N., DE MORAES, M., MAZZONETTO, R. & MOREIRA, R. W. F. 2010. Influence of Diameter and Length of Implant on Early Dental Implant Failure. *Journal of Oral and Maxillofacial Surgery*, 68, 414-419.
- OLMEDO, D. G., DUFFO, G., CABRINI, R. L. & GUGLIELMOTTI, M. B. 2008. Local effect of titanium implant corrosion: an experimental study in rats. *International Journal of Oral and Maxillofacial Surgery*, 37, 1032-8.

- OLMEDO, D. G., NALLI, G., VERDÚ, S., PAPARELLA, M. L. & CABRINI, R. L. 2012. Exfoliative Cytology and Titanium Dental Implants: A Pilot Study. *Journal of Periodontology*, 84, 78-83.
- PALMER, R. 1999. Dental implants: Teeth and implants. *British Dental Journal*, 187, 183-188.
- PAN, C., KUMAR, C., BOHL, S., KLINGMUELLER, U. & MANN, M. 2009. Comparative proteomic phenotyping of cell lines and primary cells to assess preservation of cell type-specific functions. *Molecular & Cellular Proteomics* : 8, 443-50.
- PARK, E. J., YI, J., CHUNG, K. H., RYU, D. Y., CHOI, J. & PARK, K. 2008. Oxidative stress and apoptosis induced by titanium dioxide nanoparticles in cultured BEAS-2B cells. *Toxicology Letters*, 180, 222-9.
- PAYNE, C. M., GLASSER, L., TISCHLER, M. E., WYCKOFF, D., CROMEY, D., FIEDERLEIN, R. & BOHNERT, O. 1994. Programmed cell death of the normal human neutrophil: an in vitro model of senescence. *Microscopy Research and Technique*, 28, 327-44.
- PETERS, K., UNGER, R. E., KIRKPATRICK, C. J., GATTI, A. M. & MONARI, E. 2004. Effects of nano-scaled particles on endothelial cell function in vitro: studies on viability, proliferation and inflammation. *Journal of Materials Science: Materials in Medicine*, 15, 321-5.
- PETIBOIS, C., DELERIS, G., PICCININI, M., CESTELLI-GUIDI, M. & MARCELLI, A. 2009. A bright future for synchrotron imaging. *Nature Photonics*, 3, 179-179.
- PETKOVIĆ, A. B., MATIĆ, S. M., STAMATOVIĆ, N. V., VOJVODIĆ, D. V., TODOROVIĆ, T. M., LAZIĆ, Z. R. & KOZOMARA, R. J. 2010. Proinflammatory cytokines (IL-1 β and TNF α) and chemokines (IL8 and MIP-1 α) as markers of peri-implant tissue condition. *International Journal of Oral and Maxillofacial Surgery*, 39, 478-485.
- PFÄFFL, M. W., TICHOPAD, A., PRGOMET, C. & NEUVIANS, T. P. 2004. Determination of stable housekeeping genes, differentially regulated target genes and sample integrity: BestKeeper - Excel-based tool using pair-wise correlations. *Biotechnology Letters*, 26, 509-515.
- PIANGPRACH, T., HENGTRAKOOL, C., KUKIATTRAKOON, B. & KEDJARUNE-LEGGAT, U. 2009. The effect of salivary factors on dental erosion in various age groups and tooth surfaces. *Journal of the American Dental Association*, 140, 1137-43.
- PRIME, S. S., GAME, S. M., MATTHEWS, J. B., STONE, A., DONNELLY, M. J., YEUDALL, W. A., PATEL, V., SPOSTO, R., SILVERTHORNE, A. & SCULLY, C. 1994. Epidermal growth factor and transforming growth factor alpha characteristics of human oral carcinoma cell lines. *British Journal of Cancer*, 69, 8-15.
- PRIME, S. S., NIXON, S. V., CRANE, I. J., STONE, A., MATTHEWS, J. B., MAITLAND, N. J., REMNANT, L., POWELL, S. K., GAME, S. M. & SCULLY, C. 1990. The behaviour of human oral squamous cell carcinoma in cell culture. *Journal of Pathology*, 160, 259-69.

- QIAN, Y., ZHANG, X. L., ZENG, B. F., JIANG, Y., SHEN, H. & WANG, Q. 2013. Substance P enhanced titanium particles-induced RANKL expression in fibroblasts from periprosthetic membrane. *Connective Tissue Research*, 54, 361-366.
- QUINTART, J., LEROY-HOUYET, M. A., TROUET, A. & BAUDHUIN, P. 1979. Endocytosis and chloroquine accumulation during the cell cycle of hepatoma cells in culture. *The Journal of Cell Biology*, 82, 644-53.
- RAINOV, N. G., TRUMPLER, C., QUINONES, A., SPEAR, M. A. & KRAMM, C. M. 2000. Improved method for transport of living cell cultures. *Biotechnology Letters*, 22, 383-385.
- RATNER, B. D. H., ALAN S; SCHOEN, FREDERICK J; LEMONS, JACK E 2013. *Biomaterials Science - An Introduction to Materials in Medicine*, Oxford: Academic Press.
- REMIJSEN, Q., KUIJPERS, T. W., WIRAWAN, E., LIPPENS, S., VANDENABEELE, P. & VANDEN BERGHE, T. 2011. Dying for a cause: NETosis, mechanisms behind an antimicrobial cell death modality. *Cell Death and Differentiation*, 18, 581-588.
- RENVERT, S., AGHAZADEH, A., HALLSTROM, H. & PERSSON, G. R. 2014. Factors related to peri-implantitis - a retrospective study. *Clinical Oral Implants Research*, 25, 522-9.
- RENVERT, S., ROOS-JANSÅKER, A.-M. & CLAFFEY, N. 2008. Non-surgical treatment of peri-implant mucositis and peri-implantitis: a literature review. *Journal of Clinical Periodontology*, 35, 305-315.
- RIEUX, A. D., RAGNARSSON, E. G. E., GULLBERG, E., PRÉAT, V., SCHNEIDER, Y.-J. & ARTURSSON, P. 2005. Transport of nanoparticles across an in vitro model of the human intestinal follicle associated epithelium. *European Journal of Pharmaceutical Sciences*, 25, 455-465.
- RISS, T. L. & MORAVEC, R. A. 2004. Use of multiple assay endpoints to investigate the effects of incubation time, dose of toxin, and plating density in cell-based cytotoxicity assays. *Assays and Drug Development Technology*, 2, 51-62.
- ROBERTS, A., MATTHEWS, J. B., SOCRANSKY, S. S., FREESTONE, P. P., WILLIAMS, P. H. & CHAPPLE, I. L. 2002. Stress and the periodontal diseases: effects of catecholamines on the growth of periodontal bacteria in vitro. *Oral Microbiology and Immunology*, 17, 296-303.
- ROBERTS, H. M., LING, M. R., INSALL, R., KALNA, G., SPENGLER, J., GRANT, M. M. & CHAPPLE, I. L. 2015. Impaired neutrophil directional chemotactic accuracy in chronic periodontitis patients. *Journal of Clinical Periodontology*, 42, 1-11.
- ROOS-JANSÄKER, A. M., LINDAHL, C., RENVERT, H. & RENVERT, S. 2006. Nine- to fourteen-year follow-up of implant treatment. Part I: implant loss and associations to various factors. *Journal of Clinical Periodontology*, 33, 283-9.
- ROQUES, C. G., EL KADDOURI, S., BARTHET, P., DUFFORT, J. F. & ARELLANO, M. 2000. Fusobacterium nucleatum involvement in adult periodontitis and possible modification of strain classification. *Journal of Periodontology*, 71, 1144-50.
- SAHINGUR, S. E. & YEUDALL, W. A. 2015. Chemokine function in periodontal disease and oral cavity cancer. *Frontiers in Immunology*, 6, 214.

- SANZ, M., CHAPPLE, I. L. & WORKING GROUP 4 OF THE, V. E. W. O. P. 2012. Clinical research on peri-implant diseases: consensus report of Working Group 4. *Journal of Clinical Periodontology*, 39 Suppl 12, 202-6.
- SCHAEFER, B. M., KOCH, J., WIRZBACH, A. & KRAMER, M. D. 2001. Expression of the helix-loop-helix protein ID1 in keratinocytes is upregulated by loss of cell-matrix contact. *Experimental Cell Research*, 266, 250-9.
- SCHIFF, N., GROSGOGGAT, B., LISSAC, M. & DALARD, F. 2002. Influence of fluoride content and pH on the corrosion resistance of titanium and its alloys. *Biomaterials*, 23, 1995-2002.
- SCHROTT, A. R., JIMENEZ, M., HWANG, J.-W., FIORELLINI, J. & WEBER, H.-P. 2009. Five-year evaluation of the influence of keratinized mucosa on peri-implant soft-tissue health and stability around implants supporting full-arch mandibular fixed prostheses. *Clinical Oral Implants Research*, 20, 1170-1177.
- SETTEM, R. P., EL-HASSAN, A. T., HONMA, K., STAFFORD, G. P. & SHARMA, A. 2012. *Fusobacterium nucleatum* and *Tannerella forsythia* induce synergistic alveolar bone loss in a mouse periodontitis model. *Infection and Immunity*, 80, 2436-43.
- SHALABI, M. M., GORTEMAKER, A., VAN'T HOF, M. A., JANSEN, J. A. & CREUGERS, N. H. 2006. Implant surface roughness and bone healing: a systematic review. *Journal of Dental Research*, 85, 496-500.
- SHUKLA, R. K., KUMAR, A., GURBANI, D., PANDEY, A. K., SINGH, S. & DHAWAN, A. 2013. TiO₂ nanoparticles induce oxidative DNA damage and apoptosis in human liver cells. *Nanotoxicology*, 7, 48-60.
- SHUKLA, R. K., KUMAR, A., PANDEY, A. K., SINGH, S. S. & DHAWAN, A. 2011a. Titanium dioxide nanoparticles induce oxidative stress-mediated apoptosis in human keratinocyte cells. *Journal of Biomedical Nanotechnology*, 7, 100-1.
- SHUKLA, R. K., SHARMA, V., PANDEY, A. K., SINGH, S., SULTANA, S. & DHAWAN, A. 2011b. ROS-mediated genotoxicity induced by titanium dioxide nanoparticles in human epidermal cells. *Toxicology in Vitro* ;, 25, 231-41.
- SILVERMAN, N. & MANIATIS, T. 2001. NFκB signaling pathways in mammalian and insect innate immunity. *Genes and Development*, 15, 2321-42.
- SINGH, S., SHI, T., DUFFIN, R., ALBRECHT, C., VAN BERLO, D., HOHR, D., FUBINI, B., MARTRA, G., FENOGLIO, I., BORM, P. J. & SCHINS, R. P. 2007. Endocytosis, oxidative stress and IL8 expression in human lung epithelial cells upon treatment with fine and ultrafine TiO₂: role of the specific surface area and of surface methylation of the particles. *Toxicology and Applied Pharmacology*, 222, 141-51.
- SMITH, P. J., GIROUD, M., WIGGINS, H. L., GOWER, F., THORLEY, J. A., STOLPE, B., MAZZOLINI, J., DYSON, R. J. & RAPPOPORT, J. Z. 2012. Cellular entry of nanoparticles via serum sensitive clathrin-mediated endocytosis, and plasma membrane permeabilization. *International Journal of Nanomedicine*, 7, 2045-55.

- SMYTH, G. K. 2004. Linear models and empirical bayes methods for assessing differential expression in microarray experiments. *Statistical Applications in Genetics and Molecular Biology*, 3, Article3.
- SOCRANSKY, S. S., HAFFAJEE, A. D., CUGINI, M. A., SMITH, C. & KENT, R. L. 1998. Microbial complexes in subgingival plaque. *Journal of Clinical Periodontology*, 25, 134-144.
- SQUIER, C. A. & KREMER, M. J. 2001b. Biology of oral mucosa and esophagus. *Journal of the National Cancer Institute Monographs*, 7-15.
- SRIVASTAVA, R. K., RAHMAN, Q., KASHYAP, M. P., SINGH, A. K., JAIN, G., JAHAN, S., LOHANI, M., LANTOW, M. & PANT, A. B. 2013. Nano-titanium dioxide induces genotoxicity and apoptosis in human lung cancer cell line, A549. *Human and Experimental Toxicology*, 32, 153-66.
- STAJER, A., UNGVARI, K., PELSOCI, I. K., POLYANKA, H., OSZKO, A., MIHALIK, E., RAKONCZAY, Z., RADNAI, M., KEMENY, L., FAZEKAS, A. & TURZO, K. 2008. Corrosive effects of fluoride on titanium: investigation by X-ray photoelectron spectroscopy, atomic force microscopy, and human epithelial cell culturing. *Journal of Biomedical Materials Research A*, 87, 450-8.
- SUL, Y.-T., JOHANSSON, C. B., PETRONIS, S., KROZER, A., JEONG, Y., WENNERBERG, A. & ALBREKTSSON, T. 2002. Characteristics of the surface oxides on turned and electrochemically oxidized pure titanium implants up to dielectric breakdown. *Biomaterials*, 23, 491-501.
- TAUROZZI, J. S., HACKLEY, V. A. & WIESNER, M. R. 2013. A standardised approach for the dispersion of titanium dioxide nanoparticles in biological media. *Nanotoxicology*, 7, 389-401.
- TAYLOR-PAPADIMITRIOU, J., SHEARER, M. & STOKER, M. G. P. 1977. Growth requirements of human mammary epithelial cells in culture. *International Journal of Cancer*, 20, 903-908.
- THOMAS, P. D., KEJARIWAL, A., GUO, N., MI, H., CAMPBELL, M. J., MURUGANUJAN, A. & LAZAREVA-ULITSKY, B. 2006. Applications for protein sequence-function evolution data: mRNA/protein expression analysis and coding SNP scoring tools. *Nucleic Acids Research*, 34, W645-50.
- THOMAS, S. R., SHUKLA, D. & LATHAM, P. D. 2004. Corrosion of cemented titanium femoral stems. *Journal of Bone and Joint Surgery (British Volume)*, 86, 974-8.
- TORGERSEN, S., GJERDET, N. R., ERICHSEN, E. S. & BANG, G. 1995. Metal particles and tissue changes adjacent to miniplates. A retrieval study. *Acta Odontologica Scandinavica*, 53, 65-71.
- TRIBBLE, G. D. & LAMONT, R. J. 2010. Bacterial invasion of epithelial cells and spreading in periodontal tissue. *Periodontology 2000*, 52, 68-83.
- TSCHERNITSCHKE, H., BORCHERS, L. & GEURTSSEN, W. 2006. Nonalloyed titanium as a bioinert metal—A review. *The Journal of Prosthetic Dentistry*, 96, 12.

- TSCHOPP, J. & SCHRODER, K. 2010. NLRP3 inflammasome activation: the convergence of multiple signalling pathways on ROS production? *Nature Reviews Immunology*, 10, 210-215.
- TUOMIKOSKI, T., FELIX, M. A., DOREE, M. & GRUENBERG, J. 1989. Inhibition of endocytic vesicle fusion in vitro by the cell-cycle control protein kinase cdc2. *Nature*, 342, 942-5.
- UNGER, R. E., KRUMP-KONVALINKOVA, V., PETERS, K. & KIRKPATRICK, C. J. 2002. In vitro expression of the endothelial phenotype: comparative study of primary isolated cells and cell lines, including the novel cell line HPMEC-ST1.6R. *Microvascular Research*, 64, 384-97.
- VAMANU, C. I., CIMPAN, M. R., HOL, P. J., SORNES, S., LIE, S. A. & GJERDET, N. R. 2008. Induction of cell death by TiO₂ nanoparticles: studies on a human monoblastoid cell line. *Toxicology in vitro*, 22, 1689-96.
- VAN WINKELHOFF, A. J., LOOS, B. G., VAN DER REIJDEN, W. A. & VAN DER VELDEN, U. 2002. Porphyromonas gingivalis, Bacteroides forsythus and other putative periodontal pathogens in subjects with and without periodontal destruction. *Journal of Clinical Periodontology*, 29, 1023-8.
- VEGA, L. G. & BILBAO, A. 2010. Alveolar Distraction Osteogenesis for Dental Implant Preparation: An Update. *Oral and Maxillofacial Surgery Clinics of North America*, 22, 369-385.
- VERANTH, J. M., KASER, E. G., VERANTH, M. M., KOCH, M. & YOST, G. S. 2007. Cytokine responses of human lung cells (BEAS-2B) treated with micron-sized and nanoparticles of metal oxides compared to soil dusts. *Particle and Fibre Toxicology*, 4, 2.
- VOYICH, J. M., BRAUGHTON, K. R., STURDEVANT, D. E., WHITNEY, A. R., SAID-SALIM, B., PORCELLA, S. F., LONG, R. D., DORWARD, D. W., GARDNER, D. J., KREISWIRTH, B. N., MUSSER, J. M. & DELEO, F. R. 2005. Insights into mechanisms used by Staphylococcus aureus to avoid destruction by human neutrophils. *Journal of immunology*, 175, 3907-19.
- WANG, G. F., LI, J. H., LV, K. G., ZHANG, W. J., DING, X., YANG, G. Z., LIU, X. Y. & JIANG, X. Q. 2016. Surface thermal oxidation on titanium implants to enhance osteogenic activity and in vivo osseointegration. *Scientific Reports*, 6, 31769.
- WANG, Z., LI, Y. & SARKAR, F. H. 2010. Signaling mechanism(s) of reactive oxygen species in Epithelial-Mesenchymal Transition reminiscent of cancer stem cells in tumor progression. *Current Stem Cell Research & Therapy*, 5, 74-80.
- WEISS, C. M. & JUDY, K. W. 1974. Intramucosal inserts--solve patients' problems with maxillary dentures. II. *Quintessence International: Dental Digest*, 5, 9-15.
- WEISS, M. B. & ROSTOKER, W. 1981. Development of a new endosseous dental implant. Part I: Animal studies. *Journal of Prosthetic Dentistry*, 46, 646-51.
- WERTZ, P. W. & SQUIER, C. A. 1991. Cellular and molecular basis of barrier function in oral epithelium. *Critical Reviews in Therapeutic Drug Carrier Systems*, 8, 237-69.

- WILLERT, H. G., BROBACK, L. G., BUCHHORN, G. H., JENSEN, P. H., KOSTER, G., LANG, I., OCHSNER, P. & SCHENK, R. 1996. Crevice corrosion of cemented titanium alloy stems in total hip replacements. *Clinical Orthopaedics and Related Research*, 51-75.
- WILSON, D., ZAQOUT, M., HEO, J. H., PARK, E. K., OAK, C. H. & UENO, S. 2012. Nuclear factor-kappa B is not involved in titanium dioxide-induced inflammation. *Journal of University of Occupational and Environmental Health*, 34, 183-91.
- WILSON, M. R., STONE, V., CULLEN, R. T., SEARL, A., MAYNARD, R. L. & DONALDSON, K. 2000. In vitro toxicology of respirable Montserrat volcanic ash. *Occupational and Environmental Medicine*, 57, 727-33.
- WRIGHT, H. J., MATTHEWS, J. B., CHAPPLE, I. L., LING-MOUNTFORD, N. & COOPER, P. R. 2008. Periodontitis associates with a type 1 IFN signature in peripheral blood neutrophils. *Journal of Immunology*, 181, 5775-84.
- WRIGHT, H. L., MOOTS, R. J., BUCKNALL, R. C. & EDWARDS, S. W. 2010. Neutrophil function in inflammation and inflammatory diseases. *Rheumatology*, 49, 1618-31.
- WYLIE, C. M., DAVENPORT, A. J., COOPER, P. R. & SHELTON, R. M. 2010. Oral keratinocyte responses to nickel-based dental casting alloys in vitro. *Journal of Biomaterials Applications*, 25, 251-67.
- YILMAZ, O., WATANABE, K. & LAMONT, R. J. 2002. Involvement of integrins in fimbriae-mediated binding and invasion by *Porphyromonas gingivalis*. *Cellular Microbiology*, 4, 305-14.
- YILMAZ, O., YOUNG, P. A., LAMONT, R. J. & KENNY, G. E. 2003. Gingival epithelial cell signalling and cytoskeletal responses to *Porphyromonas gingivalis* invasion. *Microbiology*, 149, 2417-26.
- YU, F., ADDISON, O., BAKER, S. J. & DAVENPORT, A. J. 2015a. Lipopolysaccharide inhibits or accelerates biomedical titanium corrosion depending on environmental acidity. *International Journal of Oral Science*, 7, 179-186.
- YU, F., ADDISON, O. & DAVENPORT, A. J. 2015b. A synergistic effect of albumin and H₂O₂ accelerates corrosion of Ti6Al4V. *Acta Biomaterialia*, 26, 355-365.
- ZHANG, G. & GHOSH, S. 2001. Toll-like receptor-mediated NFkappaB activation: a phylogenetically conserved paradigm in innate immunity. *The Journal of Clinical Investigation*, 107, 13-9.
- ZHANG, W. 2014. Nanoparticle aggregation: principles and modeling. *Advances in Experimental Medicine and Biology*, 811, 19-43.